

การวิเคราะห์และการประยุกต์ของสมการ โคชีอินทิกรัลแบบหลายมิติด้วยจำนวนคลิฟฟอร์ดเพื่อ
คำนวณการกระเจิงและการแผ่ของคลื่นแม่เหล็กไฟฟ้า

นายอจลวิษญ์ ฉันทวีโรจน์

วิทยานิพนธ์นี้เป็นส่วนหนึ่งของการศึกษาตามหลักสูตรปริญญาวิศวกรรมศาสตรดุษฎีบัณฑิต

สาขาวิชาวิศวกรรมไฟฟ้า ภาควิชาวิศวกรรมไฟฟ้า

คณะวิศวกรรมศาสตร์ จุฬาลงกรณ์มหาวิทยาลัย

ปีการศึกษา 2552

ลิขสิทธิ์ของจุฬาลงกรณ์มหาวิทยาลัย

ANALYSIS AND APPLICATIONS OF MULTI-DIMENSIONAL CAUCHY INTEGRAL
EQUATION BASED ON CLIFFORD NUMBER TO SCATTERING AND
RADIATION OF ELECTROMAGNETIC FIELDS



Mr. Ajalawit Chantaveerod

คณบดีบัณฑิตยศาสตร์
A Dissertation Submitted in Partial Fulfillment of the Requirements
for the Degree of Doctor of Philosophy Program in Electrical Engineering

Department of Electrical Engineering

Faculty of Engineering
Chulalongkorn University

จุฬาลงกรณ์มหาวิทยาลัย
Academic Year 2009

Copyright of Chulalongkorn University

Thesis Title ANALYSIS AND APPLICATIONS OF MULTI-DIMENSIONAL
CAUCHY INTEGRAL EQUATION BASED ON CLIFFORD
NUMBER TO SCATTERING AND RADIATION OF ELEC-
TROMAGNETIC FIELDS

By Mr. Ajalawit Chantaveerod

Field of Study Electrical Engineering

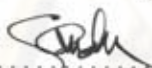
Thesis Advisor Assistant Professor Tuptim Angkaew, D.Eng.

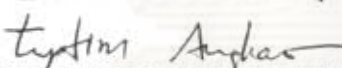
Thesis Co-advisor Andrew Seagar, Ph.D.

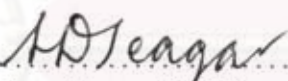
Accepted by the Faculty of Engineering, Chulalongkorn University in Partial Fulfillment
of the Requirements for the Doctoral Degree

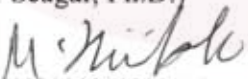

..... Dean of the Faculty of Engineering
(Associate Professor Boonsom Lerdhirunwong, Dr.Ing.)

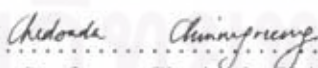
THESIS COMMITTEE

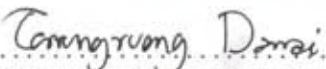

..... Chairman
(Associate Professor Somchai Jitapunkul, Dr.Ing.)


..... Thesis Advisor
(Assistant Professor Tuptim Angkaew, D.Eng.)


..... Thesis Co-advisor
(Andrew Seagar, Ph.D.)


..... Member
(Professor Monai Krairiksh, D.Eng.)


..... Member
(Associate Professor Chedsada Chinrungrueng, Ph.D.)


..... Member
(Assistant Professor Danai Torrungrueng, Ph.D.)

อจลวิษณุ ฉันทวีโรจน์ : การวิเคราะห์และการประยุกต์ของสมการ โคชีอินทิกรัลแบบหลาย มิติด้วยจำนวนคลิฟฟอร์ดเพื่อคำนวณการกระเจิงและการแผ่ของคลื่นสนามแม่เหล็กไฟฟ้า. (Analysis and Applications of Multi-Dimensional Cauchy Integral Equation Based on Clifford Number to Scattering and Radiation of Electromagnetic Fields) อ. ที่ปรึกษา วิทยานิพนธ์หลัก: ศศ.คร.ทับทิม อ่างแก้ว, อ. ที่ปรึกษาวิทยานิพนธ์ร่วม: ดร.แอนครูว์ จีการ์, 139 หน้า.

ระเบียบวิธีสมการอินทิกรัลสำหรับการคำนวณสนามแม่เหล็กไฟฟ้า ยังคงได้รับการสนใจอย่างมากจากนักวิจัย ผู้ซึ่งต้องการวิเคราะห์สมรรถนะของสายอากาศในบริเวณที่ไร้ขอบเขต ระเบียบวิธีเหล่านี้ถูกสร้างขึ้นจากสมการอินทิกรัลของสนามไฟฟ้าหรือสมการอินทิกรัลของสนามแม่เหล็ก อย่างใดอย่างหนึ่ง โดยที่ผลเฉลยแปลกปลอมยังคงเกิดขึ้น ถึงแม้ว่าการอนุพันธ์ของฟังก์ชันเอกฐานใน เคอร์เนลของการอินทิกรัลได้รับการประมาณค่าอย่างระมัดระวัง ปัญหาเหล่านี้ถูกหลีกเลี่ยงโดยการ รวบรวมทั้งสมการอินทิกรัลของสนามไฟฟ้าและสมการอินทิกรัลของสนามแม่เหล็กเข้าด้วยกัน ซึ่ง ถูกเรียกว่า สมการอินทิกรัลของสนามแม่เหล็กไฟฟ้า จุดประสงค์ของวิทยานิพนธ์ฉบับนี้ คือ การ เสนอสมการอินทิกรัลของสนามแม่เหล็กไฟฟ้าในรูปแบบใหม่ เพื่อนำไปใช้ในการแก้ปัญหาดังกล่าว

ระเบียบวิธีใหม่นี้ ถูกนำเสนอขึ้นเพื่อคำนวณผลเฉลยของสมการแมกซ์เวลล์ ซึ่งถูกประยุกต์ มาจากสมการ โคชีด้วยพีชคณิตของคลิฟฟอร์ด สนามแม่เหล็กและสนามไฟฟ้าถูกผูกไว้ด้วยกัน ภายในจำนวนคลิฟฟอร์ดหนึ่งจำนวน การอธิบายความสัมพันธ์ของสมการอินทิกรัลจะถูกตีความด้วย รูปเรขาคณิตและนำไปสู่ผลเฉลยที่สามารถใช้เทคนิคของการทำซ้ำ ซึ่งในทางทฤษฎีสามารถพิสูจน์ ความถูกต้องและการเข้าสู่ของผลเฉลยได้ง่าย โดยที่ครอบคลุมปัญหาที่พื้นผิวขอบเขตทำให้เกิดการ ส่งผ่านทั้งหมดและการสะท้อนกลับทั้งหมดของสนามแม่เหล็กไฟฟ้า ระเบียบวิธีนี้หลีกเลี่ยงการ แสดงอย่างชัดเจนของเวกเตอร์ความหนาแน่นกระแสบนพื้นผิวของตัวนำไฟฟ้าสมบูรณ์ ผลการ คำนวณแสดงให้เห็นว่า ระเบียบวิธีที่เสนอสามารถถูกนำไปใช้ในการบรรยายสนามที่กระเจิงและ แพร่ภายในบริเวณ ไร้ขอบเขตของระบบสามมิติได้

ภาควิชา.....วิศวกรรมไฟฟ้า.....
สาขาวิชา.....วิศวกรรมไฟฟ้า.....
ปีการศึกษา..... 2552.....

ลายมือชื่อนิสิต.....
ลายมือชื่อ อ. ที่ปรึกษาวิทยานิพนธ์หลัก.....
ลายมือชื่อ อ. ที่ปรึกษาวิทยานิพนธ์ร่วม.....

จุฬาลงกรณ์มหาวิทยาลัย

##4771862021: MAJOR ELECTRICAL ENGINEERING

KEY WORDS: MAXWELL'S EQUATIONS / CAUCHY INTEGRAL / CLIFFORD ALGEBRA / BOUNDARY INTEGRAL / NEAR-FIELD TO FAR-FIELD TRANSFORMATION / SCATTERING PROBLEMS

AJALAWIT CHANTAVEEROD: ANALYSIS AND APPLICATIONS OF MULTI-DIMENSIONAL CAUCHY INTEGRAL EQUATION BASED ON CLIFFORD NUMBER TO SCATTERING AND RADIATION OF ELECTROMAGNETIC FIELDS, THESIS ADVISOR: ASST. PROF. TUPTIM ANGKAEW, D.Eng., THESIS COADVISOR: ANDREW SEAGAR, Ph.D., 139 pp.

Integral equation methods in computational electromagnetics have been particularly attractive for researchers who need to analyse the performance of antennas in unbounded region. These methods are formulated either from the electric field integral equation (EFIE) or from the magnetic field integral equation (MFIE). However spurious solutions can appear at some frequencies, even when the differentiation of the singular function in the kernel under the integral is approximated carefully. The problem is often avoided by using some combination of EFIE and MFIE, that is to say a combined field integral equation or CFIE. It is the purpose of this thesis to provide a particular combination of EFIE and MFIE which solves the same problem but in a different way.

A new method is presented for calculating the solution of Maxwell's equations based on the Cauchy integral and formulated in the guise of Clifford algebra. Electric and magnetic fields are embedded together as a single entity in a single Clifford number. The formulation has a geometric interpretation leading to an iterative method of solution which is easily proven as convergent and valid for both perfectly reflective and perfectly transmissive objects. The method avoids any explicit representation of current density vector on the surface of perfect electric conductors. The numerical results prove that the method can be employed to describe the behaviour of scattered and radiated fields in unbounded regions of three dimensional space.

Department: Electrical Engineering Student's signature
 Field of study: Electrical Engineering Advisor's signature
 Academic year: 2009 Co-advisor's signature

Acknowledgements

I would like to express my great gratitude to my advisor, Assist. Prof. Dr. Tuptim Angkaew, my co-advisor, Dr. Andrew Seagar. Their encouragement, in-depth support and expert guidance have been invaluable until finishing the Ph.D. thesis. I have also greatly appreciated their warm and kind personality which makes them a truly great Ph.D. supervisor. I would like to thank my thesis committee members, Assoc. Prof. Dr. Somchai Jitapunkul, Prof. Dr. Monai Krairiksh, Assoc. Prof. Dr. Chedsada Chinrungrueng and Assist. Prof. Dr. Danai Torrungrueng for their suggestions and important comments.

I would like to express my sincere gratitude Walailak University for granting me a full scholarship without which my study at Chulalongkorn University would not be possible.

Many thanks to my all colleagues in EMRL (Electromagnetic Research Laboratory) for some help with academic documents and programming/data information. Many thanks also to my colleagues in DSPRL (Digital Signal Processing Laboratory) and TSRL (Telecommunication System Research Laboratory) for supply of HPC (High-Performance Computing) Computers. In particular I thank the administrative staffs for all their help.

Finally, I would like to thank my family. I am very grateful to my father, Wanchai Chantaveerod, my mother, Kanlaya Chantaveerod, my sister, Sarissa Chantaveerod and Assist. Prof. Dr. Nittaya Seagar, who always encourage and give me all happiness during a difficult part of my life.

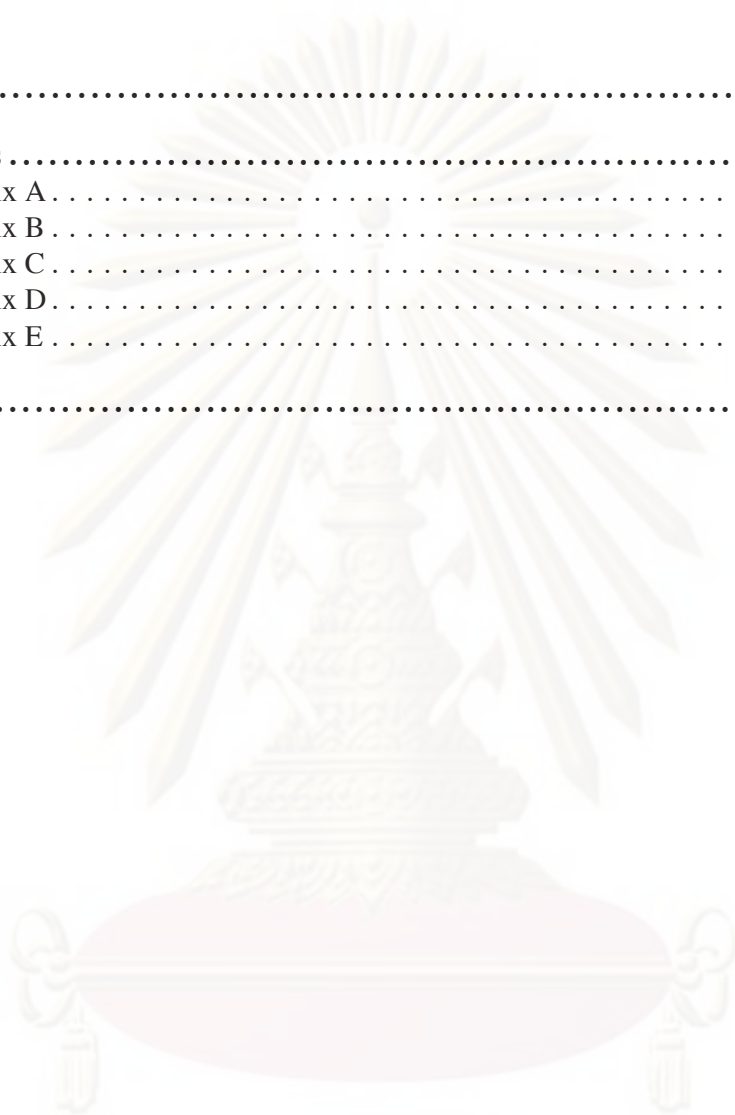
ศูนย์วิทยทรัพยากร
จุฬาลงกรณ์มหาวิทยาลัย

Contents

	Page
Abstract in Thai	iv
Abstract in English	v
Acknowledgements	vi
Contents	vii
List of Tables	x
List of Figures	xi
I Introduction	1
1.1 Background and Significance of the Research Problems	1
1.2 Literature Review	2
1.3 Objectives of the Research	7
1.4 Scopes of the Dissertation	7
1.5 Expected Results and Benefits	8
1.6 Research Procedure	8
II Integral Equations for Electromagnetic fields	10
2.1 Clifford Number and Arithmetic	10
2.2 Clifford Fields	11
2.3 Maxwell-Dirac Equation	12
2.3.1 Helmholtz Equation on Vector Form	12
2.3.2 Maxwell-Dirac Equation on Clifford Form	13
2.3.3 Fundamental Solution of Maxwell-Dirac Operator	14
2.4 Reproducing Formula	15
2.5 Cauchy Extension Operator	17
2.6 Cauchy Integral Operator	20
2.7 Hardy Projection Operator	21
III Geometric Solutions of Integral Equation for Boundary Value Problems	23
3.1 Perfect Transmission Problem	24
3.1.1 Boundary Value Problem in Perfect Transmission	24
3.1.1.1 The Cookie Cutter Problem	24
3.1.1.2 Boundary Conditions in Perfect Transmission	25
3.1.2 Normal Solutions for Perfect Transmission	26
3.1.2.1 Normal Solution of Inward Field	26
3.1.2.2 Normal Solution of Outward Field	28
3.1.3 Iterative Solution for Perfect Transmission	31
3.1.3.1 Iterative Solution of Inward Field	31
3.1.3.2 Iterative Solution of Outward Field	32

Chapter	Page
3.2 Perfect Reflection Problem	35
3.2.1 Boundary Value Problem in Perfect Reflection	35
3.2.1.1 Good Conductors	35
3.2.1.2 Boundary Conditions in Perfect Reflection	35
3.2.2 Normal Solutions for Perfect Reflection	36
3.2.3 Iterative Solution for Perfect Reflection	39
IV Methodology	41
4.1 Geometry of Boundary	41
4.1.1 Boundary	41
4.1.2 Discretisation of Boundary	42
4.2 Boundary Element Method	44
4.2.1 Discretization of Cauchy extension operator	44
4.2.2 Discretization of Cauchy integral operator	47
4.2.3 Discretization of Hardy projection operators	49
4.2.4 Procedure of Calculation	51
V Numerical Results	52
5.1 Test Cases	52
5.1.1 Boundary condition of transparent boundary	52
5.1.2 Definition of errors in test cases	53
5.1.3 Verification of Cauchy extension operator	55
5.1.4 Verification of Hardy Projection Operator	57
5.1.5 Verification of Geometric solution	60
5.2 Far-Field Cases	71
5.2.1 Boundary Condition of Near-Fields on Boundary	71
5.2.2 Definition of errors in far-field cases	72
5.2.3 Calculation of Far-Field from All Components \mathbf{E} , \mathbf{H} of Near-Field . .	73
5.2.4 Calculation of Near-Field from components \mathbf{E}_t , \mathbf{H}_n of Near-Field . .	75
5.2.5 Calculation of Far-Field from components \mathbf{E}_t , \mathbf{H}_n of Near-Field . . .	85
5.3 Scattering Cases	87
5.3.1 Boundary condition of Perfect Electric Conductor (PEC)	87
5.3.2 Definition of errors in scattering cases	87
5.3.3 Calculation of surface field on PEC from components \mathbf{E}_t , \mathbf{H}_n of incident field	88
5.3.4 Calculation of radar cross section at Far-Field	97
5.3.5 Calculation of reflection coefficient	107
5.4 Summary	107
VI Conclusions	111
6.1 Conclusions of Desertation	111
6.2 Future Research	113

Chapter	Page
References	114
Appendices	119
Appendix A	120
Appendix B	129
Appendix C	131
Appendix D	137
Appendix E	138
Vitae	139



ศูนย์วิทยทรัพยากร
จุฬาลงกรณ์มหาวิทยาลัย

List of Tables

Table	Page
2.1 Hardy and Cauchy integral operators.	22
4.1 Angular ratios on cube.	49
5.1 Errors of Hardy projection in full field when at $\frac{4s}{\lambda}=0.6366$	57
5.2 CPU time (seconds).	110



ศูนย์วิทยทรัพยากร
จุฬาลงกรณ์มหาวิทยาลัย

List of Figures

Figure	Page
2.1	Calculation of field $\mathbf{u}(\mathbf{p})$ in region Ω^+ and Ω^- from its trace $\mathbf{u}(\mathbf{q})$ on boundary Σ . 16
2.2	Propagating field $\mathbf{u}(\mathbf{p})$ in region Ω^+ and Ω^- from its trace $\mathbf{u}(\mathbf{q})$ on boundary Σ . . 18
2.3	Cauchy extensions \mathbf{u}^\pm and Hardy projections $\mathbf{P}^\pm \mathbf{u}$ for the surface field \mathbf{u} on Σ . . 21
3.1	Three cases of electromagnetic boundary value problems. 23
3.2	Three different functions: \mathbf{u}^+ , \mathbf{u}^- and \mathbf{u} along Ω^+ , Ω^- and Σ , respectively. . . . 24
3.3	Solution of Maxwell's equations as intersection in Banach space of dotted line through boundary conditions \mathbf{g} and coordinate axis OP, OP' for the inward field in case of perfect transmission. 27
3.4	Construction for solution of inward field given data $\mathbf{g} = \mathbf{Q}^- \mathbf{u}^{tr}$ 27
3.5	Solution of Maxwell's equations as intersection in Banach space of dotted line through boundary conditions \mathbf{g} and coordinate axis OP, OP' for the outward field in case of the perfect transmission. 29
3.6	Construction for solution of outward field given data $\mathbf{g} = \mathbf{Q}^- \mathbf{u}^{tr}$ 30
3.7	Iterative solution of inward field. Adding correction $\Delta \mathbf{u}_0^{tr}$ to initial estimate \mathbf{u}_0^{tr} gives improved estimate \mathbf{u}_1^{tr} , and adding $\Delta \mathbf{u}_1^{tr}$ to \mathbf{u}_0^{tr} gives \mathbf{u}_2^{tr} 31
3.8	The difference of the solutions of inward fields $\mathbf{u}_k^{tr} - \mathbf{u}_{k-1}^{tr}$ between consecutive estimates of solution \mathbf{u}^{tr} approaching zero as the iteration proceeds. 32
3.9	The difference between estimate \mathbf{u}_k^{tr} and solution of inward field \mathbf{u}^{tr} is the same after projections $\mathbf{P}^+ \mathbf{Q}^-$ only if $\mathbf{u}_k^{tr} - \mathbf{u}^{tr} = 0$, showing convergence to correct solution of inward field $\mathbf{u}_k^{tr} = \mathbf{u}^{tr}$ 32
3.10	Iterative solution of outward field. Adding correction $\Delta \mathbf{u}_0^{tr}$ to initial estimate \mathbf{u}_0^{tr} gives improved estimate \mathbf{u}_1^{tr} , and adding $\Delta \mathbf{u}_1^{tr}$ to \mathbf{u}_0^{tr} gives \mathbf{u}_2^{tr} 33
3.11	The difference of the solutions of outward fields $\mathbf{u}_k^{tr} - \mathbf{u}_{k-1}^{tr}$ between consecutive estimates of solution \mathbf{u}^{tr} approaching zero as the iteration proceeds. 33
3.12	The difference between the estimate \mathbf{u}_k^{tr} and solution of the outward field \mathbf{u}^{tr} is the same after projections $\mathbf{P}^- \mathbf{Q}^-$ only if $\mathbf{u}_k^{tr} - \mathbf{u}^{tr} = 0$, showing convergence to correct solution of outward field $\mathbf{u}_k^{tr} = \mathbf{u}^{tr}$ 34
3.13	Solution of Maxwell's equations as intersection in Banach space of dotted line through boundary conditions \mathbf{g} and coordinate axis OP, OP' for the reflected field in case of perfect reflection. 37
3.14	Construction for solution of reflected field given data $\mathbf{g} = \mathbf{Q}^- \mathbf{u}^{sc}$ 37
3.15	Iterative solution of reflected field. Adding correction $\Delta \mathbf{u}_0^{sc}$ to initial estimate \mathbf{u}_0^{sc} gives improved estimate \mathbf{u}_1^{sc} , and adding $\Delta \mathbf{u}_1^{sc}$ to \mathbf{u}_0^{sc} gives \mathbf{u}_2^{sc} 39
3.16	The difference of the solutions of reflected fields $\mathbf{u}_k^{sc} - \mathbf{u}_{k-1}^{sc}$ between consecutive estimates of solution \mathbf{u}^{sc} approaching zero as the iteration proceeds. 40
3.17	The difference between estimate \mathbf{u}_k^{sc} and solution of reflected field \mathbf{u}^{sc} is the same after projections $\mathbf{P}^- \mathbf{Q}^-$ only if $\mathbf{u}_k^{sc} - \mathbf{u}^{sc} = 0$, showing convergence to correct solution of reflected field $\mathbf{u}_k^{sc} = \mathbf{u}^{sc}$ 40
4.1	The six surfaces consist of the cube as boundary Σ 42
4.2	Discretisation of boundary Σ_j 42
4.3	Rotations to bring local coordinates into alignment with common coordinates. . . 43
4.4	Element of boundary Σ_j with local coordinates on face. 44

Figure	Page	
4.5	Procedure for calculating the iterative solutions of boundary field problems.	50
5.1	Propagation of the incident and transmitted fields in test cases.	53
5.2	Error of inward field in iterative solution.	54
5.3	Error (%) of Cauchy extension operator in full field at a centre of a cube $p(0.0,0.0,0.0)$ when varying boundary elements: 150, 384, 600 and $\frac{4s}{\lambda} \in (0.6,2.6)$	56
5.4	Error (%) of Cauchy extension operator in full field near a surface of a cube $p(0.0,0.0,0.45)$ when varying boundary elements: 150, 384, 600 and $\frac{4s}{\lambda} \in (0.6,2.6)$	56
5.5	Error (%) of Hardy projection operator in full field of all corner points on 150 rectangular boundary elements and $\frac{4s}{\lambda}=0.6366$	58
5.6	Error (%) of Hardy projection operator in full field of all corner points on 384 rectangular boundary elements and $\frac{4s}{\lambda}=0.6366$	58
5.7	Error (%) of Hardy projection operator in full field of all corner points on 600 rectangular boundary elements and $\frac{4s}{\lambda}=0.6366$	59
5.8	Averaged error (%) of Hardy projection operator in full field calculated from all corner points on boundary elements: 150, 384, 600 and $\frac{4s}{\lambda} \in (0.6,2.6)$	59
5.9	Percentage averaged error in full field during iteration towards plane wave solution. Boundary elements N: 150, 384, 600 and $\frac{4s}{\lambda}=0.6366$	60
5.10	Percentage averaged error in full field during iteration towards plane wave solution. Boundary elements N: 150, 384, 600 and $\frac{4s}{\lambda}=0.7640$	61
5.11	Percentage averaged error in full field during iteration towards plane wave solution. Boundary elements N: 150, 384, 600 and $\frac{4s}{\lambda}=0.8913$	61
5.12	Percentage averaged error in full field during iteration towards plane wave solution. Boundary elements N: 150, 384, 600 and $\frac{4s}{\lambda}=1.0185$	62
5.13	Percentage averaged error in full field during iteration towards plane wave solution. Boundary elements N: 150, 384, 600 and $\frac{4s}{\lambda}=1.1460$	62
5.14	Percentage averaged error in full field during iteration towards plane wave solution. Boundary elements N: 150, 384, 600 and $\frac{4s}{\lambda}=1.2732$	63
5.15	Percentage averaged error in full field during iteration towards plane wave solution. Boundary elements N: 150, 384, 600 and $\frac{4s}{\lambda}=1.4005$	63
5.16	Percentage averaged error in full field during iteration towards plane wave solution. Boundary elements N: 150, 384, 600 and $\frac{4s}{\lambda}=1.5278$	64
5.17	Percentage averaged error in full field during iteration towards plane wave solution. Boundary elements N: 150, 384, 600 and $\frac{4s}{\lambda}=1.6552$	64
5.18	Percentage averaged error in full field during iteration towards plane wave solution. Boundary elements N: 150, 384, 600 and $\frac{4s}{\lambda}=1.7825$	65
5.19	Percentage averaged error in full field during iteration towards plane wave solution. Boundary elements N: 150, 384, 600 and $\frac{4s}{\lambda}=1.9098$	65
5.20	Percentage averaged error in full field during iteration towards plane wave solution. Boundary elements N: 150, 384, 600 and $\frac{4s}{\lambda}=2.0371$	66
5.21	Percentage averaged error in full field during iteration towards plane wave solution. Boundary elements N: 150, 384, 600 and $\frac{4s}{\lambda}=2.1645$	66

Figure	Page
5.22 Percentage averaged error in full field during iteration towards plane wave solution. Boundary elements N: 150, 384, 600 and $\frac{4s}{\lambda}=2.2918$	67
5.23 Percentage averaged error in full field during iteration towards plane wave solution. Boundary elements N: 150, 384, 600 and $\frac{4s}{\lambda}=2.4192$	67
5.24 Percentage averaged error in full field during iteration towards plane wave solution. Boundary elements N: 150, 384, 600 and $\frac{4s}{\lambda}=2.5465$	68
5.25 The last averaged error (%) of iterative solution towards plane wave solution in full field at corner point on boundary elements 150, 384, 600 and $\frac{4s}{\lambda} \in (0.6,2.6)$	68
5.26 The last averaged error- ϵ_1 (%) of iterative solution towards plane wave solution in full field at corner point on boundary elements 150, 384, 600 and $\frac{4s}{\lambda} \in (0.6,2.6)$	69
5.27 The last averaged error- ϵ_2 (%) of iterative solution towards plane wave solution in full field at corner point on boundary elements 150, 384, 600 and $\frac{4s}{\lambda} \in (0.6,2.6)$	69
5.28 The last averaged error- ϵ_3 (%) of iterative solution towards plane wave solution in full field at corner point on boundary elements 150, 384, 600 and $\frac{4s}{\lambda} \in (0.6,2.6)$	70
5.29 The last averaged error- ϵ_4 (%) of iterative solution towards plane wave solution in full field at corner point on boundary elements 150, 384, 600 and $\frac{4s}{\lambda} \in (0.6,2.6)$	70
5.30 Radiated fields by Hertzian dipole source at near-field and far-field.	71
5.31 Error of outward field in iterative solution.	73
5.32 Error (%) in far field at $r = 0.6283$ m., $\theta=0^\circ$ generated by all components \mathbf{E} , \mathbf{H} of field when varying boundary elements: 150, 384, 600 and frequency $\in (40,170)$ MHz.	74
5.33 Error (%) in far field at $r = 62.83$ m., $\theta=0^\circ$ generated by all components \mathbf{E} , \mathbf{H} of field when varying boundary elements: 150, 384, 600 and frequency $\in (40,170)$ MHz.	74
5.34 Error (%) in far field at $r = 628.3$ m., $\theta=0^\circ$ generated by all components \mathbf{E} , \mathbf{H} of field when varying boundary elements: 150, 384, 600 and frequency $\in (40,170)$ MHz.	75
5.35 Percentage averaged error in full field during iteration towards the radiated solution of Hertzian dipole antenna. Boundary elements N: 150, 384, 600 and frequency $f=47.746$ MHz.	76
5.36 Percentage averaged error in full field during iteration towards the radiated solution of Hertzian dipole antenna. Boundary elements N: 150, 384, 600 and frequency $f=57.295$ MHz.	76
5.37 Percentage averaged error in full field during iteration towards the radiated solution of Hertzian dipole antenna. Boundary elements N: 150, 384, 600 and frequency $f=66.845$ MHz.	77
5.38 Percentage averaged error in full field during iteration towards the radiated solution of Hertzian dipole antenna. Boundary elements N: 150, 384, 600 and frequency $f=76.394$ MHz.	77
5.39 Percentage averaged error in full field during iteration towards the radiated solution of Hertzian dipole antenna. Boundary elements N: 150, 384, 600 and frequency $f=85.943$ MHz.	78

Figure	Page
5.40 Percentage averaged error in full field during iteration towards the radiated solution of Hertzian dipole antenna. Boundary elements N: 150, 384, 600 and frequency $f=95.492\text{MHz}$	78
5.41 Percentage averaged error in full field during iteration towards the radiated solution of Hertzian dipole antenna. Boundary elements N: 150, 384, 600 and frequency $f=105.042\text{MHz}$	79
5.42 Percentage averaged error in full field during iteration towards the radiated solution of Hertzian dipole antenna. Boundary elements N: 150, 384, 600 and frequency $f=114.592\text{MHz}$	79
5.43 Percentage averaged error in full field during iteration towards the radiated solution of Hertzian dipole antenna. Boundary elements N: 150, 384, 600 and frequency $f=124.140\text{MHz}$	80
5.44 Percentage averaged error in full field during iteration towards the radiated solution of Hertzian dipole antenna. Boundary elements N: 150, 384, 600 and frequency $f=133.690\text{MHz}$	80
5.45 Percentage averaged error in full field during iteration towards the radiated solution of Hertzian dipole antenna. Boundary elements N: 150, 384, 600 and frequency $f=143.240\text{MHz}$	81
5.46 Percentage averaged error in full field during iteration towards the radiated solution of Hertzian dipole antenna. Boundary elements N: 150, 384, 600 and frequency $f=152.789\text{MHz}$	81
5.47 Percentage averaged error in full field during iteration towards the radiated solution of Hertzian dipole antenna. Boundary elements N: 150, 384, 600 and frequency $f=162.338\text{MHz}$	82
5.48 The last averaged error (%) of iterative solution towards the radiated solution of Hertzian dipole antenna in full field at corner point on boundary elements 150, 384, 600 and frequency $\in (40,170)$ MHz.	82
5.49 The last averaged error- ϵ_1 (%) of iterative solution towards the radiated solution of Hertzian dipole antenna in full field at corner point on boundary elements 150, 384, 600 and frequency $\in (40,170)$ MHz.	83
5.50 The last averaged error- ϵ_2 (%) of iterative solution towards the radiated solution of Hertzian dipole antenna in full field at corner point on boundary elements 150, 384, 600 and frequency $\in (40,170)$ MHz.	83
5.51 The last averaged error- ϵ_3 (%) of iterative solution towards the radiated solution of Hertzian dipole antenna in full field at corner point on boundary elements 150, 384, 600 and frequency $\in (40,170)$ MHz.	84
5.52 The last averaged error- ϵ_4 (%) of iterative solution towards the radiated solution of Hertzian dipole antenna in full field at corner point on boundary elements 150, 384, 600 and frequency $\in (40,170)$ MHz.	84
5.53 Error (%) in far field at $r = 0.6283$ m., $\theta=0^\circ$ generated by components \mathbf{E}_t , \mathbf{H}_n of field when varying boundary elements: 150, 384, 600 and frequency $\in (40,170)$ MHz.	85

Figure	Page
5.54 Error (%) in far field at $r = 62.83$ m., $\theta=0^\circ$ generated by components $\mathbf{E}_t, \mathbf{H}_n$ of field when varying boundary elements: 150, 384, 600 and frequency $\in (40,170)$ MHz.	86
5.55 Error (%) in far field at $r = 628.3$ m., $\theta=0^\circ$ generated by components $\mathbf{E}_t, \mathbf{H}_n$ of field when varying boundary elements: 150, 384, 600 and frequency $\in (40,170)$ MHz.	86
5.56 Error of reflected field in iterative solution.	88
5.57 Percentage averaged error- ϵ_2 in full field during iteration towards solution of reflected field on PEC. Boundary elements N: 150, 384, 600 and $\frac{4s}{\lambda}=0.6366$. . .	89
5.58 Percentage averaged error- ϵ_2 in full field during iteration towards solution of reflected field on PEC. Boundary elements N: 150, 384, 600 and $\frac{4s}{\lambda}=0.7640$. . .	89
5.59 Percentage averaged error- ϵ_2 in full field during iteration towards solution of reflected field on PEC. Boundary elements N: 150, 384, 600 and $\frac{4s}{\lambda}=0.8913$. . .	90
5.60 Percentage averaged error- ϵ_2 in full field during iteration towards solution of reflected field on PEC. Boundary elements N: 150, 384, 600 and $\frac{4s}{\lambda}=1.0185$. . .	90
5.61 Percentage averaged error- ϵ_2 in full field during iteration towards solution of reflected field on PEC. Boundary elements N: 150, 384, 600 and $\frac{4s}{\lambda}=1.1460$. . .	91
5.62 Percentage averaged error- ϵ_2 in full field during iteration towards solution of reflected field on PEC. Boundary elements N: 150, 384, 600 and $\frac{4s}{\lambda}=1.2732$. . .	91
5.63 Percentage averaged error- ϵ_2 in full field during iteration towards solution of reflected field on PEC. Boundary elements N: 150, 384, 600 and $\frac{4s}{\lambda}=1.4005$. . .	92
5.64 Percentage averaged error- ϵ_2 in full field during iteration towards solution of reflected field on PEC. Boundary elements N: 150, 384, 600 and $\frac{4s}{\lambda}=1.5278$. . .	92
5.65 Percentage averaged error- ϵ_2 in full field during iteration towards solution of reflected field on PEC. Boundary elements N: 150, 384, 600 and $\frac{4s}{\lambda}=1.6552$. . .	93
5.66 Percentage averaged error- ϵ_2 in full field during iteration towards solution of reflected field on PEC. Boundary elements N: 150, 384, 600 and $\frac{4s}{\lambda}=1.7825$. . .	93
5.67 Percentage averaged error- ϵ_2 in full field during iteration towards solution of reflected field on PEC. Boundary elements N: 150, 384, 600 and $\frac{4s}{\lambda}=1.9098$. . .	94
5.68 Percentage averaged error- ϵ_2 in full field during iteration towards solution of reflected field on PEC. Boundary elements N: 150, 384, 600 and $\frac{4s}{\lambda}=2.0371$. . .	94
5.69 Percentage averaged error- ϵ_2 in full field during iteration towards solution of reflected field on PEC. Boundary elements N: 150, 384, 600 and $\frac{4s}{\lambda}=2.1645$. . .	95
5.70 Percentage averaged error- ϵ_2 in full field during iteration towards solution of reflected field on PEC. Boundary elements N: 150, 384, 600 and $\frac{4s}{\lambda}=2.2918$. . .	95
5.71 The last averaged error- ϵ_2 (%) of iterative solution of perfect reflection in full field at corner point on boundary elements 150, 384, 600 and $\frac{4s}{\lambda} \in (0.6,2.3)$. . .	96
5.72 The last averaged error- ϵ_3 (%) of iterative solution of perfect reflection in full field at corner point on boundary elements 150, 384, 600 and $\frac{4s}{\lambda} \in (0.6,2.3)$. . .	96
5.73 Broadside of backscattering RCS at $r=1$ km. computed using EHFD solution and iterative method using 150-element compared with measured data.	98

Figure	Page
5.74 Broadside of backscattering RCS at r=1km. RCS computed using EHFD solution and iterative method using 384-element compared with measured data.	98
5.75 Broadside of backscattering RCS at r=1km. RCS computed using EHFD solution and iterative method using 600-element compared with measured data.	99
5.76 E-plane and H-plane Bi-static RCS at r=1km. in (a) and (b), respectively. RCS computed using iterative method when varying boundary elements: 150, 384, 600 and $\frac{4s}{\lambda}=0.6366$	99
5.77 E-plane and H-plane Bi-static RCS at r=1km. in (a) and (b), respectively. RCS computed using iterative method when varying boundary elements: 150, 384, 600 and $\frac{4s}{\lambda}=0.7640$	100
5.78 E-plane and H-plane Bi-static RCS at r=1km. in (a) and (b), respectively. RCS computed using iterative method when varying boundary elements: 150, 384, 600 and $\frac{4s}{\lambda}=0.8913$	100
5.79 E-plane and H-plane Bi-static RCS at r=1km. in (a) and (b), respectively. RCS computed using iterative method when varying boundary elements: 150, 384, 600 and $\frac{4s}{\lambda}=1.0185$	101
5.80 E-plane and H-plane Bi-static RCS at r=1km. in (a) and (b), respectively. RCS computed using iterative method when varying boundary elements: 150, 384, 600 and $\frac{4s}{\lambda}=1.1460$	101
5.81 E-plane and H-plane Bi-static RCS at r=1km. in (a) and (b), respectively. RCS computed using iterative method when varying boundary elements: 150, 384, 600 and $\frac{4s}{\lambda}=1.2732$	102
5.82 E-plane and H-plane Bi-static RCS at r=1km. in (a) and (b), respectively. RCS computed using iterative method when varying boundary elements: 150, 384, 600 and $\frac{4s}{\lambda}=1.4005$	102
5.83 E-plane and H-plane Bi-static RCS at r=1km. in (a) and (b), respectively. RCS computed using iterative method when varying boundary elements: 150, 384, 600 and $\frac{4s}{\lambda}=1.5278$	103
5.84 E-plane and H-plane Bi-static RCS at r=1km. in (a) and (b), respectively. RCS computed using iterative method when varying boundary elements: 150, 384, 600 and $\frac{4s}{\lambda}=1.6552$	103
5.85 E-plane and H-plane Bi-static RCS at r=1km. in (a) and (b), respectively. RCS computed using iterative method when varying boundary elements: 150, 384, 600 and $\frac{4s}{\lambda}=1.7825$	104
5.86 E-plane and H-plane Bi-static RCS at r=1km. in (a) and (b), respectively. RCS computed using iterative method when varying boundary elements: 150, 384, 600 and $\frac{4s}{\lambda}=1.9098$	104
5.87 E-plane and H-plane Bi-static RCS at r=1km. in (a) and (b), respectively. RCS computed using iterative method when varying boundary elements: 150, 384, 600 and $\frac{4s}{\lambda}=2.0371$	105

Figure	Page
5.88 E-plane and H-plane Bi-static RCS at $r=1\text{km}$. in (a) and (b), respectively. RCS computed using iterative method when varying boundary elements: 150, 384, 600 and $\frac{4s}{\lambda}=2.1645$	105
5.89 E-plane and H-plane Bi-static RCS at $r=1\text{km}$. in (a) and (b), respectively. RCS computed using iterative method when varying boundary elements: 150, 384, 600 and $\frac{4s}{\lambda}=2.2918$	106
5.90 Percentage averaged error- ϵ_2 in full field during iteration towards solution of reflected field on PEC. Boundary elements N: 600 and $\frac{4s}{\lambda}=3.0$	106
5.91 E-plane and H-plane Bi-static RCS at $r=1\text{Km}$. in (a) and (b), respectively. RCS computed using iterative method when using boundary elements: 600 and $\frac{4s}{\lambda}=3.0$	107
5.92 Reflection coefficient at backscattering when using boundary elements: 150, 384 and 600 elements.	108

CHAPTER I

INTRODUCTION

1.1 Background and Significance of the Research Problems

The application of electromagnetic radiation is seen in various disciplines such as antennas, scattering, radar, radio and astronomy, quantum electronics and solid-state circuits and devices, electro-mechanical energy conversion, and even computer. Although the behaviors of electromagnetic fields in the practical system are very complicated to recognize properly, physicists and engineers are making research and developing various methods to solve these fields such as experimental method, analytical method and numerical method. The experimental methods are expensive, time consuming, sometimes hazardous, and usually do not allow much flexibility in parameter variation. The analytical methods can investigate the solutions of partial differential equations (PDE) by using analytical evaluation such as Separation of Variables, Series Expansion, Conformal Mapping, Integral Solution and Perturbation Method. These techniques work out the uncomplicated problems; however, they need mathematical knowledge at high level for realistic problems. Therefore, engineers resort to solve the complex PDE using numerical methods.

Maxwell's equations that are a set of four first order partial differential equations can represent the relationship between electric and magnetic fields that occurs when two fields are time-varying. The numerical methods can approximate effectively the solutions of Maxwell's equations into both differential form and integral form. The differential equation methods are used to solve Maxwell's equations in differential form such as Finite Difference Method (FDM), Finite Element Method (FEM), Finite-Difference Time-Domain (FD-TD), Transmission-Line Method (TLM), etc. The integral equation methods are used to solve Maxwell's equations in integral form such as Moment Method (MoM) and Boundary Element Method (BEM). The integral equation methods have emerged as powerful alternative to differential equation methods particularly in case where the domain extends to infinity. Formulation of these methods when analyzing thought out homogeneous medium requires discretization of only the boundary (surface or curve) and not interior of the region under consideration. Accordingly, computer codes of the integral equation methods are easier to employ with existing solid modelers and mesh generators.

There are two main integral equations based on vector calculus such as Electric Field Integral Equation (EFIE) and Magnetic Field Integral Equations (MFIE). They are proved from Helmholtz equations. The kernels of these integral equations are not only constructed from the fundamental solution of Helmholtz operator, Green's function, but they also contain the differentiation of those fundamental solutions. Numerical integration of the kernel is difficult because of that differential component of the fundamental solution, and often produces (at least at some frequencies) a very badly conditioned system of equations. These effects give the spurious solutions, when the EFIE or MFIE are operated with boundary conditions in order to formulate the system of linear equations. Both EFIE and MFIE are involving with current densities along the boundary. After the current densities have been evaluated by inversion, they are used to be the equivalent source to generate the radiated field around the

boundary.

This thesis presents a new integral equation based on Clifford algebra that can construct the solutions of the original four Maxwell's equations without modification. In Clifford framework, Maxwell's equations are embedded into a single differential equation called k -Dirac equation or Maxwell-Dirac equation. The integral equations are derived from the boundary theorem and the fundamental solutions of k -Dirac equations. Their kernels contain only the singular functions without the differentiation of them. The integral equations are applied to formulate some integral operators that they can be used to describe the radiation of the fields from boundary. The integral operators are the key tools for solving the linear system of the boundary value problem by using iterative method.

1.2 Literature Review

In electromagnetics, the relationships between time varying electric field and magnetic field quantities can describe into mathematical expressions as called Maxwell's equations. Maxwell's equations in differential form in [1–3] are derived to solve the bounded problems in order to explain and analyze the fields inside waveguide by using numerical methods such as FEM, FETD in [4–7]. Moreover, Maxwell's equations have widely accepted, since these powerful equations give details of behaviors of the radiated fields by the antenna and clarify effects of the scattered fields of any conducting objects. Consequently, they have been used to model and to design functional antennas for important practical problems. Generally engineers who apply for the antennas propagation problems in exterior regions must simplify Maxwell's equations into various modified versions of integral form [8–10] such as integro-differential equation, Fredholm integral equation and the others. The examples of unbounded problems are to analyze the far-field radiation and the scattered fields in [11–15].

Earlier numerical integral technique is a wire-grid model by J. H. Richmond in [16] that reforms simple relationship between the electric field and current distribution for studying the scattered electric field by conducting bodies of arbitrary shapes. He approximates the unidentified current distribution with any constant functions and work out the electric field with solution of inhomogeneous vector potential wave equation by integrating over surface of the wire. After that, numerical results are obtained by formulating a system of linear equation with the point-matching techniques.

The literature of [4] is discussed that the EFIE has advantages of being applicable to both open and small closed bodies such as a thin-wire antenna, whereas the MFIE applied by only to closed surface, especially those having large smooth surfaces. Both formulations of integral equations are used with MoM in [17, 18] to develop a simple and efficient numerical procedure for treating problems of scattering from arbitrarily shaped objects. The Numerical Electromagnetic Code (NEC) [19] is a computer program for analyzing the electromagnetic response of arbitrary structure consisting of wires and surfaces in free space or over ground plane. The NEC program use both EFIE and MFIE to model the response of general structures, since each has advantages particular structure types. The applications of EFIE are found in [20–32]. The applications of MFIE, which fails for the thin wire case, is more attractive for voluminous structures, especially those having large smooth surfaces. The examples of MFIE are found in [33–40].

C. M. Butler and D. R. Wilton in [20] investigate the efficiency of various numerical schemes based on EFIE when solving the scattered fields by thin-wire structures. The schemes are constructed using different basis functions for approximating the current dis-

tribution, for example, piecewise sinusoidal, piecewise linear and trigonometric. These unknown current distributions are formulated in Hallen's equation and Pocklington's equation for formulating linear equation system. The results are delineated that the solution methods applied to Hallen's equation govern quantities which are less sensitive to discontinuities in the current approximation and its derivative than Pocklington's equation. Then, for the convergence rate of solutions to Pocklington's equation, it must eliminate the effects of these discontinuities by rendering the equation insensitive to them. Moreover, the kernel functions of EFIE that contain singular functions must be reduced particularly to more convenient implementation as [21] by C. M. Butler. Many researches attempt to evade the use of the exact kernel function of EFIE; thus, the other choices are available that they avoid the singularity of those kernel. In [22], they discuss about the property of both Hallen's equation and Pocklington's equation when using the reduced and exact kernel functions, and they propose a new reduced derivation of integral equation. With these integral equations the unknown current distribution are determined their behavior directly in the time-domain and indirectly in the frequency-domain; consequently, their results agree with the common opinion that numerical space and time differentiation should be avoided as much as possible.

However, the reduced kernel integrals cause the erroneous numerical solutions, the exact kernel integrals are employed again. In order to reduce the complicated evaluation of the exact kernels of integro-differential equations, the researchers attempt to describe these exact kernels into various forms for particular problems. For example, when integrating the exact kernel over very thin wire the scalar potential function is approximated into infinite series by [23] and over arbitrary closed surfaces the vector potential function is approximated into various infinite series by [24, 25]. Potential integrals involved in EFIE occur often singular, and therefore necessitate special numerical considerations of their evaluation. The [26] does not only realize the singularity of Green's functions on a plane triangle but their gradients also. Then, their singularity causes the complexity of the numerical integration and is eliminated with the singularity extraction (subtraction) techniques by [27]. These various techniques that are offered for expressing numerically the exact kernel integral can eliminate the need of singularity extraction when analyzing the thin wire. In [28], D. R. Wilton and N. J. Champagne propose transforming the discontinuous approximated current distribution into smooth integrand with quadrature schemes. It is necessary that the assumptions of the wire antenna calculate using line integrals and construct from two kinds of elements of lines; observation point is contained inside and outside these elements. When an observation point holds on and off the elements of the line, line integrals employ the Ma, Rohkin, Wandzura (MRW) quadrature scheme and Gauss-Legendre scheme, respectively. Unfortunately, it is only appropriate for very extreme thin wire and more difficult to be relevant real scattering objects. Moreover, the drawbacks of the singularity extraction (subtraction) techniques are discussed into the literature review of [29], and then this research improves the numerical singularity cancellation method techniques for evaluating the singular and near-singular potential integration. This new method is demonstrated to solve scattering fields from thin wires in two dimensions [30].

On the other hand, Rao, Wilton and Glisson in [31] model the surfaces of scatterer with planar triangular patches in order to get effective formulation of integral equation is applicable to both open and close surfaces. Thus, the set of individual sub-domain basis functions that can be defined on pairs of adjacent triangular patches and yield a current representation free of line or point charges at sub-domain boundaries. After that, their basis functions have been of interest by many researchers as known as RWG basis functions. The EFIE associated with RWG basis function can solve efficiently the scattering problem

for very thin wire; and then, the [32] proposes this method to apply for large problem on three dimensional geometry. However, the strength of the singularity in the integrand being strongly singular has been not eliminated. The strong singular of kernel integral has been the limitation of the numerical integration.

N. C. Albersen, J. E. Hansen and N. E. Jensen in [33] present a theoretical formulation for electromagnetic problems in which one or more wire antenna are connected to conducting body of arbitrary shape. The MFIE are combined with EFIE in order to obtain good advantages of both integral equations. Although, this is primary implementation of integral equation for analyzing scattering field on conducting bodies, it confirms that the integral equation method is more efficient tool. However, the current distribution formulated in MFIE and EFIE has been critical to approximate the derivative of singular kernel function. In 2004, O. Ergul and L. Gurel in [34] verify that MFIE cannot give more accurate results as compared to EFIE for the solution electromagnetic scattering problems with RWG basis function of current distribution [35]; moreover, it is more evident when the results in [36] are discussed. They also investigate the inaccuracy of MFIE discretized with four different basis functions of current distributions, such as RWG, TL, $n \times$ RWG and $n \times$ TL defined on the planar triangles. Their efficiency is measured by induced current on scatterer and radar cross section. The scatterer is a cube with edge and is triangulated with mesh size. The results notify that TL and $n \times$ TL are more accurate than RWG and $n \times$ RWG. Although the use of TL and $n \times$ TL functions can improve the efficiency in [37], computational cost has been significantly increased. At the same time, [38] presented by C. P. Davis and K. F. Warnick is another research group attempting to develop the formulation of MFIE with a low-order discretization in two dimensions. In their literature it is discussed that MFIE kernel is more continuous than EFIE kernel, but MFIE scattering solution is one-order less accuracy than EFIE solution for polarizations. They conclude that the identity operator associated with MFIE causes inaccuracy in MoM solutions of MFIE. This identity operator is not only very specific for implementing MFIE on MoM, but it also has not developed to three dimensional scatterer. The various basis functions of MFIE are improved for efficient numerical solutions; moreover, the singularity of the kernel integral is analyzed. In [39] O. Ergul and L. Gurel show that the solution of MFIE by MoM on planar triangulation have the singularity both in the inner integrals on the basis function and also in the outer integrals on the testing functions. Therefore, they propose the singularity extraction method for computation of the outer integrals, similar to the way inner integral singularities are handled. Otherwise, in [40] they redevelop both linear normal and liner tangential basis functions to describe the basis and testing functions of MFIE.

Recently, A.F. Peterson and M.M. Bibby [41] discuss about the implementation of EFIE and MFIE for the detail procedure of MoM. In their literature, researchers have been improving the evaluation of the MoM matrix entries by using higher-order polynomial basis functions, since it is possible that these individual basis functions assist in such validation and verification in several respects. They investigate the error by comparing the results of two uncomplicated cases with exact solutions in two dimensions. The first case is to calculate the current density and scattering cross section of circular cylinder of one wavelength. Another case is to measure the residue error in the continuous equation of a TM-illuminated flat strip, which can be estimated by over-determined matrix. In two cases of their experiences with higher order discretizations of EFIE and MFIE suggest that the error in the current density, scattering cross section and residuals follow predictable trends indicative of higher order solutions. Moreover, these results are interesting in their own right, and can be used to confirm the correctness of computer implementation.

A variety of formulations to remedy the spurious solution of the scattered fields from the perfect conductor have been presented: the combined field integral equation (CFIE) formulation, the combined source integral equation formulation (CSIE), the augmented boundary condition method, the augmented integral equation method, and the minimum norm solution. Firstly, the combination of EFIE and MFIE as called CFIE are utilized for modeling the scattered fields from the mixture of the thin wire antennas and conducting bodies by [33]. Then the CFIE are used for improving the conditioning of MoM matrix, since they can help avoiding the spurious solutions of the EFIE and MFIE. Therefore, the CFIE are modified into various several formulations such as [42–44]. In 1996, C.C. Lu, W.C. Chew and J.M. Song as [42] implement the numerical algorithm with utilizing the flat-triangular patch and RWG basis functions, after EFIE, MFIE and CFIE are formulated by using MoM. Their results show that the CFIE in iterative solver provides more accurate radar cross section and faster convergence. Otherwise, [43] proposes the basis functions for MoM solution of CFIE for three dimensional problems. These basis functions are higher order functions that the Lagrange interpolation points are chosen to be the same as the nodes of the well-developed Gaussian quadratures. Therefore, the evaluations of the integrals in the MoM is greatly simplified. However, this formulation never considers the particular behavior of the electric and magnetic fields. The different CFIE proposed in [44] uses the different basis functions between EFIE and MFIE. Consequently, there are at least two different forms of the CFIE. One version, known as the PMCHW formulations involves two equations, one of which is obtained by combining an electric field equation for the interior region with an electric field equation for the exterior region of the problem domain. A second equation is obtained when a magnetic field equation for the interior region is combined with a magnetic field equation for the exterior region. A second type of the CFIE is obtained when the electric and magnetic equations for the interior region are combined and the electric and magnetic equations for the exterior region are combined [45]. This latter form of the CFIE is of interest because the exterior equations alone can be combined and used a radiation boundary condition to truncate the computational domain of differential equation formulations [46]. However, the solutions of this form are failed at interior resonance [47] when are implemented for considered electrically large problems.

It is the fact that any tools in electrical engineering, which are employed for computing electromagnetic fields, are only in the vector framework. Although, Maxwell's four equations represent on vector calculus, their solutions cannot be solve directly in vector framework. Because a single vector cannot contain both electric and magnetic fields at the same time. However, other framework in NEC is differential forms (DFs) which is applied from exterior algebra in order to express various laws of physics. DFs form on various degrees and identify them with field intensity, flux density, current density, charge density and scalar potential. A number in DFs can represent both the electric field and the magnetic flux into the different groups. Otherwise, the multiplication of two groups needs to use the basic laws of exterior algebra. In paper [2], this article by M.J. Bluck, A. Hatzipetros and S.P. Walker introduces the relevance of the exterior calculus to EMs and proposes the application of DFs. And it describes the representation of electromagnetic fields and definition of relationship between the curl, gradient and divergence operators of vector calculus in terms of DFs. Moreover, it is applied to solve the reduced versions of Maxwell's equations by using numerical method, such as FDM and FEM by L.E. Garcia-Castillo, M. Salazar-Palma, T.K. Sarkar and R.S. Adve [3], in order to decrease the system matrix of problem. K.F. Warnick, R.H. Selfridge and D.V. Arnold [48], this is another paper to define DFs in order to clarify the relationship between field intensity and flux density by using graphical

representations in order to teach engineering EMs. Otherwise, it uses these DFs to express Maxwell's equations in integral forms. Recently, differential forms are developed for computational works in EMs. It uses for Boundary Integral Equations (BIE) which consider by discretization. S. Kurz, *et al.* [49] show how the integral equations of EMs can be expressed in language of DFs. For frequency domain EM problems, G.A. Deschamps [50] propose the appropriate integral equations for Helmholtz equation but not for original Maxwell's equations. Then, Green's functions are used for the fundamental solution of Helmholtz operator. Consequently, this method is also to solve Maxwell's equations with integral form which are applied by using Green theorem based on DFs. All literature reviews about DFs, they can not only represent Maxwell's equations, but also they are encode both electric and magnetic fields. Unfortunately, they have still not been employed for evaluating both fields in electromagnetics. Moreover, it is not possible to apply integral equation for scattering problems on DFs.

A great deal of freedom exists in exactly how to formulate integral equation techniques firstly at the level of the equations themselves and secondly at the level of the numerical solution. Formulation of integral equations can be carried either by using potentials and differentiations or by avoiding them altogether. One approach of the latter kind uses a multi-dimensional version of the Cauchy integral [51] to invert differential equations in the form of fields directly into the corresponding boundary integral equations [52]. This multi-dimensional Cauchy integral was not used when the approaches based on Green's functions were first developed for the simple reason that, at that time (cf. [53]), it had yet to be discovered. Only recently [51] has this alternative approach appeared in the mathematical literature.

From a mathematical viewpoint, the method is based on extending the properties of analytic functions of complex variables in the plane, to multiple dimensions [54] as what are called *monogenic* functions of Clifford variables in N -dimensional space, where $N \geq 2$. (Of course, in electromagnetism only $N = 4$ dimensions are required, three for space and one for time or frequency). Such a generalization of complex variables into multiple dimensions has long been sought, engineers well recognizing their invaluable properties for solving field problems which conform to a two-dimensional planar geometry. That the generalization has proved somewhat elusive is in part because it is not to be found amongst the familiar mathematical tools of real or complex variables, algebra and arithmetic. Rather, the generalization is to be found amongst the (less familiar) tools of *Clifford* variables, algebra and arithmetic. These tools were actually developed for the specific purpose of making Maxwell's equations easier to solve a long time ago by Clifford [55], a student of Maxwell's [56], but were for some reason or the other, overlooked. However, a growing interest in applying Clifford's algebra to problems in mathematical physics including electromagnetism, gravitation and multi-particle quantum mechanics [57] has appeared within the last few years.

The approach involving the Cauchy integral and Clifford algebra bears a formal similarity to integral methods involving Green's functions. However, they are by no means directly equivalent. The kernel for the Cauchy integral solves a first order differential equation whereas the Green's functions solve a second order differential equation. The singularities that appear in each differ, for example $(-1)e^{-ikr}/4\pi r$ for the Green's function in the frequency domain and $\{-(\vec{r}/r^2) + ik(i\epsilon_0 - \vec{r}/r)\}e^{-ikr}/4\pi r$ for the Cauchy kernel, where k , is wavenumber, \vec{r} is displacement vector and r is magnitude of \vec{r} .

The Cauchy integral is known to apply to Lipschitz surfaces [52, 58], i.e. those with sharp corners and edges, such as cubes and wedges. It correctly accommodates fields which approach infinity at such points (cf [59, 60]) provided that the basis functions for the fields

on the boundary are chosen correctly. The functional analysis has been carried in two cases: one for fields on the boundary in the L^2 (square integrable) functional space [52, 58], and one for functions in a more complicated functional space denoted in [61] as \mathcal{X}^2 . The second choice ensures that the field *off* the boundary is locally square integrable (i.e. finite energy, L^2).

This research proposes a new tool used for solving scattering fields of arbitrary objects in free space. It is anticipated that original Maxwell's equations are solved by implementing the integral equation on Clifford algebra. The innovative form of integral equation not only reproduces the full electromagnetic field but does so (provided a little bit of care is taken) without introducing any significant problem when numerically integrating over the singularity in the kernel. This produces a (numerically) more stable linear system. Since the kernel function is the fundamental solution of first order of partial differential equation (k-Dirac operator) as a point source of full fields already, it is not necessary to do any derivative operation. Moreover, the approximated current distributions are without complicated functions whenever they are computed by numerical methods.

1.3 Objectives of the Research

The objectives of the research are:

1. To propose new method for solving Maxwell's equations using Clifford algebra and multi-dimensional Cauchy integral equation.
2. To apply the Cauchy integral equation based on Clifford number for analyzing scattering and radiation of electromagnetic fields.

1.4 Scopes of the Dissertation

The research will recast Maxwell's equations (for regions of uniform, linear and isotropic material properties) from vector calculus into a single first-order partial differential equation on Clifford algebra in order to improve methodology and solve directly for full solution of Maxwell's equations by using a novel integral equation form. The scope of the research covered here is limited to the following five topics:

1. To study and analyze the method of solving Maxwell's equations by Clifford algebra and the multi-dimensional Cauchy integral.
2. To formulate and to show the utility of the integral operator over a closed surface in the near-field, in the role of determining the electromagnetic field in the far-field.
3. To analyze and formulate an implementation of the integral operator over closed surface in the near-field back onto itself, as a prerequisite for using it to solve a boundary value problem.
4. To construct linear equation system in case of scattering problems by using integral operator, and to solve this system by iterative methods.
5. To compare calculated results with measured results or analytical solutions.

1.5 Expected Results and Benefits

Solution of Maxwell's equations using Clifford algebra is expected to be easier than other methods when it is computed with integral equation method. The Clifford algebra itself is equivalent to the algebras of Dirac matrices and to Cartan's algebra, and has no special advantages over other algebras. However, the Clifford algebra carries with it the multi-dimensional Cauchy integral, other algebras themselves do not directly support. This integral is a direct inverse for Maxwell's homogeneous (source free) equations, similar in form to a Green's function integral, but operating directly on the field instead of the potential. Eliminating any need for using a potential makes the solution simpler. This in turn makes it easier to develop a reliable implementation.

From an educational viewpoint, use of Clifford algebra is much more straightforward than, for example, vector calculus. Rather than a pair of products (dot and cross) and a collection of identities which are difficult to remember, as for vector calculus, Clifford algebra has a single product which relies only on two simple rules which can be easily remembered. From the view of an instructor teaching, or a student learning, it is expected that Clifford algebra makes a more effective tool than does vector calculus.

The method of solution using Clifford algebra and the multi-dimensional Cauchy integral leads to a solution in the domain of Banach space. The form of the solution is different from most conventional techniques. It is the form of a linear system, but is not a form that can be solved directly by a single matrix inversion. It is therefore expected that any numerical implementation of the solution directly in Banach space will behave differently from a solution in the form of a matrix inversion. It may be possible to exploit the different behavior to obtain some numerical advantages, such as increased accuracy or faster solution.

1.6 Research Procedure

1. Study previous research papers relevant to the research works of the dissertation.
2. Study Clifford algebra
3. Study and represent Maxwell's equations on vector calculus into Maxwell-Dirac equation on Clifford form.
4. Study and apply the integral equations for solving Maxwell-Dirac equation.
5. Publish the conference paper in topic of solving Maxwell's equations by the Cauchy integral equation on Clifford algebra.
6. Implement and test the efficiency of the proposed integral operator with numerical method.
7. Publish the conference paper in topic of application of the proposed integral operators
8. Improve the accuracy of integral operator for solving boundary value problems.
9. Study and formulate the linear system equations in the perfect transmission problems with the proposed integral operator.

10. Study and formulate the linear system equations in the perfect reflection problems with the proposed integral operator.
11. Construct the indirect inversion of the linear equations by iterative techniques.
12. Publish the international journal
13. Check whether the conclusions meet all the objectives of the research work of the dissertation.
14. Write the dissertation.



ศูนย์วิทยทรัพยากร
จุฬาลงกรณ์มหาวิทยาลัย

CHAPTER II

INTEGRAL EQUATIONS FOR ELECTROMAGNETIC FIELDS

This chapter describes the mathematical material applied in this thesis. The main focus is on the behavior of electromagnetic fields as described through integral equations and operators. However, reference is first made to Maxwell's equations in the well known differential form based on vector notation in order to introduce another version of Maxwell's equations based on Clifford algebra. After that, their integral form based on Clifford algebra is described. Finally, integral operators are constructed for focusing on boundary value problems.

2.1 Clifford Number and Arithmetic

Four dimensional Clifford numbers take the general form:

$$\begin{aligned} \mathbf{a} = & a_0 + a_1\mathbf{e}_0 + a_2\mathbf{e}_1 + a_3\mathbf{e}_2 + a_4\mathbf{e}_3 \\ & + a_5\mathbf{e}_0\mathbf{e}_1 + a_6\mathbf{e}_0\mathbf{e}_2 + a_7\mathbf{e}_1\mathbf{e}_2 + a_8\mathbf{e}_0\mathbf{e}_3 + a_9\mathbf{e}_1\mathbf{e}_3 + a_{10}\mathbf{e}_2\mathbf{e}_3 \\ & + a_{11}\mathbf{e}_0\mathbf{e}_1\mathbf{e}_2 + a_{12}\mathbf{e}_0\mathbf{e}_1\mathbf{e}_3 + a_{13}\mathbf{e}_0\mathbf{e}_2\mathbf{e}_3 + a_{14}\mathbf{e}_1\mathbf{e}_2\mathbf{e}_3 \\ & + a_{15}\mathbf{e}_0\mathbf{e}_1\mathbf{e}_2\mathbf{e}_3. \end{aligned} \quad (2.1)$$

The a_i are complex-valued numeric coefficients. The \mathbf{e}_i are symbolic entities known as Clifford units. For the purposes of electromagnetism the Clifford units \mathbf{e}_i play the role of four Cartesian basis vectors, the (compound) units $\mathbf{e}_i\mathbf{e}_j$ play the role of bivectors (oriented areas), the $\mathbf{e}_i\mathbf{e}_j\mathbf{e}_k$ play the role of trivectors (oriented volumes), and $\mathbf{e}_0\mathbf{e}_1\mathbf{e}_2\mathbf{e}_3$ plays the role of the four dimensional pseudo-scalar.

The arithmetic operations required are those of addition and multiplication, as shown in detail in Appendix A. Addition $\mathbf{a} + \mathbf{b}$ is simply a matter of adding all the corresponding complex coefficients. Multiplication $\mathbf{a}\mathbf{b}$ entails use of the distributive law of multiplication over addition. The 256 terms produced are then further reduced by applying the two rules for multiplication of Clifford units:

$$\mathbf{e}_i\mathbf{e}_j = \begin{cases} -1 & \text{if } i = j \\ -\mathbf{e}_j\mathbf{e}_i & \text{if } i \neq j. \end{cases} \quad (2.2)$$

The first rule has the same characteristics as the rule $i^2 = -1$ for squaring the unit imaginary number i . The second rule has the same anti-commutative property as the rule for the vector cross product, $\vec{x} \times \vec{y} = -\vec{y} \times \vec{x}$, if \vec{x} and \vec{y} are vectors.

2.2 Clifford Fields

When using the vector form of electromagnetic fields in three spatial dimensions separate electric and magnetic fields vectors are written:

$$\begin{cases} \vec{E} &= E_x \vec{a}_x + E_y \vec{a}_y + E_z \vec{a}_z \\ \vec{H} &= H_x \vec{a}_x + H_y \vec{a}_y + H_z \vec{a}_z. \end{cases} \quad (2.3)$$

Here, each vector is transformed into three dimensional Clifford number, in which the Clifford units \mathbf{e}_1 , \mathbf{e}_2 and \mathbf{e}_3 play the role of Cartesian unit vectors \vec{a}_x , \vec{a}_y and \vec{a}_z , respectively,

$$\mathbf{e}_1 \Leftrightarrow \vec{a}_x, \mathbf{e}_2 \Leftrightarrow \vec{a}_y, \mathbf{e}_3 \Leftrightarrow \vec{a}_z. \quad (2.4)$$

Then, each of the magnitudes (or numeric parts) of both vectors (\vec{E}, \vec{H}) have a one to one correspondence to each of the magnitudes of both Clifford numbers (\mathbf{E}, \mathbf{H}) by following:

$$\left\{ \begin{array}{l} E_x \vec{a}_x \Leftrightarrow E_x \mathbf{e}_1 \\ E_y \vec{a}_y \Leftrightarrow E_y \mathbf{e}_2 \\ E_z \vec{a}_z \Leftrightarrow E_z \mathbf{e}_3 \end{array} \right\} \quad \text{and} \quad \left\{ \begin{array}{l} H_x \vec{a}_x \Leftrightarrow H_x \mathbf{e}_1 \\ H_y \vec{a}_y \Leftrightarrow H_y \mathbf{e}_2 \\ H_z \vec{a}_z \Leftrightarrow H_z \mathbf{e}_3 \end{array} \right\}. \quad (2.5)$$

Therefore, both electric and magnetic fields are described with the vector parts or grade 1 (Λ^1) of three dimensional Clifford numbers:

$$\begin{cases} \mathbf{E} &= E_x \mathbf{e}_1 + E_y \mathbf{e}_2 + E_z \mathbf{e}_3 \\ \mathbf{H} &= H_x \mathbf{e}_1 + H_y \mathbf{e}_2 + H_z \mathbf{e}_3. \end{cases} \quad (2.6)$$

Although, both electric and magnetic fields in (2.6) are expressed into three Cartesian space, they are still separate. However, the dimension of time can help to attach their relationship together. It is necessary to consider three dimensions of space and one dimension of time. Therefore, the two Clifford field (\mathbf{E}, \mathbf{H}) are encoded into a four dimensional Clifford number:

$$\mathbf{u} = \sqrt{\mu} \mathbf{H} \sigma + j \sqrt{\epsilon} \mathbf{E} \mathbf{e}_0, \quad (2.7)$$

where ϵ and μ are the electric permittivity (farad/metre) and the magnetic permeability (henry/metre), respectively. The Clifford unit \mathbf{e}_0 plays the role of time dimension, and σ is Clifford space units in Λ^3 that denoted $-\mathbf{e}_1 \mathbf{e}_2 \mathbf{e}_3$.

The Clifford number \mathbf{u} consists of sixteen components such as a scalar, four vectors, six bivectors, four tri-vector and a pseudo-scalar. In here, all components of bi-vector or Λ^2 are used to represent both the electric and magnetic fields. In the right hand side of (2.7), there are two groups such as groups of magnetic and electric fields. The first group is used to describe the bi-vector field which involves the spatial components of Λ^2 such as $\mathbf{e}_1 \mathbf{e}_2$, $\mathbf{e}_2 \mathbf{e}_3$, $\mathbf{e}_1 \mathbf{e}_3$, so that they keep the magnetic field. The second group is used to describe the bi-vector field which involves the temporal components of Λ^2 such as $\mathbf{e}_1 \mathbf{e}_0$, $\mathbf{e}_2 \mathbf{e}_0$, $\mathbf{e}_3 \mathbf{e}_0$, so that they keep the electric field:

$$\begin{aligned} \mathbf{u} &= \sqrt{\mu} \mathbf{H} \sigma + j \sqrt{\epsilon} \mathbf{E} \mathbf{e}_0 \\ &= \sqrt{\mu} (H_x \mathbf{e}_1 + H_y \mathbf{e}_2 + H_z \mathbf{e}_3) \sigma + j \sqrt{\epsilon} (E_x \mathbf{e}_1 + E_y \mathbf{e}_2 + E_z \mathbf{e}_3) \mathbf{e}_0 \\ &= \sqrt{\mu} (H_x \mathbf{e}_2 \mathbf{e}_3 - H_y \mathbf{e}_1 \mathbf{e}_3 + H_z \mathbf{e}_1 \mathbf{e}_2) + j \sqrt{\epsilon} (E_x \mathbf{e}_1 \mathbf{e}_0 + E_y \mathbf{e}_2 \mathbf{e}_0 + E_z \mathbf{e}_3 \mathbf{e}_0). \end{aligned} \quad (2.8)$$

2.3 Maxwell-Dirac Equation

For the purpose of simplification the discussion here is limited to electromagnetic fields which are time harmonic as $e^{j\omega t}$ with an angular frequency ω , in source free region of space where the material properties are uniform, linear and isotropic. In this case Maxwell's equations can be written in vector notation as

$$\begin{cases} \nabla \cdot \vec{E} = 0 \\ \nabla \times \vec{H} - j\omega\epsilon\vec{E} = 0 \\ \nabla \times \vec{E} + j\omega\mu\vec{H} = 0 \\ \nabla \cdot \vec{H} = 0 \end{cases}, \quad (2.9)$$

where $\vec{E} = E_x\vec{a}_x + E_y\vec{a}_y + E_z\vec{a}_z$ and $\vec{H} = H_x\vec{a}_x + H_y\vec{a}_y + H_z\vec{a}_z$ are the electric and magnetic fields respectively. The reduced (homogeneous or source free) version of Maxwell's equations (2.9) are derived into the appropriate form for retrieving their solution on vector framework and Clifford algebras.

2.3.1 Helmholtz Equation on Vector Form

To solve Maxwell's equations on vector framework, one may first convert the first-order differential equations involving two field quantities into second-order differential equations involving only one field quantity. Therefore, the differential equations for \vec{E} can be obtained by eliminating \vec{H} with the aid of the constitutive relations:

$$\nabla \times \left(\frac{1}{\mu} \nabla \times \vec{E} \right) - \omega^2 \epsilon \vec{E} = 0. \quad (2.10)$$

Similarly, one can eliminate \vec{E} to find the equation for \vec{H} as

$$\nabla \times \left(\frac{1}{\epsilon} \nabla \times \vec{H} \right) - \omega^2 \mu \vec{H} = 0. \quad (2.11)$$

Note that k is the wavenumber ($k = \omega\sqrt{\mu\epsilon}$). Taking the vector identity $\nabla \times \nabla \times \vec{E} = \nabla(\nabla \cdot \vec{E}) - \nabla^2 \vec{E}$ and $\nabla \cdot \vec{E} = 0$, and then (2.10) can be written:

$$\nabla^2 \vec{E} + k^2 \vec{E} = 0. \quad (2.12)$$

And taking the vector identity $\nabla \times \nabla \times \vec{H} = \nabla(\nabla \cdot \vec{H}) - \nabla^2 \vec{H}$ and $\nabla \cdot \vec{H} = 0$, and then (2.11) can be written:

$$\nabla^2 \vec{H} + k^2 \vec{H} = 0. \quad (2.13)$$

In (2.12) and (2.13), these equations are the partial differential equations of the electric and magnetic fields respectively, which are the derivation of the vector fields operated by Helmholtz operator. The Helmholtz operator denotes that

$$\Pi = \nabla^2 + k^2. \quad (2.14)$$

2.3.2 Maxwell-Dirac Equation on Clifford Form

On vector form, the differential operators $\nabla \cdot$ and $\nabla \times$ are used to describe the relationship of electromagnetic field in (2.9). They play the same role as the Dirac derivative or Clifford gradient \mathbf{D} (see Appendix A) based on Clifford algebra. The \mathbf{D} -operator can write the vector differential operators both divergence and curl; however, it can not explain the behavior of the electromagnetic field in time dimension. Therefore, another operator is considered:

$$\mathbf{D}_k = \mathbf{D} - k\mathbf{e}_0, \quad (2.15)$$

which is called 'k-Dirac operator' or 'Maxwell-Dirac operator' in [52, 62]. In frequency domain an additional dimension is used to accommodate the wavenumber k . The Clifford unit \mathbf{e}_0 plays the role of the time dimension. The Clifford units \mathbf{e}_1 , \mathbf{e}_2 and \mathbf{e}_3 similarly play the role of the Cartesian unit vectors, respectively. The properties of \mathbf{D}_k -operator are satisfying with the electromagnetic field in three spatial and one temporal dimensions. Therefore, the frequency domain version of homogeneous form of Maxwell's equations in (2.9) are written as the Maxwell-Dirac equation [52]:

$$\mathbf{D}_k \mathbf{u} = 0. \quad (2.16)$$

Here the electromagnetic field \mathbf{u} of (2.7) is a monogenic function since the source term on the right is zero. Such a field could represent the total field in a region without source, or some aspect of a field in a region containing sources (such as the field reflected from or transmitted through a boundary). The Maxwell-Dirac equation (2.16) can be expanded into components by using (2.15) and (2.7), along with the multiplication of Clifford units:

$$\begin{aligned} \mathbf{D}_k \mathbf{u} &= (\mathbf{D} - k\mathbf{e}_0) (\sqrt{\mu} \mathbf{H} \sigma + j\sqrt{\epsilon} \mathbf{E} \mathbf{e}_0) \\ &= \sqrt{\mu} (\mathbf{D} \mathbf{H}) \sigma + j\sqrt{\epsilon} (\mathbf{D} \mathbf{E}) \mathbf{e}_0 - k\sqrt{\mu} (\mathbf{e}_0 \mathbf{H} \sigma) - kj\sqrt{\epsilon} (\mathbf{e}_0 \mathbf{E} \mathbf{e}_0). \end{aligned} \quad (2.17)$$

Taking the gradient operator \mathbf{D} identity of a Clifford number \mathbf{v} when the vector \vec{v} is encoded into Λ^1 of \mathbf{v} :

$$\begin{aligned} \mathbf{D} \mathbf{v} &= -[\nabla \cdot \vec{v}]^0 - [\nabla \times \vec{v}]^1 \mathbf{e}_1 \mathbf{e}_2 \mathbf{e}_3 \\ &= -[\nabla \cdot \vec{v}]^0 + [\nabla \times \vec{v}]^1 \sigma, \end{aligned} \quad (2.18)$$

and then substituting into (2.17) yield:

$$\begin{aligned} \mathbf{D}_k \mathbf{u} &= \sqrt{\mu} \left(-[\nabla \cdot \vec{H}]^0 + [\nabla \times \vec{H}]^1 \sigma \right) \sigma + j\sqrt{\epsilon} \left(-[\nabla \cdot \vec{E}]^0 + [\nabla \times \vec{E}]^1 \sigma \right) \mathbf{e}_0 \\ &\quad - k\sqrt{\mu} (\mathbf{e}_0 \mathbf{H} \sigma) - kj\sqrt{\epsilon} (\mathbf{e}_0 \mathbf{E} \mathbf{e}_0) \\ &= -\sqrt{\mu} [\nabla \cdot \vec{H}]^0 \sigma + \sqrt{\mu} [\nabla \times \vec{H}]^1 - j\sqrt{\epsilon} [\nabla \cdot \vec{E}]^0 \mathbf{e}_0 + j\sqrt{\epsilon} [\nabla \times \vec{E}]^1 \sigma \mathbf{e}_0 \\ &\quad - k\sqrt{\mu} [\vec{H}]^1 \sigma \mathbf{e}_0 - kj\sqrt{\epsilon} [\vec{E}]^1 \\ &= 0. \end{aligned} \quad (2.19)$$

In order to show that Maxwell-Dirac equation can contain four Maxwell's equations in vector form (2.9), then (2.19) are rearranged into different grades:

$$\mathbf{D}_k \mathbf{u} = \left\{ \begin{array}{l} - j\sqrt{\epsilon} [\nabla \cdot \vec{E}]^0 \mathbf{e}_0 \quad \in T\Lambda^1 \\ + \sqrt{\mu} \left([\nabla \times \vec{H}]^1 - j\omega\epsilon [\vec{E}]^1 \right) \quad \in S\Lambda^1 \\ + j\sqrt{\epsilon} \left([\nabla \times \vec{E}]^1 + j\omega\mu [\vec{H}]^1 \right) \sigma \mathbf{e}_0 \in T\Lambda^3 \\ - \sqrt{\mu} [\nabla \cdot \vec{H}]^0 \sigma \quad \in S\Lambda^3 \end{array} \right\} = 0. \quad (2.20)$$

The resulting Clifford number occupies time-like components T (containing the time unit \mathbf{e}_0) and space-like components S (where the unit \mathbf{e}_0 is missing) of both Λ^1 and Λ^3 . These four components in the order listed represent respectively source free differential statements of Gauss's law, the Ampere-Maxwell law, Faraday's law, and a magnetic version of Gauss's law.

2.3.3 Fundamental Solution of Maxwell-Dirac Operator

Before the fundamental solution of k-Dirac operator as (2.15) is described in here, let us discuss the solution of Helmholtz operator (2.14) since the fundamental solution of k-Dirac operator can be derived from the fundamental solution of Helmholtz operator.

If B_k is the fundamental solution of Helmholtz operator (2.14), then it is satisfied in

$$\Pi B_k = (\nabla^2 + k^2) B_k(\mathbf{p}) = \delta(\mathbf{p} - \mathbf{0}), \quad (2.21)$$

where \mathbf{p} is Clifford number in Λ^1 which is defined the location of the point in Cartesian coordinates ($\mathbf{p} = x\mathbf{e}_1 + y\mathbf{e}_2 + z\mathbf{e}_3$), and $\delta(\mathbf{p} - \mathbf{0})$ is Dirac delta function for an impulse function acting at the origin defined as

$$\delta(\mathbf{p} - \mathbf{0}) = 0, \quad \text{if } \mathbf{p} \neq \mathbf{0}, \quad (2.22)$$

and that the integral over any finite region including $\mathbf{p} = \mathbf{0}$ is unity, i.e.

$$\int_{\Omega} \delta(\mathbf{p} - \mathbf{0}) d\sigma = 1, \quad (2.23)$$

where $d\sigma$ is the elemental measure of space within the region Ω .

Moreover, Helmholtz operator can derive from the term of k-Dirac operator. Simple algebra using the rules of multiplication of Clifford numbers shows that:

$$\begin{aligned} \mathbf{D}_k^2 &= (\mathbf{D} - k\mathbf{e}_0)^2 \\ &= \mathbf{D}^2 - \mathbf{D}(k\mathbf{e}_0) - (k\mathbf{e}_0)\mathbf{D} + k^2\mathbf{e}_0\mathbf{e}_0 \\ &= \mathbf{D}^2 - \mathbf{D}(k\mathbf{e}_0) + \mathbf{D}(k\mathbf{e}_0) - k^2 \\ &= \mathbf{D}^2 - k^2 \\ &= -\left(\frac{\partial^2}{\partial x^2} + \frac{\partial^2}{\partial y^2} + \frac{\partial^2}{\partial z^2}\right) - k^2 \\ &= -(\nabla^2 + k^2) \\ &= -\Pi. \end{aligned} \quad (2.24)$$

The resulting Clifford number is (minus) Helmholtz operator that is a scalar operator, and it is in Λ^0 of a Clifford number.

After the relationship of both Helmholtz operator and k -Dirac operator is shown, it is used to explain constructing the solution of k -Dirac operator from Helmholtz operator. When applying Helmholtz operator in (2.21) by using (2.24):

$$\begin{aligned}(\nabla^2 + k^2)B_k(\mathbf{p}) &= \delta(\mathbf{p} - \mathbf{0}) \\ (-\mathbf{D}_k^2)B_k(\mathbf{p}) &= \delta(\mathbf{p} - \mathbf{0}) \\ \mathbf{D}_k(-\mathbf{D}_k B_k)(\mathbf{p}) &= \delta(\mathbf{p} - \mathbf{0}) \\ \mathbf{D}_k \mathbf{F}_k(\mathbf{p}) &= \delta(\mathbf{p} - \mathbf{0}),\end{aligned}\tag{2.25}$$

where $\mathbf{F}_k(p)$ is the fundamental solution of k -Dirac operator. Therefore, the fundamental solution of k -Dirac operator can be calculated simply by applying (minus) the k -Dirac operator to the fundamental solution of the Helmholtz operator:

$$\mathbf{F}_k = -\mathbf{D}_k B_k(\mathbf{p}).\tag{2.26}$$

In here the electromagnetic fields in three dimensions are of interest, so that the fundamental solution of Helmholtz operator by [63] are

$$B_k = -\frac{1}{4\pi|\mathbf{p}|} e^{jk|\mathbf{p}|}.\tag{2.27}$$

Therefore the fundamental solution of k -Dirac operator in three dimensions is given by

$$\begin{aligned}\mathbf{F}_k(\mathbf{p}) &= -\mathbf{D}_k B_k(\mathbf{p}) \\ &= (\mathbf{D} - k\mathbf{e}_0) \left\{ \frac{1}{4\pi|\mathbf{p}|} e^{jk|\mathbf{p}|} \right\} \\ &= \frac{1}{4\pi} \left\{ \mathbf{D} \frac{1}{|\mathbf{p}|} e^{jk|\mathbf{p}|} - k\mathbf{e}_0 \frac{1}{|\mathbf{p}|} e^{jk|\mathbf{p}|} \right\} \\ &= \frac{e^{jk|\mathbf{p}|}}{4\pi|\mathbf{p}|} \left\{ -\frac{\mathbf{p}}{|\mathbf{p}|^2} + jk \left(j\mathbf{e}_0 + \frac{\mathbf{p}}{|\mathbf{p}|} \right) \right\} \\ &= \frac{e^{jkr}}{4\pi r} \left\{ \left(\frac{-1 + jkr}{r^2} \right) \mathbf{p} - k\mathbf{e}_0 \right\},\end{aligned}\tag{2.28}$$

where $r = |\mathbf{p}|$.

The fundamental solution of k -Dirac operator (\mathbf{F}_k) as (2.28) are represented by the four dimensional Clifford number. The part of the spatial component does not only involve with the magnitude of position vector, $|\mathbf{p}|$, but also it depends on the vector \mathbf{p} . Otherwise, the part of the temporal component still appears and relates with the wavenumber k . Although the two fundamental solutions which are considered are different (the fundamental solution of Helmholtz operator B_k as scalar but the fundamental solution k -Dirac \mathbf{F}_k as Clifford field), they have satisfied with the property of Dirac delta function as (2.23). In the following sections, they can be used for developing the boundary integral equation method.

2.4 Reproducing Formula

Construction of an integral equation for potential is based on the fundamental solution of the Helmholtz operator together with Green's function. For the field, it is the fundamental

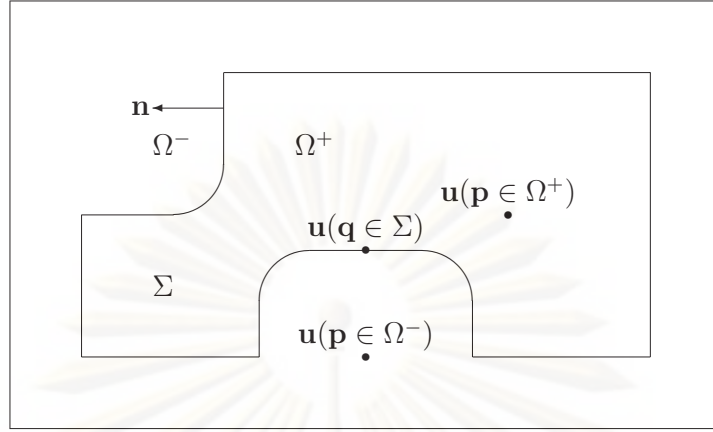


Figure 2.1: Calculation of field $\mathbf{u}(\mathbf{p})$ in region Ω^+ and Ω^- from its trace $\mathbf{u}(\mathbf{q})$ on boundary Σ .

solution of the k -Dirac operator and boundary theorem which are used instead [52]. Reproducing formula, reproduces the value of a function $\mathbf{u}(\mathbf{p})$ within a region Ω^+ (see Fig.2.1) from the trace of the function $\mathbf{u}(\mathbf{q})$ on the boundary of the region Σ . The boundary theorem can be written for two functions \mathbf{f} and \mathbf{g}

$$\int_{\Sigma} \mathbf{g}(\mathbf{q}) \mathbf{n}(\mathbf{q}) \mathbf{f}(\mathbf{q}) d\sigma(\mathbf{q}) = \int_{\Omega^+} \{(\mathbf{g}\mathbf{D})(\mathbf{q})\mathbf{f}(\mathbf{q}) + \mathbf{g}(\mathbf{q})\mathbf{D}\mathbf{f}(\mathbf{q})\} d\mathbf{q}, \quad (2.29)$$

where $\mathbf{D} = \mathbf{D}_{k=0} = \frac{\partial}{\partial x}\mathbf{e}_1 + \frac{\partial}{\partial y}\mathbf{e}_2 + \frac{\partial}{\partial z}\mathbf{e}_3$ is the Dirac operator [58], \mathbf{q} is a Clifford number representing a point on the boundary Σ or within its interior Ω^+ , \mathbf{n} is a Clifford number representing the outward unit normal, $d\sigma(\mathbf{q})$ is differential measure of area on the boundary.

In Fig. 2.1, the boundary theorem is more general than Green's theorem since the latter can be recovered from the former. This is achieved by first putting $\mathbf{g}(\mathbf{q}) = 0$, which gives both Stokes' theorem and the divergence theorem, and then by substituting into the divergence theorem as usual a vector field constructed from two scalar fields and their gradients. In the case of electromagnetic fields, it is more useful when the function $\mathbf{g}(\mathbf{q}) = 0$ of the differential operator \mathbf{D} is zero at everywhere except at $\mathbf{q} = \mathbf{0}$, and that the integral over any finite region including $\mathbf{q} = \mathbf{0}$ is unity as the delta function. In Axelsson's work [52], the fundamental solution of k -Dirac operator is derived for the full field associated with a point source of radiation. It satisfies the Clifford-valued relationship $\mathbf{D}_k \mathbf{F}_k(\mathbf{q}) = \delta(|\mathbf{q}|)$ where \mathbf{D}_k is the k -Dirac operator, and $\delta(|\mathbf{q}|)$ is a delta function at the origin $\mathbf{q} = \mathbf{0}$.

Now choose $\mathbf{g}(\mathbf{q}) = \mathbf{g}(\mathbf{q}; \mathbf{p}) = \mathbf{E}_k(\mathbf{q} - \mathbf{p}) = -\mathbf{F}_k(\mathbf{p} - \mathbf{q})$, then $\mathbf{E}_k(\mathbf{q} - \mathbf{p})$ is actually a function of two points \mathbf{p} and \mathbf{q} . Although they can both vary normally we think that one of them is fixed (at least temporarily) while we perform operations like differentiation or integration with respect to the other one. When the point \mathbf{p} can be placed anywhere: inside Ω^+ , or inside Ω^- , or on the boundary Σ , the effect of placing \mathbf{p} at different locations is to translate the function \mathbf{E}_k . The function \mathbf{E}_k is closely related to the fundamental solution of the k -Dirac operator, \mathbf{F}_k . The function \mathbf{f} is taken as the monogenic field \mathbf{u} as (2.7). We simply use the stated properties of \mathbf{E}_k and \mathbf{u} , giving:

$$\int_{\Sigma} \mathbf{E}_k(\mathbf{q} - \mathbf{p}) \mathbf{n}(\mathbf{q}) \mathbf{u}(\mathbf{q}) d\sigma(\mathbf{q}) \quad \left\{ \begin{array}{l} = \int_{\Omega^+} \mathbf{E}_k(\mathbf{D} - k\mathbf{e}_0)(\mathbf{q} - \mathbf{p}) \mathbf{u}(\mathbf{q}) d\mathbf{q} \\ = \int_{\Omega^+} \delta(\mathbf{q} - \mathbf{p}) \mathbf{u}(\mathbf{q}) d\mathbf{q}. \end{array} \right. \quad (2.30)$$

Therefore, the boundary value theorem then reduces to a different integral formulation:

$$\int_{\Sigma} \mathbf{E}_k(\mathbf{q} - \mathbf{p}) \mathbf{n}(\mathbf{q}) \mathbf{u}(\mathbf{q}) d\sigma(\mathbf{q}) = \begin{cases} \mathbf{u}(\mathbf{p}) & ; \mathbf{p} \in \Omega^+ \\ \frac{1}{2} \mathbf{u}(\mathbf{p}) & ; \mathbf{p} \in \Sigma \\ 0 & ; \mathbf{p} \in \Omega^- \end{cases}, \quad (2.31)$$

for the field \mathbf{u} at one point \mathbf{p} inside the region Ω^+ from its value \mathbf{u} at every point \mathbf{q} on the boundary Σ (see Fig. 2.1). This results is in the form of Cauchy integral with Clifford-valued functions in 4 dimensions rather than the complex-valued function in 2 dimensions as is usually the case. It is called *reproducing formula*. Note that, if the point \mathbf{q} is placed on a non-smooth part of the boundary the factor of $\frac{1}{2}$ must be changed to represent the local geometry of the boundary.

Eq. (2.31) is not the same style of integral as, for example, a Fredholm integral equation. There is no equation here to solve. Eq. (2.31) instead plays the role of a theorem that, for a function \mathbf{u} which is *monogenic* (i.e., a solution to (2.16)) within some region Υ of space/time spanned by Λ^1 of an n -dimensional Clifford algebra, states the following: “given any Cauchy surface Σ within Υ the trace of \mathbf{u} on Σ can reproduce \mathbf{u} in the sub-domain Ω^+ of Υ enclosed by Σ ”. In terms of applications in electromagnetics this theorem may be restated as: “given the electromagnetic field on any closed surface in a source free region it is possible to reconstruct the field inside”.

2.5 Cauchy Extension Operator

Although the reproducing formula are used to describe the relationship of the trace of the field between on the boundary and inside the boundary, they cannot be used for calculating the field outside the boundary. In the problem of electromagnetics, it is necessary to analyze the behavior of field both inside and outside of the boundary. Therefore, in this section the reproducing formula are applied to the different integral operator for considering the fields on both sides of the boundary.

In Fig. 2.2, the closed surface Σ is the boundary which split separately for the interior region Ω^+ and the exterior region Ω^- . The position of a point on Σ is denoted by \mathbf{q} and called *boundary point*. The position of a point in Ω^+ or Ω^- is denoted by \mathbf{p} and called an *internal point* or *external point*, respectively. The normal vector \mathbf{n}^+ , which identifies the closed surface covering over the interior region, gives direction from Ω^+ to Ω^- . The normal vector \mathbf{n}^- , which identifies the closed surface covering over the exterior region, gives direction from Ω^- to Ω^+ . Let us define three kinds of the fields on Σ . The first field that is propagating away from Σ into Ω^+ is called *the inward field* on Σ denoted as $\mathbf{u}^+(\mathbf{q})$. The second field that is propagating away from Σ into Ω^- is called *the outward field* on Σ denoted as $\mathbf{u}^-(\mathbf{q})$. The third field that combines $\mathbf{u}^+(\mathbf{q})$ and $\mathbf{u}^-(\mathbf{q})$ is called *the total field on Σ* denoted as $\mathbf{u}(\mathbf{q})$. For understanding easier, let us express the relationship of the reproducing formula and the field on both sides of Σ by separating into three cases, such as the inward propagation, outward propagation and total field of inward and outward propagations on Σ .

- The first case: Inward propagation

The surface equivalence theorem is referred in order to discuss the field propagating from Σ to Ω^+ . In Fig. 2.2(a), it assumes that the surface field produces the inward field from Σ into Ω^+ , and it does not generate the outward field from Σ to Ω^- . Accordingly, the outward field in Ω^- is zero, and the inward field in Ω^+ is monogenic function satisfied with

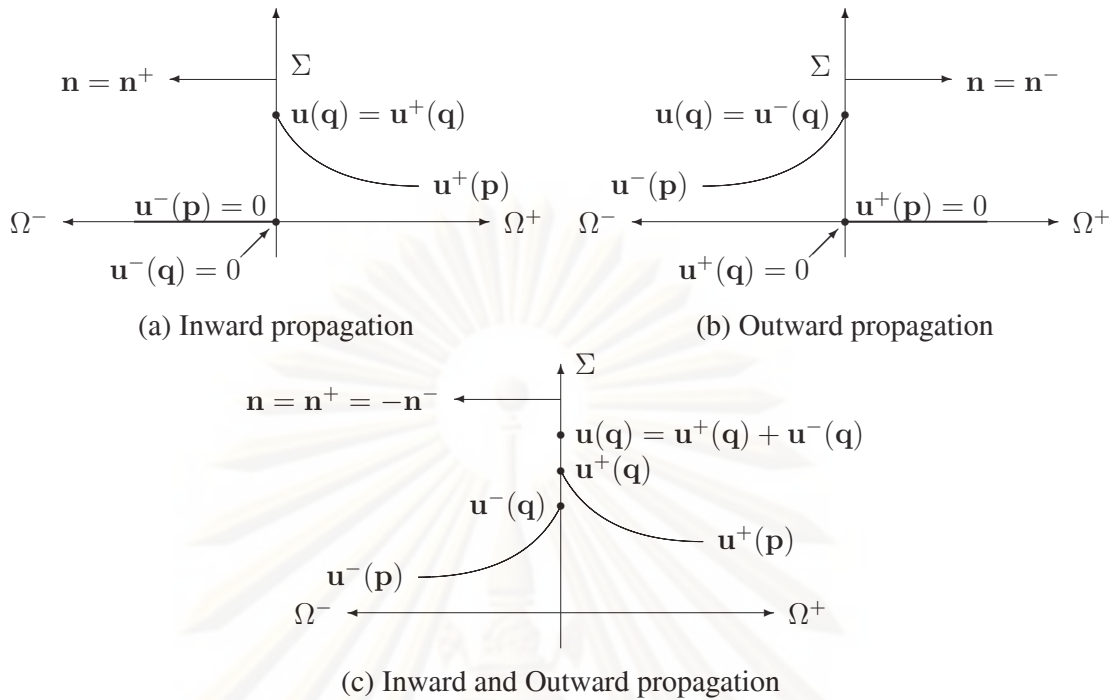


Figure 2.2 Propagating field $\mathbf{u}(\mathbf{p})$ in region Ω^+ and Ω^- from its trace $\mathbf{u}(\mathbf{q})$ on boundary Σ .

(2.16). On the boundary, the total of the field is $\mathbf{u}(\mathbf{q}) = \mathbf{u}^+(\mathbf{q})$ since $\mathbf{u}^-(\mathbf{q}) = 0$. Moreover, the normal unit of Σ is defined as $\mathbf{n} = \mathbf{n}^+$. Finally, applying the reproducing formula in (2.31) into:

$$\int_{\Sigma} \mathbf{E}_k(\mathbf{q} - \mathbf{p}) \mathbf{n}^+(\mathbf{q}) \mathbf{u}^+(\mathbf{q}) d\sigma(\mathbf{q}) = \begin{cases} \mathbf{u}^+(\mathbf{p}) & \text{if } \mathbf{p} \in \Omega^+ \\ 0 & \text{if } \mathbf{p} \in \Omega^- \end{cases} \quad (2.32)$$

It reproduces $\mathbf{u}^+(\mathbf{p})$ in Ω^+ from Σ and give zero in Ω^- .

- The second case: Outward propagation

The surface equivalence theorem is referred in order to discuss the field propagating from Σ to Ω^- . In Fig. 2.2(b), it assumes that the surface field produces the outward field from Σ into Ω^- , and it does not generate the inward field from Σ to Ω^+ . Accordingly, the inward field in Ω^+ is zero, and the outward field in Ω^- is monogenic function satisfied with (2.16). On the boundary, the total of the field is $\mathbf{u}(\mathbf{q}) = \mathbf{u}^-(\mathbf{q})$ since $\mathbf{u}^+(\mathbf{q}) = 0$. Moreover, the normal unit of Σ is defined as $\mathbf{n} = \mathbf{n}^-$. Finally, applying the reproducing formula in (2.31) into:

$$\int_{\Sigma} \mathbf{E}_k(\mathbf{q} - \mathbf{p}) \mathbf{n}^-(\mathbf{q}) \mathbf{u}^-(\mathbf{q}) d\sigma(\mathbf{q}) = \begin{cases} 0 & \text{if } \mathbf{p} \in \Omega^+ \\ \mathbf{u}^-(\mathbf{p}) & \text{if } \mathbf{p} \in \Omega^- \end{cases} \quad (2.33)$$

It reproduces $\mathbf{u}^-(\mathbf{p})$ in Ω^- from Σ and give zero in Ω^+ .

- The third case: Inward and Outward propagations

In Fig. 2.2(c), it assumes that the surface field produces both the inward and outward fields from Σ to Ω^+ and Ω^- , respectively. Both inward and outward fields have been being

the monogenic function and satisfying with (2.16). On the boundary, the total of the field is $\mathbf{u}(\mathbf{q}) = \mathbf{u}^+(\mathbf{q}) + \mathbf{u}^-(\mathbf{q})$, and the normal unit of boundary Σ is defined as $\mathbf{n}(\mathbf{q}) = \mathbf{n}^+(\mathbf{q}) = -\mathbf{n}^-(\mathbf{q})$.

Firstly, considering the propagating field in the interior region ($\mathbf{p} \in \Omega^+$), (2.32) is applied into:

$$\begin{aligned} \mathbf{u}^+(\mathbf{p}) &= \int_{\Sigma} \mathbf{E}_k(\mathbf{q} - \mathbf{p}) \mathbf{n}^+(\mathbf{q}) \mathbf{u}^+(\mathbf{q}) d\sigma(\mathbf{q}) \\ &= \int_{\Sigma} \mathbf{E}_k(\mathbf{q} - \mathbf{p}) \mathbf{n}(\mathbf{q}) (\mathbf{u}(\mathbf{q}) - \mathbf{u}^-(\mathbf{q})) d\sigma(\mathbf{q}), \end{aligned} \quad (2.34)$$

and (2.33) is applied into:

$$\begin{aligned} 0 &= \int_{\Sigma} \mathbf{E}_k(\mathbf{q} - \mathbf{p}) \mathbf{n}^-(\mathbf{q}) \mathbf{u}^-(\mathbf{q}) d\sigma(\mathbf{q}) \\ &= - \int_{\Sigma} \mathbf{E}_k(\mathbf{q} - \mathbf{p}) \mathbf{n}(\mathbf{q}) (\mathbf{u}^-(\mathbf{q})) d\sigma(\mathbf{q}). \end{aligned} \quad (2.35)$$

Subtracting (2.34) by (2.35) to eliminate the terms of $\mathbf{u}^-(\mathbf{q})$ yields:

$$\begin{aligned} \mathbf{u}^+(\mathbf{p}) &= \int_{\Sigma} \mathbf{E}_k(\mathbf{q} - \mathbf{p}) \mathbf{n}(\mathbf{q}) \mathbf{u}(\mathbf{q}) d\sigma(\mathbf{q}) - \int_{\Sigma} \mathbf{E}_k(\mathbf{q} - \mathbf{p}) \mathbf{n}(\mathbf{q}) \mathbf{u}^-(\mathbf{q}) d\sigma(\mathbf{q}) \\ &\quad - \left(- \int_{\Sigma} \mathbf{E}_k(\mathbf{q} - \mathbf{p}) \mathbf{n}(\mathbf{q}) \mathbf{u}^-(\mathbf{q}) d\sigma(\mathbf{q}) \right) \\ &= \int_{\Sigma} \mathbf{E}_k(\mathbf{q} - \mathbf{p}) \mathbf{n}(\mathbf{q}) \mathbf{u}(\mathbf{q}) d\sigma(\mathbf{q}) \quad \text{if } \mathbf{p} \in \Omega^+. \end{aligned} \quad (2.36)$$

Therefore, this resulting integral equation can be used to explain the inward field in interior region, $\mathbf{u}(\mathbf{p} \in \Omega^+)$, that is involved with any surface fields on boundary $\mathbf{u}(\mathbf{q} \in \Sigma)$.

Secondly, considering the propagating field in the exterior region ($\mathbf{p} \in \Omega^-$), (2.32) is applied into:

$$\begin{aligned} 0 &= \int_{\Sigma} \mathbf{E}_k(\mathbf{q} - \mathbf{p}) \mathbf{n}^+(\mathbf{q}) \mathbf{u}^+(\mathbf{q}) d\sigma(\mathbf{q}) \\ &= \int_{\Sigma} \mathbf{E}_k(\mathbf{q} - \mathbf{p}) \mathbf{n}(\mathbf{q}) (\mathbf{u}(\mathbf{q}) - \mathbf{u}^-(\mathbf{q})) d\sigma(\mathbf{q}), \end{aligned} \quad (2.37)$$

and (2.33) is applied into:

$$\begin{aligned} \mathbf{u}^-(\mathbf{p}) &= \int_{\Sigma} \mathbf{E}_k(\mathbf{q} - \mathbf{p}) \mathbf{n}^-(\mathbf{q}) \mathbf{u}^-(\mathbf{q}) d\sigma(\mathbf{q}) \\ &= - \int_{\Sigma} \mathbf{E}_k(\mathbf{q} - \mathbf{p}) \mathbf{n}(\mathbf{q}) (\mathbf{u}^-(\mathbf{q})) d\sigma(\mathbf{q}). \end{aligned} \quad (2.38)$$

Subtracting (2.37) by (2.38) to eliminate the terms of $\mathbf{u}^-(\mathbf{q})$ yields:

$$\begin{aligned} 0 - \mathbf{u}^-(\mathbf{p}) &= \int_{\Sigma} \mathbf{E}_k(\mathbf{q} - \mathbf{p}) \mathbf{n}(\mathbf{q}) \mathbf{u}(\mathbf{q}) d\sigma(\mathbf{q}) - \int_{\Sigma} \mathbf{E}_k(\mathbf{q} - \mathbf{p}) \mathbf{n}(\mathbf{q}) \mathbf{u}^-(\mathbf{q}) d\sigma(\mathbf{q}) \\ &\quad - \left(- \int_{\Sigma} \mathbf{E}_k(\mathbf{q} - \mathbf{p}) \mathbf{n}(\mathbf{q}) \mathbf{u}^-(\mathbf{q}) d\sigma(\mathbf{q}) \right) \\ -\mathbf{u}^-(\mathbf{p}) &= \int_{\Sigma} \mathbf{E}_k(\mathbf{q} - \mathbf{p}) \mathbf{n}(\mathbf{q}) \mathbf{u}(\mathbf{q}) d\sigma(\mathbf{q}) \quad \text{if } \mathbf{p} \in \Omega^-. \end{aligned} \quad (2.39)$$

Therefore, this resulting integral equation can be used to explain the outward field in exterior region, $\mathbf{u}(\mathbf{p} \in \Omega^-)$, that is involved with any surface fields on the boundary $\mathbf{u}(\mathbf{q} \in \Sigma)$.

Notice in these formula that the inward and outward fields, in (2.36) and (2.39) respectively, are created from any same surface fields $\mathbf{u}(\mathbf{q}) = \mathbf{u}^+(\mathbf{q}) + \mathbf{u}^-(\mathbf{q})$. Now declare Ω^+ as the “official” inside, and always use normal unit $\mathbf{n} = \mathbf{n}^+$. Then replace \mathbf{n}^- with $-\mathbf{n}^+ = \mathbf{n}$ so that:

$$\int_{\Sigma} \mathbf{E}_k(\mathbf{q} - \mathbf{p}) \mathbf{n}(\mathbf{q}) \mathbf{u}(\mathbf{q}) d\sigma(\mathbf{q}) = \begin{cases} \mathbf{u}^+(\mathbf{p}) & \text{if } \mathbf{p} \in \Omega^+ \\ -\mathbf{u}^-(\mathbf{p}) & \text{if } \mathbf{p} \in \Omega^- \end{cases}. \quad (2.40)$$

Both fields are propagating away from the boundary. Note that \mathbf{u}^+ and \mathbf{u}^- are usually discontinuous across the boundary, both in value and in derivatives. It is possible to have continuity in value and derivatives if neither Ω^+ and Ω^- extends to infinity then continuity in value and in derivatives can only be achieved if \mathbf{u}^+ and \mathbf{u}^- are zero everywhere. Now define an integral operator \mathbf{C} , which operates on some function $\mathbf{u}(\mathbf{q} \in \Sigma)$ and produces a different function $\mathbf{C}\mathbf{u}(\mathbf{p} \in \Omega^+ \cup \Omega^-)$, according to the formula:

$$\mathbf{C}\mathbf{u}(\mathbf{p} \in \Omega^+ \cup \Omega^-) = \int_{\Sigma} \mathbf{E}_k(\mathbf{q} - \mathbf{p}) \mathbf{n}(\mathbf{q}) \mathbf{u}(\mathbf{q}) d\sigma(\mathbf{q}). \quad (2.41)$$

The operator \mathbf{C} is called the *Cauchy extension*. Thus $\mathbf{C}\mathbf{u}$ is the Cauchy extension of \mathbf{u} in both Ω^+ and Ω^- . Therefore, Eq. (2.31) are applied to the inward and outward fields in terms of Cauchy extension operator as:

$$\mathbf{C}\mathbf{u}(\mathbf{p}) = \begin{cases} \mathbf{u}^+(\mathbf{p}) & \text{if } \mathbf{p} \in \Omega^+ \\ -\mathbf{u}^-(\mathbf{p}) & \text{if } \mathbf{p} \in \Omega^- \end{cases}. \quad (2.42)$$

The Cauchy extension operator is used to explain the propagation of both inward and outward fields from the Σ in Ω^+ and Ω^- , and it is used to apply the integral equation for solving boundary value problems.

2.6 Cauchy Integral Operator

After Cauchy extension operator is constructed for describing the radiation of the field from the boundary, this section introduces another integral operator for analyzing the field on the boundary. The integral operator is derived from reproducing formula. It is used to identify the difference of the trace of the fields on the boundary.

Let us refer to the third case of Section 2.5, the field on the surface equivalent is $\mathbf{u}(\mathbf{q}) = \mathbf{u}^+(\mathbf{q}) + \mathbf{u}^-(\mathbf{q})$. The observation point inside the interior and exterior regions ($\mathbf{p} \in \Omega^+ \cup \Omega^-$) moves into the boundary ($\mathbf{p} \in \Sigma$). Therefore, in here to define operator \mathbf{C}_{Σ} , which operates on some function $\mathbf{u}(\mathbf{q})$ and produces a different function $(\mathbf{C}_{\Sigma}\mathbf{u})(\mathbf{p})$, according to the formula:

$$\left\{ \begin{aligned} (\mathbf{C}_{\Sigma}\mathbf{u})(\mathbf{p}) &= 2 \text{ p.v. } \int_{\Sigma} \mathbf{E}_k(\mathbf{q} - \mathbf{p}) \mathbf{n}(\mathbf{q}) \mathbf{u}(\mathbf{q}) d\sigma(\mathbf{q}) \\ &= 2 \text{ p.v. } \int_{\Sigma} \mathbf{E}_k(\mathbf{q} - \mathbf{p}) \mathbf{n}(\mathbf{q}) (\mathbf{u}^+(\mathbf{q}) + \mathbf{u}^-(\mathbf{q})) d\sigma(\mathbf{q}) \\ &= 2 \text{ p.v. } \int_{\Sigma} \mathbf{E}_k(\mathbf{q} - \mathbf{p}) \mathbf{n}(\mathbf{q}) \mathbf{u}^+(\mathbf{q}) d\sigma(\mathbf{q}) \\ &\quad + 2 \text{ p.v. } \int_{\Sigma} \mathbf{E}_k(\mathbf{q} - \mathbf{p}) \mathbf{n}(\mathbf{q}) \mathbf{u}^-(\mathbf{q}) d\sigma(\mathbf{q}) \\ &= \mathbf{u}^+(\mathbf{p}) - \mathbf{u}^-(\mathbf{p}) \quad \text{if } \mathbf{p} \in \Sigma. \end{aligned} \right. \quad (2.43)$$

The operator \mathbf{C}_{Σ} is called the “principal value (p.v.) Cauchy integral”. Thus $\mathbf{C}_{\Sigma}\mathbf{u}$ is the (principal value) Cauchy integral of \mathbf{u} on Σ .

When Cauchy integral operator operates any field functions on the boundary, their results are the difference of the inward and outward propagating fields on the boundary. This property is very powerful for solving the boundary value problems, such as the perfect transmission and perfect reflection problems.

2.7 Hardy Projection Operator

After Cauchy extension operator is constructed for describing the radiation of the field from the boundary, this section introduces another integral operator for analyzing the field on boundary. The integral operator is derived from the reproducing formula. It is used to identify the difference of the trace of the fields on the boundary.

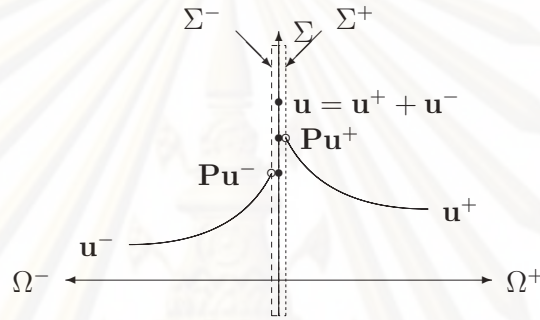


Figure 2.3 Cauchy extensions u^\pm and Hardy projections $P^\pm u$ for the surface field u on Σ .

Fig. 2.3 shows some part of the boundary Σ in order to describe the two ideal boundary Σ^+ and Σ^- . Both Σ^+ and Σ^- are placed on very close up to Σ , but it is never the same place on Σ (Σ^+ and Σ^- are membered onto the domains Ω^+ and Ω^- , respectively). And then the function $u^+(\mathbf{p} \in \Sigma^+)$ and $u^-(\mathbf{p} \in \Sigma^-)$ are the trace of the field on Σ^+ and Σ^- , respectively.

If the \mathbf{p}^+ point, which is placed on Σ^+ , approaches closely at the point \mathbf{p} on the Σ from Ω^+ ($\mathbf{p}^+ = \mathbf{p} \rightarrow \Sigma$), then the limit of Cauchy extension operator by taking function $u(\mathbf{q} \in \Sigma)$ that:

$$\mathbf{P}^+ \mathbf{u}(\mathbf{p}) = \lim_{\mathbf{p}^+ \rightarrow \Sigma} \mathbf{C}u(\mathbf{p}^+) = u^+(\mathbf{p}) \quad \text{if } \mathbf{p} \in \Sigma, \quad (2.44)$$

where \mathbf{P}^+ is *the plus Hardy projection*. So that $\mathbf{P}^+ \mathbf{u}(\mathbf{p})$ can be used to predict the trace of $u^+(\mathbf{p})$ function on Σ . On the other hand, if the \mathbf{p}^- point, which is placed on Σ^- , approaches closely at the point \mathbf{p} on the Σ from Ω^- ($\mathbf{p}^- = \mathbf{p} \rightarrow \Sigma$), then the limit of Cauchy extension operator by taking function $u(\mathbf{q} \in \Sigma)$ that:

$$\mathbf{P}^- \mathbf{u}(\mathbf{p}) = - \lim_{\mathbf{p}^- \rightarrow \Sigma} \mathbf{C}u(\mathbf{p}^-) = u^-(\mathbf{p}) \quad \text{if } \mathbf{p} \in \Sigma, \quad (2.45)$$

where \mathbf{P}^- is *the minus Hardy projection*. So that $\mathbf{P}^- \mathbf{u}(\mathbf{p})$ can be used to predict the trace of $u^-(\mathbf{p})$ function on Σ .

The original field $u(\mathbf{p} \in \Sigma)$ can recover by the summation of two projection operator, \mathbf{P}^+ and \mathbf{P}^- as described (2.44) and (2.45):

$$\mathbf{u}(\mathbf{p}) = \mathbf{P}^+ \mathbf{u}(\mathbf{p}) + \mathbf{P}^- \mathbf{u}(\mathbf{p}) = u^+(\mathbf{p}) + u^-(\mathbf{p}). \quad (2.46)$$

Therefore, it is possible to obtain the following identities for the Hardy projection:

- Idempotent:

$$\begin{cases} (\mathbf{P}^+)^2 = \mathbf{P}^+ \\ (\mathbf{P}^-)^2 = \mathbf{P}^- \end{cases} \quad (2.47)$$

- Mutually Exclusive:

$$\begin{cases} \mathbf{P}^+\mathbf{P}^- = 0 \\ \mathbf{P}^-\mathbf{P}^+ = 0 \end{cases} \quad (2.48)$$

- Complementary

$$\mathbf{P}^+ + \mathbf{P}^- = \mathbf{I} \quad (2.49)$$

Eq. (2.47) confirms that the two Hardy projections are indeed projection operators; *i.e.*, the result of repeated applications of one operator is not different from the result of a single application. Eq. (2.48) states that these two projections are orthogonal; *i.e.*, the information preserved by one is entirely independent of that preserved by the other. Eq. (2.49) shows that the two projections are complementary, *i.e.* the information preserved by one matches exactly that lost by the other.

The two Hardy projection operators have defined already, but they have not been employed for solving boundary value problems. It is necessary to construct the term of the Cauchy integral operator on the boundary in order to split the trace of the field $\mathbf{u}(\mathbf{p})$ into $\mathbf{u}^+(\mathbf{p})$ and $\mathbf{u}^-(\mathbf{p})$. When Cauchy integral operator is written into the terms of two Hardy projection operators by substituting (2.44) and (2.45) into (2.43), then

$$\mathbf{C}_\Sigma \mathbf{u}(\mathbf{p}) = \mathbf{P}^+ \mathbf{u}(\mathbf{p}) + \mathbf{P}^- \mathbf{u}(\mathbf{p}). \quad (2.50)$$

The sum and difference of the two unknown fields on Σ are represented in (2.46) and (2.50), they can be written by separately:

$$\begin{cases} \mathbf{u}^+ = \frac{1}{2}(\mathbf{I} + \mathbf{C}_\Sigma)\mathbf{u} = \mathbf{P}^+\mathbf{u} \\ \mathbf{u}^- = \frac{1}{2}(\mathbf{I} - \mathbf{C}_\Sigma)\mathbf{u} = \mathbf{P}^-\mathbf{u} \end{cases} \quad (2.51)$$

Table 2.1 summaries the effects of the Cauchy integral and Hardy operators on three particular fields; one with only an inward propagating field, one with only an outward propagating field, and one with both inward and outward propagating fields. Note that the Hardy projections play role of decomposing the field on the boundary into its inward and outward propagating fields.

Table 2.1 Hardy and Cauchy integral operators.

surface field $\mathbf{u}(\mathbf{q} \in \Sigma)$	Cauchy integral $\mathbf{C}_\Sigma \mathbf{u}(\mathbf{q} \in \Sigma)$	Hardy projection $\mathbf{P}^+ \mathbf{u}(\mathbf{q} \in \Sigma)$	Hardy projection $\mathbf{P}^- \mathbf{u}(\mathbf{q} \in \Sigma)$
\mathbf{u}^+	\mathbf{u}^+	\mathbf{u}^+	0
\mathbf{u}^-	$-\mathbf{u}^-$	0	\mathbf{u}^-
$\mathbf{u}^+ + \mathbf{u}^-$	$\mathbf{u}^+ - \mathbf{u}^-$	\mathbf{u}^+	\mathbf{u}^-

CHAPTER III

GEOMETRIC SOLUTIONS OF INTEGRAL EQUATION FOR BOUNDARY VALUE PROBLEMS

Electromagnetic boundary value problems fall naturally into three different cases, as shown in Fig. 3.1, according to the behavior of the field at the boundary: (a) perfect transmission, (b) perfect reflection and (c) partial transmission and reflection. In all cases the method of solution involves calculating the the transmitted and reflected fields, \mathbf{u}^{tr} and \mathbf{u}^{sc} , on the boundary from the incident field, \mathbf{u}^{in} .

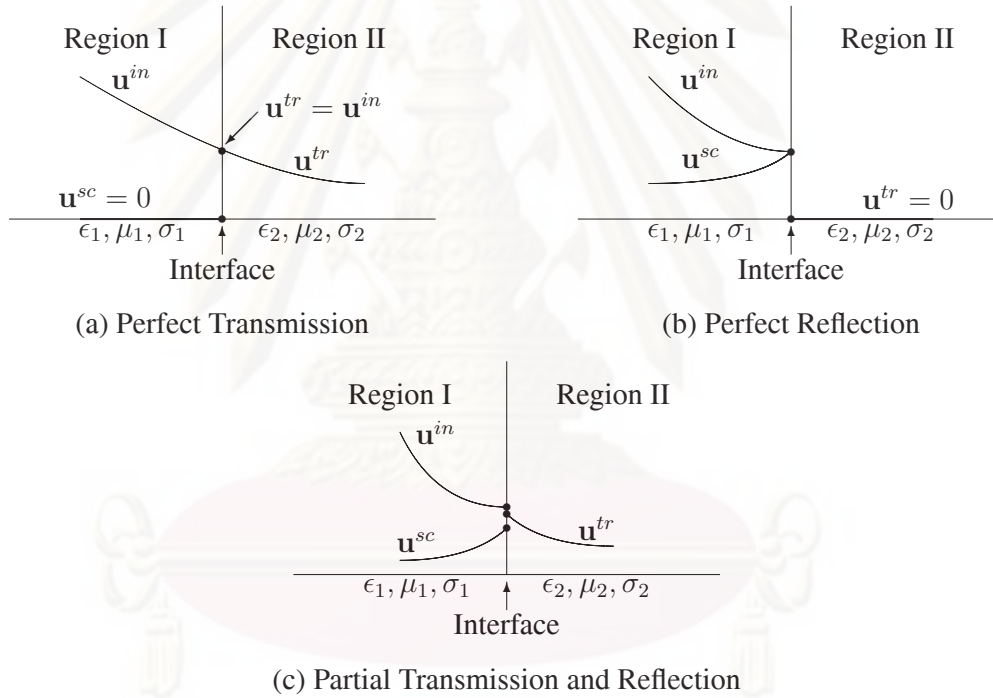


Figure 3.1 Three cases of electromagnetic boundary value problems.

For the perfect transmission, the incident and transmitted fields exhibit same behavior when the mediums in region I and region II are same ($\epsilon_1 = \epsilon_2, \mu_1 = \mu_2, \sigma_1 = \sigma_2 \neq \infty$). For the perfect reflection, the current density induced on PEC interface ($\sigma_2 = \infty$) by the incident field will produce the reflected field. For the partial of transmission and reflection, both the transmitted and reflected fields are propagating into the medium I ($\epsilon_1, \mu_1, \sigma_1 \neq \infty$) and medium II ($\epsilon_2, \mu_2, \sigma_2 \neq \infty$), respectively, when the incident field arrive at the interface.

The three cases can be ordered according to complexity (and difficulty) from the perfect transmission as the simplest, to the partial transmission as the most complicated. Here the perfect transmission case and the perfect reflection case are described separately in Sections 3.1 and 3.2, respectively. Each of these two sections describes the Maxwell-Dirac

equation in the integral form, the solution of integral operator, and applied solution of integral operator for iteration.

Together, the Maxwell-Dirac equation (differential) (see in Chapter II) and the boundary conditions lead to sufficient equations for determining the unknown fields (transmitted or reflected or both). For each region where one field is unknown, two equations can be written. The first derives from the general properties of k -monogenic functions as solutions to the Maxwell-Dirac equation. This gives the Hardy projection, relating the field on the boundary to the field immediately adjacent to the boundary. The second comes from the boundary conditions, recast in the form of one of two boundary data projections (see detail in Appendix C). Each of these two projections relates one half of the unknown field on the boundary to one half of the incident field on the boundary.

For the case of perfect transmission and perfect reflection this process reduces the entire problem to two simultaneous equations: one Hardy-style and one data-style. The Hardy projections are already of a form that can be used immediately to construct a coordinate system in Banach space. The boundary conditions known well in vector form can be recast as boundary data projections of a suitable form. This is easy for the cases of perfect transmission and perfect reflection, because it is only necessary to deal with one side of the boundary and one value of permittivity and permeability.

3.1 Perfect Transmission Problem

3.1.1 Boundary Value Problem in Perfect Transmission

3.1.1.1 The Cookie Cutter Problem

Fig. 3.2 shows a rectangular subregion within a larger (infinite) region Ω of uniform material properties μ , ϵ and σ . There are no sources within the subregion, but electromagnetic radiation propagates through the subregion from some distant monochromatic source. The magnitude of the phaser \mathbf{u} representing the field in the subregions is a k -monogenic function as given by the Maxwell-Dirac equation.

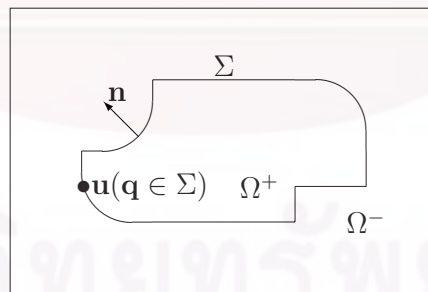


Figure 3.2 Three different functions: \mathbf{u}^+ , \mathbf{u}^- and \mathbf{u} along Ω^+ , Ω^- and Σ , respectively.

Imagine now tracing some arbitrary (non-intersecting) closed boundary Σ separating Ω into an interior region Ω^+ and an exterior region Ω^- (extending to infinity), taking in the process a copy of the value of the field $\mathbf{u}(\mathbf{p} \in \Sigma)$ on the boundary. If the external region Ω^- is cut away the boundary field is maintained by some equivalent electromagnetic source located on the boundary, the field in the interior Ω^+ remains the same. This problem is called the “*Cookie Cutter*” problem since its construction bears many similarities to the way cookie

of various shapes are cut out of a sheet of uniform dough. The Cookies Cutter problem can be used to generate simple boundary value test problems in which there is a single uniform region of arbitrary shape, and in which the (equivalent) boundary sources can be varied by changing the real (external) sources of the field according to taste. External sources for which analytical solutions are known are preferable in order to make it easy to calculate the (equivalent) boundary sources.

Unlike the problems described in the next section, the incident field gives directly the solution without calculation: both on the boundary and inside. Discarding one half of the boundary field at the outset and retaining the other half to serve as the boundary conditions establishes a simple non-trivial boundary value test problem for which the correct answer is known both on the boundary and inside. This makes it possible to break the work of developing an algorithm to calculate the solution numerically into decoupled sections, and verify their numerical validity independently. Such an approach with checks at all possible stages is essential in developing a trustworthy numerical solution since the numerical methods which must be used are far from trivial; littered with all sorts of traps awaiting the unwary developer. It is also worth noting that the solution of the Cookie Cutter problem is effectively the same as the solution for the case of perfect reflection. Whereas the former may seem contrived, the latter is of definite practical importance.

3.1.1.2 Boundary Conditions in Perfect Transmission

In case of perfect transmission, the boundary conditions in vector form is:

$$\begin{cases} \vec{n} \cdot \vec{E}^{in} = \vec{n} \cdot \vec{E}^{tr} \\ \vec{n} \times \vec{H}^{in} = \vec{n} \times \vec{H}^{tr} \\ \vec{n} \times \vec{E}^{in} = \vec{n} \times \vec{E}^{tr} \\ \vec{n} \cdot \vec{H}^{in} = \vec{n} \cdot \vec{H}^{tr} \end{cases}, \quad (3.1)$$

where \vec{E}^{in} and \vec{H}^{in} are incident electric and magnetic fields, respectively, and \vec{E}^{tr} and \vec{H}^{tr} are transmitted electric and magnetic fields, respectively. The behavior of the fields on the interface does not create the reflection; therefore, the incident field is same as the transmitted field.

The incident and transmitted fields on boundary conditions on the vector form in (3.1) can be divided into four groups by considering the direction of normal unit identifying the boundary. The first pair of the groups are the normal components of electric and magnetic fields (\vec{E}_n, \vec{H}_n) and another one are the tangential component of both fields (\vec{E}_t, \vec{H}_t). All these fields are described into Clifford number according to (2.7):

$$\begin{cases} \mathbf{u}^{in} = \mu_-^{\frac{1}{2}} \mathbf{H}^{in} \sigma + j \epsilon_-^{\frac{1}{2}} \mathbf{E}^{in} \mathbf{e}_0 \\ \mathbf{u}^{tr} = \mu_+^{\frac{1}{2}} \mathbf{H}^{tr} \sigma + j \epsilon_+^{\frac{1}{2}} \mathbf{E}^{tr} \mathbf{e}_0 \end{cases}, \quad (3.2)$$

where (μ_-, ϵ_-) and (μ_+, ϵ_+) are the electric permittivity and permeability in the exterior and interior regions, respectively. The material properties μ and ϵ take complex number scalar values. This accommodates lossy material in frequency domain as non-zero imaginary part of ϵ , but excludes anisotropic media. In order to capture two appropriate components of the fields either (\vec{E}_t, \vec{H}_n) or (\vec{E}_n, \vec{H}_t) in Clifford algebra the data projection operators \mathbf{Q}^\pm are employed and their details are described in Appendix C. Therefore, the boundary conditions

in (3.1) are rewritten into Clifford formalism with the data projections:

$$\begin{cases} \mathbf{Q}^+ \mathbf{u}^{tr} &= \mu_+^{\frac{1}{2}} \mathbf{H}_t^{tr} \sigma + j \epsilon_+^{\frac{1}{2}} \mathbf{E}_n^{tr} \mathbf{e}_0 &= \mu_-^{\frac{1}{2}} \mathbf{H}_t^{in} \sigma + j \epsilon_-^{\frac{1}{2}} \mathbf{E}_n^{in} \mathbf{e}_0 &= \mathbf{Q}^+ \mathbf{u}^{in} \\ \mathbf{Q}^- \mathbf{u}^{tr} &= \mu_+^{\frac{1}{2}} \mathbf{H}_n^{tr} \sigma + j \epsilon_+^{\frac{1}{2}} \mathbf{E}_t^{tr} \mathbf{e}_0 &= \mu_-^{\frac{1}{2}} \mathbf{H}_n^{in} \sigma + j \epsilon_-^{\frac{1}{2}} \mathbf{E}_t^{in} \mathbf{e}_0 &= \mathbf{Q}^- \mathbf{u}^{in} \end{cases} \quad (3.3)$$

3.1.2 Normal Solutions for Perfect Transmission

In case of perfect transmission, there are two main situations such as consideration of the inward field or the outward field. Firstly, when the incident field is propagating from the exterior region onto the boundary, the inward field is reproduced in the interior region. Secondly, when the incident field is propagating from the interior region onto the boundary, the outward field is reproduced on the exterior region. Therefore, both situations are shown in this section.

3.1.2.1 Normal Solution of Inward Field

When the incident field produced by any actual source in the exterior region arrives at the boundary, this field is equivalent source or secondary source along boundary that can generate the inward field propagating in the interior region. Their characteristics of these fields are satisfied with Maxwell-Dirac equation in the form of Hardy projections (2.51). When \mathbf{u}^+ is used instead of \mathbf{u}^{tr} , and \mathbf{u}^- is zero since the reflected field does not appear. Therefore, the total field on the boundary \mathbf{u} is \mathbf{u}^{tr} :

$$\begin{cases} \mathbf{P}^+ \mathbf{u}^{tr} &= \mathbf{u}^{tr} \\ \mathbf{P}^- \mathbf{u}^{tr} &= 0 \end{cases} \quad (3.4)$$

And the boundary conditions of perfect transmission in (3.3) can be shown as

$$\begin{cases} \mathbf{f} &= \mathbf{Q}^+ \mathbf{u}^{tr} \\ \mathbf{g} &= \mathbf{Q}^- \mathbf{u}^{tr} \end{cases} \quad (3.5)$$

where \mathbf{f} and \mathbf{g} are Clifford functions. The function \mathbf{f} is used to describe the normal components of the electric field and the tangential field of the magnetic field ($\mathbf{E}_n^{tr}, \mathbf{H}_t^{tr}$). In practice, these components of the fields are unknown, since it cannot be measured directly. However, the function \mathbf{g} that is used to describe the normal components of the magnetic field and the tangential field of the electric field ($\mathbf{H}_n^{tr}, \mathbf{E}_t^{tr}$) can be evaluated without using complicated techniques. Therefore, the function \mathbf{g} that is some parts of the transmitted field is employed as the input data in order to solve its full parts.

In order to visualize the solutions to (3.4) and (3.5) it is useful to represent them in a geometric form. Since \mathbf{P}^\pm and \mathbf{Q}^\pm are operators which take the projections of functions rather than points, the appropriate geometrical space to use is one of functions \mathbf{u}^{tr} , as shown in Fig. 3.3, rather than points. In here, only two equations are chosen for formulating the linear system:

$$\begin{cases} \mathbf{P}^+ \mathbf{u}^{tr} &= \mathbf{u}^{tr} \\ \mathbf{g} &= \mathbf{Q}^- \mathbf{u}^{tr} \end{cases} \quad (3.6)$$

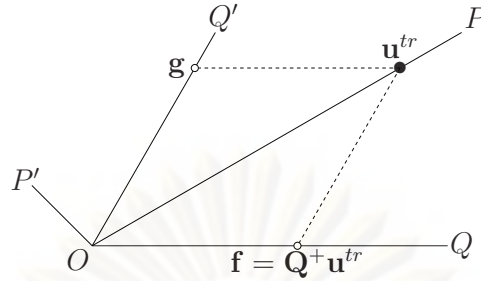


Figure 3.3: Solution of Maxwell's equations as intersection in Banach space of dotted line through boundary conditions g and coordinate axis OP, OP' for the inward field in case of perfect transmission.

In Banach space this means the solution u^{tr} lies somewhere along the dotted lines parallel to the OQ -axis and through function g on the OQ' -axis, as shown in Fig. 3.3. Simple geometry dictates that the intersection between the dotted line and the OP -axis gives a unique solution u^{tr} as long as the OP -axis and the OQ' -axis are not coincident. This is known already, since from their definitions the projections Q^- and P^+ are definitely not the same.

The solution u^{tr} can be represented in terms of Cartesian components in either the P -system and Q -system:

$$\begin{cases} u^{tr} = u^{tr} + 0 & P\text{-system} \\ u^{tr} = f + g & Q\text{-system} \end{cases} \quad (3.7)$$

where $f = Q^+ u^{tr}$ (as shown in Fig. 3.3) is the missing half of the boundary field.

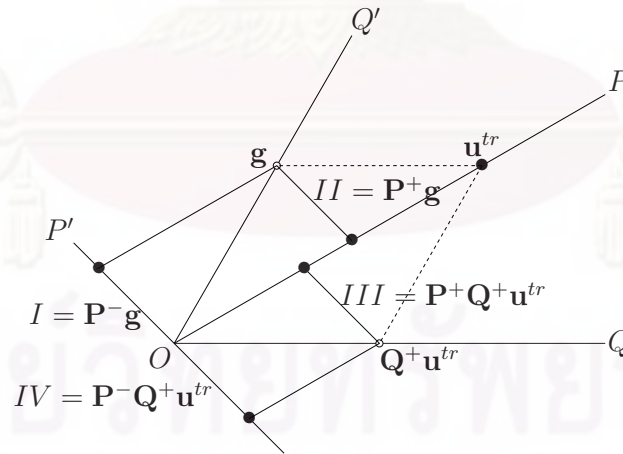


Figure 3.4 Construction for solution of inward field given data $g = Q^- u^{tr}$.

A solution in either system can be formulated by inspection of Fig. 3.4. The figure shows the solution u^{tr} on the OP -axis, split into two components $Q^+ u^{tr}$ and $g = Q^- u^{tr}$ in the Q -system, each of which are themselves further split into two more components back in the P -system. All of the triangles and rectangles in the figure which appear by casual inspection to be similar, are indeed similar.

The value of the four components produced in the P -system by the splitting process are represented in Fig. 3.4 by the four line segments I, II, III and IV. Adding these line segments as vectors produces a resultant vector from the origin to the solution \mathbf{u}^{tr} :

$$I + II + III + IV = \mathbf{P}^- \mathbf{g} + \mathbf{P}^+ \mathbf{g} + \mathbf{P}^+ \mathbf{Q}^+ \mathbf{u}^{tr} + \mathbf{P}^- \mathbf{Q}^+ \mathbf{u}^{tr} = \mathbf{u}^{tr}. \quad (3.8)$$

Eq. (3.8) is actually rather trivial, and rather useless in its own right since it is easily reduced to either of the forms in (3.7). Of more interest and more immediate use are its projections into the P system. Projection onto the two axes of the P -system gives:

$$\begin{cases} \mathbf{P}^+ \mathbf{Q}^+ \mathbf{u}^{tr} + \mathbf{P}^+ \mathbf{g} = \mathbf{u}^{tr} \\ \mathbf{P}^- \mathbf{Q}^+ \mathbf{u}^{tr} + \mathbf{P}^- \mathbf{g} = 0 \end{cases}, \quad (3.9)$$

where use has been made of $(\mathbf{P}^\pm)^2 = \mathbf{P}^\pm$, $\mathbf{P}^\pm \mathbf{P}^\mp = 0$ and $\mathbf{P}^+ \mathbf{u}^{tr} = \mathbf{u}^{tr}$.

Inspection of Fig. 3.4 shows that $\mathbf{P}^+ \mathbf{Q}^+ \mathbf{u}^{tr} \neq \mathbf{u}^{tr}$ unless the OP -axis is coincident with the OQ' -axis; a situation which has already been ruled out. It is therefore possible to subtract $\mathbf{P}^+ \mathbf{Q}^+ \mathbf{u}^{tr}$ from both sides of (3.9) to obtain:

$$\mathbf{P}^+ \mathbf{g} = (\mathbf{I} - \mathbf{P}^+ \mathbf{Q}^+) \mathbf{u}^{tr}, \quad (3.10)$$

with the assurance that both sides are non-zero.

The right hand side contains the product of two singular operators $\mathbf{P}^+ \mathbf{Q}^+$, itself singular. The sum of this product with the (non-singular) identity operator gives the term $\mathbf{I} - \mathbf{P}^+ \mathbf{Q}^+$ which is sure to be non-singular. It is therefore possible to invert this term, giving:

$$\mathbf{u}^{tr} = (\mathbf{I} - \mathbf{P}^+ \mathbf{Q}^+)^{-1} \mathbf{P}^+ \mathbf{g}. \quad (3.11)$$

This is the solution of inward field in case of perfect transmission problem.

Note that (3.10) is not in the form of a Fredholm integral equation. Writing (3.10) in full integral form shows that the operator $(\mathbf{I} - \mathbf{P}^+ \mathbf{Q}^+)$ embeds \mathbf{u}^{tr} with non-commutative multiplication from both sides. For a Fredholm integral equation the multiplication is from one side only. Whereas a direct matrix inverse style of solution for a discrete approximation to a Fredholm integral equation is possible, the same cannot be said for (3.10). The formal solution as written in (3.11) is symbolic only, and should not be mistaken for some kind of matrix inverse.

3.1.2.2 Normal Solution of Outward Field

When the incident field produced by any actual source in the interior region arrives onto the boundary, this field is equivalent source or secondary source along boundary that can generate the outward field propagating in the exterior region. The characteristics of these fields are satisfied with the Maxwell-Dirac equation in form of Hardy projections (2.51). When \mathbf{u}^- is used instead of \mathbf{u}^{tr} , and \mathbf{u}^+ is zero since the reflected field does not appear. Therefore, the total field on the boundary \mathbf{u} is \mathbf{u}^{tr} :

$$\begin{cases} \mathbf{P}^- \mathbf{u}^{tr} = \mathbf{u}^{tr} \\ \mathbf{P}^+ \mathbf{u}^{tr} = 0 \end{cases}. \quad (3.12)$$

The boundary conditions of perfect transmission in (3.3) can be shown again as

$$\begin{cases} \mathbf{f} = \mathbf{Q}^+ \mathbf{u}^{tr} \\ \mathbf{g} = \mathbf{Q}^- \mathbf{u}^{tr} \end{cases}. \quad (3.13)$$

This boundary conditions for analyzing the outward field is same as the the inward field.

The Maxwell-Dirac equation in the form of Hardy projections (3.12) and boundary conditions (3.13) are described together on Banach space in order to construct the solution of the outward field. In here, only two equations are chosen for formulating the linear system:

$$\begin{cases} \mathbf{P}^- \mathbf{u}^{tr} = \mathbf{u}^{tr} \\ \mathbf{g} = \mathbf{Q}^- \mathbf{u}^{tr} \end{cases} \quad (3.14)$$

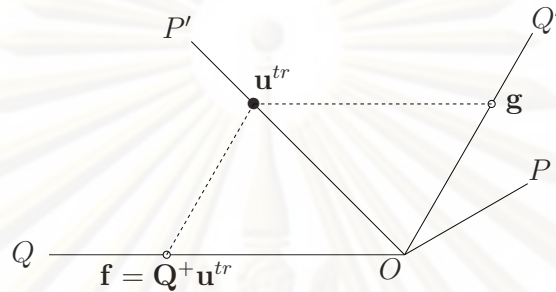


Figure 3.5: Solution of Maxwell's equations as intersection in Banach space of dotted line through boundary conditions \mathbf{g} and coordinate axis OP, OP' for the outward field in case of the perfect transmission.

In Banach space this means the solution \mathbf{u}^{tr} lies somewhere along the dotted lines parallel to the OQ -axis and through function \mathbf{g} on the OQ' -axis, as shown in Fig. 3.5. Simple geometry dictates that the intersection between the dotted line and the OP' -axis gives a unique solution \mathbf{u}^{tr} as long as the OP' -axis and the OQ' -axis are not coincident. This is known already, since from their definitions the projections \mathbf{Q}^- and \mathbf{P}^- are definitely not the same.

The solution \mathbf{u}^{tr} can be represented in terms of Cartesian components in either the P -system and Q -system:

$$\begin{cases} \mathbf{u}^{tr} = \mathbf{u}^{tr} + 0 & P\text{-system} \\ \mathbf{u}^{tr} = \mathbf{f} + \mathbf{g} & Q\text{-system} \end{cases} \quad (3.15)$$

where $\mathbf{f} = \mathbf{Q}^+ \mathbf{u}^{tr}$ (as shown in Fig. 3.5) is the missing half of the boundary field.

A solution in either system can be formulated by inspection of Fig. 3.6. The figure shows the solution \mathbf{u}^{tr} on the OP' -axis, split into two components $\mathbf{Q}^+ \mathbf{u}^{tr}$ and $\mathbf{g} = \mathbf{Q}^- \mathbf{u}^{tr}$ in the Q -system, each of which are themselves further split into two more components back in the P -system. All of the triangles and rectangles in the figure which appear by casual inspection to be similar, are indeed similar.

The value of the four components produced in the P -system by the splitting process are represented in Fig. 3.6 by the four line segments I, II, III and IV. Adding these line segments as vectors produces a resultant vector from the origin to the solution \mathbf{u}^{tr} :

$$I + II + III + IV = \mathbf{P}^+ \mathbf{g} + \mathbf{P}^- \mathbf{g} + \mathbf{P}^- \mathbf{Q}^+ \mathbf{u}^{tr} + \mathbf{P}^+ \mathbf{Q}^+ \mathbf{u}^{tr} = \mathbf{u}^{tr}. \quad (3.16)$$

Eq. (3.16) is actually rather trivial, and rather useless in its own right since it is easily reduced to either of the forms in (3.15). Of more interest and more immediate use its projections into

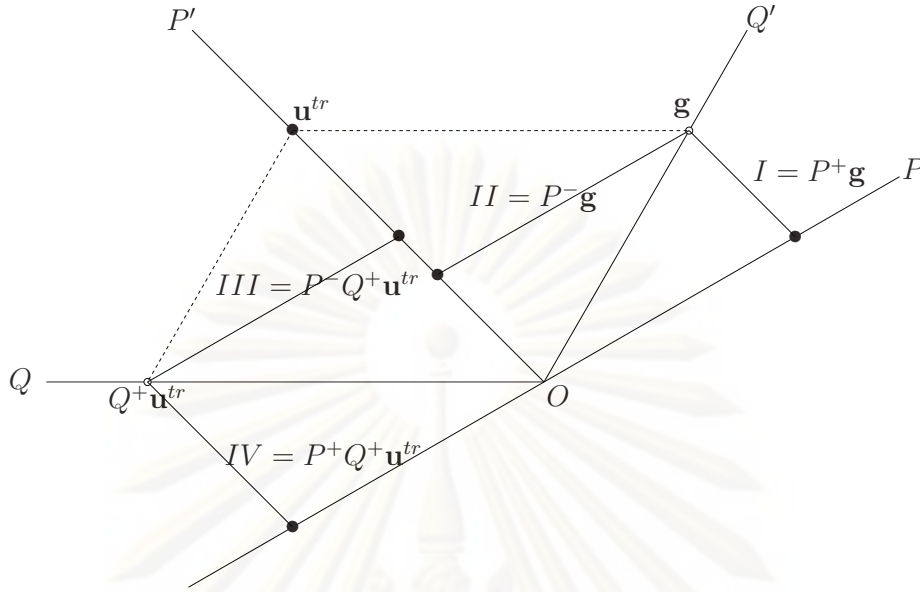


Figure 3.6 Construction for solution of outward field given data $\mathbf{g} = \mathbf{Q}^- \mathbf{u}^{tr}$.

the P systems. Projection onto the two axes of the P -system gives:

$$\begin{cases} \mathbf{P}^- \mathbf{Q}^+ \mathbf{u}^{tr} + \mathbf{P}^- \mathbf{g} = \mathbf{u}^{tr} \\ \mathbf{P}^+ \mathbf{Q}^+ \mathbf{u}^{tr} + \mathbf{P}^+ \mathbf{g} = 0 \end{cases} \quad (3.17)$$

where has been made of $(\mathbf{P}^\pm)^2 = \mathbf{P}^\pm$, $\mathbf{P}^\pm \mathbf{P}^\mp = 0$ and $\mathbf{P}^- \mathbf{u}^{tr} = \mathbf{u}^{tr}$.

Inspection of Fig. 3.6 shows that $\mathbf{P}^- \mathbf{Q}^+ \mathbf{u}^{tr} \neq \mathbf{u}^{tr}$ unless the OP' -axis is coincident with the OQ' -axis; a situation which has already been ruled out. It is therefore possible to subtract $\mathbf{P}^- \mathbf{Q}^+ \mathbf{u}^{tr}$ from both sides of (3.17) to obtain:

$$\mathbf{P}^- \mathbf{g} = (\mathbf{I} - \mathbf{P}^- \mathbf{Q}^+) \mathbf{u}^{tr}, \quad (3.18)$$

with the assurance that both sides are non-zero.

The right hand side contains the product of two singular operators $\mathbf{P}^- \mathbf{Q}^+$, itself singular. The sum of this product with the (non-singular) identity operator gives the term $\mathbf{I} - \mathbf{P}^- \mathbf{Q}^+$ which is sure to be non-singular. It is therefore possible to invert this term, giving:

$$\mathbf{u}^{tr} = (\mathbf{I} - \mathbf{P}^- \mathbf{Q}^+)^{-1} \mathbf{P}^- \mathbf{g}. \quad (3.19)$$

This is the solution of outward field in case of perfect transmission problem. The $(\mathbf{I} - \mathbf{P}^- \mathbf{Q}^+)$ that is the compound operators can simulate its inversion similar to the inversion of $(\mathbf{I} - \mathbf{P}^+ \mathbf{Q}^+)$ as (3.11).

3.1.3 Iterative Solution for Perfect Transmission

3.1.3.1 Iterative Solution of Inward Field

In principle the solution of the inward field \mathbf{u}^{tr} in (3.11) need not involve a direct inversion of the compound operator $(\mathbf{I} - \mathbf{P}^+\mathbf{Q}^+)$. An iterative procedure can be used, as shown in Fig. 3.7.

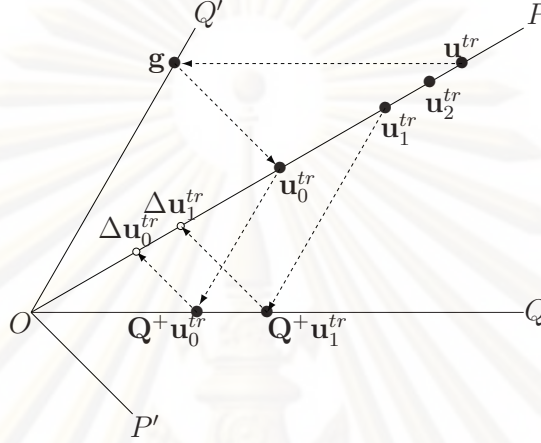


Figure 3.7: Iterative solution of inward field. Adding correction $\Delta \mathbf{u}_0^{tr}$ to initial estimate \mathbf{u}_0^{tr} gives improved estimate \mathbf{u}_1^{tr} , and adding $\Delta \mathbf{u}_1^{tr}$ to \mathbf{u}_0^{tr} gives \mathbf{u}_2^{tr} .

Firstly, an initial estimate:

$$\mathbf{u}_0^{tr} = \mathbf{P}^+ \mathbf{g}, \quad (3.20)$$

is obtained by projecting the boundary condition \mathbf{g} onto the OP -axis. A correction $\Delta \mathbf{u}_0^{tr} = \mathbf{P}^+\mathbf{Q}^+\mathbf{u}_0^{tr}$ is calculated by projecting \mathbf{u}_0^{tr} first onto the OQ -axis and then back onto the OP -axis. A new estimate $\mathbf{u}_1^{tr} = \mathbf{u}_0^{tr} + \Delta \mathbf{u}_0^{tr}$ is obtained by adding the correction to initial estimate. As a second iteration, an improved correction $\Delta \mathbf{u}_1^{tr} = \mathbf{P}^+\mathbf{Q}^+\mathbf{u}_1^{tr}$ is used to give a better estimate $\mathbf{u}_2^{tr} = \mathbf{u}_0^{tr} + \Delta \mathbf{u}_1^{tr}$. Note that the correction is always added to the initial estimate \mathbf{u}_0^{tr} , not to the most recent estimate. The general form of the k^{th} estimate \mathbf{u}_k^{tr} is:

$$\mathbf{u}_k^{tr} = \mathbf{u}_0^{tr} + \mathbf{P}^+\mathbf{Q}^+\mathbf{u}_{k-1}^{tr} = \sum_{m=0}^k (\mathbf{P}^+\mathbf{Q}^+)^m \mathbf{u}_0^{tr}. \quad (3.21)$$

This is iterative solution of inward field in case of perfect transmission. The solution takes the form of Neumann iteration, with initial guess \mathbf{u}_0 calculated directly from the boundary conditions \mathbf{g} . A different field $\mathbf{u}'_0 = \mathbf{P}^+\mathbf{v}$ could also be chosen for an initial guess. This would make sense if it is known that \mathbf{u}'_0 is closer to the solution than \mathbf{u}_0 .

Moreover, the convergence of the iterative solution in (3.21) is discussed in here. The difference between consecutive estimates is:

$$\mathbf{u}_k^{tr} - \mathbf{u}_{k-1}^{tr} = (\mathbf{P}^+\mathbf{Q}^+)^k \mathbf{u}_0^{tr}. \quad (3.22)$$

which, as shown in Fig. 3.8, approaches zero as k approaches infinity at a rate proportional to the size of the difference. In principle, the difference reduces to zero after an infinite number of iterations. At that stage $\mathbf{u}_k^{tr} = \mathbf{u}_{k-1}^{tr}$, so that:

$$\mathbf{u}_k^{tr} = \mathbf{u}_0^{tr} + \mathbf{P}^+\mathbf{Q}^+\mathbf{u}_{k-1}^{tr} = \mathbf{u}_0^{tr} + \mathbf{P}^+\mathbf{Q}^+\mathbf{u}_k^{tr}. \quad (3.23)$$

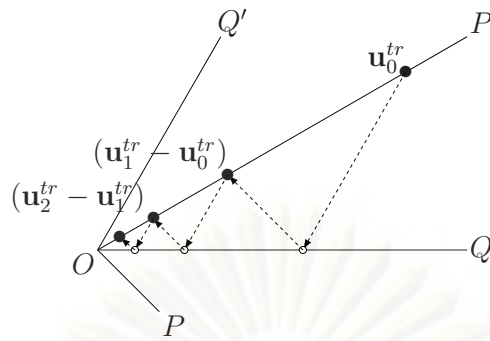


Figure 3.8: The difference of the solutions of inward fields $\mathbf{u}_k^{tr} - \mathbf{u}_{k-1}^{tr}$ between consecutive estimates of solution \mathbf{u}^{tr} approaching zero as the iteration proceeds.

The difference from the correct solution \mathbf{u} can be found by subtracting (3.10):

$$(\mathbf{u}_k^{tr} - \mathbf{u}^{tr}) = \mathbf{P}^+ \mathbf{Q}^+ (\mathbf{u}_k^{tr} - \mathbf{u}^{tr}), \quad (3.24)$$

which by inspection of Fig. 3.9 can only be true if $\mathbf{u}_k^{tr} - \mathbf{u}^{tr}$ is sitting at the origin, so that $\mathbf{u}_k^{tr} = \mathbf{u}^{tr}$. It therefore follows that the iterative method in (3.20) and (3.21) converges and, furthermore, converges to the correct solution.

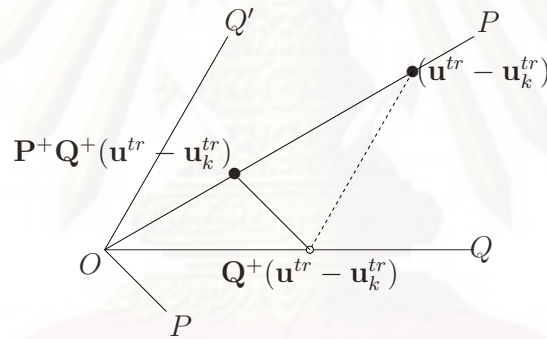


Figure 3.9: The difference between estimate \mathbf{u}_k^{tr} and solution of inward field \mathbf{u}^{tr} is the same after projections $\mathbf{P}^+ \mathbf{Q}^+$ only if $\mathbf{u}_k^{tr} - \mathbf{u}^{tr} = 0$, showing convergence to correct solution of inward field $\mathbf{u}_k^{tr} = \mathbf{u}^{tr}$.

3.1.3.2 Iterative Solution of Outward Field

In principal the solution of the outward field \mathbf{u}^{tr} in (3.19) need not involve a direct inversion of the compound operator $(\mathbf{I} - \mathbf{P}^- \mathbf{Q}^+)$. An iterative procedure can be used, as shown in Fig. 3.10.

Firstly, an initial estimate:

$$\mathbf{u}_0^{tr} = \mathbf{P}^- \mathbf{g}, \quad (3.25)$$

is obtained by projecting the boundary conditions \mathbf{g} onto the OP' -axis. A correction $\Delta \mathbf{u}_0^{tr} = \mathbf{P}^- \mathbf{Q}^+ \mathbf{u}_0^{tr}$ is calculated by projecting \mathbf{u}_0^{tr} first onto the OQ -axis and then back onto the OP' -axis. A new estimate $\mathbf{u}_1^{tr} = \mathbf{u}_0^{tr} + \Delta \mathbf{u}_0^{tr}$ is obtained by adding the correction to initial estimate. As a second iteration, an improved correction $\Delta \mathbf{u}_1^{tr} = \mathbf{P}^- \mathbf{Q}^+ \mathbf{u}_1^{tr}$ is used to give

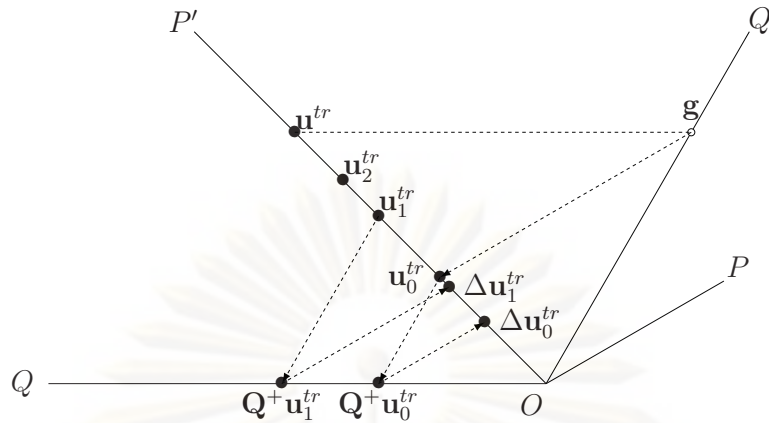


Figure 3.10: Iterative solution of outward field. Adding correction $\Delta \mathbf{u}_0^{tr}$ to initial estimate \mathbf{u}_0^{tr} gives improved estimate \mathbf{u}_1^{tr} , and adding $\Delta \mathbf{u}_1^{tr}$ to \mathbf{u}_0^{tr} gives \mathbf{u}_2^{tr} .

a better estimate $\mathbf{u}_2^{tr} = \mathbf{u}_0^{tr} + \Delta \mathbf{u}_1^{tr}$. Note that the correction is always added to the initial estimate \mathbf{u}_0^{tr} , not to the most recent estimate. The general form of the k^{th} estimate \mathbf{u}_k^{tr} is:

$$\mathbf{u}_k^{tr} = \mathbf{u}_0^{tr} + \mathbf{P}^- \mathbf{Q}^+ \mathbf{u}_{k-1}^{tr} = \sum_{m=0}^k (\mathbf{P}^- \mathbf{Q}^+)^m \mathbf{u}_0^{tr}. \quad (3.26)$$

This is iterative solution of outward field in case of perfect transmission. The solution takes the form of Neumann iteration, with initial guess \mathbf{u}_0 calculated directly from the boundary conditions \mathbf{g} . A different field $\mathbf{u}'_0 = \mathbf{P}^- \mathbf{v}$ could also be chosen for an initial guess. This would make sense if it is known that \mathbf{u}'_0 is closer to the solution than \mathbf{u}_0 .

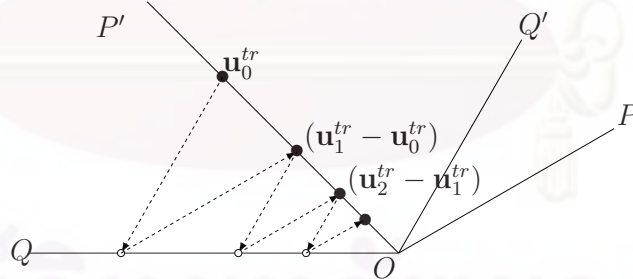


Figure 3.11: The difference of the solutions of outward fields $\mathbf{u}_k^{tr} - \mathbf{u}_{k-1}^{tr}$ between consecutive estimates of solution \mathbf{u}^{tr} approaching zero as the iteration proceeds.

Moreover, the convergence of the iterative solution in (3.26) is discussed in here. The difference between consecutive estimates is:

$$\mathbf{u}_k^{tr} - \mathbf{u}_{k-1}^{tr} = (\mathbf{P}^- \mathbf{Q}^+)^k \mathbf{u}_0^{tr}, \quad (3.27)$$

which, as shown in Fig. 3.11, approaches zero as k approaches infinity at a rate proportional to the size of the difference. In principle, the difference reduces to zero after an infinite

number of iterations. At that stage $\mathbf{u}_k^{tr} = \mathbf{u}_{k-1}^{tr}$, so that:

$$\mathbf{u}_k^{tr} = \mathbf{u}_0^{tr} + \mathbf{P}^- \mathbf{Q}^+ \mathbf{u}_{k-1}^{tr} = \mathbf{u}_0^{tr} + \mathbf{P}^- \mathbf{Q}^+ \mathbf{u}_k^{tr}. \quad (3.28)$$

The difference from the correct solution \mathbf{u} can be found by subtracting (3.18):

$$(\mathbf{u}_k^{tr} - \mathbf{u}^{tr}) = \mathbf{P}^- \mathbf{Q}^+ (\mathbf{u}_k - \mathbf{u}), \quad (3.29)$$

which by inspection of Fig. 3.12 can only be true if $\mathbf{u}_k^{tr} - \mathbf{u}^{tr}$ is sitting at the origin, so that $\mathbf{u}_k^{tr} = \mathbf{u}^{tr}$. It therefore follows that the iterative method in (3.25) and (3.26) converges and, furthermore, converges to the correct solution.

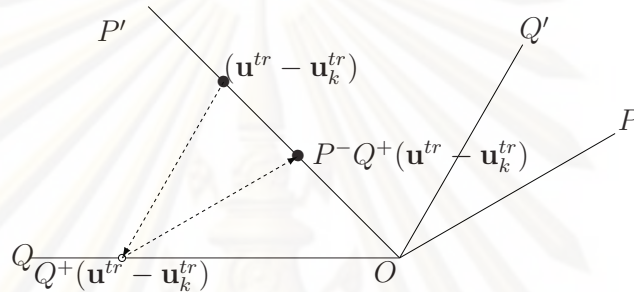


Figure 3.12: The difference between the estimate \mathbf{u}_k^{tr} and solution of the outward field \mathbf{u}^{tr} is the same after projections $\mathbf{P}^- \mathbf{Q}^-$ only if $\mathbf{u}_k^{tr} - \mathbf{u}^{tr} = 0$, showing convergence to correct solution of outward field $\mathbf{u}_k^{tr} = \mathbf{u}^{tr}$.

3.2 Perfect Reflection Problem

3.2.1 Boundary Value Problem in Perfect Reflection

3.2.1.1 Good Conductors

Conductors are solids or liquids in which the flow of current is supported by charge carriers moving at a constant average (drift) velocity through the material. In linear conductors this flow of current can be described at the macroscopic level by Ohm's Law, and is called "conduction" current. In good conductors the flow of current is supported predominantly by conduction current. Other mechanisms of current flow, such as convection current and displacement current, are (by definition) negligible. They can normally be ignored. The idea of a good conductor is a conceptual ideal. In practice only superconductors really fit the description, but many metals also behave like good conductors.

When external electromagnetic fields interact with a good conductor, the external fields drop abruptly to zero at the surface of the conductor. Inside, the internal fields in a good conductor are in principle identically zero. The abrupt change in the value of the field is effected by charges and currents induced in an infinitesimally thin layer immediately inside the conductor. In principle the layer is only infinitesimally thin if the conductivity is infinite, *i.e.* in the case of a superconductor. In the case of real conductors such as metal, the charge and current layer is of non-zero thickness, and the fields inside the conductor decay exponentially from the value at the surface of the conductor to zero value a short distance inside. When external electromagnetic fields interact with a good conductor none of the field is transmitted into the conductor. All of the field is reflected.

3.2.1.2 Boundary Conditions in Perfect Reflection

In case of perfect reflection the boundary conditions in vector form is:

$$\begin{cases} \vec{n} \cdot \epsilon_- (\vec{E}^{in} + \vec{E}^{sc}) = \rho_s \\ \vec{n} \times (\vec{H}^{ic} + \vec{H}^{sc}) = \vec{J}_s \\ \vec{n} \times (\vec{E}^{in} + \vec{E}^{sc}) = 0 \\ \vec{n} \cdot \mu_- (\vec{H}^{in} + \vec{H}^{sc}) = 0 \end{cases}, \quad (3.30)$$

where ϵ_- and μ_- are the electric permittivity and permeability in space region (exterior region). The fields \vec{E}^{in} and \vec{H}^{in} are incident electric and magnetic fields respectively, and \vec{E}^{sc} and \vec{H}^{sc} are reflected electric and magnetic fields, respectively. The behavior of the fields on the interface does not create the transmission; therefore, the incident field reproduces the surface charge density ρ_s the current density \vec{J}_s and also generates the reflected field around the boundary.

The incident and reflected fields on boundary conditions on vector form in (3.30) can be divided into four groups by considering the direction of normal unit identifying the boundary. The first pair of the groups are the normal components of the electric field involving with the charge density, and the tangential components of the magnetic field involving with the current density. And another one are the tangential components of the electric field and the normal components of the magnetic field involving without any source on the boundary. All

these fields are described into Clifford number that satisfying with (2.7):

$$\begin{cases} \mathbf{u}^{in} &= \mu_-^{\frac{1}{2}} \mathbf{H}^{in} \sigma + j \epsilon_-^{\frac{1}{2}} \mathbf{E}^{in} \mathbf{e}_0 \\ \mathbf{u}^{sc} &= \mu_-^{\frac{1}{2}} \mathbf{H}^{sc} \sigma + j \epsilon_-^{\frac{1}{2}} \mathbf{E}^{sc} \mathbf{e}_0 \end{cases}, \quad (3.31)$$

where μ_- and ϵ_- are the electric permittivity and permeability in the exterior. In order to capture two appropriate components of the fields (\vec{E}_t, \vec{H}_n) in Clifford algebra the data projection operators \mathbf{Q}^\pm are employed and their details are described as Appendix C. Therefore, the boundary conditions in (3.30) are rewritten into Clifford formalism with the data projections:

$$\begin{cases} \mathbf{Q}^+ \mathbf{u}^{in} + \mathbf{Q}^+ \mathbf{u}^{sc} &= \zeta(\rho_s, \mathbf{J}_s) \\ \mathbf{Q}^- \mathbf{u}^{in} + \mathbf{Q}^- \mathbf{u}^{sc} &= 0 \end{cases}, \quad (3.32)$$

where $\zeta(\rho_s, \mathbf{J}_s)$ is the unknown function of the surface charge and current densities. The boundary conditions for solving the reflected field is:

$$\begin{aligned} \mathbf{Q}^- \mathbf{u}^{sc} &= \mu_-^{\frac{1}{2}} \mathbf{H}_n^{sc} \sigma + j \epsilon_-^{\frac{1}{2}} \mathbf{E}_t^{sc} \mathbf{e}_0 \\ &= - \left(\mu_-^{\frac{1}{2}} \mathbf{H}_n^{in} \sigma + j \epsilon_-^{\frac{1}{2}} \mathbf{E}_t^{in} \mathbf{e}_0 \right) \\ &= -\mathbf{Q}^- \mathbf{u}^{in} \end{aligned} \quad (3.33)$$

3.2.2 Normal Solutions for Perfect Reflection

When the incident field that is produced by any actual source in the exterior region arrives onto the boundary, this field induces the charge and current densities along the interface. These densities that are equivalent sources generate the scattered or reflected field around the boundary in the exterior region. Their characteristics of these fields are satisfied with the Maxwell-Dirac equation in form of Hardy projections (2.51). When \mathbf{u}^- is used instead of \mathbf{u}^{sc} , and \mathbf{u}^+ is zero since the transmitted field does not appear. Therefore, the total field on the boundary \mathbf{u} is \mathbf{u}^{sc} ,

$$\begin{cases} \mathbf{P}^- \mathbf{u}^{sc} &= \mathbf{u}^{sc} \\ \mathbf{P}^+ \mathbf{u}^{sc} &= 0 \end{cases}. \quad (3.34)$$

The boundary conditions of perfect reflected in (3.33) can be shown as

$$\begin{cases} \mathbf{f} &= \mathbf{Q}^+ \mathbf{u}^{sc} \\ \mathbf{g} &= \mathbf{Q}^- \mathbf{u}^{sc} \end{cases}, \quad (3.35)$$

where \mathbf{f} and \mathbf{g} are Clifford functions. The function \mathbf{f} is used to describe the normal components of the electric field and the tangential field of the magnetic field $(\mathbf{E}_n^{sc}, \mathbf{H}_t^{sc})$, and it can be used to evaluate the charge and current densities on the boundary. The function \mathbf{g} that is used to describe the normal components of the magnetic field and the tangential field of the electric field $(\mathbf{H}_n^{sc}, \mathbf{E}_t^{sc})$ can evaluate without using complicated techniques. Therefore, the function \mathbf{g} that is some parts of the reflected field is employed as the input data in order to solve its full parts.

The Maxwell-Dirac equation in the forms of Hardy projections (3.34) and boundary conditions (3.35) are described together on Banach space in order to construct the solution of the inward field. In here, only two equations are chosen for formulating the linear system:

$$\begin{cases} \mathbf{P}^- \mathbf{u}^{sc} &= \mathbf{u}^{sc} \\ \mathbf{g} &= \mathbf{Q}^- \mathbf{u}^{sc} \end{cases}. \quad (3.36)$$

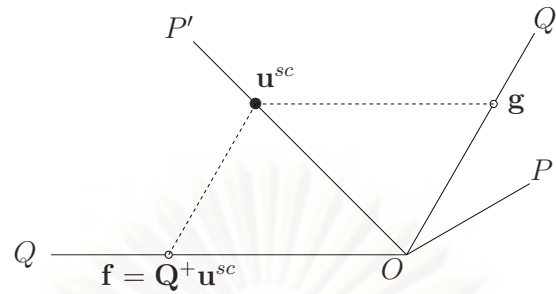


Figure 3.13: Solution of Maxwell's equations as intersection in Banach space of dotted line through boundary conditions g and coordinate axis OP, OP' for the reflected field in case of perfect reflection.

In Banach space this means the solution u^{sc} lies somewhere along the dotted lines parallel to the OQ -axis and through function g on the OQ' -axis, as shown in Fig. 3.13. Simple geometry dictates that the intersection between the dotted line and the OP' -axis gives a unique solution u^{sc} as long as the OP' -axis and the OQ' -axis are not coincident. This is known already, since from their definitions the projections Q^- and P^- are definitely not the same.

The solution u^{sc} can be represented in terms of Cartesian components in either the P -system or Q -system:

$$\begin{cases} u^{sc} = u^{sc} + 0 & P\text{-system} \\ u^{sc} = f + g & Q\text{-system} \end{cases}, \quad (3.37)$$

where $f = Q^+u^{sc}$ (as shown in Fig. 3.13) is the missing half of the boundary field.

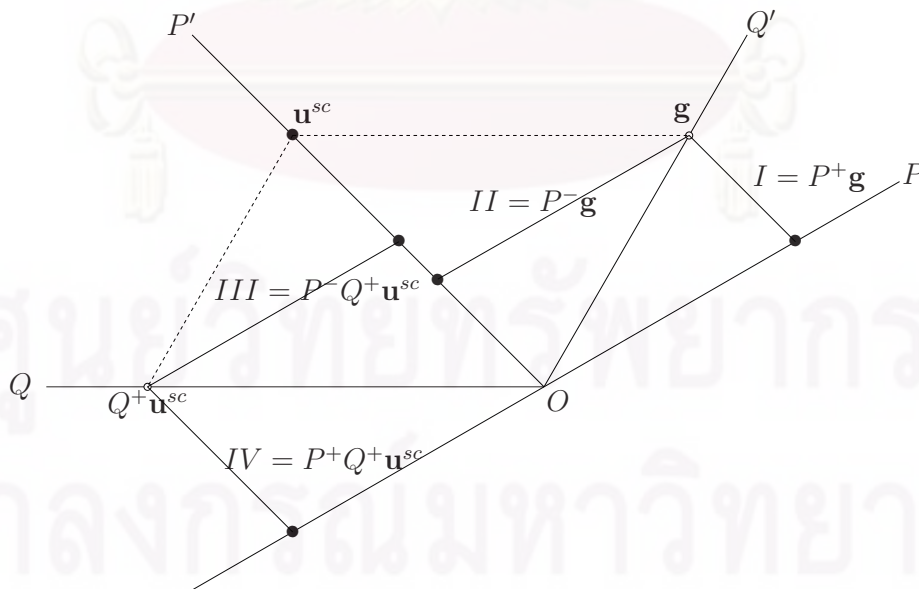


Figure 3.14 Construction for solution of reflected field given data $g = Q^-u^{sc}$.

A solution in either system can be formulated by inspection of Fig. 3.14. The figure shows the solution \mathbf{u}^{sc} on the OP' -axis, split into two components $\mathbf{Q}^+\mathbf{u}^{sc}$ and $\mathbf{g} = \mathbf{Q}^-\mathbf{u}^{sc}$ in the Q -system, each of which are themselves further split into two more components back in the P -system. All of the triangles and rectangles in the figure which appear by casual inspection to be similar, are indeed similar.

The value of the four components produced in the P -system by the splitting process are represented in Fig. 3.14 by the four line segments I, II, III and IV. Adding these line segments as vectors produces a resultant vector from the origin to the solution \mathbf{u}^{sc} :

$$I + II + III + IV = \mathbf{P}^+\mathbf{g} + \mathbf{P}^-\mathbf{g} + \mathbf{P}^-\mathbf{Q}^+\mathbf{u}^{sc} + \mathbf{P}^+\mathbf{Q}^+\mathbf{u}^{sc} = \mathbf{u}^{sc}. \quad (3.38)$$

Eq. (3.38) is actually rather trivial, and rather useless in its own right since it is easily reduced to either of the forms in (3.37). Of more interest and more immediate use its projections into the P system. Projection onto the two axes of the P -system gives:

$$\begin{cases} \mathbf{P}^-\mathbf{Q}^+\mathbf{u}^{sc} + \mathbf{P}^-\mathbf{g} = \mathbf{u}^{sc} \\ \mathbf{P}^+\mathbf{Q}^+\mathbf{u}^{sc} + \mathbf{P}^+\mathbf{g} = 0 \end{cases}. \quad (3.39)$$

where has been made of $(\mathbf{P}^\pm)^2 = \mathbf{P}^\pm$, $\mathbf{P}^\pm\mathbf{P}^\mp = 0$ and $\mathbf{P}^-\mathbf{u}^{sc} = \mathbf{u}^{sc}$.

Inspection of Fig. 3.14 shows that $\mathbf{P}^-\mathbf{Q}^+\mathbf{u}^{sc} \neq \mathbf{u}^{sc}$ unless the OP' -axis is coincident with the OQ' -axis; a situation which has already been ruled out. It is therefore possible to subtract $\mathbf{P}^-\mathbf{Q}^+\mathbf{u}^{sc}$ from both sides of (3.39) to obtain:

$$\mathbf{P}^-\mathbf{g} = (\mathbf{I} - \mathbf{P}^-\mathbf{Q}^+)\mathbf{u}^{sc}, \quad (3.40)$$

with the assurance that both sides are non-zero.

The right hand side contains the product of two singular operators $\mathbf{P}^-\mathbf{Q}^+$, itself singular. The sum of this product with the (non-singular) identity operator gives the term $\mathbf{I} - \mathbf{P}^-\mathbf{Q}^+$ which is sure to be non-singular. It is therefore possible to invert this term, giving:

$$\mathbf{u}^{sc} = (\mathbf{I} - \mathbf{P}^-\mathbf{Q}^+)^{-1} \mathbf{P}^-\mathbf{g}. \quad (3.41)$$

This is the solution of reflected field in case of perfect reflection problem. The $(\mathbf{I} - \mathbf{P}^-\mathbf{Q}^+)$ that is the compound operators can simulate its inversion similar to the inversion of $(\mathbf{I} - \mathbf{P}^+\mathbf{Q}^+)$ as (3.11).

3.2.3 Iterative Solution for Perfect Reflection

In principle the solution of the reflected field \mathbf{u}^{sc} in (3.41) need not involve a direct inversion of the compound operator $(\mathbf{I} - \mathbf{P}^- \mathbf{Q}^+)$. An iterative procedure can be used, as shown in Fig. 3.15.

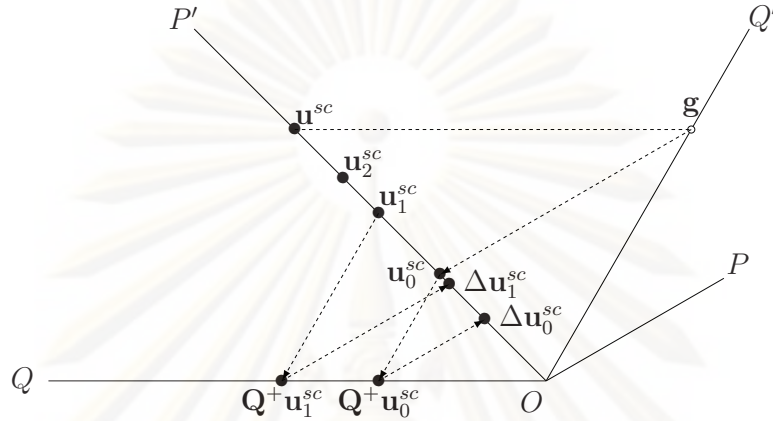


Figure 3.15: Iterative solution of reflected field. Adding correction $\Delta \mathbf{u}_0^{sc}$ to initial estimate \mathbf{u}_0^{sc} gives improved estimate \mathbf{u}_1^{sc} , and adding $\Delta \mathbf{u}_1^{sc}$ to \mathbf{u}_0^{sc} gives \mathbf{u}_2^{sc} .

Firstly, an initial estimate:

$$\mathbf{u}_0^{sc} = \mathbf{P}^- \mathbf{g}, \quad (3.42)$$

is obtained by projecting the boundary conditions \mathbf{g} onto the OP' -axis. A correction $\Delta \mathbf{u}_0^{sc} = \mathbf{P}^- \mathbf{Q}^+ \mathbf{u}_0^{sc}$ is calculated by projecting \mathbf{u}_0^{sc} first onto the OQ -axis and then back onto the OP' -axis. A new estimate $\mathbf{u}_1^{sc} = \mathbf{u}_0^{sc} + \Delta \mathbf{u}_0^{sc}$ is obtained by adding the correction to initial estimate. As a second iteration, an improved correction $\Delta \mathbf{u}_1^{sc} = \mathbf{P}^- \mathbf{Q}^+ \mathbf{u}_1^{sc}$ is used to give a better estimate $\mathbf{u}_2^{sc} = \mathbf{u}_0^{sc} + \Delta \mathbf{u}_1^{sc}$. Note that the correction is always added to the initial estimate \mathbf{u}_0^{sc} , not to the most recent estimate. The general form of the k^{th} estimate \mathbf{u}_k^{sc} is:

$$\mathbf{u}_k^{sc} = \mathbf{u}_0^{sc} + \mathbf{P}^- \mathbf{Q}^+ \mathbf{u}_{k-1}^{sc} = \sum_{m=0}^k (\mathbf{P}^- \mathbf{Q}^+)^m \mathbf{u}_0^{sc}. \quad (3.43)$$

This is iterative solution of reflected field in case of perfect reflection. The solution takes the form of Neumann iteration, with initial guess \mathbf{u}_0 calculated directly from the boundary conditions \mathbf{g} . A different field $\mathbf{u}'_0 = \mathbf{P}^- \mathbf{v}$ could also be chosen for an initial guess. This would make sense if it is known that \mathbf{u}'_0 is closer to the solution than \mathbf{u}_0 .

Moreover, the convergence of the iterative solution in (3.43) is discussed in here. The difference between consecutive estimates is:

$$\mathbf{u}_k^{sc} - \mathbf{u}_{k-1}^{sc} = (\mathbf{P}^- \mathbf{Q}^+)^k \mathbf{u}_0^{sc}, \quad (3.44)$$

which (as shown in Fig. 3.16) approaches zero as k approaches infinity at a rate proportional to the size of the difference. In principle, the difference reduces to zero after an infinite number of iterations. At that stage $\mathbf{u}_k^{sc} = \mathbf{u}_{k-1}^{sc}$, so that:

$$\mathbf{u}_k^{sc} = \mathbf{u}_0^{sc} + \mathbf{P}^- \mathbf{Q}^+ \mathbf{u}_{k-1}^{sc} = \mathbf{u}_0^{sc} + \mathbf{P}^- \mathbf{Q}^+ \mathbf{u}_k^{sc}. \quad (3.45)$$

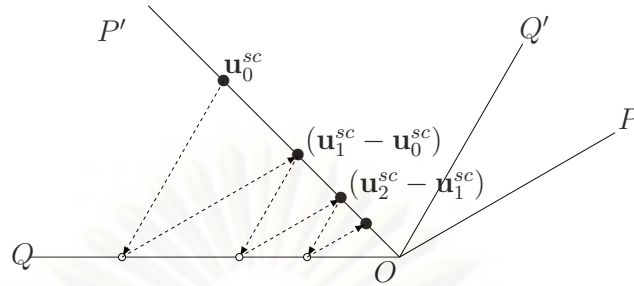


Figure 3.16: The difference of the solutions of reflected fields $\mathbf{u}_k^{sc} - \mathbf{u}_{k-1}^{sc}$ between consecutive estimates of solution \mathbf{u}^{sc} approaching zero as the iteration proceeds.

The difference from the correct solution \mathbf{u}^{sc} can be found by subtracting (3.40):

$$(\mathbf{u}_k^{sc} - \mathbf{u}^{sc}) = \mathbf{P}^- \mathbf{Q}^+ (\mathbf{u}_k^{sc} - \mathbf{u}^{sc}), \quad (3.46)$$

which by inspection of Fig. 3.17 can only be true if $\mathbf{u}_k^{sc} - \mathbf{u}^{sc}$ is sitting at the origin, so that $\mathbf{u}_k^{sc} = \mathbf{u}^{sc}$. It therefore follows that the iterative method in (3.42) and (3.43) converges and, furthermore, converges to the correct solution.

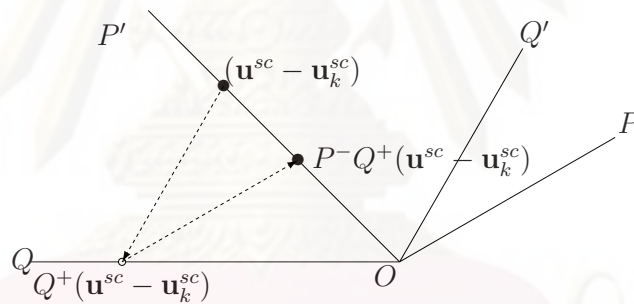


Figure 3.17: The difference between estimate \mathbf{u}_k^{sc} and solution of reflected field \mathbf{u}^{sc} is the same after projections $\mathbf{P}^- \mathbf{Q}^-$ only if $\mathbf{u}_k^{sc} - \mathbf{u}^{sc} = 0$, showing convergence to correct solution of reflected field $\mathbf{u}_k^{sc} = \mathbf{u}^{sc}$.

ศูนย์วิทยทรัพยากร
จุฬาลงกรณ์มหาวิทยาลัย

CHAPTER IV

METHODOLOGY

In this chapter, all proposed integral operators are applied to boundary element techniques. In order to realize a numerical solution according to calculate the field by using reproducing formula, it is necessary to choose a representation for the boundary Σ and the field u on the boundary which conforms to:

- the geometrical requirements of the particular application
- the known physical behavior of the field.

The shape of the boundary should be simple for approximation, since the error made by modeling the boundary can be fixed easier. The field on the boundary should be approximated with the appropriated function but being not far away from the theory [52].

4.1 Geometry of Boundary

Most electromagnetic problems in electrical engineering involve macroscopic objects with either planar or curved smooth surfaces meeting at sharp corners or edges. On a smooth surface the unit normal vector varies continuously from point to point. Edges and corners are points where two or more smooth surfaces meet with a loss of continuity in the normal. When integrating over surfaces which meet at edges and corners the integral should be carried piecewise, carefully using the normal appropriate to each individual piece. That means edges, for example, are incorporated into the overall integral two lines, with different values of normal.

Surfaces which are smooth apart from a finite number of edges and corner are known as Lipschitz surfaces. Fractal surfaces have infinite number of edges and corners, and are therefore not Lipschitz surfaces. Moreover, surfaces which have cusps, points at which the normal abruptly reverse (180 degrees) in direction, are also not Lipschitz surfaces.

The Clifford formulation and solution of Maxwell's equations presented here is mathematically proven as valid for Lipschitz surface. The same cannot be said for fractal surfaces, or surfaces with cusps. It is not clear in those case how to formulate a solution.

For many physical problems it is possible to approximate a curved smooth surface sufficiently well by a surface constructed from polygonal element (facets). However, that is not possible for problems involving electromagnetic phenomena. Electromagnetic radiation likes nothing more than colliding with edges and corners, breaking up, and scattering all directions. If smooth curved surfaces are required they must be constructed as such, from smooth elements meet without a discontinuity in the normal. This avoids art-factual scattering from edges in those places where none should exist.

4.1.1 Boundary

Boundary is defined by Cartesian system, because it is the original system which the mathematicians are use to prove the kernel of reproducing formula. Moreover, it is to help

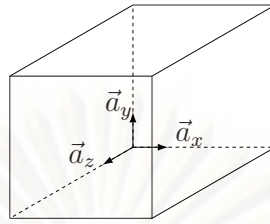


Figure 4.1 The six surfaces consist of the cube as boundary Σ .

more confident for investigating the formulation of the integral equation on previous section. The most appropriated boundary on Cartesian system is surface of a cube, as is indicated in Fig. 4.1. They consist of six planes. Therefore, this shape of the boundary is the best boundary for checking the reproducing formula and the geometric operator.

4.1.2 Discretisation of Boundary

The boundary is represented by a certain number of elements as Fig. 4.2. In here, all segments which are divided from the boundary Σ are the rectangular elements. Since they are perfectly matching with boundary Σ , the errors of the integral equations do not cause by the discretisation of the geometric boundary.

The position of points on the boundary can be encoded as vectors into $S\Lambda^1$ of a Clifford number \mathbf{x} . Individual elements (pieces) of the boundary are in general free to assume any arbitrary orientation with respect to whatever directions are used for reference. This case is shown in Fig. 4.3(a) where the reference directions are depicted by the coordinates x, y, z (common to all elements), and the orientation of a single rectangular boundary element is depicted by the local coordinates x_l, y_l, z_l fixed in one of its corners.

In a numerical implementation it is often convenient to initially treat all elements (pieces) of the boundary in terms of their own local coordinates, and to later convert any

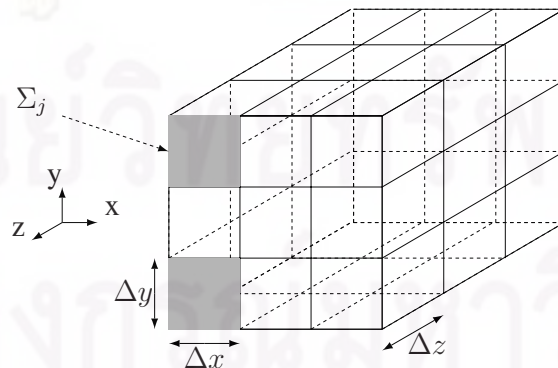


Figure 4.2 Discretisation of boundary Σ_j .

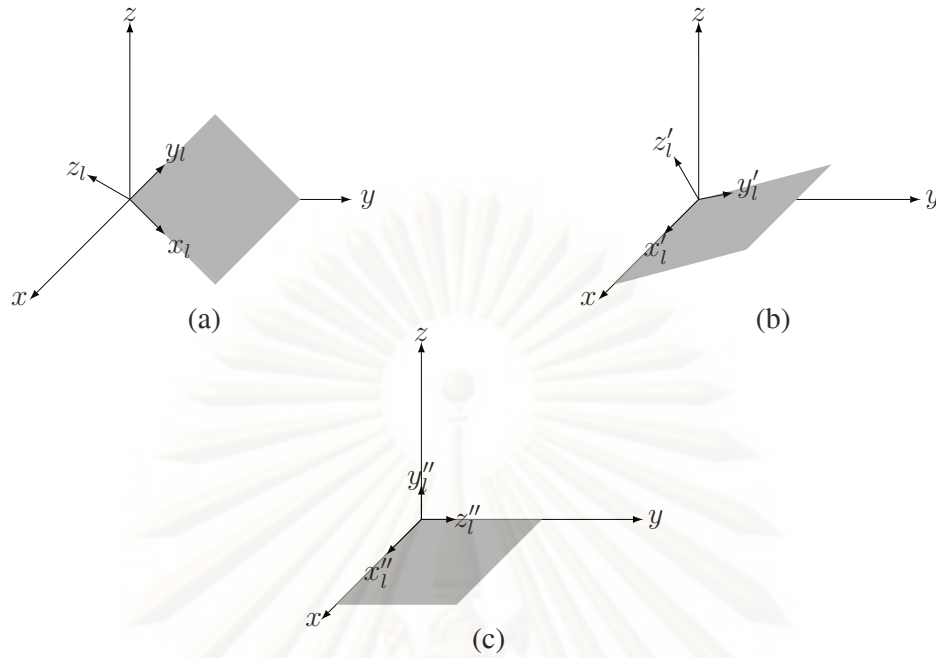


Figure 4.3 Rotations to bring local coordinates into alignment with common coordinates.

results from these coordinate systems to common set of coordinates. The conversation of results operators which have the effect of rotating each element until its local coordinates move into alignment with the common coordinates.

Fig. 4.3(b) shows the same element as in Fig. 4.3(a), after applying a rotation operator Θ_1 chosen to transport the local x-axis x_l onto a new vector x'_l lying along the common x-axis. At the same time, the local y and z axes are transported onto vectors y'_l and z'_l , both lying in the common yz -plane $x = 0$:

$$\begin{cases} x_l \rightarrow x'_l = \Theta_1 x_l & \text{on the x-axis} \\ y_l \rightarrow y'_l = \Theta_1 y_l & \text{on the y-axis} \\ z_l \rightarrow z'_l = \Theta_1 z_l & \text{on the z-axis} \end{cases} \quad (4.1)$$

Fig. 4.3(c) shows the element after applying a further rotation operator Θ_2 chosen to transport the local y -axis y'_l onto a new vector y''_l lying along the common y -axis. At the same time, the local x and z axes are transported onto x''_l and z''_l lying respectively along the common x and z axes:

$$\begin{cases} x'_l \rightarrow x''_l = \Theta_2 x'_l & \text{on the x-axis} \\ y'_l \rightarrow y''_l = \Theta_2 y'_l & \text{on the y-axis} \\ z'_l \rightarrow z''_l = \Theta_2 z'_l & \text{on the z-axis} \end{cases} \quad (4.2)$$

The rotation operators Θ_1 and Θ_2 can each be constructed from any pair of unit vector $\mathbf{n}_1, \mathbf{n}_2$ lying separated in the plane of rotation by half the angle of rotation. For Θ_1 an appropriate choice is:

$$\begin{cases} \mathbf{n}_1 = \mathcal{U}(x_l) \\ \mathbf{n}_2 = \mathcal{U}(\mathcal{U}(x_l) + \mathcal{U}(x)) = \mathcal{U}(\mathcal{U}(x_l) + \mathbf{e}_1) \end{cases}, \quad (4.3)$$

where $\mathcal{U}(r)$ is a unit vector $\mathbf{r}/|\mathbf{r}|$ and the Clifford unit \mathbf{e}_1 has been taken to represent the x -axis. For Θ_2 an appropriate choice is:

$$\begin{cases} \mathbf{n}_1 = \mathcal{U}(y'_l) \\ \mathbf{n}_2 = \mathcal{U}(\mathcal{U}(y'_l) + \mathcal{U}(y)) = \mathcal{U}(\Theta_1 \mathcal{U}(y_l) + \mathbf{e}_2) \end{cases}, \quad (4.4)$$

where the Clifford unit e_2 has been taken to represent the y -axis.

4.2 Boundary Element Method

There are three integral operators such as Cauchy extension operator (2.42), Cauchy integral operator (2.43) and Hardy projection operators (2.51) that can be discretized to system of equations from which the boundary fields can be found. The cube that is discretized boundary in three dimensions, and its surface is divided into $N = 6 \times M^2$ segments or elements as shown Fig. 4.2.

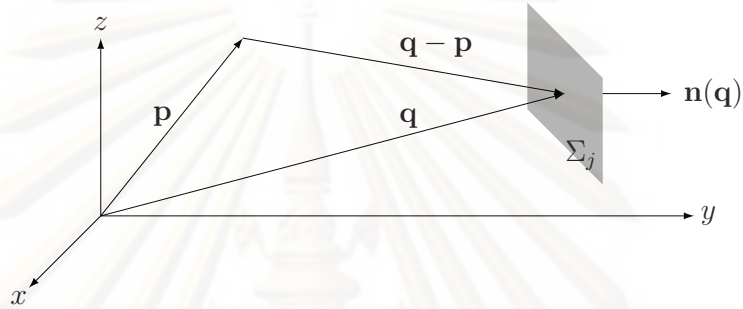


Figure 4.4 Element of boundary Σ_j with local coordinates on face.

4.2.1 Discretization of Cauchy extension operator

Cauchy extension operator (2.42) that is used to determine the fields inside and outside boundary can be constructed from the fields on the N -element of the boundary.

$$\begin{aligned}
 \mathbf{C}\mathbf{u}(\mathbf{p} \in \Omega^+ \cup \Omega^-) &= \int_{\Sigma} \mathbf{E}_k(\mathbf{q} - \mathbf{p}) \mathbf{n}(\mathbf{q}) \mathbf{u}(\mathbf{q}) d\sigma(\mathbf{q}) \\
 &= \sum_{j=1}^N \int_{\Sigma_j} \mathbf{E}_k(\mathbf{q} - \mathbf{p}) \mathbf{n}(\mathbf{q}) \mathbf{u}(\mathbf{q}) d\sigma(\mathbf{q}) \\
 &= \sum_{j=1}^N \mathbf{F}_j(\mathbf{p}),
 \end{aligned} \tag{4.5}$$

where Σ_j is the boundary of the 'j' element. The field F_j generated at any point \mathbf{p} by the field at the point \mathbf{q} inside the element of the boundary Σ_j shown in Fig. 4.4:

$$\mathbf{F}_j(\mathbf{p}) = \int_{\Sigma_j} \mathbf{E}_k(\mathbf{q} - \mathbf{p}) \mathbf{n}(\mathbf{q}) \mathbf{u}(\mathbf{q}) d\sigma(\mathbf{q}). \tag{4.6}$$

The fields on its surface generate a different value for the field at the point \mathbf{p} after translating and rotating that surface.

- **Consider first a translation:**

$$\mathbf{q}' = \mathbf{q} - \mathbf{p}, \quad (4.7)$$

which brings the point \mathbf{p} to origin and transports the element of the boundary Σ_j along with the fields on its surface in the same direction by the same distance. After translation the field \mathbf{F}'_j generated at any point \mathbf{p}' can be calculated by applying (4.6):

$$\mathbf{F}'_j(\mathbf{p}') = \int_{\Sigma'_j} \mathbf{E}'_k(\mathbf{q}' - \mathbf{p}') \mathbf{n}'(\mathbf{q}') \mathbf{u}'(\mathbf{q}') d\sigma'(\mathbf{q}'). \quad (4.8)$$

The values of all the primed variables can be obtained directly from the corresponding unprimed variables; i.e. those employed prior to translation:

$$\begin{cases} \Sigma'_{\mathbf{q}'} & = \Sigma_{\mathbf{q}} & = \Sigma_{\mathbf{q}'+\mathbf{p}} \\ \mathbf{E}'_k(\mathbf{q}'_1 - \mathbf{q}'_2) & = \mathbf{E}_k(\mathbf{q}_1 - \mathbf{q}_2) & = \mathbf{E}_k(\mathbf{q}'_1 - \mathbf{q}'_2) \\ \mathbf{n}'(\mathbf{q}') & = \mathbf{n}(\mathbf{q}) & = \mathbf{n}(\mathbf{q}' + \mathbf{p}) \\ \mathbf{u}'(\mathbf{q}') & = \mathbf{u}(\mathbf{q}) & = \mathbf{u}(\mathbf{q}' + \mathbf{p}) \\ d\sigma'(\mathbf{q}') & = d\sigma(\mathbf{q}) & = d\sigma(\mathbf{q}' + \mathbf{p}). \end{cases} \quad (4.9)$$

Note that the value of the original field can be obtained after translation by choosing $\mathbf{p}' = 0$:

$$\mathbf{F}_j(\mathbf{p}) = \mathbf{F}'_j(0) = \int_{\Sigma'_j} \mathbf{E}'_k(\mathbf{q}') \mathbf{n}'(\mathbf{q}') \mathbf{u}'(\mathbf{q}') d\sigma'(\mathbf{q}'). \quad (4.10)$$

- **Consider second a rotation**

which brings the local axes x_l, y_l, z_l into a chosen orientation and transports the element of the boundary Σ'_j along with the fields on its surface in the same direction by the same angle. After rotation the field \mathbf{F}''_j generated at any point \mathbf{p}'' can be calculated by applying (4.6):

$$\mathbf{F}''_j(\mathbf{p}'') = \int_{\Sigma''_j} \mathbf{E}''_k(\mathbf{q}'' - \mathbf{p}'') \mathbf{n}''(\mathbf{q}'') \mathbf{u}''(\mathbf{q}'') d\sigma''(\mathbf{q}''). \quad (4.11)$$

The values of all of doubly primed variables can be obtained directly from the corresponding singly primed variables, i.e. those employed immediately prior to rotation:

$$\begin{cases} \Sigma''_{\mathbf{q}''} & = \Theta \Sigma'_{\mathbf{q}'} & = \Theta \Sigma'_{\Theta^{-1}\mathbf{q}''} \\ \mathbf{E}''_k(\mathbf{q}'') & = \Theta \mathbf{E}'_k(\mathbf{q}') & = \mathbf{E}'_k(\mathbf{q}'') \\ \mathbf{n}''(\mathbf{q}'') & = \Theta \mathbf{n}'(\mathbf{q}') & = \Theta \mathbf{n}'(\Theta^{-1}\mathbf{q}'') \\ \mathbf{u}''(\mathbf{q}'') & = \Theta \mathbf{u}'(\mathbf{q}') & = \Theta \mathbf{u}'(\Theta^{-1}\mathbf{q}'') \\ d\sigma''(\mathbf{q}'') & = d\sigma'(\mathbf{q}') & = d\sigma'(\Theta^{-1}\mathbf{q}''). \end{cases} \quad (4.12)$$

Note that a rotated version of the original field can be obtained after rotation by choosing $\mathbf{p}'' = 0$:

$$\Theta \mathbf{F}_j(\mathbf{p}) = \Theta \mathbf{F}'_j(0) = \mathbf{F}''_j(0) = \int_{\Sigma''_j} \mathbf{E}''_k(\mathbf{q}'') \mathbf{n}''(\mathbf{q}'') \mathbf{u}''(\mathbf{q}'') d\sigma''(\mathbf{q}''). \quad (4.13)$$

The rotation Θ can be chosen separately to bring the local coordinates for each element of boundary Σ_j into alignment with the common coordinates. Adopting this choice for the front face of Σ_j gives $d\sigma''(\mathbf{q}'') = dx dy$, $\mathbf{n}''(\mathbf{q}'') = \mathbf{e}_3$ and:

$$\begin{aligned}
\mathbf{F}_j(\mathbf{p}) &= \Theta^{-1} \int_{\Sigma_j''} \mathbf{E}_k''(\mathbf{q}'') \mathbf{e}_3 \mathbf{u}''(\mathbf{q}'') dx dy \\
&= \Theta^{-1} \int_{\Sigma_j''} \mathbf{E}_k'(\mathbf{q}'') \mathbf{e}_3 \Theta \mathbf{u}'(\Theta^{-1} \mathbf{q}'') dx dy \\
&= \Theta^{-1} \int_{\Sigma_j''} \mathbf{E}_k(\mathbf{q}'') \mathbf{e}_3 \Theta \mathbf{u}(\mathbf{p} + \Theta^{-1} \mathbf{q}'') dx dy \\
&= \int_{\Sigma_j''} \Theta^{-1} \{ \mathbf{E}_k(\mathbf{q}'') \mathbf{e}_3 \} \mathbf{u}(\mathbf{p} + \Theta^{-1} \mathbf{q}'') dx dy \\
&= \int_{\Sigma_j''} \Theta^{-1} \{ \mathbf{E}_k(\mathbf{q}'') \mathbf{e}_3 \} \mathbf{u}(\mathbf{q}) dx dy,
\end{aligned} \tag{4.14}$$

where the Clifford unit \mathbf{e}_3 has been taken to represent the z -axis.

Equation (4.14) can be used to calculate the field generated by all Σ_j , simply by choosing different values for the rotation Θ —each to bring the local coordinates into alignment with the common coordinates.

The field $\mathbf{u}(\mathbf{q})$ on each element is approximated by a bilinear function:

$$\mathbf{u}(\mathbf{q}) = \mathbf{u}(\mathbf{q}(x, y)) = \sum_{i=1}^4 \mathbf{A}_{ij} f_i(x, y), \tag{4.15}$$

in a local coordinates system x, y . The coefficients \mathbf{A}_{ij} are the values of the field at the four corners, and the function f_i which interpolate the field elsewhere are:

$$f_i(x, y) = \begin{cases} (1 - x/\ell)(1 - y/\ell) & ; i = 1 \\ (x/\ell)(1 - y/\ell) & ; i = 2 \\ (x/\ell)(y/\ell) & ; i = 3 \\ (1 - x/\ell)(y/\ell) & ; i = 4 \end{cases}, \tag{4.16}$$

for an element with edges of the length l .

It is always difficult when choosing a basis to know whether it is a good one for any particular problem. The judgement of what is good and what is not good lies in part in mathematical rigour and in part in the accuracy required in any particular application. The mathematical rigour tells us that by choosing for the functions on the boundary a basis which spans either the L^2 functional space [62] or the \mathcal{X}^2 functional space [58] leads to results with a predictable behavior. In the first case the solutions for the functions on the boundary are guaranteed to be square integrable, *i.e.* finite energy but accommodating isolated integrable singularities. In the second case the same condition applies for the fields *off* the boundaries.

Here, the particular application needs only to meet the accuracy of other published numerical solutions in order to verify, to that accuracy, that the technique described here is at least as viable as any other. In this situation it is an expedient to choose the simplest basis which allows us to meet that stated objective. The choice here, then, is to adopt a bilinear

basis. This basis is a subset of the L^2 functional space. It resides fully inside but does not span all of it. In particular, the bilinear basis does not accommodate singularities of any kind. From a practical viewpoint that means the field at certain points is likely to be more smooth than if an L^2 basis were chosen.

For the case of perfectly transmissive objects this makes no difference, since the field is everywhere smooth; there are no singularities. That is the reason the tests in Section 3.1 on perfectly transmissive objects are important. For the case of perfectly reflective objects it is likely that the fields at the corners and edges, if closely examined, have a lower accuracy than at other points. It is for that reason the comparative tests in Sections 3.2 to other published results are so important.

The integrals $\mathbf{F}_j(\mathbf{p})$ in (4.14) over each element are carried in the local coordinate system.

$$\mathbf{F}_j(\mathbf{p}) = \sum_{i=1}^4 \mathbf{G}_{ij}(\mathbf{p}) \mathbf{A}_{ij}, \quad (4.17)$$

where

$$\mathbf{G}_{ij}(\mathbf{p}) = \int_{\Sigma_j''} \Theta^{-1} \{ \mathbf{E}_k(\mathbf{q}''(x, y)) \mathbf{e}_3 \} f_i(x, y) dx dy. \quad (4.18)$$

Two-dimensional Gauss quadrature integration for rectangular region [64] is used to here to evaluate these value numerically,

$$\left\{ \begin{array}{l} \mathbf{G}_{ij}(\mathbf{p}) = \sum_{\alpha=1}^{n_g} \sum_{\beta=1}^{n_g} \Theta^{-1} \{ \mathbf{E}_k(\mathbf{q}''(x(\zeta_\alpha, \eta_\beta), y(\zeta_\alpha, \eta_\beta))) \mathbf{e}_3 \} \\ f_i(x(\zeta_\alpha, \eta_\beta), y(\zeta_\alpha, \eta_\beta)) J w_\alpha w_\beta \end{array} \right., \quad (4.19)$$

where ζ_α, η_β are integration point coordinates, and w_α, w_β are the weight factors, and J is the Jacobian of common and local coordinates.

4.2.2 Discretization of Cauchy integral operator

Cauchy integral operator (2.43) that is used to determine the field on boundary in order to make the reflection operator for solving the boundary field problem. It can be constructed from the field on the N-element of the boundary,

$$\begin{aligned} \mathbf{C}_\Sigma \mathbf{u}(\mathbf{p} \in \Sigma) &= 2 \text{ p.v.} \int_{\Sigma} \mathbf{E}_k(\mathbf{q} - \mathbf{p}) \mathbf{n}(\mathbf{q}) \mathbf{u}(\mathbf{q}) d\sigma(\mathbf{q}) \\ &= \sum_{j=1}^N 2 \text{ p.v.} \int_{\Sigma_j} \mathbf{E}_k(\mathbf{q} - \mathbf{p}) \mathbf{n}(\mathbf{q}) \mathbf{u}(\mathbf{q}) d\sigma(\mathbf{q}) \\ &= \sum_{j=1}^N \mathbf{F}_{\Sigma_j}(\mathbf{p}), \end{aligned} \quad (4.20)$$

where Σ_j is the boundary of the 'j' element. The field F_{Σ_j} generated at any point \mathbf{p} by the field at the point \mathbf{q} inside the element of the boundary Σ_j shown in Fig. 4.4

$$\mathbf{F}_{\Sigma_j}(\mathbf{p}) = 2 \text{ p.v.} \int_{\Sigma_j} \mathbf{E}_k(\mathbf{q} - \mathbf{p}) \mathbf{n}(\mathbf{q}) \mathbf{u}(\mathbf{q}) d\sigma(\mathbf{q}). \quad (4.21)$$

The fields on its surface generate a different value for the field at the point \mathbf{p} after translating and rotating that surface. Therefore, the transformation of $\mathbf{F}_{\Sigma,j}$ from the local coordinates to the common coordinate is similar to $\mathbf{F}_{\Sigma,j}$ in (4.14) by using the translation and rotation,

$$\mathbf{F}_{\Sigma,j}(\mathbf{p}) = 2 \text{ p.v.} \int_{\Sigma_j''} \Theta^{-1} \{ \mathbf{E}_k(\mathbf{q}'') \mathbf{e}_3 \} \mathbf{u}(\mathbf{q}) dx dy, \quad (4.22)$$

where the Clifford unit \mathbf{e}_3 has been taken to represent the z-axis. Moreover, the field $\mathbf{u}(\mathbf{q})$ on each element is approximated by a bilinear that is same as (4.15). Therefore, the integral $\mathbf{F}_{\Sigma,j}$ in (4.22) over each element are carried in the local coordinate system,

$$\mathbf{F}_{\Sigma,j}(\mathbf{p}) = \sum_{i=1}^4 \mathbf{G}_{\Sigma,ij}(\mathbf{p}) \mathbf{A}_{ij}, \quad (4.23)$$

where,

$$\mathbf{G}_{\Sigma,ij}(\mathbf{p}) = 2 \text{ p.v.} \int_{\Sigma_j''} \Theta^{-1} \{ \mathbf{E}_k(\mathbf{q}''(x, y)) \mathbf{e}_3 \} f_i(x, y) dx dy. \quad (4.24)$$

Two-dimensional Gauss quadrature integration for rectangular region [64] is used to here to evaluate these value numerically.

$$\left\{ \begin{array}{l} \mathbf{G}_{\Sigma,ij}(\mathbf{p}) = 2 \sum_{\alpha=1}^{n_g} \sum_{\beta=1}^{n_g} \Theta^{-1} \{ \mathbf{E}_k(\mathbf{q}''(x(\zeta_\alpha, \eta_\beta), y(\zeta_\alpha, \eta_\beta))) \mathbf{e}_3 \} \\ f_i(x(\zeta_\alpha, \eta_\beta), y(\zeta_\alpha, \eta_\beta)) J w_\alpha w_\beta \end{array} \right., \quad (4.25)$$

where ζ_α, η_β are integration point coordinates, and w_α, w_β are the weight factors, and J is the Jacobian of common and local coordinates.

For a single step in the iteration the Cauchy integral is calculated at every point \mathbf{p}_m at the corners of every element. However, it is only necessary to evaluate the geometric components $\mathbf{G}_{\Sigma,ij}(\mathbf{p}_m)$ once, since the entire set of values does not change as the iteration proceeds. Gauss-Legendre integration [64] is used here to evaluate these values numerically. The calculations required for each iteration then amount to the product of a matrix $\mathbf{G}'_j(\mathbf{p}_m)$ and a vector \mathbf{A}'_j :

$$\mathbf{C}_\Sigma \mathbf{u}(\mathbf{p}_m) = \sum_{j=1}^N \sum_{i=1}^4 \mathbf{G}_{\Sigma,ij}(\mathbf{p}_m) \mathbf{A}_{ij} = \sum_{j=1}^{N+2} \mathbf{G}'_{\Sigma,j}(\mathbf{p}_m) \mathbf{A}'_j, \quad (4.26)$$

both of which contain Clifford-valued quantities. The vector \mathbf{A}_{ij} contains multiple copies of the points at the corners of the elements. The values in the matrix $\mathbf{G}'_j(\mathbf{p}_m)$ are obtained from the matrix $\mathbf{G}_{ij}(\mathbf{p}_m)$ by adding together columns which operate on common points. For any particular problem the matrix is fixed, and the vector \mathbf{A}'_j represents the most recent estimate of the field at all $N+2$ points on the boundary. For example of the single step in iteration, the Cauchy integral operator at every point on the boundary can be described into the matrix form:

$$\mathbf{B} = \mathcal{G}' \mathbf{A}, \quad (4.27)$$

where

$$\mathcal{G}' = \begin{bmatrix} \mathbf{G}'_{\Sigma,1}(\mathbf{p}_1) & \mathbf{G}'_{\Sigma,2}(\mathbf{p}_1) & \cdots & \mathbf{G}'_{\Sigma,j}(\mathbf{p}_1) & \cdots & \mathbf{G}'_{\Sigma,N+2}(\mathbf{p}_1) \\ \mathbf{G}'_{\Sigma,1}(\mathbf{p}_2) & \mathbf{G}'_{\Sigma,2}(\mathbf{p}_2) & \cdots & \mathbf{G}'_{\Sigma,j}(\mathbf{p}_2) & \cdots & \mathbf{G}'_{\Sigma,N+2}(\mathbf{p}_2) \\ \cdots & \cdots & \cdots & \cdots & \cdots & \cdots \\ \mathbf{G}'_{\Sigma,1}(\mathbf{p}_m) & \mathbf{G}'_{\Sigma,2}(\mathbf{p}_m) & \cdots & \mathbf{G}'_{\Sigma,j}(\mathbf{p}_m) & \cdots & \mathbf{G}'_{\Sigma,N+2}(\mathbf{p}_m) \\ \cdots & \cdots & \cdots & \cdots & \cdots & \cdots \\ \mathbf{G}'_{\Sigma,1}(\mathbf{p}_{N+2}) & \mathbf{G}'_{\Sigma,2}(\mathbf{p}_{N+2}) & \cdots & \mathbf{G}'_{\Sigma,j}(\mathbf{p}_{N+2}) & \cdots & \mathbf{G}'_{\Sigma,N+2}(\mathbf{p}_{N+2}) \end{bmatrix}, \quad (4.28)$$

$$\mathcal{A}^T = [\mathbf{A}'_1 \quad \mathbf{A}'_2 \cdots \mathbf{A}'_m \cdots \mathbf{A}'_{N+2}], \quad (4.29)$$

$$\mathcal{B}^T = [\mathbf{C}_\Sigma \mathbf{u}(\mathbf{p}_1) \quad \mathbf{C}_\Sigma \mathbf{u}(\mathbf{p}_2) \cdots \mathbf{C}_\Sigma \mathbf{u}(\mathbf{p}_m) \cdots \mathbf{C}_\Sigma \mathbf{u}(\mathbf{p}_{N+2})]. \quad (4.30)$$

Table 4.1 Angular ratios on cube.

position	ratio τ^\pm	
	interior field	exterior field
corner	1/4	7/4
edge	1/2	3/2
smooth	1	1

4.2.3 Discretization of Hardy projection operators

A cubic boundary Σ in Fig. 4.1 is used to verify the iterative solutions of the inward field in Fig. 3.7, the outward field in Fig. 3.10 and the reflected field in Fig. 3.15. For this boundary minor modifications in Cauchy integral and Hardy projections are required at the corners and edges. Equations (2.43) and (2.51) strictly apply only to points on smooth surfaces. In the case of the points on edges and corners for boundary field problems, the equations should be written more generally as:

$$\begin{aligned} \mathbf{C}_\Sigma \mathbf{u}(\mathbf{p}) &= 2p.v. \int_{\Sigma} \mathbf{E}_k(\mathbf{q} - \mathbf{p}) \mathbf{n}(\mathbf{q}) \mathbf{u}(\mathbf{q}) d\sigma(\mathbf{q}) \\ &= \tau^+ \mathbf{u}^+(\mathbf{p}) - \tau^- \mathbf{u}^-(\mathbf{p}), \end{aligned} \quad (4.31)$$

and

$$\begin{cases} \mathbf{u}^+ &= \frac{1}{2}(\tau^- \mathbf{I} + \mathbf{C}_\Sigma) \mathbf{u} = \mathbf{P}^+ \mathbf{u} \\ \mathbf{u}^- &= \frac{1}{2}(\tau^+ \mathbf{I} - \mathbf{C}_\Sigma) \mathbf{u} = \mathbf{P}^- \mathbf{u} \end{cases}. \quad (4.32)$$

Here the parameter $\tau^\pm = \theta_i / \theta_{ii}$ is the ratio of two angles: (i) the angle on the side of the boundary indicated by the superscript $x \in \{+, -\}$ subtended to a point on an edge or a corner, and (ii) the angle subtended to a point *not* on an edge or corner. The ratios at edges and corners, when calculating the Hardy projections for the interior and exterior fields, are as listed in Table 4.1.

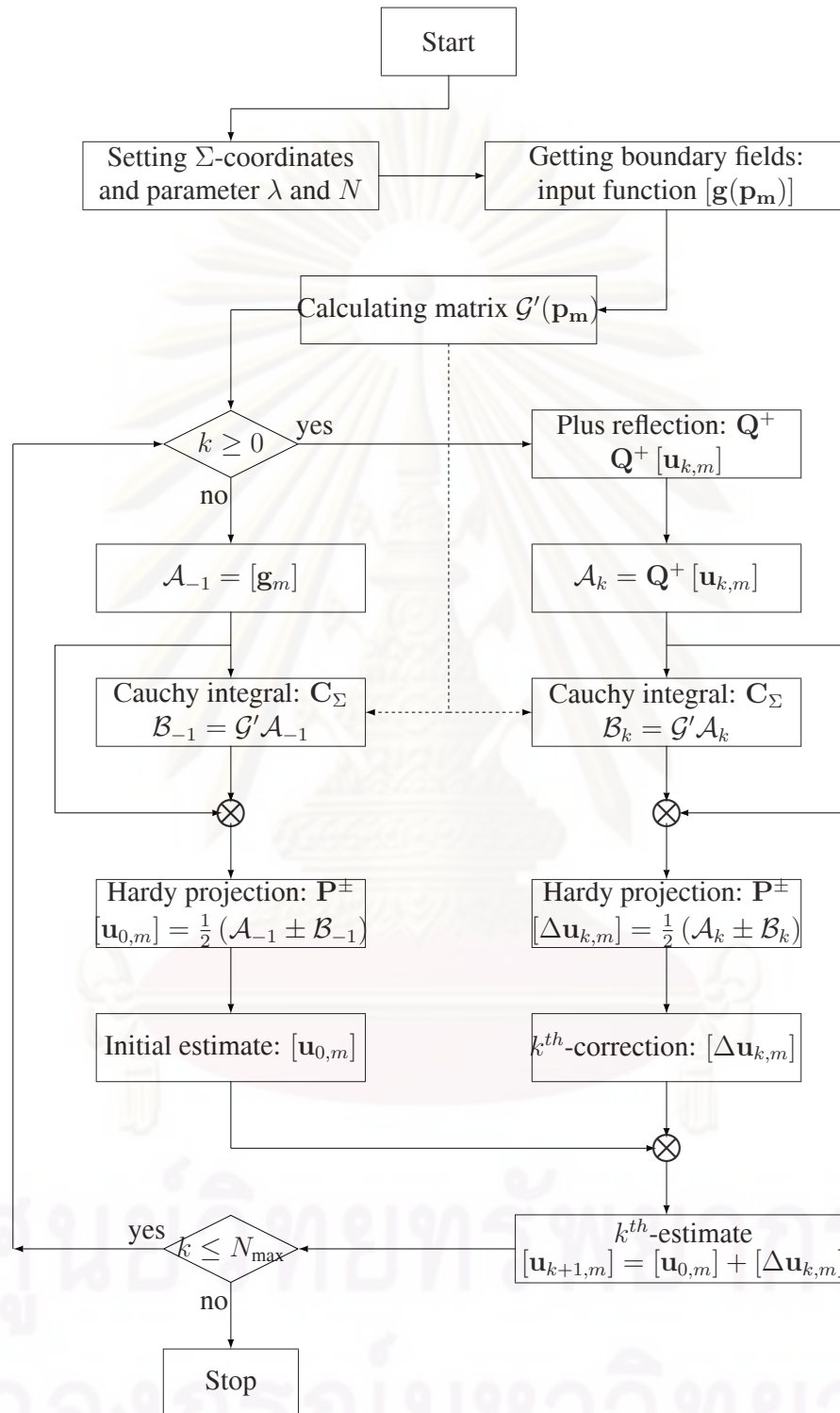


Figure 4.5 Procedure for calculating the iterative solutions of boundary field problems.

4.2.4 Procedure of Calculation

This section describes a procedure for calculating the iterative solution of the boundary field. The main step is the discretisation of both Cauchy integral and Hardy projection as described in the previous sections. Although the iterative solutions of three cases are different, the Cauchy integral and Hardy projection operator is operated into the process at Fig. 4.5 can be covered them. Then each steps are explained by following:

1. The first step is to prepare the important parameters; for examples, the boundary Σ considered is described in the Cartesian system and divided into N rectangular elements Σ_j . And the frequency of the field is defined through the wavelength λ .
2. After the coordinates of the discretized boundary Σ_j are generated, they are used to evaluate the field function g at any point \mathbf{p}_m . All $(N + 2)$ -function g are arranged into the matrix $[\mathbf{g}_m]$.
3. In this step, the geometric function $\mathbf{G}'_{\Sigma,j}$ of any point \mathbf{p}_m are prepared for calculating Cauchy integral by (4.26), and they are collected into matrix \mathcal{G}' as (4.28).
4. In order to calculate the initial estimate of iterative solution, the value of k is fixed as -1 . Then matrix \mathcal{A}_{-1} in (4.29) is used to contain every input function g at any point \mathbf{p}_m .
5. In matrix \mathcal{B}_{-1} in (4.30) contains the $(N + 2)$ Clifford functions that each of them $\mathbf{C}_{\Sigma}\mathbf{u}(\mathbf{p}_m)$ are constructed from the geometric function $\mathbf{G}'_{\Sigma,j}$ inside matrix \mathcal{G}' and the field function \mathbf{A}'_j inside matrix \mathcal{A}_{-1} by using the multiplication of two Clifford numbers. Therefore, the multiplication of them are employed $(N + 2)$ times for $(N + 2)$ Clifford functions $\mathbf{C}_{\Sigma}\mathbf{u}(\mathbf{p}_m)$.
6. Hardy projection of the Clifford field at any point \mathbf{p}_m can construct from the field function g in matrix \mathcal{A}_{-1} and the field function $\mathbf{C}_{\Sigma}\mathbf{g}(\mathbf{p}_m)$ in matrix \mathcal{B}_{-1} by using the addition of two Clifford numbers. Then, the results of Hardy projection that consist of $(N + 2)$ functions are collected into matrix $[\mathbf{u}_{0,m}]$ for being the initial estimate.
7. Next iteration the value of k is increased as 0 , then the field functions in matrix $[\mathbf{u}_{0,m}]$ are operated with plus reflection operator. The results of the plus reflection operator, $\mathbf{Q}^+[\mathbf{u}_{k,m}]$, is collected into matrix \mathcal{A}_0 .
8. In matrix \mathcal{B}_0 the field function $\mathbf{C}_{\Sigma}\mathbf{u}(\mathbf{p}_m)$ are constructed from the same geometric function $\mathbf{G}'_{\Sigma,j}$ inside \mathcal{G}' and the field function \mathcal{A}'_m inside matrix \mathcal{A}_0 by using the multiplication of two Clifford numbers.
9. Hardy projection of the Clifford field at \mathbf{p}_m can be constructed from the plus reflection of the field function, $\mathbf{Q}^+[\mathbf{u}_{0,m}]$ in matrix \mathcal{A}_0 , and the field function $\mathbf{C}_{\Sigma}\mathbf{u}(\mathbf{p}_m)$ in matrix \mathcal{B}_0 by using the addition of two Clifford numbers. Then the results are the corrections of the initial estimate, $[\Delta\mathbf{u}_{0,j}]$.
10. All the new estimate of Clifford field in matrix $[\mathbf{u}_{1,j}]$ can calculate by addition of the initial estimate in matrix $[\mathbf{u}_{0,m}]$ and $[\Delta\mathbf{u}_{0,j}]$.
11. The step (7) to (10) have been reconsidered for improving the, estimate, $[\mathbf{u}_{k,m}]$, until the iterative solutions converge.

CHAPTER V

NUMERICAL RESULTS

This chapter is to show numerical results used for verifying the theoretical geometric and iterative solutions. These solutions of boundary field problems are offered by boundary element method (BEM). The solutions of both perfect transmission and perfect reflection are described as Chapter III. The normal and iterative solutions of inward field in Section 3.1.2.1 and Section 3.1.3.1, respectively, are demonstrated into test cases as Section 5.1. And then, both solutions of outward field in section 3.1.2.2 and section 3.1.3.2, respectively, are confirmed into far-field cases as Section 5.2. In the perfect reflection, the normal and iterative solutions of reflected field in Section 3.2.2 and Section 3.2.3 respectively are verified into scattering cases as Section 5.3. The convergence of all iterative solution can examine the trends of the error in the full field toward the normal solution. The definition of error are described in the next section.

5.1 Test Cases

Cauchy integral equations that are established on Clifford algebra by mathematicians can be employed to illustrate theoretically some behaviors of the fields according with Maxwell's equations. However, they are never applied for solving practically the boundary field problem in electrical engineering. It is difficult to study and to modify Cauchy integral equations in the impenetrable problem directly. Therefore, the suitable situations that are used to prove Cauchy integral equations by mathematicians have still been used to verify their results by using computational techniques.

The test case focuses initially in simple case of perfect transmission problem in order to achieve various central benefits. The first aim is to prove that Cauchy extension and Cauchy integral operators can be used to construct properly the solution of Maxwell's equations. The second aim is to evaluate efficiency of the integral operators when be relevant with boundary element method, before these operators are used as tool in the iterative solution. The third aim is to prove that the geometric solution gives unique answer certainly and to demonstrate the development of the iterative solution. Otherwise, the capability of both these integral operators and the iterative solutions can be analyzed in this case easier, since it is without the complicated phenomena of the fields.

5.1.1 Boundary condition of transparent boundary

Six surfaces of a cube that is described as Section 4.1 is the considered boundary. The centre of a cube is the origin. A cube of 1 m^3 with edges aligns to the axes of Cartesian system. In this case, the boundary is transparent surface that is used to analyze the surface field in free space (ϵ_0, μ_0) according with the boundary condition of perfect transmission as Section 3.1. In Fig. 5.1 the incident field from outside boundary. The incident field is a uniform plane wave traveling in the positive z direction, written in terms of electric and

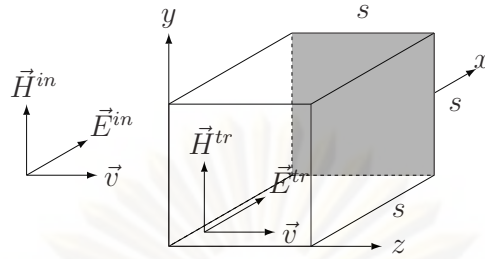


Figure 5.1 Propagation of the incident and transmitted fields in test cases.

magnetic fields as [1]:

$$\begin{cases} \vec{E}^{in}(x, y, z) = E_x \vec{a}_x = E_0 e^{j\beta z} \vec{a}_x \\ \vec{H}^{in}(x, y, z) = H_y \vec{a}_y = H_0 e^{j\beta z} \vec{a}_y \end{cases} \quad (5.1)$$

Numerical values of $E_0 = 120\pi V/m$ and $H_0 = 1A/m$ were taken for the magnitude of electric and magnetic fields, respectively, and β is the wavenumber. Both vector fields are encoded into Clifford form by following (2.6):

$$\begin{cases} \mathbf{E}^{in}(x, y, z) = E_0 e^{j\beta z} \mathbf{e}_1 \\ \mathbf{H}^{in}(x, y, z) = H_0 e^{j\beta z} \mathbf{e}_2 \end{cases} \quad (5.2)$$

Both Clifford field are described into the full components of the incident field in free space by (3.2):

$$\begin{cases} \mathbf{u}^{in} = \mu_0^{\frac{1}{2}} \mathbf{H}^{in} \sigma + j\epsilon_0^{\frac{1}{2}} \mathbf{E}^{in} \mathbf{e}_0 \\ = \mu_0^{\frac{1}{2}} H_0 e^{j\beta z} (-\mathbf{e}_1 \mathbf{e}_3) + j\epsilon_0^{\frac{1}{2}} E_0 e^{j\beta z} \mathbf{e}_1 \mathbf{e}_0 \end{cases} \quad (5.3)$$

Therefore, the inward field can be evaluated by incident field with boundary condition as (3.3):

$$\begin{cases} \mathbf{Q}^+ \mathbf{u}^{tr} = \mu_0^{\frac{1}{2}} \mathbf{H}_t^{tr} + j\epsilon_0^{\frac{1}{2}} \mathbf{E}_n^{tr} \mathbf{e}_0 = \mu_0^{\frac{1}{2}} \mathbf{H}_t^{in} + j\epsilon_0^{\frac{1}{2}} \mathbf{E}_n^{in} \mathbf{e}_0 = \mathbf{Q}^+ \mathbf{u}^{in} \\ \mathbf{Q}^- \mathbf{u}^{tr} = \mu_0^{\frac{1}{2}} \mathbf{H}_n^{tr} + j\epsilon_0^{\frac{1}{2}} \mathbf{E}_t^{tr} \mathbf{e}_0 = \mu_0^{\frac{1}{2}} \mathbf{H}_n^{in} + j\epsilon_0^{\frac{1}{2}} \mathbf{E}_t^{in} \mathbf{e}_0 = \mathbf{Q}^- \mathbf{u}^{in} \end{cases} \quad (5.4)$$

The medium inside boundary is same as outside, so that on the interface the inward field is the incident field

$$\mathbf{u}^{tr} = \mathbf{u}^{in}. \quad (5.5)$$

Then \mathbf{u}^{tr} represents all components of the inward field on the boundary, and it can rewritten as:

$$\mathbf{u}^{tr} = \mathbf{f} + \mathbf{g}, \quad (5.6)$$

where $\mathbf{f} = \mathbf{Q}^+ \mathbf{u}^{tr}$ and $\mathbf{g} = \mathbf{Q}^- \mathbf{u}^{tr}$ are Clifford function that stand for some components of the inward field on boundary.

5.1.2 Definition of errors in test cases

Errors are classified into two groups. The first group of errors involves with the full field at any point that is reproduced by the integral operators. Another group involves with the iterative solution of the full field that are presented on Banach space.

In the first group there are two types of the errors. They are the error of the full field at any point that is used to evaluate the accuracy of the integral operators such as Cauchy extension, Cauchy integral and Hardy projections. The definition of the first type of error is:

$$\% \xi(\mathbf{p}) = \frac{|\mathbf{u}(\mathbf{p}) - \tilde{\mathbf{u}}(\mathbf{p})|}{|\mathbf{u}(\mathbf{p})|} \times 100, \quad (5.7)$$

which $\mathbf{u}(\mathbf{p})$ and $\tilde{\mathbf{u}}(\mathbf{p})$ is the analytical solution (or exact solution) and the numerical result of the full field at any point \mathbf{p} , respectively. And another type of error is:

$$\%_{\text{av. error}} = \frac{\sum_{i=1}^{N+2} \xi(\mathbf{p}_i)}{N+2}, \quad (5.8)$$

where N is the number of elements. It is the average of the ξ at any point \mathbf{p} , when Hardy projections are considered at all points on boundary.

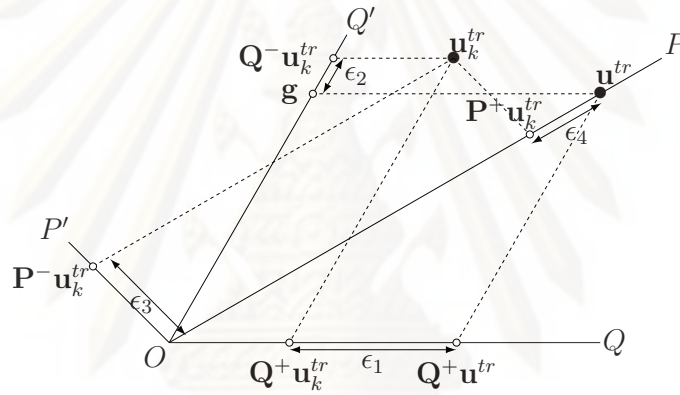


Figure 5.2 Error of inward field in iterative solution.

In the second group there are four types of the errors. They are used to check error in iterative solution. Fig. 5.2 shows for the case of inward field the solution \mathbf{u}^{tr} of Maxwell's equations as intersection between the dotted line through the data $\mathbf{g} = \mathbf{Q}^- \mathbf{u}^{tr}$ and the OP-axis.

Also shown is an estimate of the solution \mathbf{u}_k^{tr} . Note that the error $\mathbf{u}^{tr} - \mathbf{u}_k^{tr}$ can be measured in terms of its projections:

$$\begin{cases} \epsilon_1 = \mathbf{Q}^+ \mathbf{u}_k^{tr} - \mathbf{Q}^+ \mathbf{u}^{tr} \\ \epsilon_2 = \mathbf{Q}^- \mathbf{u}_k^{tr} - \mathbf{g} \\ \epsilon_3 = \mathbf{P}^- \mathbf{u}_k^{tr} - \mathbf{P}^- \mathbf{g} \\ \epsilon_4 = \mathbf{P}^+ \mathbf{u}_k^{tr} - \mathbf{P}^+ \mathbf{u}^{tr} \end{cases} \quad (5.9)$$

The value of the solution \mathbf{u}^{tr} is known, so all errors can be calculated. However, they can be normalized as a percentage:

$$\begin{cases} \% \epsilon_1 = \frac{|\epsilon_1|}{|\mathbf{Q}^+ \mathbf{u}^{tr}|} \times 100 \\ \% \epsilon_2 = \frac{|\epsilon_2|}{|\mathbf{g}|} \times 100 \\ \% \epsilon_3 = \frac{|\epsilon_3|}{|\mathbf{P}^- \mathbf{g}|} \times 100 \\ \% \epsilon_4 = \frac{|\epsilon_4|}{|\mathbf{P}^+ \mathbf{u}^{tr}|} \times 100 \end{cases} \quad (5.10)$$

5.1.3 Verification of Cauchy extension operator

In this calculation, the numerical results are used to verify both theory and application of Cauchy extension in sections 2.5 and 4.2.1, respectively. The Cauchy extension operator reproduces the full field at any points inside the considered region, after all components of the field are forced on the surfaces of a cube by according with (5.5). The six surfaces of a cube are divided into the definite number of elements such as 150, 384 and 600. The inward field at any points inside a cube are compared with the solution of uniform plane wave in order to make the error of the full field by following as (5.7).

Fig. 5.3 illustrates some errors in the full fields at a point in the centre of the cube ($x = y = z = 0$), and Fig. 5.4 illustrates some errors in the full field at a point close to one surface of the cube ($x = y = 0, z = 0.45$). The error between the value delivered by Cauchy extension and known solution of uniform plane wave depends on both the wavelength of the surface fields and the number of points q used as samples to represent the field on boundary. The errors can be reduced if the number of elements is increased as Figs. 5.3 and 5.4. These figures show the percentage error at the points inside a cube for the full fields as the number of boundary elements is increased from 150, 384 and 600.

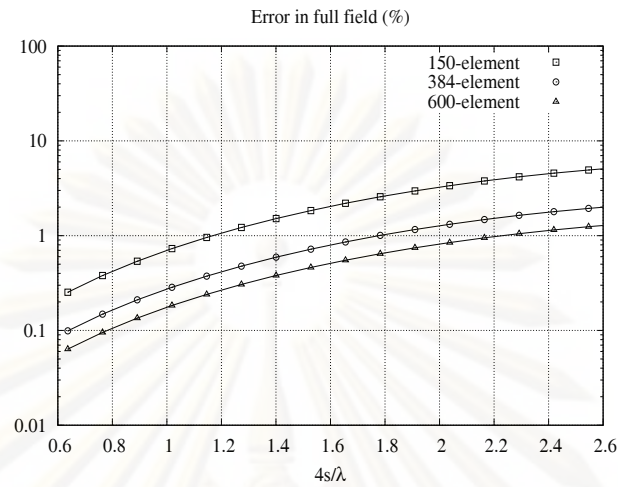


Figure 5.3: Error (%) of Cauchy extension operator in full field at a centre of a cube $p(0.0,0.0,0.0)$ when varying boundary elements: 150, 384, 600 and $\frac{4s}{\lambda} \in (0.6,2.6)$.

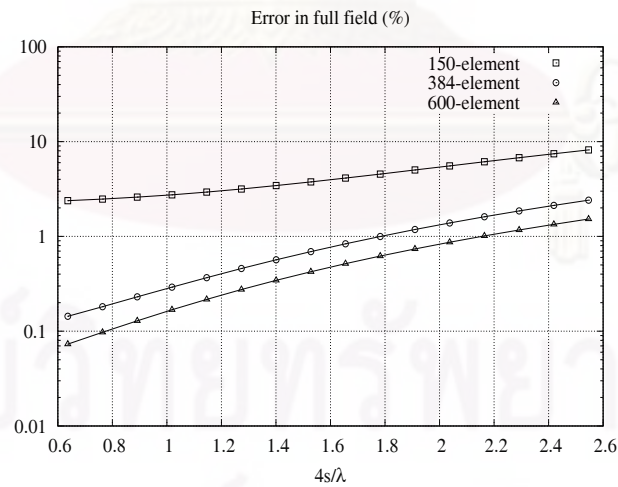


Figure 5.4: Error (%) of Cauchy extension operator in full field near a surface of a cube $p(0.0,0.0,0.45)$ when varying boundary elements: 150, 384, 600 and $\frac{4s}{\lambda} \in (0.6,2.6)$.

5.1.4 Verification of Hardy Projection Operator

In this calculation, the numerical results are used to verify both theory and application of Hardy projections in Sections 2.7 and 4.2.3, respectively. The Hardy projections operates with the trace of the inward or outward fields that are collected on the surfaces of a cube by according with (5.5). The six surfaces of a cube are divided into the definite number of elements such as 150, 384 and 600. The trace of the inward fields at any points on the boundary are compared with known solution of uniform plane wave in order to make the error of the full field by following as (5.7) and (5.8).

Table 5.1 Errors of Hardy projection in full field when at $\frac{4s}{\lambda}=0.6366$.

Positions	Averaged error (%)		
	150-element	384-element	600-element
corner	0.12392	0.05507	0.03855
edge	0.17626	0.08343	0.06089
middle	0.17419	0.09132	0.07800

Table 5.1 shows the error in the full field at three different positions such as the points at corner, edge and middle of the surface of a cube. The error between the value delivered by Hardy projections and known solution depends on both the particular positions and the number of points q used as samples to represent the field on boundary.

Fig. 5.5 illustrates some averages of errors in the full fields at all points q placed on rectangular boundary elements of a cube, when the number of elements are 150. And then, these errors as the numbers of elements are 384 and 600 are shown in Figs. 5.6 and 5.7, respectively. When Figs. 5.5 to 5.7 are considered, the error can be reduced if the number of elements is increased. These figures show the percentage error at all points on the cube as the number of the elements is increased from 150, 384 and 600. Otherwise, these errors depend on the wavelength of the surface fields as shown in Fig. 5.8. The averaged error decreases, when the wavelength of the field is increasing as constant boundary elements.

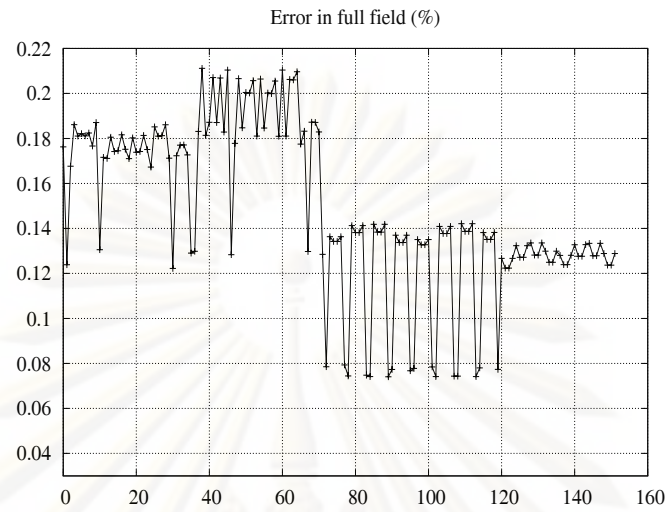


Figure 5.5: Error (%) of Hardy projection operator in full field of all corner points on 150 rectangular boundary elements and $\frac{4s}{\lambda}=0.6366$.

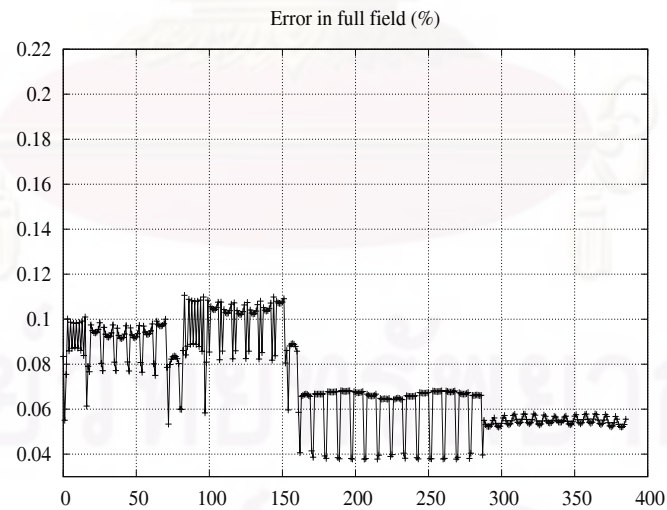


Figure 5.6: Error (%) of Hardy projection operator in full field of all corner points on 384 rectangular boundary elements and $\frac{4s}{\lambda}=0.6366$.

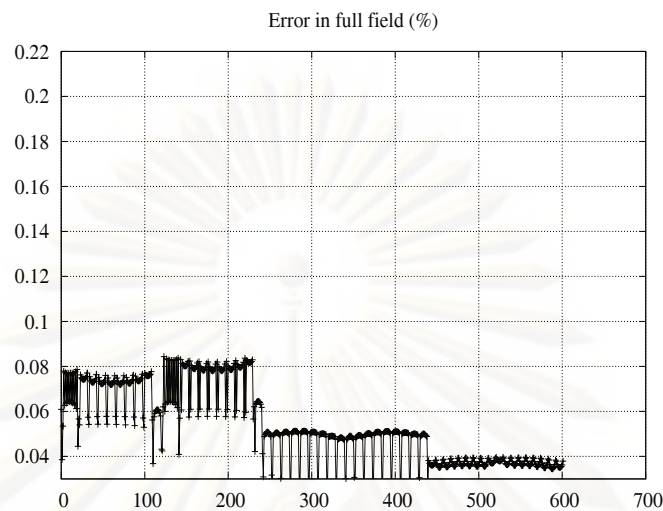


Figure 5.7: Error (%) of Hardy projection operator in full field of all corner points on 600 rectangular boundary elements and $\frac{4s}{\lambda}=0.6366$.

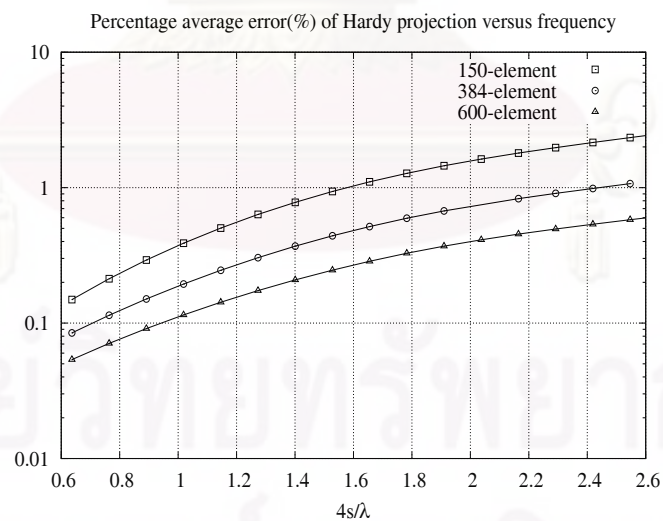


Figure 5.8: Averaged error (%) of Hardy projection operator in full field calculated from all corner points on boundary elements: 150, 384, 600 and $\frac{4s}{\lambda} \in (0.6, 2.6)$.

5.1.5 Verification of Geometric solution

In this calculation, the numerical results are used to verify both normal and iterative solutions of inward field in sections 3.1.2.1 and section 3.1.3.1, respectively. All components of the inward field on the boundary are constructed from the function f and g as (5.6). This boundary condition is considered to test the iterative algorithm in (3.21), and the function g is chosen for making the initial term of iterative solution.

There are sixteen different wavelengths of the incident field, $\frac{4s}{\lambda} \in (0.6, 2.6)$, focused in here. Figs. 5.9 to 5.24 show the averaged error in full field, that is evaluated by (5.8), decreasing as the iterative algorithm processes towards known solution of uniform plane wave. In each figure, the three curves are for different conditions, with the cubic boundary divided into either $N = 150, 384$ or 600 elements. With each condition the solution obtained has a finite error. The error decreases as the number of boundary elements is increased.

Fig. 5.25 shows at the last iteration of all cases the averaged error in the full field. Figs. 5.26 to 5.29 show at the last iteration of all cases the error- ϵ_1 to error- ϵ_4 in Banach space, respectively. The averaged error and four error- ϵ_i have the behaviors similarly. Their value decreases when the wavelength of the field is increasing as constant boundary elements, and it decreases when the number of boundary elements increases.

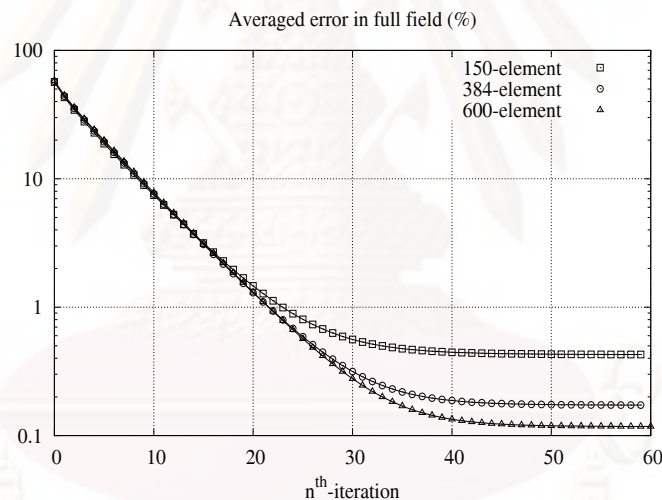


Figure 5.9: Percentage averaged error in full field during iteration towards plane wave solution. Boundary elements $N: 150, 384, 600$ and $\frac{4s}{\lambda} = 0.6366$.

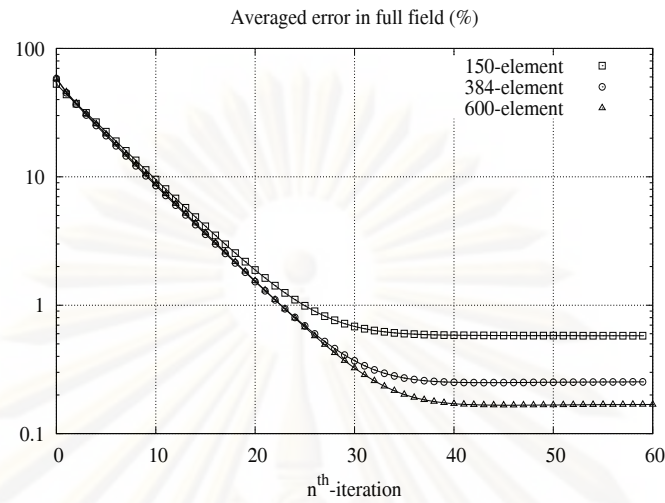


Figure 5.10: Percentage averaged error in full field during iteration towards plane wave solution. Boundary elements N: 150, 384, 600 and $\frac{4s}{\lambda}=0.7640$.

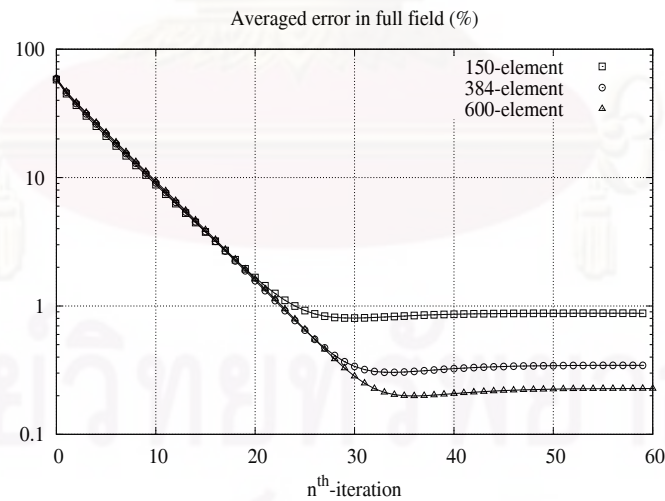


Figure 5.11: Percentage averaged error in full field during iteration towards plane wave solution. Boundary elements N: 150, 384, 600 and $\frac{4s}{\lambda}=0.8913$.

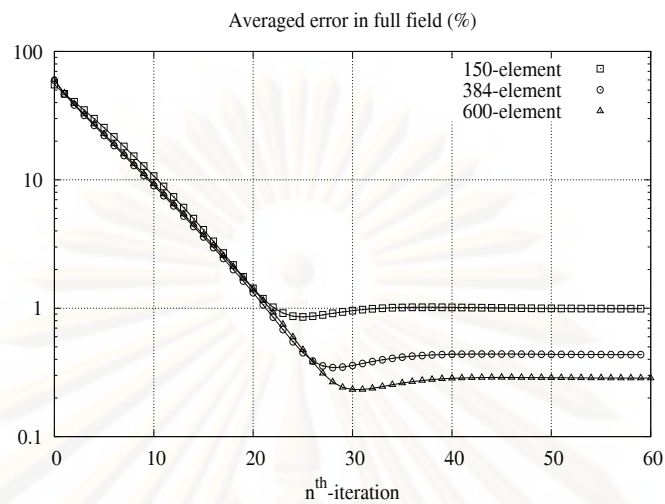


Figure 5.12: Percentage averaged error in full field during iteration towards plane wave solution. Boundary elements N : 150, 384, 600 and $\frac{4s}{\lambda}=1.0185$.

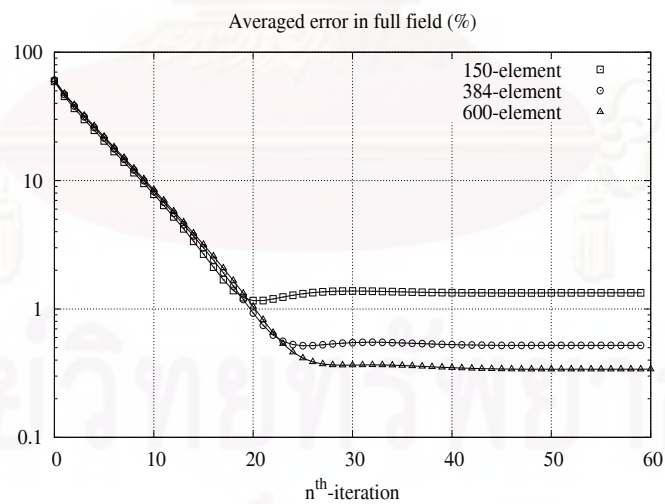


Figure 5.13: Percentage averaged error in full field during iteration towards plane wave solution. Boundary elements N : 150, 384, 600 and $\frac{4s}{\lambda}=1.1460$.

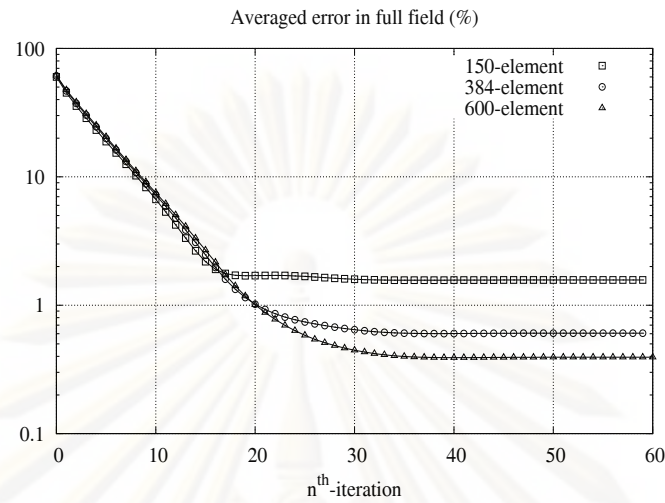


Figure 5.14: Percentage averaged error in full field during iteration towards plane wave solution. Boundary elements N : 150, 384, 600 and $\frac{4s}{\lambda}=1.2732$.

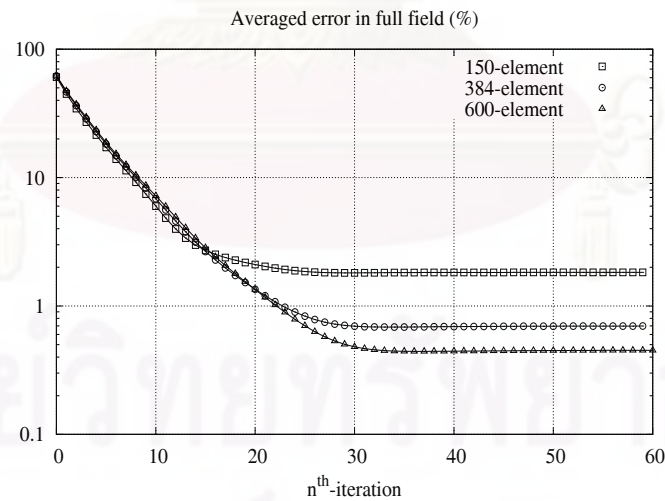


Figure 5.15: Percentage averaged error in full field during iteration towards plane wave solution. Boundary elements N : 150, 384, 600 and $\frac{4s}{\lambda}=1.4005$.

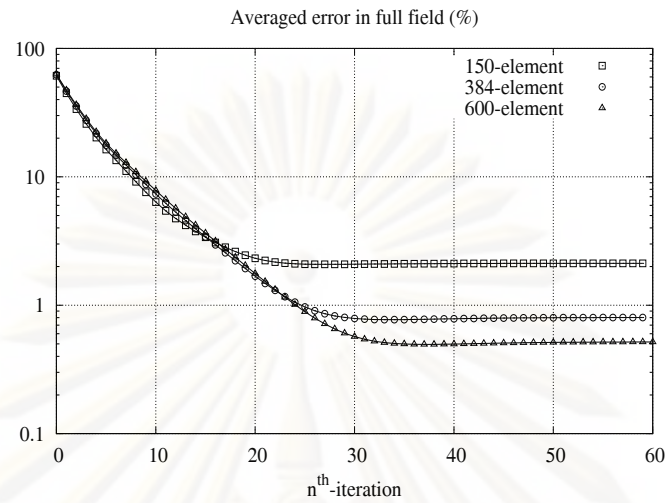


Figure 5.16: Percentage averaged error in full field during iteration towards plane wave solution. Boundary elements N: 150, 384, 600 and $\frac{4s}{\lambda}=1.5278$.

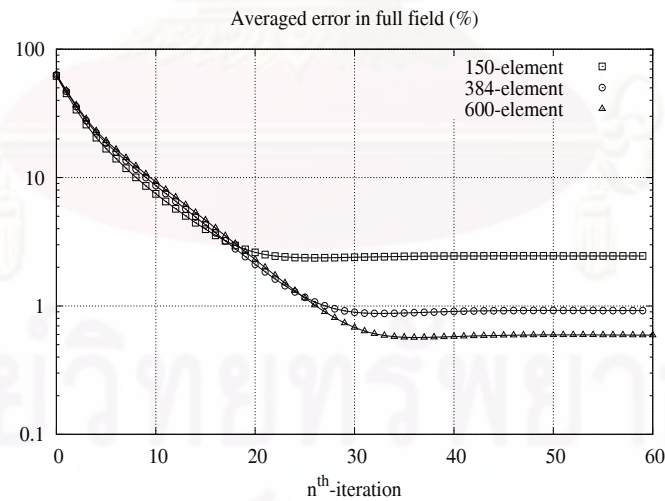


Figure 5.17: Percentage averaged error in full field during iteration towards plane wave solution. Boundary elements N: 150, 384, 600 and $\frac{4s}{\lambda}=1.6552$.

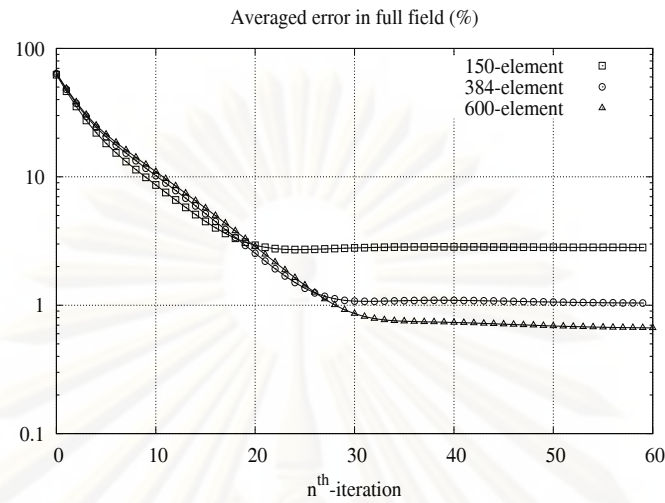


Figure 5.18: Percentage averaged error in full field during iteration towards plane wave solution. Boundary elements N : 150, 384, 600 and $\frac{4s}{\lambda}=1.7825$.

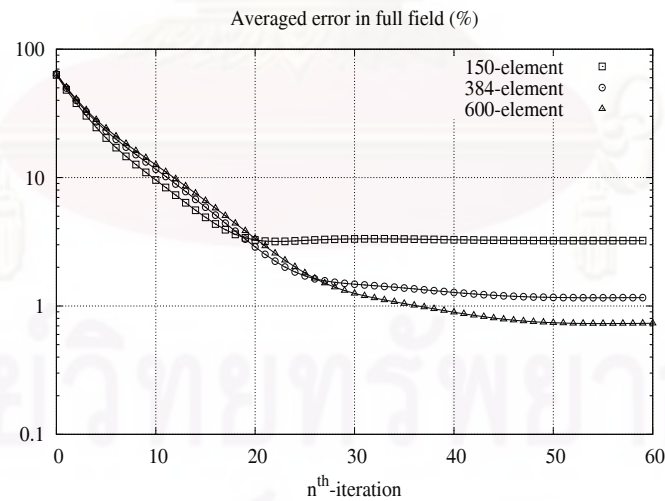


Figure 5.19: Percentage averaged error in full field during iteration towards plane wave solution. Boundary elements N : 150, 384, 600 and $\frac{4s}{\lambda}=1.9098$.

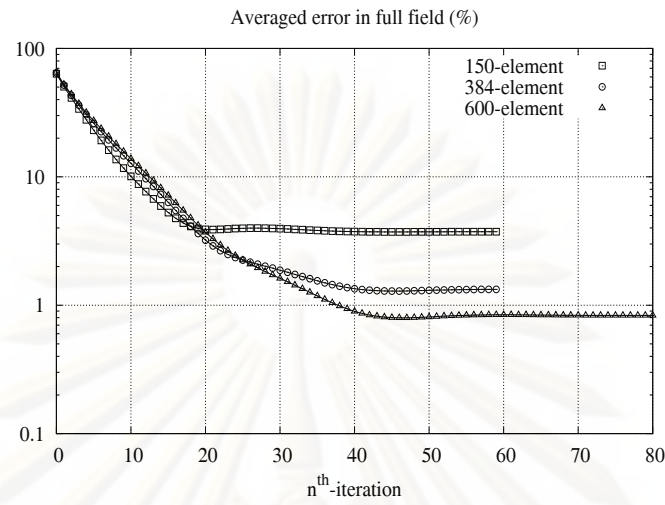


Figure 5.20: Percentage averaged error in full field during iteration towards plane wave solution. Boundary elements N : 150, 384, 600 and $\frac{4s}{\lambda}=2.0371$.

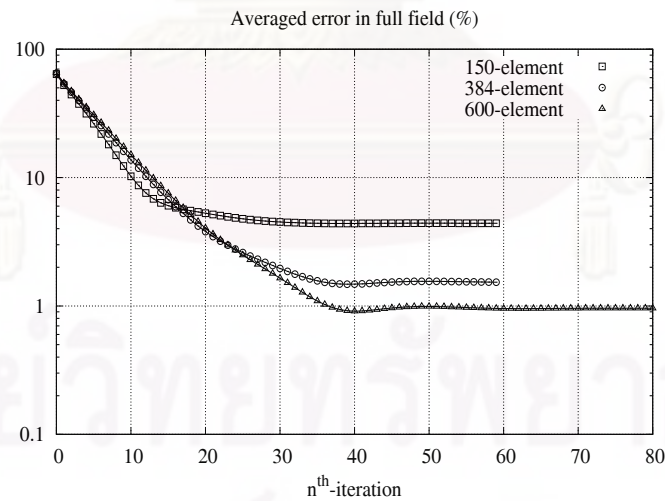


Figure 5.21: Percentage averaged error in full field during iteration towards plane wave solution. Boundary elements N : 150, 384, 600 and $\frac{4s}{\lambda}=2.1645$.

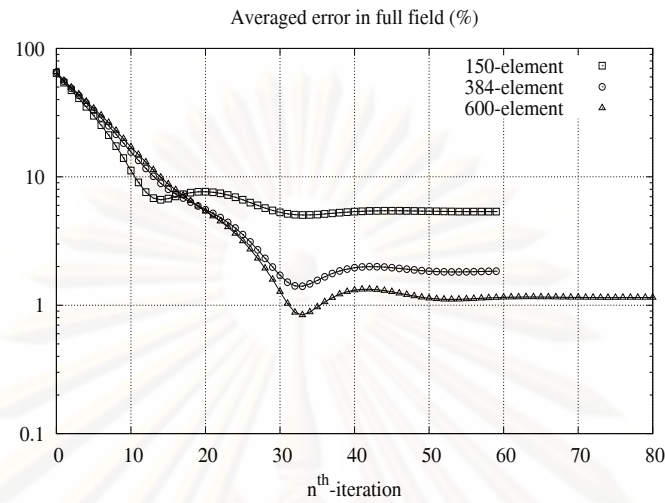


Figure 5.22: Percentage averaged error in full field during iteration towards plane wave solution. Boundary elements N : 150, 384, 600 and $\frac{4s}{\lambda}=2.2918$.

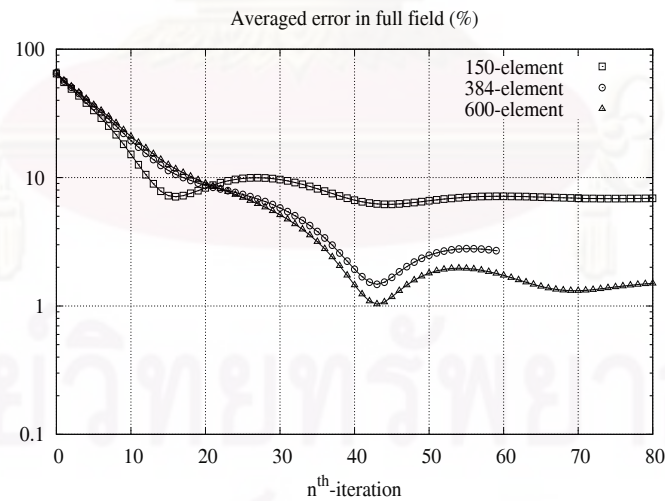


Figure 5.23: Percentage averaged error in full field during iteration towards plane wave solution. Boundary elements N : 150, 384, 600 and $\frac{4s}{\lambda}=2.4192$.

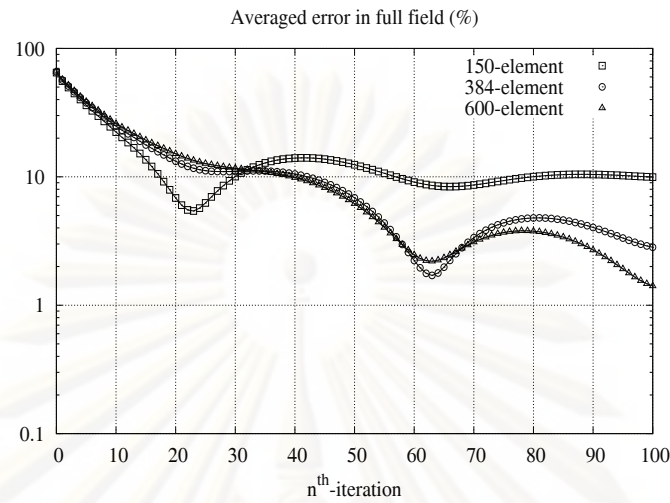


Figure 5.24: Percentage averaged error in full field during iteration towards plane wave solution. Boundary elements N : 150, 384, 600 and $\frac{4s}{\lambda}=2.5465$.

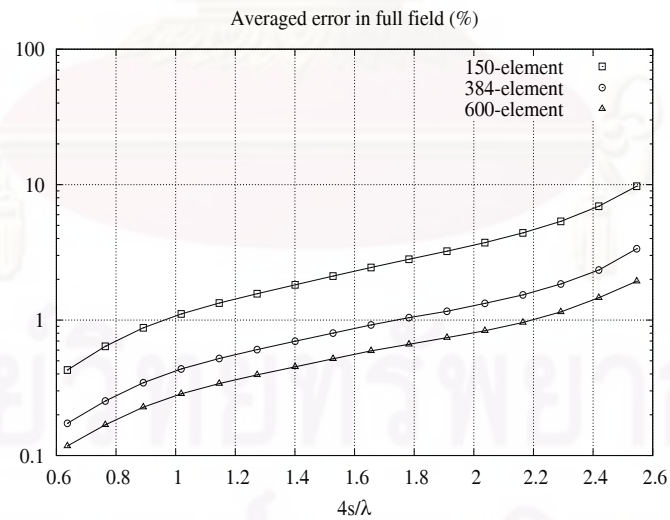


Figure 5.25: The last averaged error (%) of iterative solution towards plane wave solution in full field at corner point on boundary elements 150, 384, 600 and $\frac{4s}{\lambda} \in (0.6, 2.6)$.

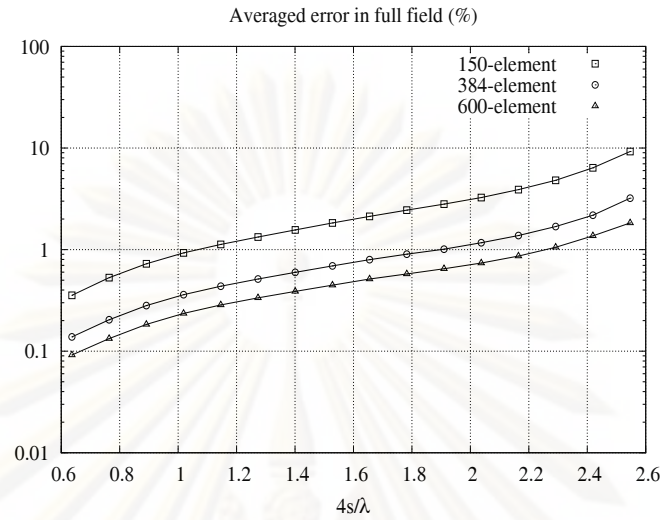


Figure 5.26: The last averaged error- ϵ_1 (%) of iterative solution towards plane wave solution in full field at corner point on boundary elements 150, 384, 600 and $\frac{4s}{\lambda} \in (0.6, 2.6)$.

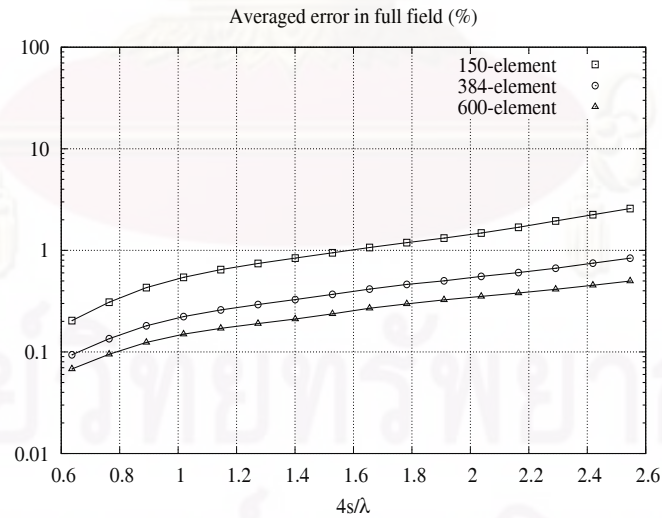


Figure 5.27: The last averaged error- ϵ_2 (%) of iterative solution towards plane wave solution in full field at corner point on boundary elements 150, 384, 600 and $\frac{4s}{\lambda} \in (0.6, 2.6)$.

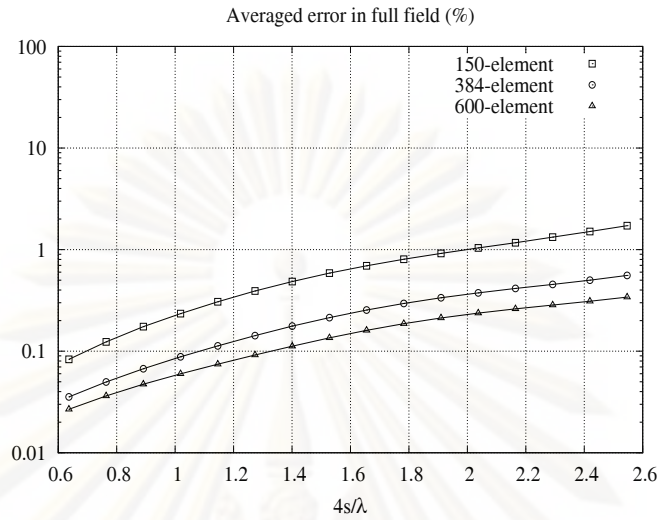


Figure 5.28: The last averaged error- ϵ_3 (%) of iterative solution towards plane wave solution in full field at corner point on boundary elements 150, 384, 600 and $\frac{4s}{\lambda} \in (0.6, 2.6)$.

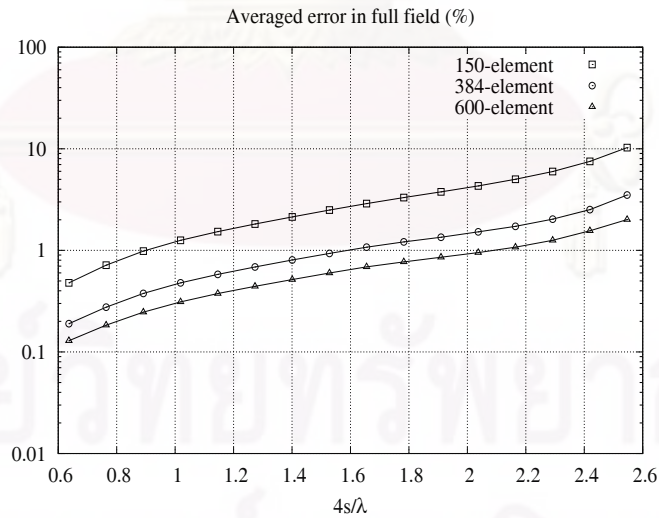


Figure 5.29: The last averaged error- ϵ_4 (%) of iterative solution towards plane wave solution in full field at corner point on boundary elements 150, 384, 600 and $\frac{4s}{\lambda} \in (0.6, 2.6)$.

5.2 Far-Field Cases

Typically, it is difficult to determine directly the far-field pattern of antenna; therefore, the far-field is simulated for predicting and understanding its characteristic. Ordinarily, it is the radiated power that is of interest (not the far-field pattern), and then antenna patterns are usually measured in the far-field region. The accepted formula [1] for the distances in the far-field region is

$$r \geq \frac{2D^2}{\lambda}, \quad (5.11)$$

where D is the largest dimension of the radiator or scatterer. In here, the integral equation on Clifford algebra is used for constructing the powerful techniques of the transformation from the near-field to the far-field. Cauchy extension operator that is one part of powerful tools can reproduce the full field at any points inside the considered region, when all components of the near-field on the boundary are recognized completely. Although some components of the near-field are available in the practice, they cannot be used to analyze the far field instantly. The proposed technique that is constructed with Hardy projection operators can solve all components of the near-field on the boundary.

The far-field cases point out the radiated fields in the exterior region that are generated by any sources in the interior region. The first aim is to prove the normal and iterative solutions of outward field in boundary field problem involving with the calculation of all components of the near-field. Hardy projection operators that are verified in the test cases are used to be the important tools of this application. The second aim is to show the efficiency of Cauchy extension operator when its results is reproduced by analytical and calculated solutions of the near-field.

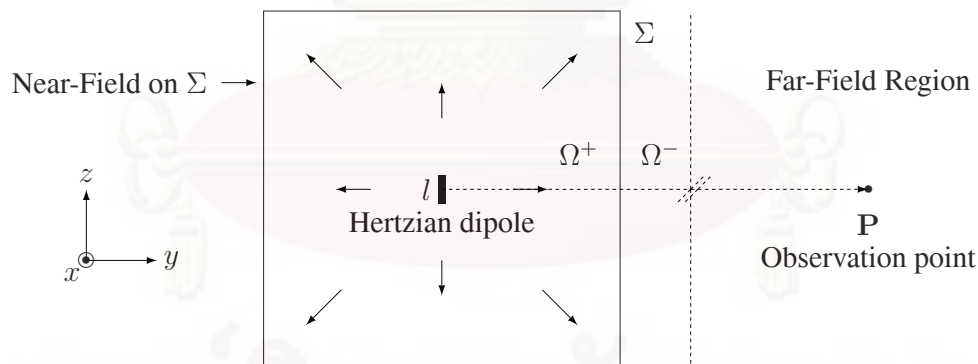


Figure 5.30 Radiated fields by Hertzian dipole source at near-field and far-field.

5.2.1 Boundary Condition of Near-Fields on Boundary

In Fig.5.30, six surfaces of a cube that is described as section 4.1 is the considered boundary. The centre of a cube is the origin. A cube of 1 m^3 with edges aligned to the axes of Cartesian system. In this case, the boundary is transparent surface that is used to analyze

the surface field in free space (ϵ_0, μ_0) according with the boundary condition of perfect transmission as section 3.1. The surface field is created by the incident field from inside boundary. The incident field emanates from a Hertzian dipole source oriented in the positive z direction at the centre of the cube, written in terms of electric and magnetic fields in spherical coordinates as [1]:

$$\begin{cases} \vec{E}(x, y, z) = E_r \vec{a}_r + E_\theta \vec{a}_\theta \\ = \frac{I_0 l}{4\pi} e^{-j\beta r} \left[\left(\frac{2\eta}{r^2} + \frac{2}{j\omega\epsilon r^3} \right) \cos\theta \vec{a}_r + \left(\frac{j\omega\mu}{r} + \frac{1}{j\omega\epsilon r^3} + \frac{\eta}{r^2} \right) \sin\theta \vec{a}_\theta \right] \\ \vec{H}(x, y, z) = H_\phi \vec{a}_\phi \\ = \frac{I_0 l}{4\pi} e^{-j\beta r} \left(\frac{j\beta}{r} + \frac{1}{r^2} \right) \sin\theta \vec{\phi} \end{cases} \quad (5.12)$$

Numerical values of $I_0 l = 0.04 Am$ was taken for the strength of the dipole, and β is the wavenumber.

Both vector fields are used to describe all components of the incident field into Clifford form similar to the incident field in the test cases as (5.3). Then, the outward field can be evaluated by incident field with the boundary condition (3.3). The medium inside and outside boundary are same, so that along the interface the outward field is the incident field. There are two kinds of the near-field on the boundary. The first kind is the outward field that contains all components of the near-field,

$$\mathbf{u}^{tr} = \mu_0^{\frac{1}{2}} \mathbf{H}^{tr} \sigma + j\epsilon_0^{\frac{1}{2}} \mathbf{E}^{tr} \mathbf{e}_0. \quad (5.13)$$

The second kind is the outward field that contains some normal components of the magnetic field and some tangential components of the electric field,

$$\mathbf{g} = \mathbf{Q}^- \mathbf{u}^{tr}. \quad (5.14)$$

5.2.2 Definition of errors in far-field cases

Equations (5.7) and (5.8) are referred to present the accuracy of the numerical solutions in the far-field cases. Another group of the errors is used to check the error in iterative solution on Banach space. The errors have the definitions similar to the error in test cases. Fig. 5.31 shows for the case of outward field the solution \mathbf{u}^{tr} of Maxwell's equations as intersection between the dotted line through the data $\mathbf{g} = \mathbf{Q}^- \mathbf{u}^{tr}$ and the OP'-axis.

Also shown is an estimate of the solution \mathbf{u}_k^{tr} . Note that the error $\mathbf{u}^{tr} - \mathbf{u}_k^{tr}$ can be measured in terms of its projections:

$$\begin{cases} \epsilon_1 = \mathbf{Q}^+ \mathbf{u}_k^{tr} - \mathbf{Q}^+ \mathbf{u}^{tr} \\ \epsilon_2 = \mathbf{Q}^- \mathbf{u}_k^{tr} - \mathbf{g} \\ \epsilon_3 = \mathbf{P}^- \mathbf{u}_k^{tr} - \mathbf{u}^{tr} \\ \epsilon_4 = \mathbf{P}^+ \mathbf{u}_k^{tr} \end{cases} \quad (5.15)$$

The value of the solution \mathbf{u}^{tr} is known, so all errors can be calculated. However, they can be normalized as a percentage:

$$\begin{cases} \% \epsilon_1 = \frac{|\epsilon_1|}{|\mathbf{Q}^+ \mathbf{u}^{tr}|} \times 100 \\ \% \epsilon_2 = \frac{|\epsilon_2|}{|\mathbf{g}|} \times 100 \\ \% \epsilon_3 = \frac{|\epsilon_3|}{|\mathbf{P}^+ \mathbf{g}|} \times 100 \\ \% \epsilon_4 = \frac{|\epsilon_4|}{|\mathbf{u}^{tr}|} \times 100 \end{cases} \quad (5.16)$$

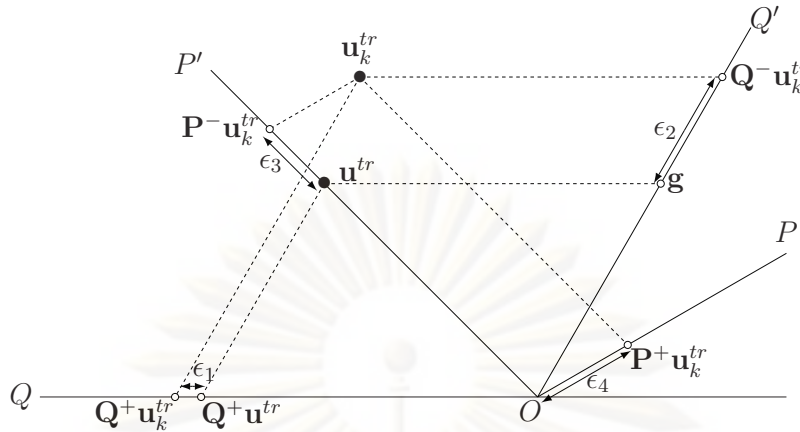


Figure 5.31 Error of outward field in iterative solution.

5.2.3 Calculation of Far-Field from All Components E, H of Near-Field

After Cauchy extension operator is verified in test case, its primary application is presented in here. The Cauchy extension operator reproduces the full field at any points outside the boundary, after all components of the near-field are forced on the surfaces of a cube according with (5.13). The six surfaces of a cube are divided into the definite number of elements such as 150, 384 and 600. The outward fields at any points outside the cube are compared with the solution of the radiated field from the Hertzian dipole antenna in order to make the error of the full field by following as (5.7).

Figs. 5.32, 5.33 and 5.34 illustrate some errors in the full fields at a point 0.6283, 62.83 and 628.3 m, respectively, from the centre of the cube when varying frequency from 40 MHz to 170 MHz. The error between the value delivered by Cauchy extension and the radiated field excited by the Hertzian dipole antenna depends on both frequency and the number of the point q used as sample to represent the field on boundary. The errors can be reduced if the number of the elements is increased as Figs. 5.32 to 5.34. These figures show the percentage error of all components of the far-field outside a cube as the number of boundary elements is increased from 150, 384 and 600.

ศูนย์วิทยทรัพยากร
จุฬาลงกรณ์มหาวิทยาลัย

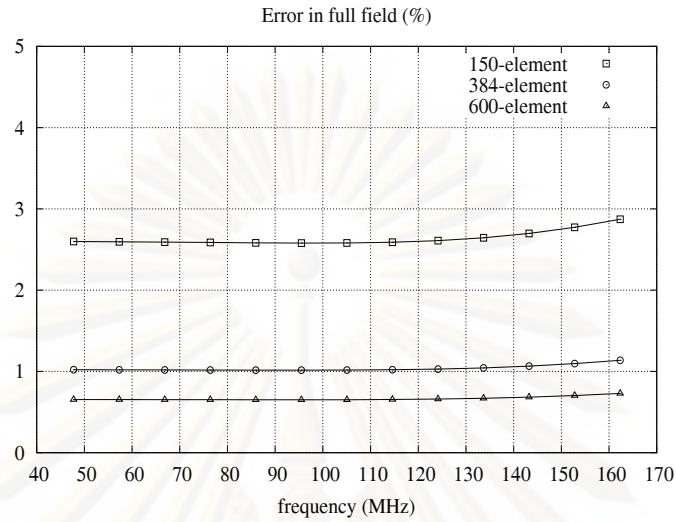


Figure 5.32: Error (%) in far field at $r = 0.6283$ m., $\theta=0^\circ$ generated by all components E , H of field when varying boundary elements: 150, 384, 600 and frequency $\in (40,170)$ MHz.

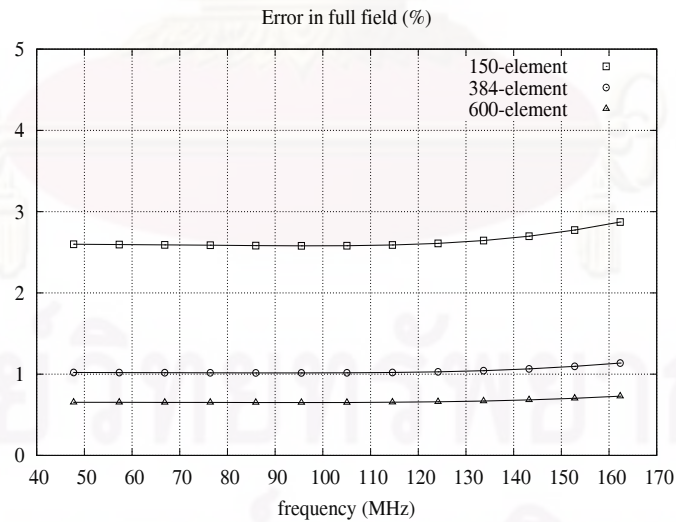


Figure 5.33: Error (%) in far field at $r = 62.83$ m., $\theta=0^\circ$ generated by all components E , H of field when varying boundary elements: 150, 384, 600 and frequency $\in (40,170)$ MHz.

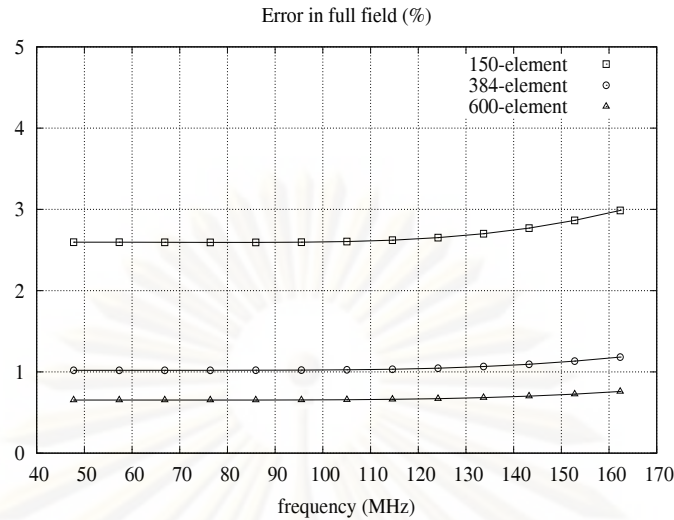


Figure 5.34: Error (%) in far field at $r = 628.3$ m., $\theta = 0^\circ$ generated by all components E , H of field when varying boundary elements: 150, 384, 600 and frequency $\in (40, 170)$ MHz.

5.2.4 Calculation of Near-Field from components E_t , H_n of Near-Field

In this calculation, the numerical results are used to verify both normal and iterative solutions of outward field in section 3.1.2.2 and sections 3.1.3.2, respectively. All components of the outward field on the boundary are constructed from function g as (5.14). This boundary condition is considered to show the iterative algorithm in (3.26), and the function g is chosen for making the initial term of iterative solution.

There are thirteen different frequency of the incident field between 40MHz and 170MHz, focused in here. Figs. 5.35 to 5.47 show the averaged error in full field, that is evaluated by (5.8), decreasing as the iterative algorithm processes towards known solution of the radiated field of Hertzian dipole antenna. In each figure, the three curves are for different conditions, with the cubic boundary divided into either $N = 150, 384$ or 600 elements. With each condition the solution obtained has a finite error. The error decreases as the number of boundary elements is increased.

Fig. 5.48 shows at the last iteration of all cases the averaged error in the full field. Figs. 5.49 to 5.52 show at the last iteration of all cases the error- ϵ_1 to error- ϵ_4 in Banach space, respectively. The averaged error and four error- ϵ_i have the behaviors similarly. Their value decreases when the wavelength of the field is increasing as constant boundary elements, and it decreases when the number of boundary elements increases. However, at 150-160 MHz of Figs. 5.50 to 5.52, the error of iterative solution by using 150 elements does not depend on the frequency, because the efficiency of the integral operator is decreased at higher frequencies. It is noticed on Figs. 5.32 to 5.34 that the integral operator by using 150 elements of the boundary has large error when comparing with 384 and 600 elements.

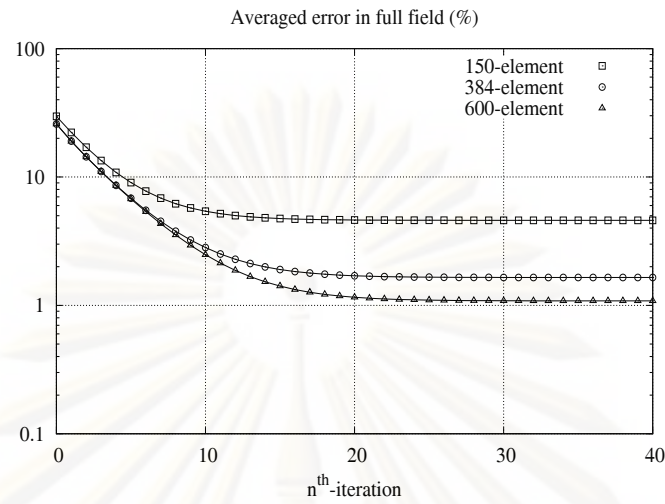


Figure 5.35: Percentage averaged error in full field during iteration towards the radiated solution of Hertzian dipole antenna. Boundary elements N: 150, 384, 600 and frequency $f=47.746\text{MHz}$.

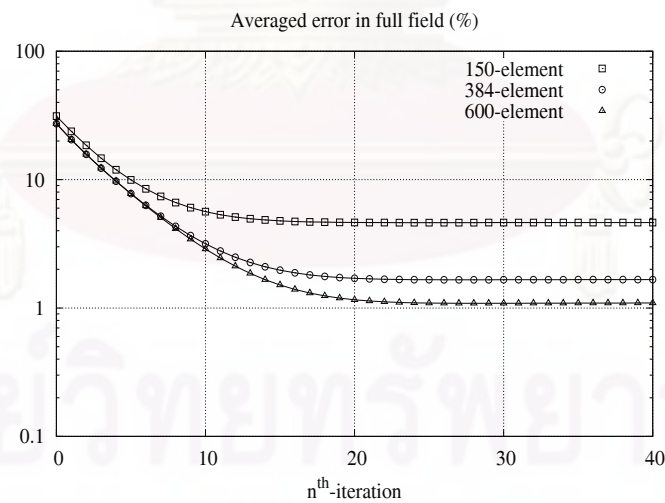


Figure 5.36: Percentage averaged error in full field during iteration towards the radiated solution of Hertzian dipole antenna. Boundary elements N: 150, 384, 600 and frequency $f=57.295\text{MHz}$.

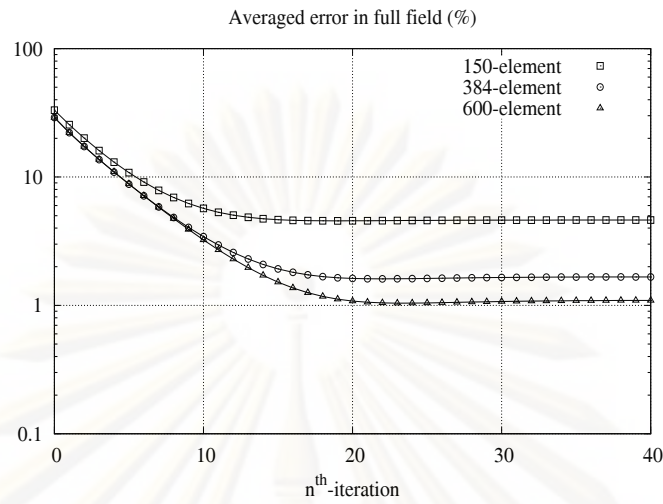


Figure 5.37: Percentage averaged error in full field during iteration towards the radiated solution of Hertzian dipole antenna. Boundary elements N: 150, 384, 600 and frequency $f=66.845\text{MHz}$.

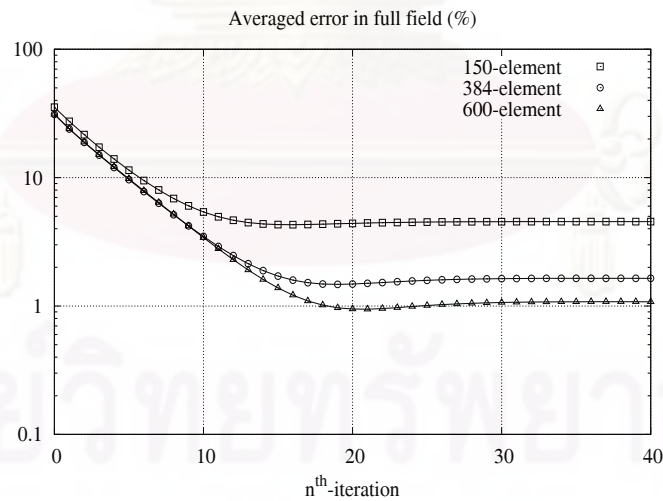


Figure 5.38: Percentage averaged error in full field during iteration towards the radiated solution of Hertzian dipole antenna. Boundary elements N: 150, 384, 600 and frequency $f=76.394\text{MHz}$.

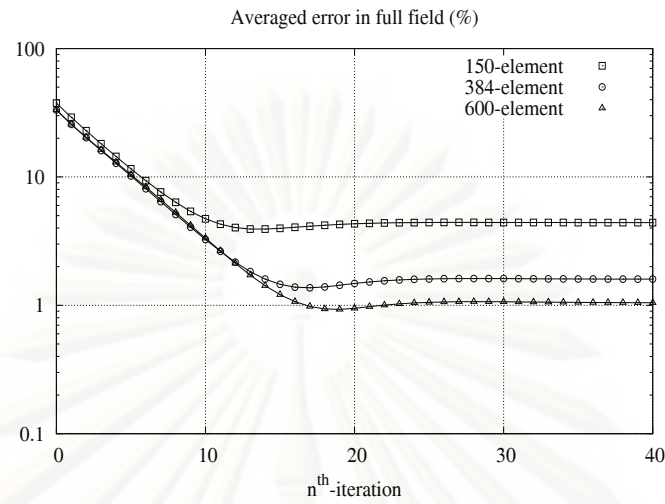


Figure 5.39: Percentage averaged error in full field during iteration towards the radiated solution of Hertzian dipole antenna. Boundary elements N: 150, 384, 600 and frequency $f=85.943\text{MHz}$.

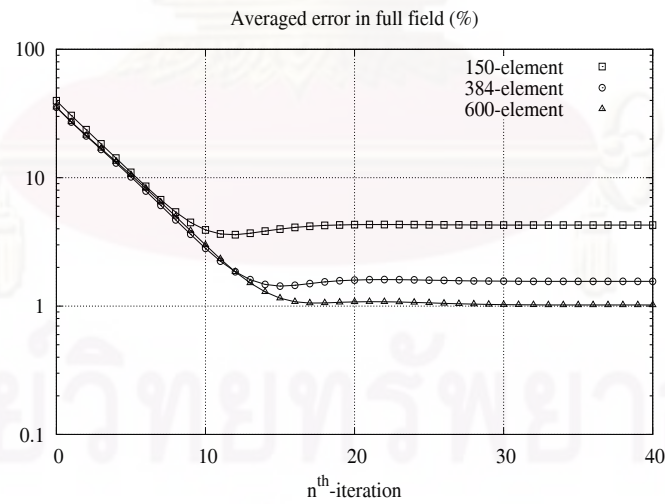


Figure 5.40: Percentage averaged error in full field during iteration towards the radiated solution of Hertzian dipole antenna. Boundary elements N: 150, 384, 600 and frequency $f=95.492\text{MHz}$.

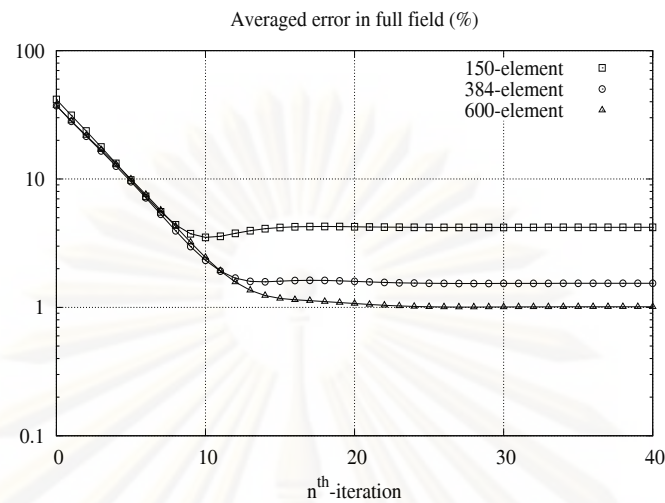


Figure 5.41: Percentage averaged error in full field during iteration towards the radiated solution of Hertzian dipole antenna. Boundary elements N: 150, 384, 600 and frequency $f=105.042\text{MHz}$.

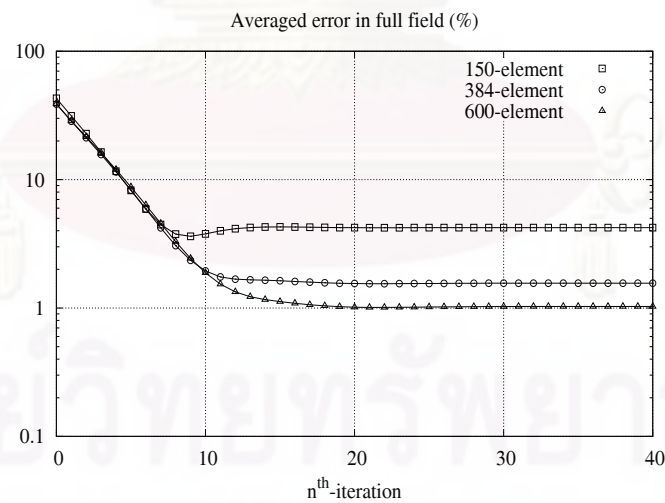


Figure 5.42: Percentage averaged error in full field during iteration towards the radiated solution of Hertzian dipole antenna. Boundary elements N: 150, 384, 600 and frequency $f=114.592\text{MHz}$.

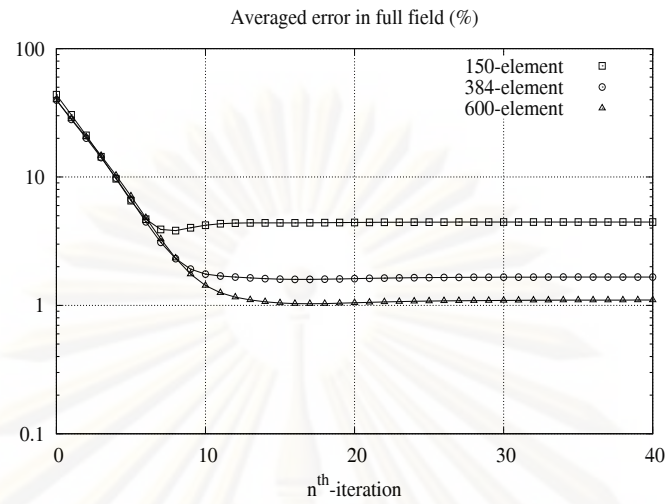


Figure 5.43: Percentage averaged error in full field during iteration towards the radiated solution of Hertzian dipole antenna. Boundary elements N: 150, 384, 600 and frequency $f=124.140\text{MHz}$.

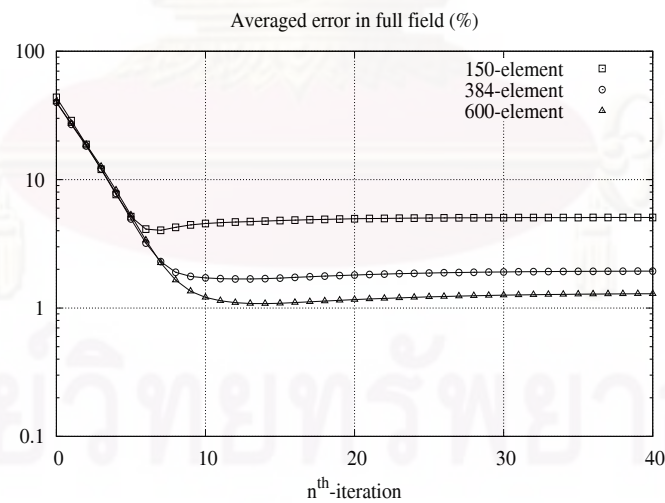


Figure 5.44: Percentage averaged error in full field during iteration towards the radiated solution of Hertzian dipole antenna. Boundary elements N: 150, 384, 600 and frequency $f=133.690\text{MHz}$.

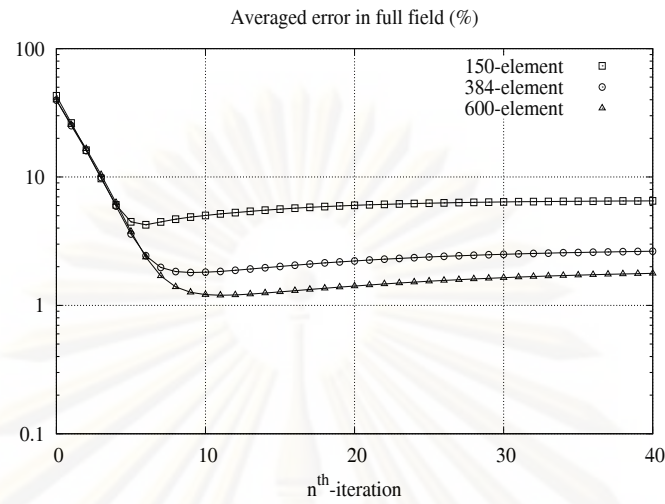


Figure 5.45: Percentage averaged error in full field during iteration towards the radiated solution of Hertzian dipole antenna. Boundary elements N: 150, 384, 600 and frequency $f=143.240\text{MHz}$.

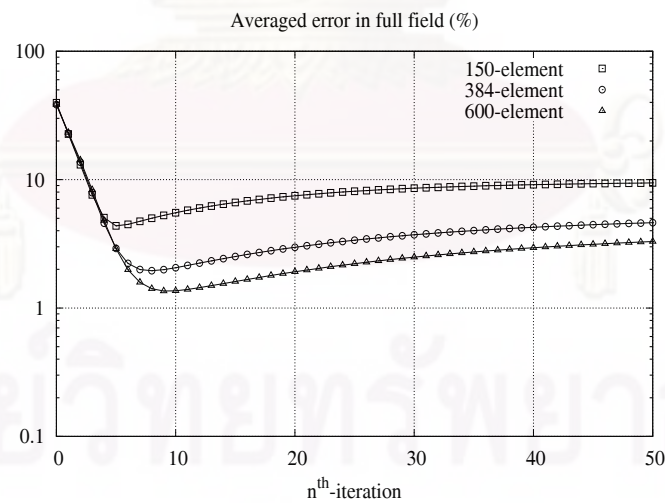


Figure 5.46: Percentage averaged error in full field during iteration towards the radiated solution of Hertzian dipole antenna. Boundary elements N: 150, 384, 600 and frequency $f=152.789\text{MHz}$.

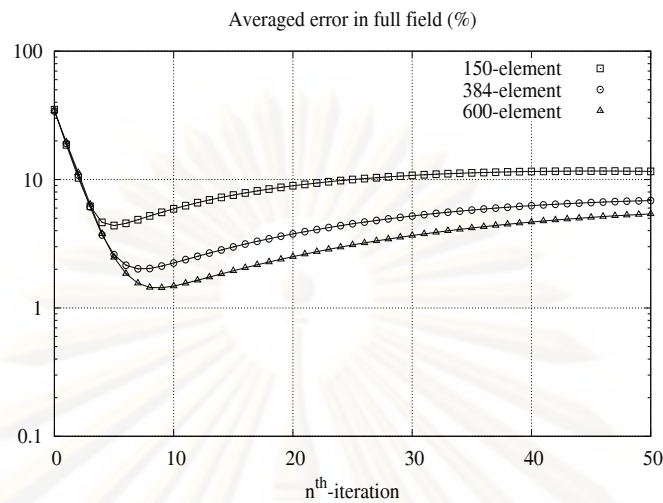


Figure 5.47: Percentage averaged error in full field during iteration towards the radiated solution of Hertzian dipole antenna. Boundary elements N : 150, 384, 600 and frequency $f=162.338\text{MHz}$.

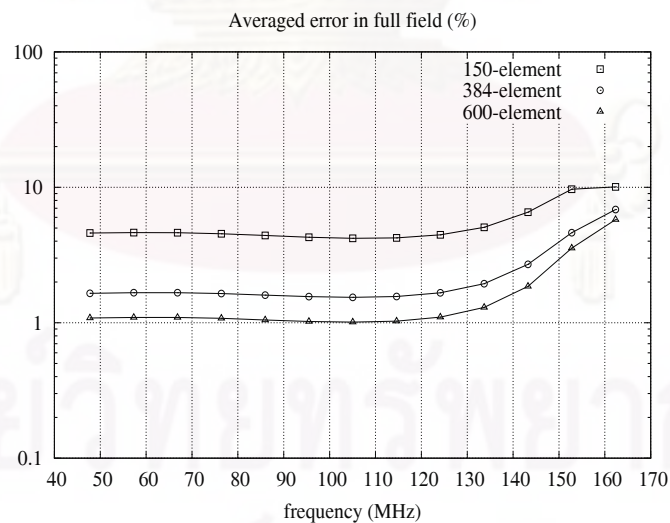


Figure 5.48: The last averaged error (%) of iterative solution towards the radiated solution of Hertzian dipole antenna in full field at corner point on boundary elements 150, 384, 600 and frequency $\in (40,170)$ MHz.

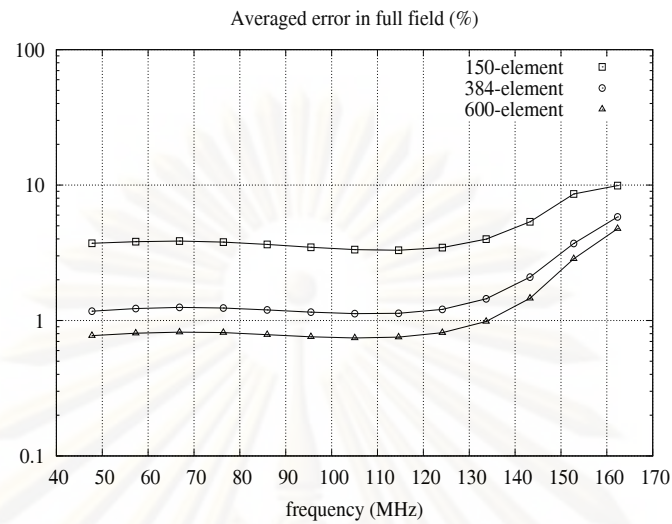


Figure 5.49: The last averaged error- ϵ_1 (%) of iterative solution towards the radiated solution of Hertzian dipole antenna in full field at corner point on boundary elements 150, 384, 600 and frequency $\in (40,170)$ MHz.

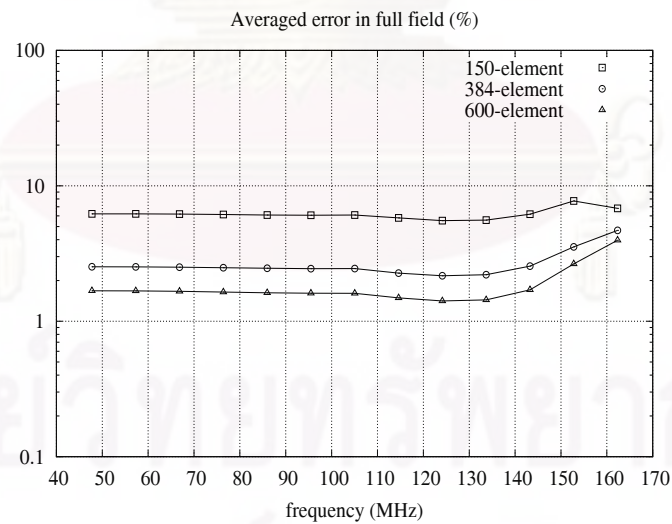


Figure 5.50: The last averaged error- ϵ_2 (%) of iterative solution towards the radiated solution of Hertzian dipole antenna in full field at corner point on boundary elements 150, 384, 600 and frequency $\in (40,170)$ MHz.

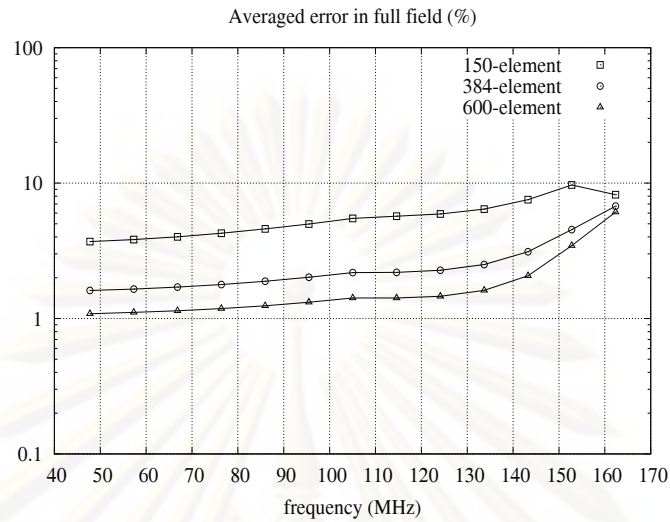


Figure 5.51: The last averaged error- ϵ_3 (%) of iterative solution towards the radiated solution of Hertzian dipole antenna in full field at corner point on boundary elements 150, 384, 600 and frequency $\in (40,170)$ MHz.

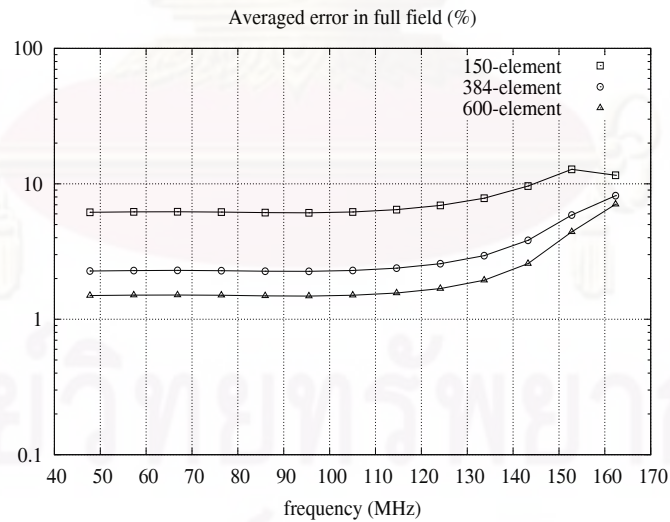


Figure 5.52: The last averaged error- ϵ_4 (%) of iterative solution towards the radiated solution of Hertzian dipole antenna in full field at corner point on boundary elements 150, 384, 600 and frequency $\in (40,170)$ MHz.

5.2.5 Calculation of Far-Field from components E_t, H_n of Near-Field

The Cauchy extension operator reproduces the full field at any points outside the boundary, after all components of the near-field are the results of the previous section. The six surfaces of a cube are divided into the definite number of elements such as 150, 384 and 600. The outward fields at any points outside the cube are compared with the solution of the radiated field from the Hertzian dipole antenna in order to make the error of the full field by following as (5.7).

Figs. 5.53, 5.54 and 5.55 illustrate some errors in the full fields at a point $0.6283, 62.83$ and $628.3 m$, respectively, from the centre of the cube when varying frequency from 40 MHz to 170 MHz. The error between the value delivered by Cauchy extension and the radiated field excited by the Hertzian dipole antenna depends on both frequency and the number of the point q used as sample to represent the field on boundary. The errors can be reduced if the number of the elements is increased as Figs. 5.53 to 5.55. These figures show the percentage error of all components of the far-field outside a cube as the number of boundary elements is increased from 150, 384 and 600.

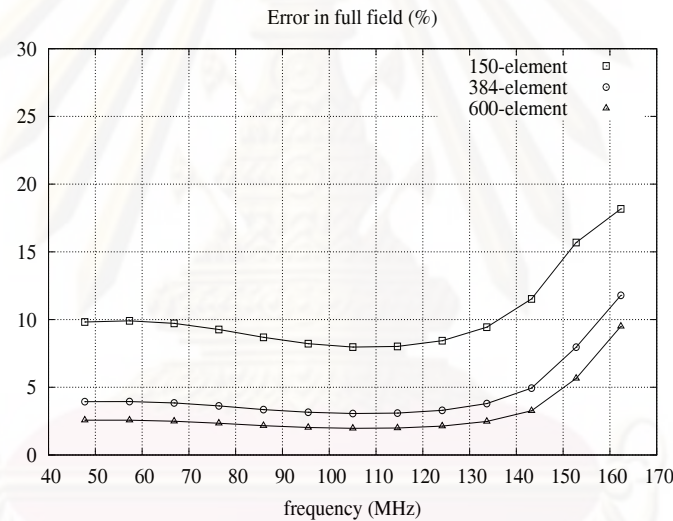


Figure 5.53: Error (%) in far field at $r = 0.6283 m$, $\theta=0^\circ$ generated by components E_t, H_n of field when varying boundary elements: 150, 384, 600 and frequency $\in (40,170)$ MHz.

ศูนย์วิทยทรัพยากร
จุฬาลงกรณ์มหาวิทยาลัย

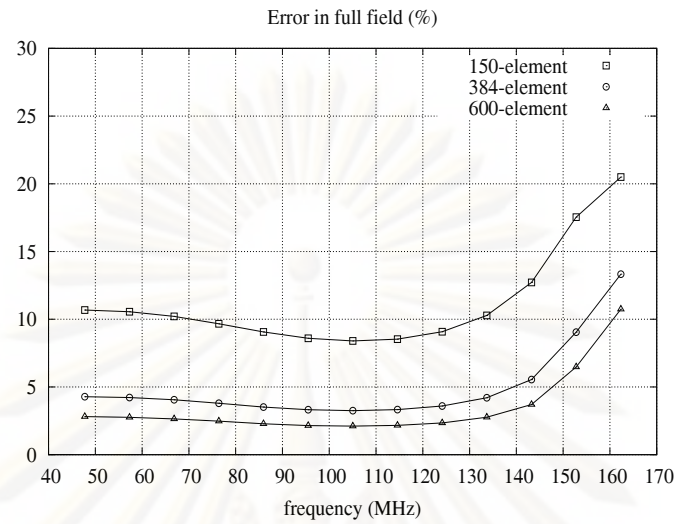


Figure 5.54: Error (%) in far field at $r = 62.83$ m., $\theta = 0^\circ$ generated by components \mathbf{E}_t , \mathbf{H}_n of field when varying boundary elements: 150, 384, 600 and frequency $\in (40, 170)$ MHz.

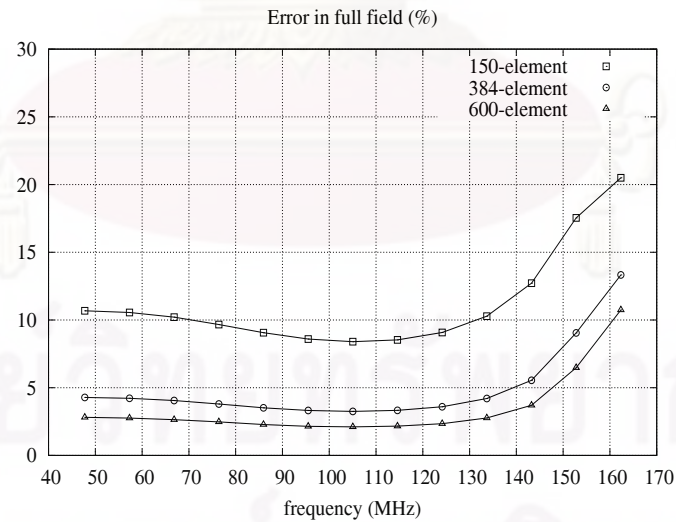


Figure 5.55: Error (%) in far field at $r = 628.3$ m., $\theta = 0^\circ$ generated by components \mathbf{E}_t , \mathbf{H}_n of field when varying boundary elements: 150, 384, 600 and frequency $\in (40, 170)$ MHz.

5.3 Scattering Cases

Currently, the scattering problems that involve the field reflected by perfect electric conductor (PEC) have been attracted by many researchers [44]. In here the integral equation on Clifford form is used to solve the scattering problems. Cauchy extension operator that is one part of the proposed tools can evaluate the full field at any points around the PEC cube, when all components of the field on the cube's surface are known. Although some components of the surface field are available in practice, they have not been used to analyze the scattered field directly. The techniques proposed here, constructed with Hardy projection operators, can solve all components of the surfaced field over the considered cube.

The scattering cases point out the reflected field in the exterior region that are generated by any artificial source such as the surface field on the boundary. The first aim is to prove the normal and iterative solutions of the reflected field in boundary field problem involving with the calculation of all components of the surface field. The second aim is to show the efficiency of Cauchy extension operator when its results are the scattered field around the PEC cube written in term of radar cross section (RCS).

5.3.1 Boundary condition of Perfect Electric Conductor (PEC)

Six surfaces of a cube that is described as section 4.1 is the considered boundary of perfect electric conductors. The cube has a volume $1 m^3$ with edges aligns to the axes of Cartesian system. In this case, the boundary is PEC surface that is used to analyze the reflected field according with the boundary condition of perfect reflection as section 3.2. The surface field is dictated by the incident field from outside boundary. The incident field is uniform plane wave traveling in the positive z direction, written in terms of electric and magnetic fields as (5.1). The numerical values are copied from the section 5.1.1 in the test cases. Moreover, the incident field in Clifford form is referred as (5.3). Therefore, some components of the reflected field can be evaluated by some components of the incident field directly with boundary condition as (3.33):

$$\mathbf{g} = \mathbf{Q}^- \mathbf{u}^{sc} = -\mathbf{Q}^- \mathbf{u}^{in}, \quad (5.17)$$

where \mathbf{g} is Clifford function that play some components of the reflected field on boundary.

5.3.2 Definition of errors in scattering cases

The group of the error is used to check the error in iterative solution on Banach space. Fig. 5.56 shows for the case of the reflected field the solution \mathbf{u}^{sc} of Maxwell's equations as intersection between the dotted line through the data $\mathbf{g} = \mathbf{Q}^- \mathbf{u}^{sc}$ and OP' -axis.

Also shown is an estimate of the solution \mathbf{u}^{sc} . Note that the error $\mathbf{u}^{sc} - \mathbf{u}_k^{sc}$ can be measured in terms of its projections:

$$\begin{cases} \epsilon_1 = \mathbf{Q}^+ \mathbf{u}_k^{sc} - \mathbf{Q}^+ \mathbf{u}^{sc} \\ \epsilon_2 = \mathbf{Q}^- \mathbf{u}_k^{sc} - \mathbf{g} \\ \epsilon_3 = \mathbf{P}^+ \mathbf{u}_k^{sc} \\ \epsilon_4 = \mathbf{P}^- \mathbf{u}_k^{sc} - \mathbf{u}^{sc} \end{cases}, \quad (5.18)$$

The value of the solution \mathbf{u}^{sc} is unknown, so it is not possible to calculate ϵ_1 and ϵ_4 . However, it is possible to calculate both ϵ_2 and ϵ_3 . Note from Fig. 5.56 that if $\epsilon_2 \rightarrow 0$ and $\epsilon_3 \rightarrow 0$ then

$\mathbf{u}_k^{sc} \rightarrow \mathbf{u}^{sc}$. It we check only $\epsilon_2 \rightarrow 0$ then \mathbf{u}_k^{sc} can be anywhere on the dotted line through \mathbf{g} . It we check only $\epsilon_3 \rightarrow 0$ then \mathbf{u}_k^{sc} can be anywhere on the OP' -axis. We therefore need to check both ϵ_2 and ϵ_3 and make sure that both of these approach zero. If we want to plot the error as a percentage, we can divide ϵ_2 by (the magnitude of) \mathbf{g} , and divide ϵ_3 by (the magnitude of) $\mathbf{P}^+\mathbf{g}$:

$$\begin{cases} \% \epsilon_2 = \frac{|\epsilon_2|}{|\mathbf{g}|} \times 100 \\ \% \epsilon_3 = \frac{|\epsilon_3|}{|\mathbf{P}^+\mathbf{g}|} \times 100 \end{cases} \quad (5.19)$$

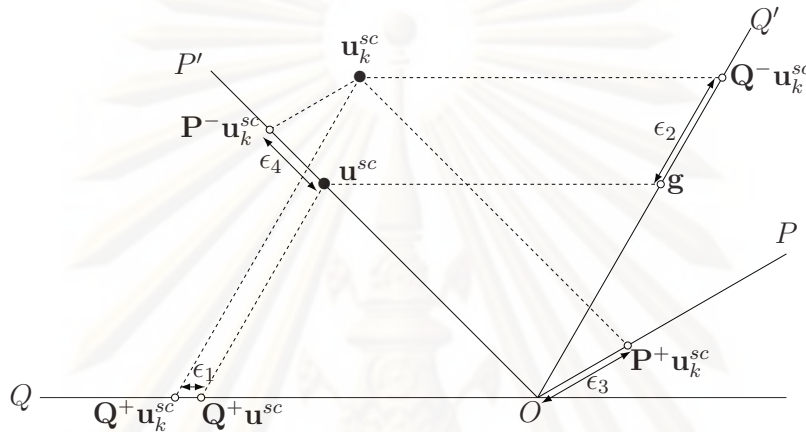


Figure 5.56 Error of reflected field in iterative solution.

5.3.3 Calculation of surface field on PEC from components $\mathbf{E}_t, \mathbf{H}_n$ of incident field

In this calculation, the numerical results are used to verify both normal and iterative solutions of reflected field in section 3.2.2 and section 3.2.3, respectively. All components of the reflected field on PEC cube are constructed from function \mathbf{g} as (5.17). This boundary condition is constructed to show the iterative algorithm in (3.43), and the function \mathbf{g} is chosen for making the initial term of the iterative solution.

There are fourteen different ratio of the side of a cube and wavelength $\frac{4s}{\lambda}$ between 0.6 and 2.3 focused in here. Figs. 5.57 to 5.70 show the error- ϵ_2 in full field, that is evaluated by (5.8), decreasing as the iterative algorithm progresses towards these components of the reflected field which are known in advance from the data. In each figure, three curves are for different conditions, with the cubic boundary divided into either $N=150, 384$ and 600 elements. With each condition the solution obtained has a finite error. The error decreases as the number of boundary elements is increased.

Fig. 5.71 and Fig. 5.72 show at the last iteration of all cases the error- ϵ_2 and the error- ϵ_3 in Banach space, respectively. For a given number of boundary elements the values of the error- ϵ_2 are more than the error- ϵ_3 in all wavelengths. The error- ϵ_2 is fluctuating slightly when $\frac{4s}{\lambda}$ between 0.6 and 2.4. The error- ϵ_3 is going up when $\frac{4s}{\lambda}$ is increasing. However, these errors can be reduced when the boundary elements increase.

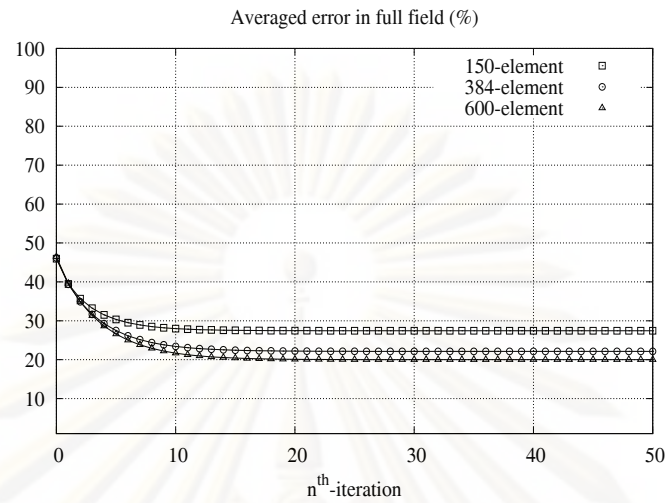


Figure 5.57: Percentage averaged error- ϵ_2 in full field during iteration towards solution of reflected field on PEC. Boundary elements N: 150, 384, 600 and $\frac{4s}{\lambda}=0.6366$.

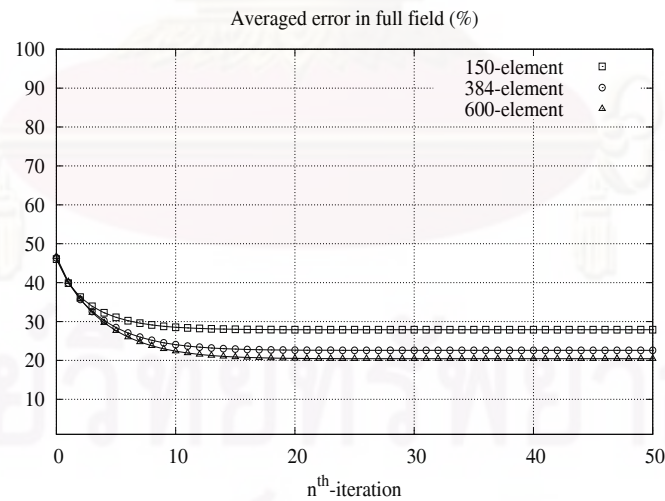


Figure 5.58: Percentage averaged error- ϵ_2 in full field during iteration towards solution of reflected field on PEC. Boundary elements N: 150, 384, 600 and $\frac{4s}{\lambda}=0.7640$.

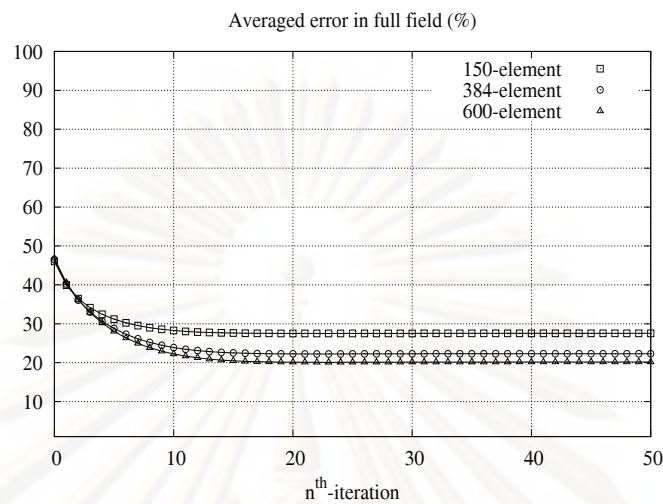


Figure 5.59: Percentage averaged error- ϵ_2 in full field during iteration towards solution of reflected field on PEC. Boundary elements N: 150, 384, 600 and $\frac{4s}{\lambda}=0.8913$.

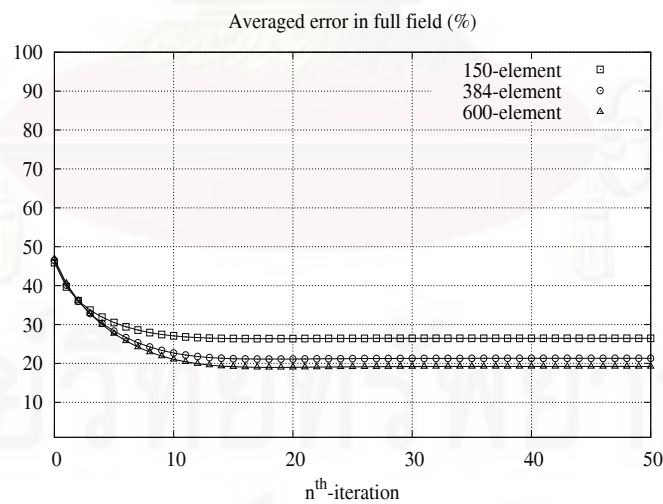


Figure 5.60: Percentage averaged error- ϵ_2 in full field during iteration towards solution of reflected field on PEC. Boundary elements N: 150, 384, 600 and $\frac{4s}{\lambda}=1.0185$.

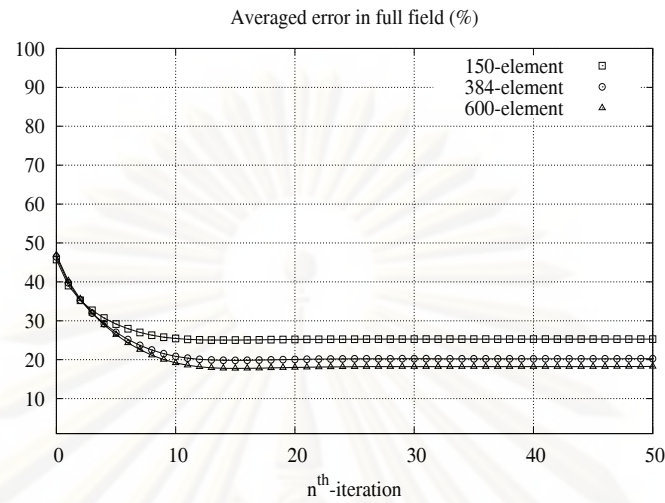


Figure 5.61: Percentage averaged error- ϵ_2 in full field during iteration towards solution of reflected field on PEC. Boundary elements N: 150, 384, 600 and $\frac{4s}{\lambda}=1.1460$.

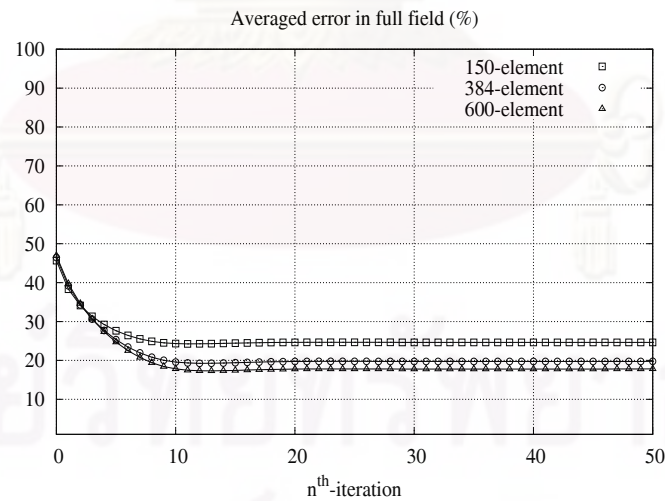


Figure 5.62: Percentage averaged error- ϵ_2 in full field during iteration towards solution of reflected field on PEC. Boundary elements N: 150, 384, 600 and $\frac{4s}{\lambda}=1.2732$.

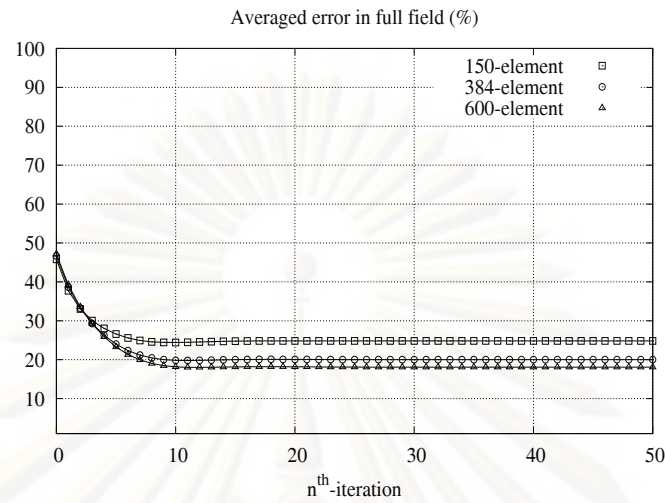


Figure 5.63: Percentage averaged error- ϵ_2 in full field during iteration towards solution of reflected field on PEC. Boundary elements N: 150, 384, 600 and $\frac{4s}{\lambda}=1.4005$.

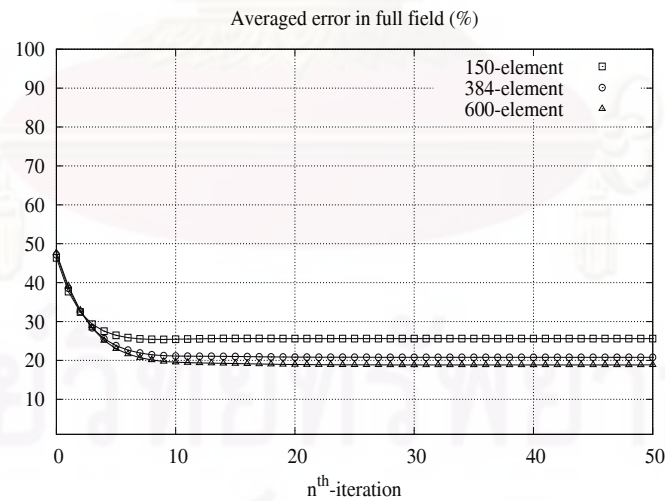


Figure 5.64: Percentage averaged error- ϵ_2 in full field during iteration towards solution of reflected field on PEC. Boundary elements N: 150, 384, 600 and $\frac{4s}{\lambda}=1.5278$.

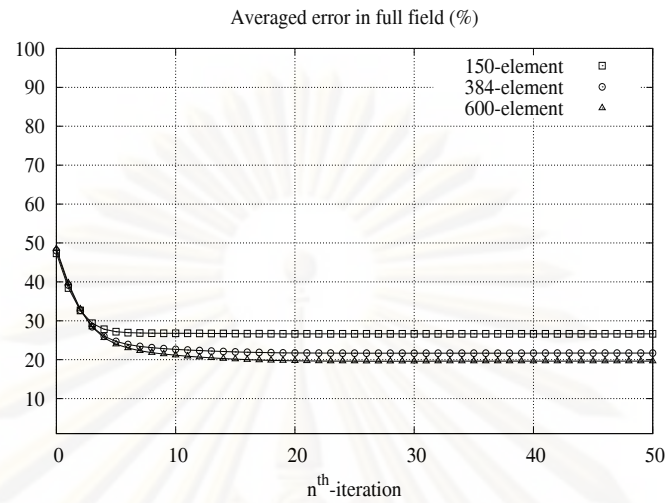


Figure 5.65: Percentage averaged error- ϵ_2 in full field during iteration towards solution of reflected field on PEC. Boundary elements N: 150, 384, 600 and $\frac{4s}{\lambda}=1.6552$.

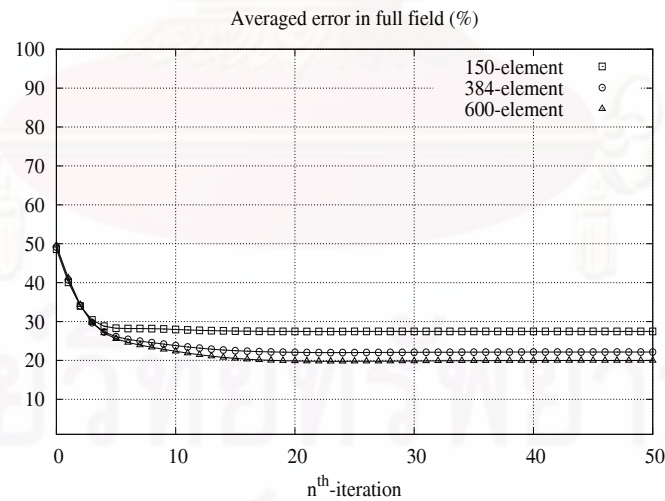


Figure 5.66: Percentage averaged error- ϵ_2 in full field during iteration towards solution of reflected field on PEC. Boundary elements N: 150, 384, 600 and $\frac{4s}{\lambda}=1.7825$.

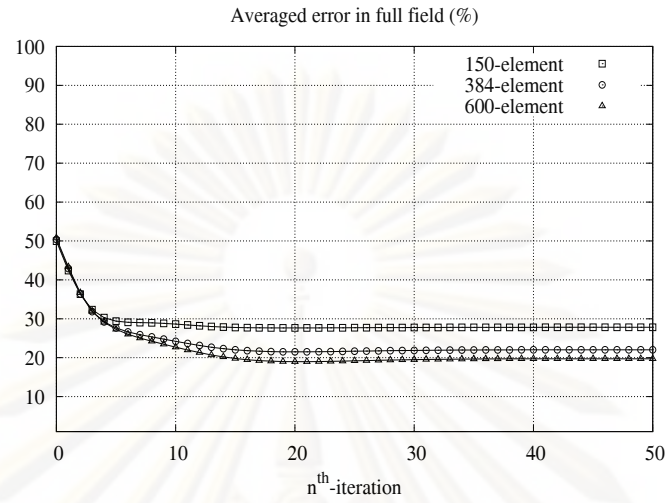


Figure 5.67: Percentage averaged error- ϵ_2 in full field during iteration towards solution of reflected field on PEC. Boundary elements N: 150, 384, 600 and $\frac{4s}{\lambda}=1.9098$.

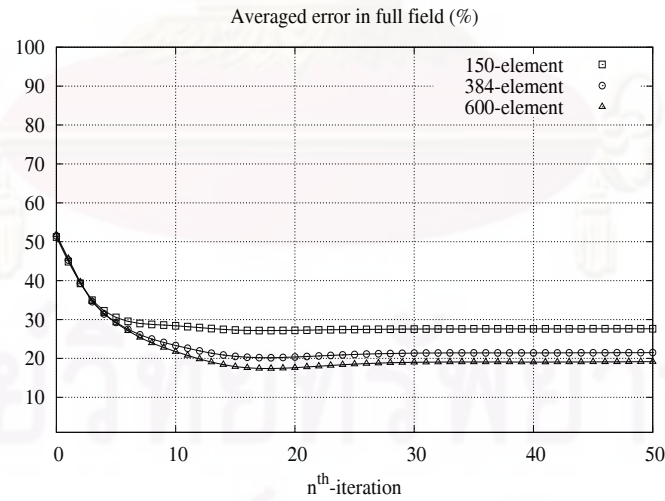


Figure 5.68: Percentage averaged error- ϵ_2 in full field during iteration towards solution of reflected field on PEC. Boundary elements N: 150, 384, 600 and $\frac{4s}{\lambda}=2.0371$.

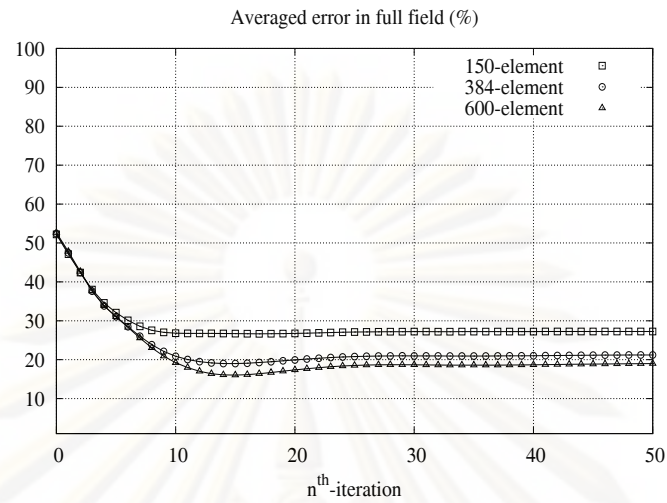


Figure 5.69: Percentage averaged error- ϵ_2 in full field during iteration towards solution of reflected field on PEC. Boundary elements N: 150, 384, 600 and $\frac{4s}{\lambda}=2.1645$.

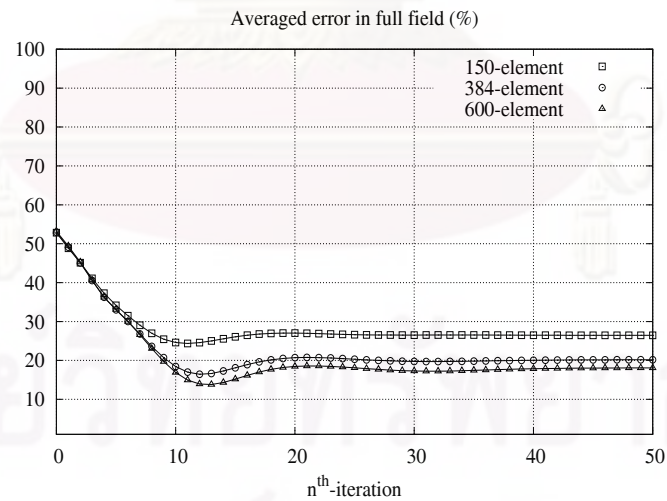


Figure 5.70: Percentage averaged error- ϵ_2 in full field during iteration towards solution of reflected field on PEC. Boundary elements N: 150, 384, 600 and $\frac{4s}{\lambda}=2.2918$.

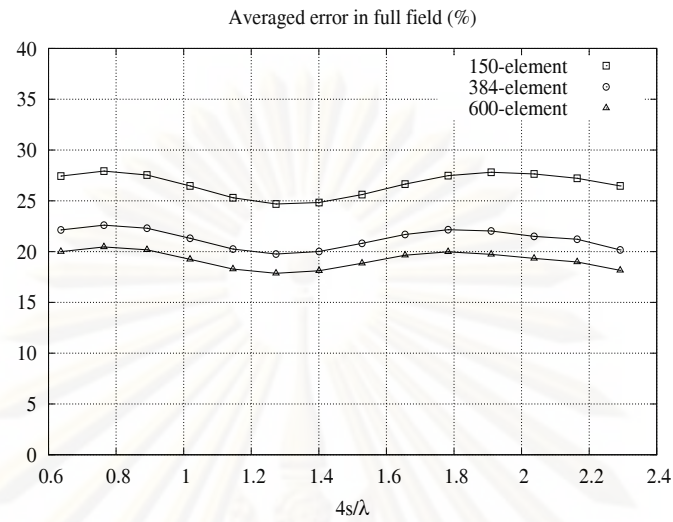


Figure 5.71: The last averaged error- ϵ_2 (%) of iterative solution of perfect reflection in full field at corner point on boundary elements 150, 384, 600 and $\frac{4s}{\lambda} \in (0.6, 2.3)$.

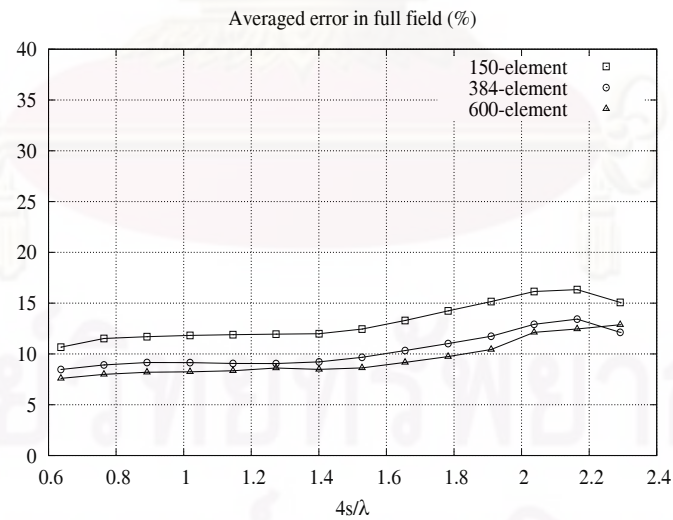


Figure 5.72: The last averaged error- ϵ_3 (%) of iterative solution of perfect reflection in full field at corner point on boundary elements 150, 384, 600 and $\frac{4s}{\lambda} \in (0.6, 2.3)$.

5.3.4 Calculation of radar cross section at Far-Field

After the iterative solutions of the reflected field on PEC cube are provided evidence by the errors on Banach space, they are double-checked in this section. These surface fields are operator with Cauchy extension operator in order to evaluate all components of the scattered field around the PEC cube. The six surfaces of a cube are divided into the definite number of elements such as 150, 384 and 600. Normally, the scattered fields are examined in the form of radar cross section:

$$\sigma = 4\pi r^2 \frac{|\vec{H}^{sc}|^2}{|H_0|}, \quad (5.20)$$

where r is the distance from the scatterer. The $|H_0|$ and $|\vec{H}^{sc}|$ are the magnitude of the magnetic field that are decoded from the incident and scattered field, respectively.

In [65] the EHFD method produces the broadside curve of backscattering RCS compared with the measured data. Then, these curves are used to examine the results of the proposed method. Figs. 5.73 to 5.75 plot the RCS curves of the EHFD method and measured data in order to compare with the numerical results when using boundary elements as 150, 384 and 600, respectively. The RCS of the proposed method has higher accuracy than the EHFD method when the wavelength of the incident field increases. The errors of RCS by the proposed method can be reduced when the number of the elements is increased as Figs. 5.73 to 5.75. Note that these errors are corresponding with the errors of the surface fields as Figs. 5.71 and 5.72. Therefore, the proposed method can give better the RCS when the number of boundary elements is increased from 150, 384 and 600.

Moreover, those surface fields on boundary that are calculated by the proposed method can evaluate the scattered field any point around the PEC cube by operating with Cauchy extension. The scattered fields are described in terms of both E-plane and H-plane Bi-static RCS at $r = 1$ km as Figs. 5.76 to 5.89. In each figure, the three curves are for different conditions, with the cubic boundary divided into either $N = 150, 384$ and 600 elements. With each condition the RCS obtained has the corresponding characteristic. The RCS curve between using 384 and 600 elements is less different than using 150 and 384 elements.

The experiment results of all cases are covered the calculation of the scattered field over $4s/\lambda \in (0.6, 2.3)$. Under this situation the iterative algorithm can reproduce the solution of the scattered field converging strongly. However, the iterative algorithm has less efficient when the value of $4s/\lambda$ is more than 2.3. For example of $4s/\lambda$ equals 3.0, the error- ϵ_2 in full field that has condition by using 600 elements is plotted for analyzing the convergence of iterative solution as shown Fig. 5.90. Although, the solution fluctuates very greatly, it can be captured to check the correction when the error- ϵ_2 is minimize value. The results are compared with the measured data [66] and they are plotted the E-plane and H-plane Bi-static RCS at $r = 1$ km as shown Fig. 5.91. The case of scattered field when $4s/\lambda$ equals 3.0 is used often to confirm the algorithm by many researchers, since the spurious solution in this case occurs from the other integral equation method [67].

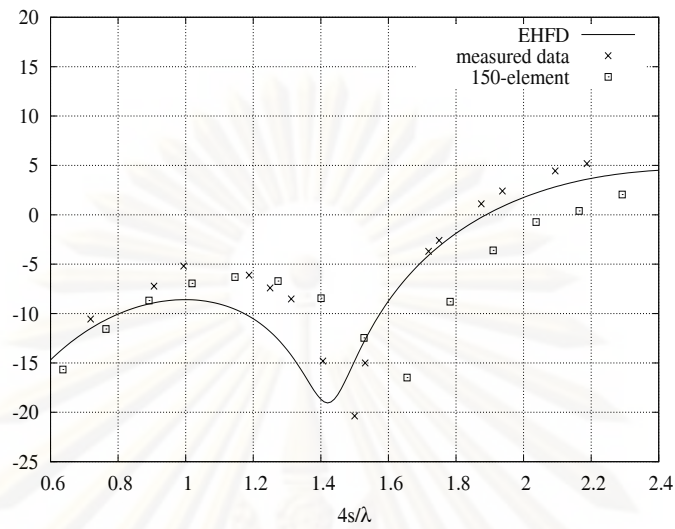


Figure 5.73: Broadside of backscattering RCS at $r=1\text{km}$. computed using EHF solution and iterative method using 150-element compared with measured data.

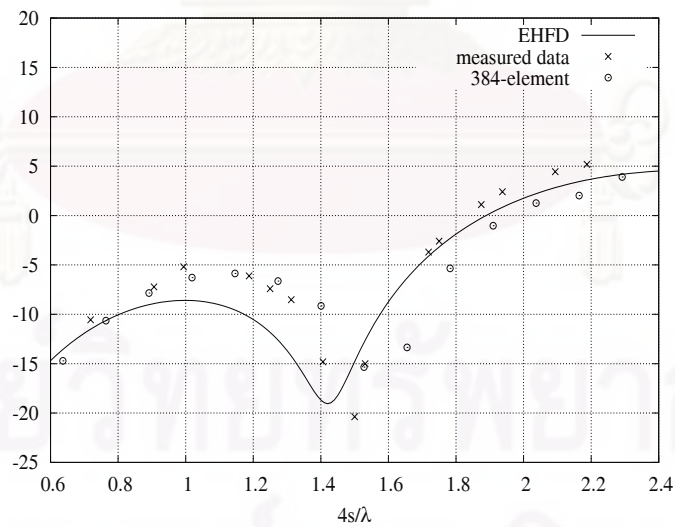


Figure 5.74: Broadside of backscattering RCS at $r=1\text{km}$. RCS computed using EHF solution and iterative method using 384-element compared with measured data.

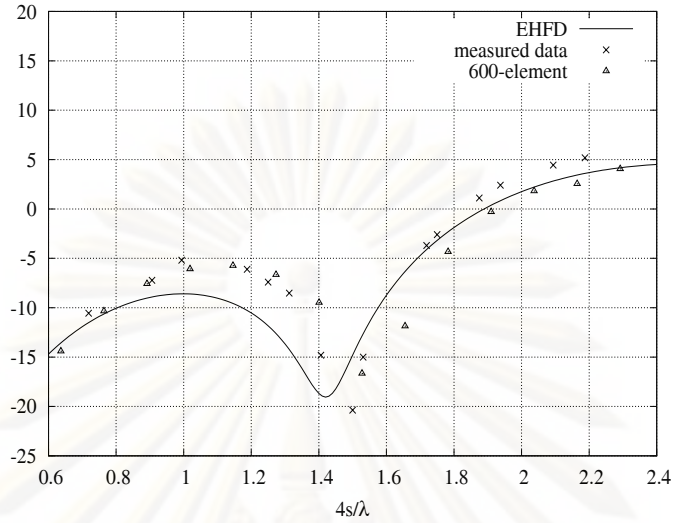


Figure 5.75: Broadside of backscattering RCS at $r=1\text{km}$. RCS computed using EHFD solution and iterative method using 600-element compared with measured data.

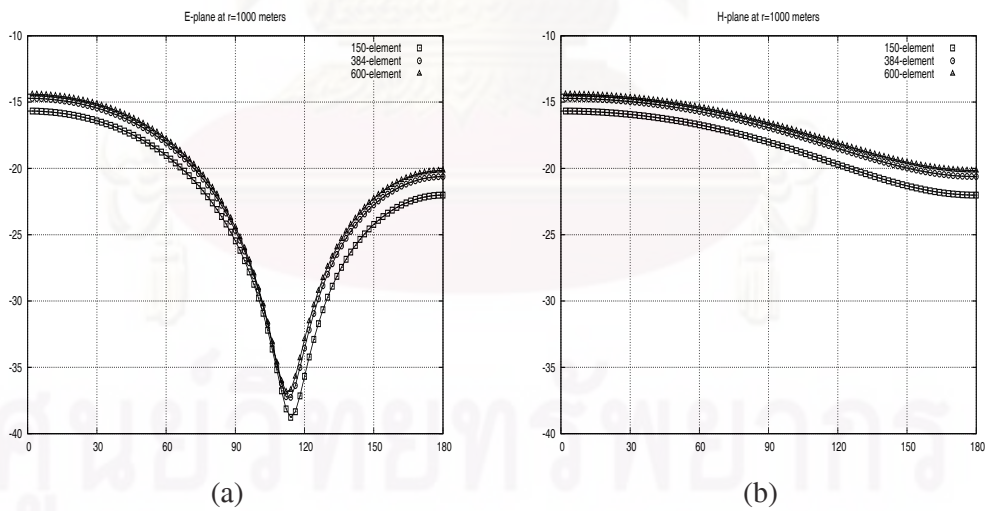


Figure 5.76: E-plane and H-plane Bi-static RCS at $r=1\text{km}$. in (a) and (b), respectively. RCS computed using iterative method when varying boundary elements: 150, 384, 600 and $\frac{4s}{\lambda}=0.6366$.

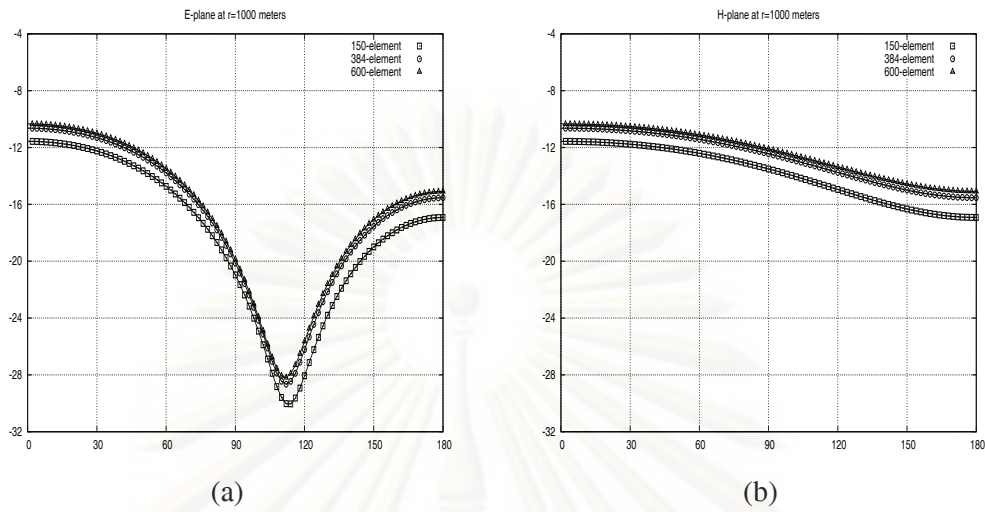


Figure 5.77: E-plane and H-plane Bi-static RCS at $r=1\text{km}$. in (a) and (b), respectively. RCS computed using iterative method when varying boundary elements: 150, 384, 600 and $\frac{4s}{\lambda}=0.7640$.

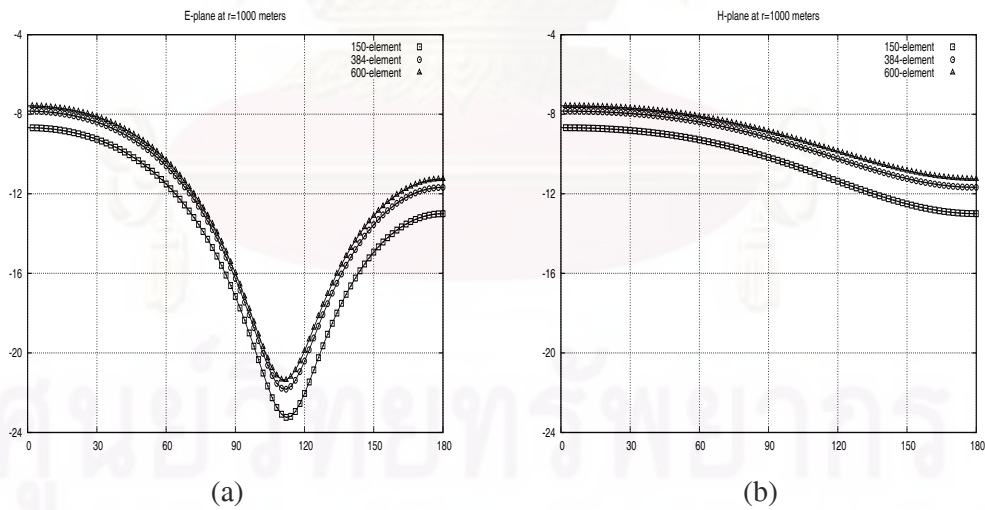


Figure 5.78: E-plane and H-plane Bi-static RCS at $r=1\text{km}$. in (a) and (b), respectively. RCS computed using iterative method when varying boundary elements: 150, 384, 600 and $\frac{4s}{\lambda}=0.8913$.

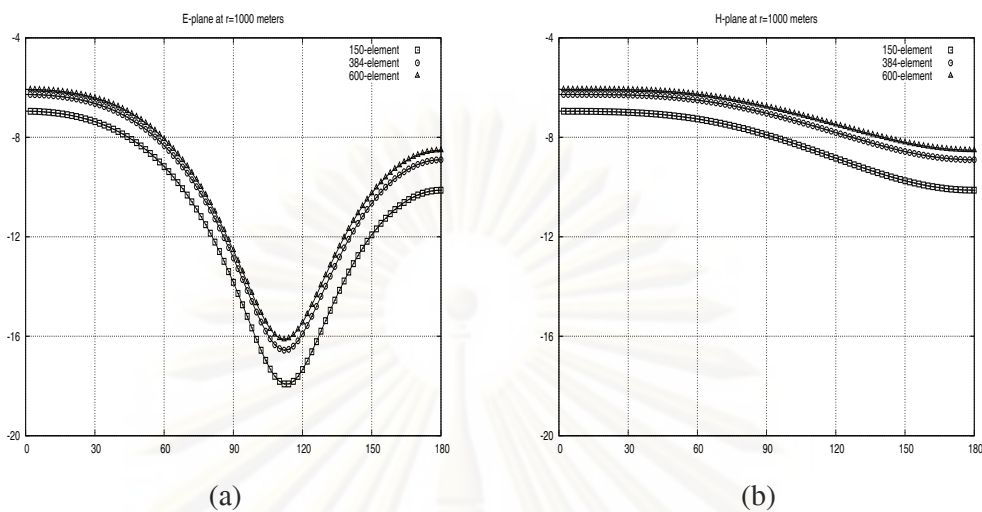


Figure 5.79: E-plane and H-plane Bi-static RCS at $r=1\text{km}$. in (a) and (b), respectively. RCS computed using iterative method when varying boundary elements: 150, 384, 600 and $\frac{4s}{\lambda}=1.0185$.

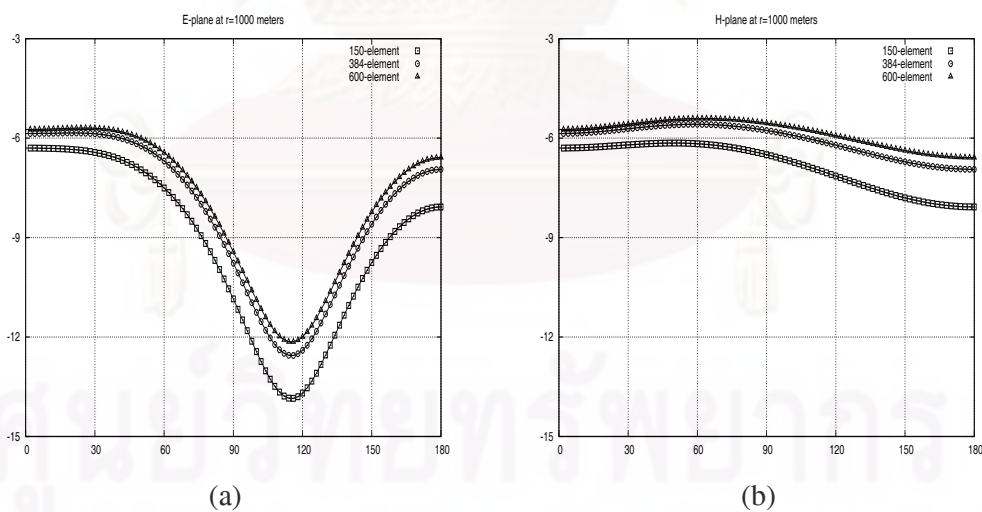


Figure 5.80: E-plane and H-plane Bi-static RCS at $r=1\text{km}$. in (a) and (b), respectively. RCS computed using iterative method when varying boundary elements: 150, 384, 600 and $\frac{4s}{\lambda}=1.1460$.

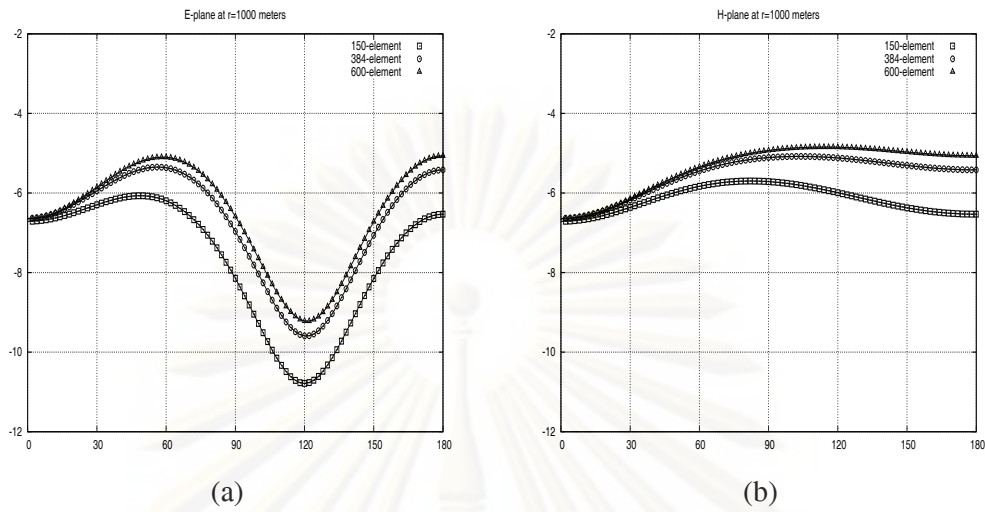


Figure 5.81: E-plane and H-plane Bi-static RCS at $r=1\text{km}$. in (a) and (b), respectively. RCS computed using iterative method when varying boundary elements: 150, 384, 600 and $\frac{4s}{\lambda}=1.2732$.

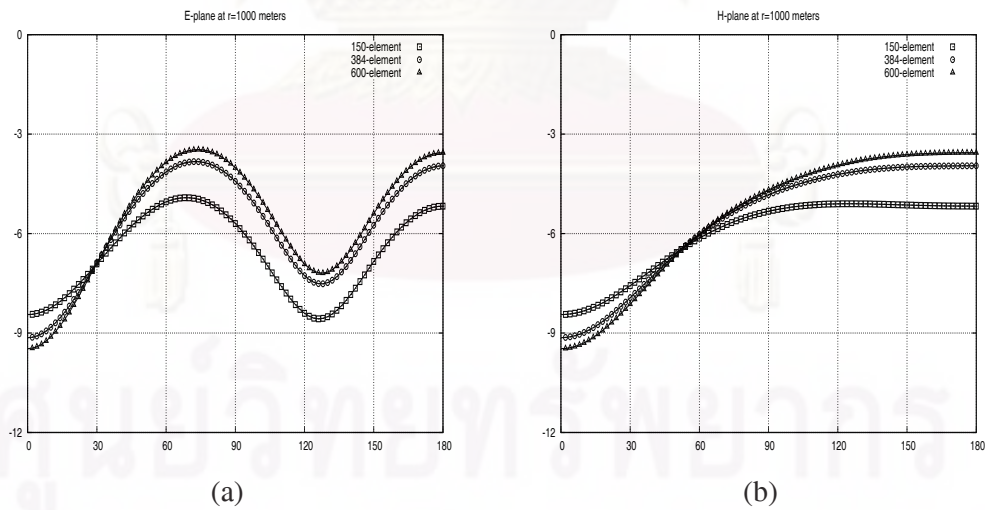


Figure 5.82: E-plane and H-plane Bi-static RCS at $r=1\text{km}$. in (a) and (b), respectively. RCS computed using iterative method when varying boundary elements: 150, 384, 600 and $\frac{4s}{\lambda}=1.4005$.

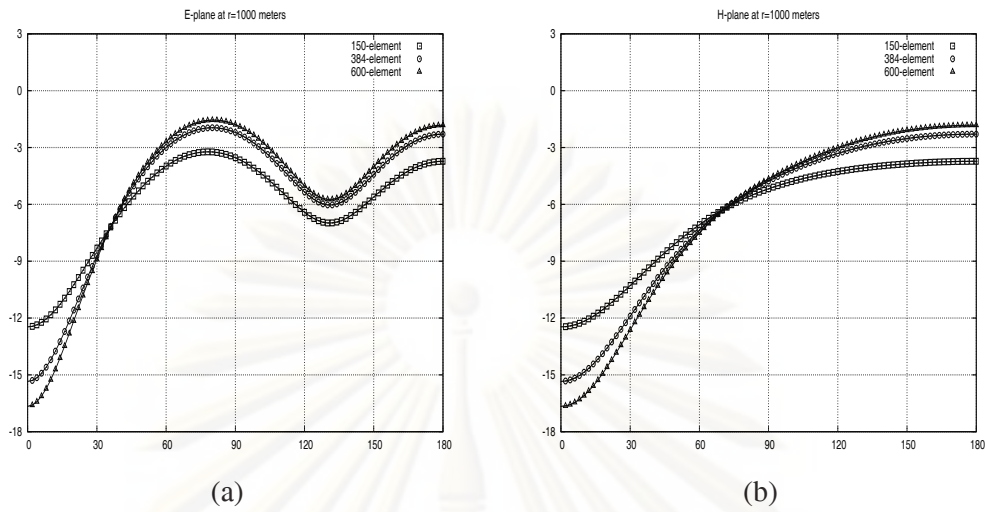


Figure 5.83: E-plane and H-plane Bi-static RCS at $r=1\text{km}$. in (a) and (b), respectively. RCS computed using iterative method when varying boundary elements: 150, 384, 600 and $\frac{4s}{\lambda}=1.5278$.

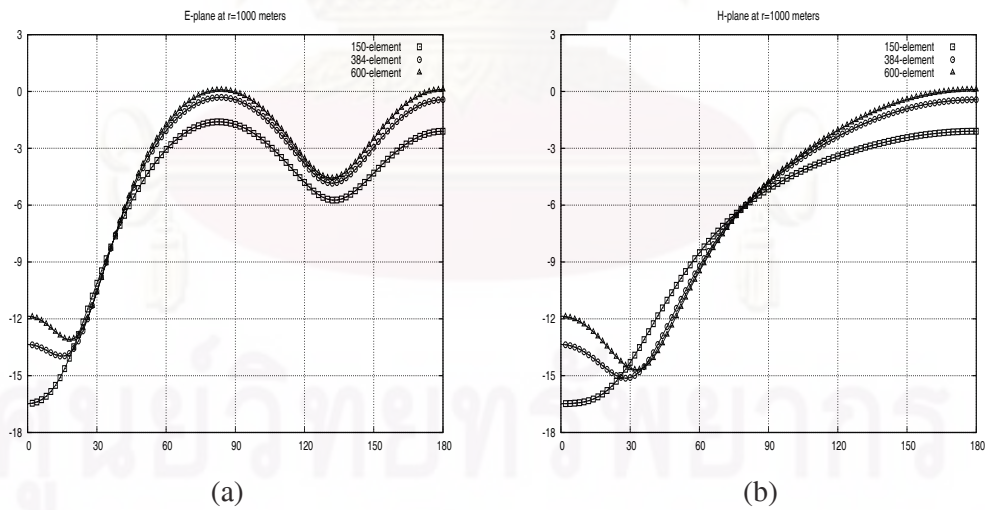


Figure 5.84: E-plane and H-plane Bi-static RCS at $r=1\text{km}$. in (a) and (b), respectively. RCS computed using iterative method when varying boundary elements: 150, 384, 600 and $\frac{4s}{\lambda}=1.6552$.

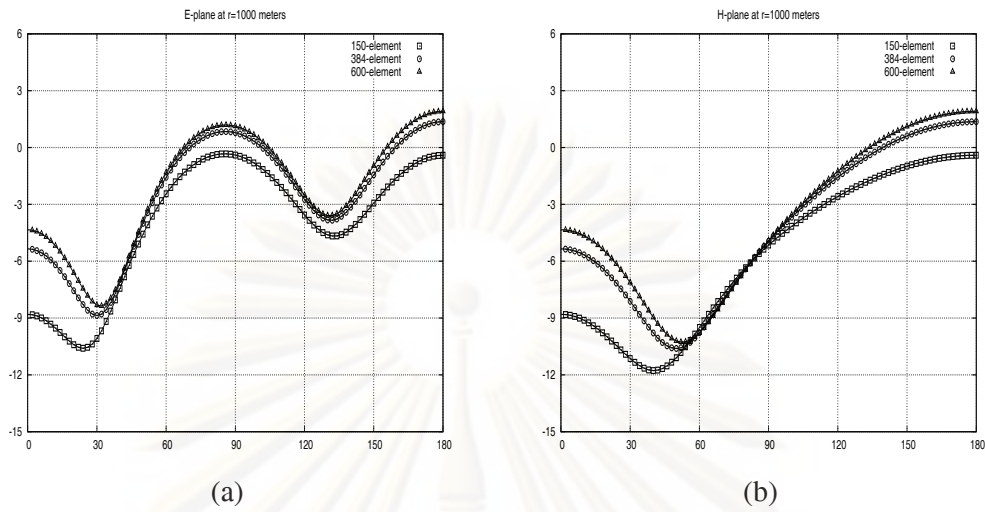


Figure 5.85: E-plane and H-plane Bi-static RCS at $r=1\text{km}$. in (a) and (b), respectively. RCS computed using iterative method when varying boundary elements: 150, 384, 600 and $\frac{4s}{\lambda}=1.7825$.

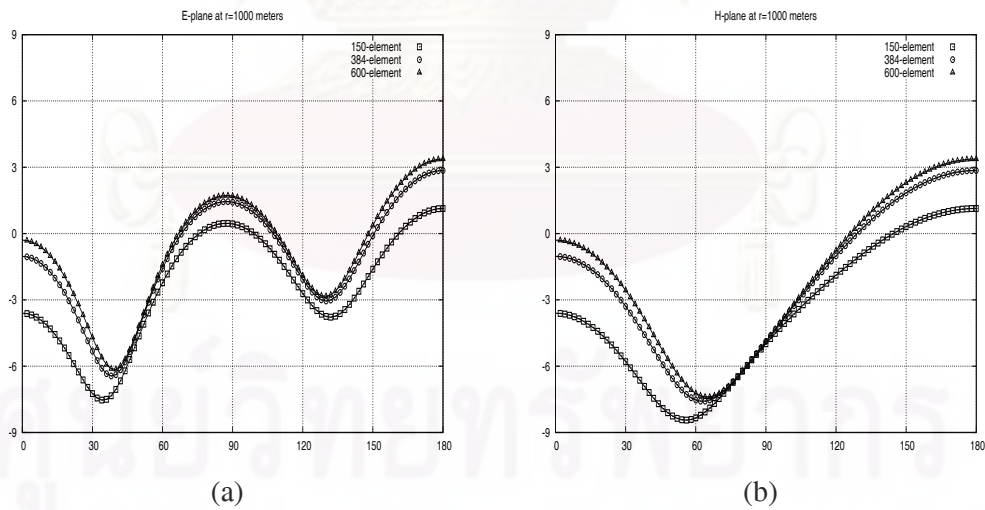


Figure 5.86: E-plane and H-plane Bi-static RCS at $r=1\text{km}$. in (a) and (b), respectively. RCS computed using iterative method when varying boundary elements: 150, 384, 600 and $\frac{4s}{\lambda}=1.9098$.

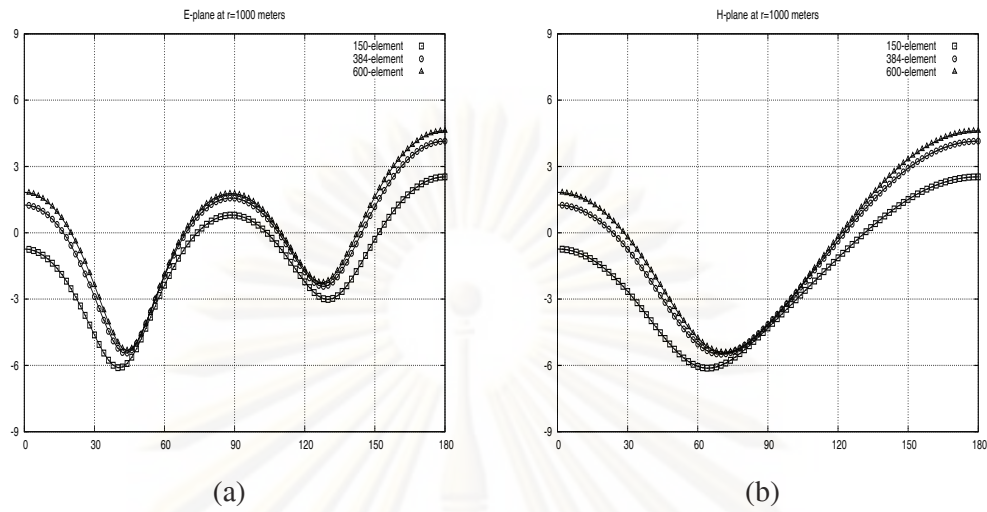


Figure 5.87: E-plane and H-plane Bi-static RCS at $r=1\text{km}$. in (a) and (b), respectively. RCS computed using iterative method when varying boundary elements: 150, 384, 600 and $\frac{4s}{\lambda}=2.0371$.

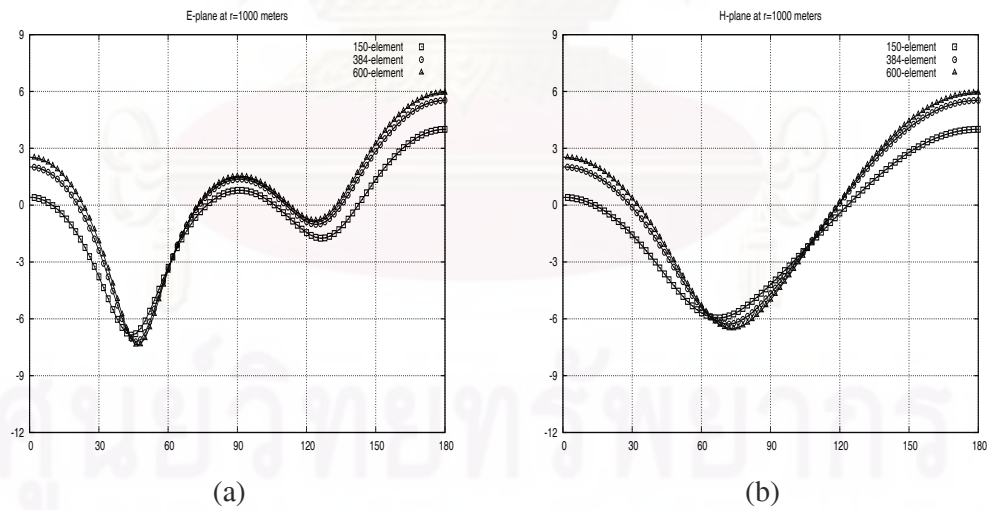


Figure 5.88: E-plane and H-plane Bi-static RCS at $r=1\text{km}$. in (a) and (b), respectively. RCS computed using iterative method when varying boundary elements: 150, 384, 600 and $\frac{4s}{\lambda}=2.1645$.

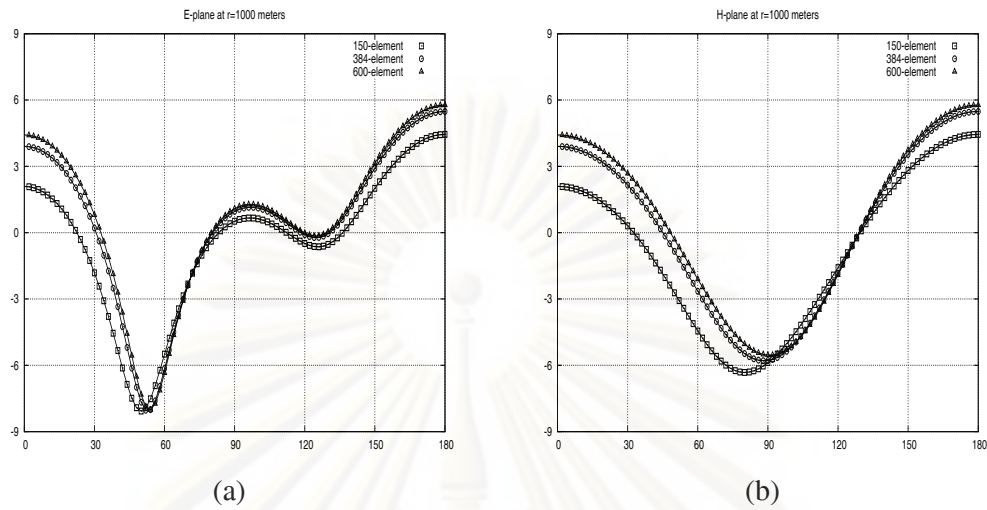


Figure 5.89: E-plane and H-plane Bi-static RCS at $r=1$ km. in (a) and (b), respectively. RCS computed using iterative method when varying boundary elements: 150, 384, 600 and $\frac{4s}{\lambda}=2.2918$.

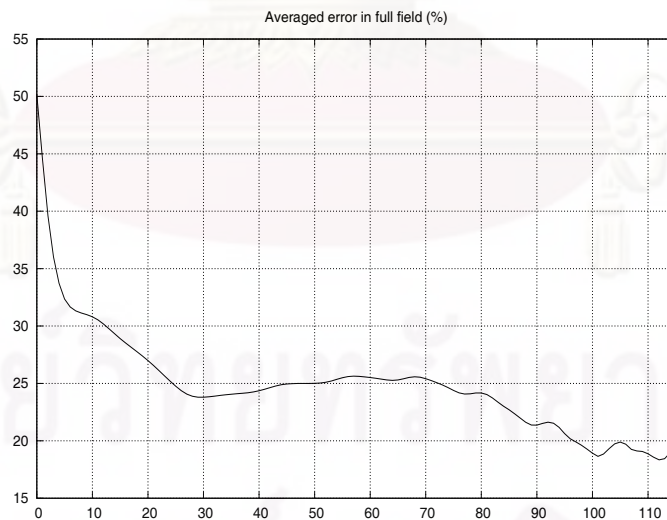


Figure 5.90: Percentage averaged error- ϵ_2 in full field during iteration towards solution of reflected field on PEC. Boundary elements N : 600 and $\frac{4s}{\lambda}=3.0$.

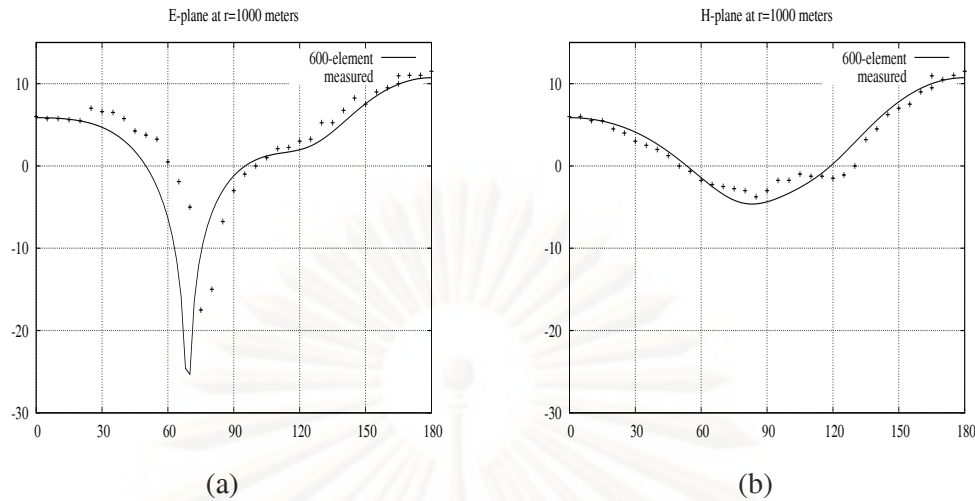


Figure 5.91: E-plane and H-plane Bi-static RCS at $r=1\text{Km}$. in (a) and (b), respectively. RCS computed using iterative method when using boundary elements: 600 and $\frac{4s}{\lambda}=3.0$.

5.3.5 Calculation of reflection coefficient

On a planar interface the tangential components of electric and magnetic fields must be continuous at the boundary between the incident and transmitting media. The reflection coefficient is given by

$$\Gamma = \frac{|\vec{E}^{sc}|}{|\vec{E}^{in}|} = -\frac{|\vec{H}^{sc}|}{|\vec{H}^{in}|}. \quad (5.21)$$

In Fig. 5.92 the reflection coefficients are evaluated by focusing the incident and scattered fields at the centre of backscattering surface of a cube by using 150, 384 and 600 elements. The results computed by 384 and 600 elements are similar more than 150 elements. Consequently, the reflection coefficients can get more accurate when the numerical results of the scattered field on boundary are close up to the exact solution.

5.4 Summary

The iterative method presented in Chapter 5 can be used for both perfectly reflective and transmissive interfaces. Here, there are three applications such as test cases, far-field cases and scattering cases. Both test and far-field cases are on the transmissive type of the interface since the results are in general known in advance. It is difficult to evaluate clearly the direction and magnitude of the reflected field in the scattering cases; however, the measured data and the numerical results by the other method have been referred here. This knowledge makes it easier to properly evaluate the performance of the algorithm.

The cube is chosen as a tested shape for reason of simplicity. For surfaces with sharp edges and corners it is usually expected that the field contains singularities at some points. That is not the cases of perfect transmission, since the incident field is transmitted through the surface without perturbation. The field everywhere, including on edges and corners, is

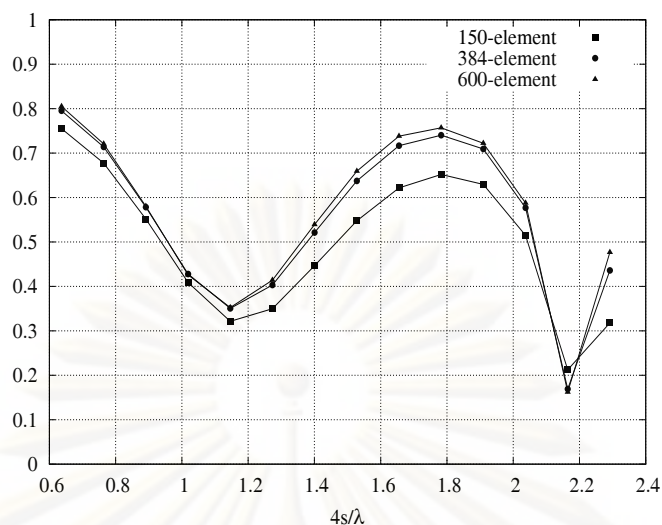


Figure 5.92: Reflection coefficient at backscattering when using boundary elements: 150, 384 and 600 elements.

that of either a plane wave or is that of a dipole source. In the first case study the field is totally void of singularities, and in the second there is one singularity at the source itself. However, the dipole here is placed off the surface, so the field on the surface is everywhere finite and well behaved. In the third the scattered field from the PEC cube is very interesting from [66]. Its numerical calculation is often involves the occurrence of spurious solutions, because the incident field is echoed diffusely over the surface and especially on edges and corners.

The efficiency of algorithm in these three applications has been analyzed in various wavelengths, after each iterative solution converges into some finite error. The accuracy achieved in Fig. 5.25 for test cases is greater than in Fig. 5.48 for dipole source. The orientation of the plane wave matches the orientation of surface and also matches the orientation of the elements into which the surface is divided. The same is not true for dipole source, where the nature of the wave is more well suited by a spherical rather than a cubic and Cartesian system. The bilinear functions and quantization chosen here are set in the Cartesian framework, and do not accommodate the dipole field as easily as they accommodate the plane wave. It then follows for any given level of quantization that the accuracy is likely to be higher for the plane wave. Nevertheless, for both applications the accuracy can be improved by increasing the number of elements. It is likely that the same would also be the true if functions of higher order than bilinear were used.

In the scattering cases error- ϵ_2 and error- ϵ_3 are considered instead of the averaged error. When considering error- ϵ_2 of three applications the accuracy of achieved in Fig. 5.27 for test cases is greater than in Fig. 5.50 for the dipole source and Fig. 5.71 for scattered field, respectively. The boundary condition for the scattered field at some points of a cube has been not complete, when some components of the reflected field as the initial data for iterative solution are computed from the incident field. Some points that located on edge and corner cause the big error when the normal unit has not identified correctly. Accordingly, the error- ϵ_3 of three applications play similarly with the error- ϵ_2 . The error in Fig. 5.28 for test cases is better than in Fig. 5.51 for far-field cases and in Fig. 5.72 for scattering cases, respectively. After that these results of iterative solutions are used to generate the radar cross section

as shown in Figs. 5.73, 5.74 and 5.75 when using number of elements as 150, 384 and 600, respectively. The RCS calculated by iterative solution is more accurate than the EHFD solution when referring with measured data. The numerical results of the reflected field have still not deteriorated near internal resonance of the PEC cube when varying wavelengths between $4s/\lambda \in (0.6, 2.4)$. It is very interesting that the basis functions are improved for the scattered field on boundary when focusing into high frequency.

Consider now the convergence of iterative solution in perfect transmission when the interface is same, but the incident field is different. The rate of convergence towards solution appears in Figs. 5.35 to 5.47 higher for the far-field cases than in Figs. 5.9 to 5.21 for the test cases, although the shape of the curve for the dipole makes it somewhat difficult to obtain a good estimate. Consider also the convergence of iterative solution when the incident field is same, but the interface is different. In this case the rate of convergence towards solution appears in Figs. 5.57 to 5.70 much higher for the scattering cases than in Figs. 5.35 to 5.47 for test cases. The accuracy accrues at a rate of five decimal place for every ten iterations in test cases, three decimal place for every five iterations in far-field cases and one decimal place for every three iterations. However, the number of iterations in scattering cases is the smallest and in test cases is the largest.

Many problems in physics can be formulated as some kind of linear system. Traditionally Maxwell's equations are formulated using a linear system constructed around Green's functions. Here, the formulation involves instead the Cauchy kernel. Both are linear systems. In both cases the solution involves determining the unknown fields or currents using some kind of linear algebra. In the case of Green's functions, it is normal to use the algebra of real or complex numbers. It is usually possible (even if it is not done) to write the system using matrix algebra. The most direct solution then involves a matrix inverse, either directly or indirectly (i.e. iteratively).

Matrix inverse of size $N \times N$ usually take of the order of N^3 operations. If some particular structure of the system can be exploited, it may be possible to reduce the number of operations. Also, an iterative technique may require fewer operations than a direct technique. However, none of that can be guaranteed. The one thing that can be guaranteed is that any solution taking more than N^3 operations is not as efficient as a matrix solution, and is therefore definitely not very good.

Here, our interest is to check that the solution either not worse than a matrix solution, or perhaps is better than a matrix solution. If either of those cases are true, then we can conclude that there is nothing really wrong or badly inefficient with the solution we use. It may of course with a lot more study be possible to develop a better (faster, more efficient) solution. However, if we are already faster than N^3 , it may not be possible to be very much faster.

The operations of multiplication and addition are carried in Clifford arithmetic, which takes more work than real arithmetic. Without taking special short cuts, a Clifford multiplication of two four-dimensional Clifford numbers, each of which have 16 complex coefficients, takes $16^2 = 64$ complex multiplications and additions when implemented as 4×4 Dirac matrices. However, for applications in electromagnetism short cuts can be achieved because many of the 16 complex coefficients are zero. The \vec{E} and \vec{H} fields together require only six non-zero complex coefficients, and simple vectors such as the normal vector \vec{n} require only three non-zero real coefficients.

Table 5.2 shows CPU time on a personal computer (AMD Athlon, 2.4 GHz) and required memory 512 MB. When using 150 elements the operation of the integral operator, construction of Matrix \mathbf{G} and each period of iteration took around 8.66, 1074.27 and 301.62

seconds, respectively. The other data using 384 and 600 elements are shown in Table 5.2.

Table 5.2 CPU time (seconds).

Number element	Number node	Integral operator	Geometry Matrix G	A period iteration
150	152	8.66	1064.27	301.62
384	386	20.40	6936.03	1948.75
600	602	31.91	16854.87	4756.24



ศูนย์วิทยทรัพยากร
จุฬาลงกรณ์มหาวิทยาลัย

CHAPTER VI

CONCLUSIONS

6.1 Conclusions of Desertation

The differential form of Maxwell's equations based on vector calculus has for a long time been widely popular when solving electromagnetic problems. These equations serve as a starting point from which to introduce another differential form based on Clifford algebra. In detail both electromagnetic fields and their differential operators on vector calculus are encoded respectively into a single number and an operator in Clifford arithmetic. The electric and magnetic fields are encoded into a four dimensional Clifford number. Both divergence and curl operators are replaced with a Clifford gradient operator. In the Clifford framework the Maxwell-Dirac equation, which reproduces faithfully all of Maxwell's equations, is the fundamental equation governing behavior of the electromagnetic field.

The Maxwell-Dirac equation (called the k -Dirac equation by mathematicians) is constructed from the k -Dirac operator and the Clifford field. The k -Dirac operator is a first order differential operator. Differentiating it reproduces the Helmholtz operator. The Helmholtz equation is the reduced version of Maxwell's equations used to make the solution of the potential, but the k -Dirac equation is the unadulterated version of Maxwell's equations and is used to make the solution of the electromagnetic field directly. The Green's function is the fundamental solution of the Helmholtz operator. Although it works in a straightforward manner when applied to the potential problem, it needs various complicated techniques when computing the field itself. The fundamental solution of the k -Dirac operator provides a much more direct approach in order to obtain the solution of Maxwell's field equations.

The integral form of the Maxwell-Dirac equation is derived from the boundary theorem by applying it to the fundamental solution of the k -Dirac operator. This integral equation describes the behavior of the full field at any point as generated by the fields on the boundary. The initial form of the integral equation considers only the field at points placed inside the boundary, but that form can be extended to evaluate the field at any points placed anywhere in the entire domain. The resulting integral equations are divided into two kinds. The first kind of the integral equation (the Cauchy extension operator) can reproduce the full field at any point placed inside and outside the boundary. It is used to analyze the behavior of the field propagating away from the boundary. Another integral equation (the Cauchy integral operator) describes the relationship of the fields at any point placed on the boundary. It not only evaluates the difference of the inward and outward fields along the boundary, but also behaves as a reflection operator accommodating Maxwell's equations.

The boundary field problems that are examined satisfy the reduced (homogeneous or source free) version of Maxwell's equations. These problems are constructed by using proposed projection operators, and their specified boundary conditions are described with data projection operators. The proposed projection operators, the plus and minus Hardy projection operators, define a Banach space in which to construct generalized geometric solutions. The geometric solution only fails to be unique if the two systems of projection operators (Hardy and data) are identically the same. However, the Hardy projection operators and the

data projection operators play quite distinct and separate roles, so that the solution obtained is very well defined. Although the proposed work has covered the boundary field problems in the case of perfect transmission and perfect reflection, it is possible to expand into the case of the partial transmission and reflection. Surface currents play no role in the proposed integral equations and appear nowhere in the geometric solutions. For that reason, it is possible to use the technique for objects which are not perfect electric conductors just as easily as for objects which are perfect electrical conductors.

The proposed integral equations are applied for solving practical problems by employing numerical techniques. The considered boundary is discretized into the number of rectangular segments. After that the integral equations are formulated with boundary element techniques. Over each element of the boundary, the kernel integral is constructed from geometric function in conjunction with the approximated surface field. The geometric function is produced by multiplying the fundamental solution of k -Dirac operator and the unit normal. For approximating the surface field, the mathematical theory [51, 52, 58, 62] behind the method presented here is quite rigorous. The implementation of the surface field departs from the rigor of the theory by making three different approximations. Firstly, the surface is quantized into a finite number of elements (here squares). Secondly, the field on each element is supposed to conform to a particular generic form (here bilinear). Thirdly, integrals over the elements are evaluated numerically (here by Gauss Legendre integration). Such departures from the theory, if taken too far, can render its support invalid. However, if departures from the theory are kept within acceptable limits, valid solutions are guaranteed. Although it is not clear in general what those limits might be, the experience here is that valid solutions are achievable (within a fixed amount of error) using relatively simple approximations. Needless to say, making improvements to those approximations is likely to yield even more accurate results.

After the applied Hardy projection operators are verified to produce an acceptably small finite error, they are used to compute the iterative solutions. The iterative solutions are obtained by expanding the inverse of the compound operators $\mathbf{I} - \mathbf{X}$ in the formal solution as a binomial series $(\mathbf{I} - \mathbf{X})^{-1} = \sum_{m=0}^{\infty} \mathbf{X}^m$. Convergence of the binomial series follows from the properties of the operator \mathbf{X} . For example in the test case of Chapter V the operator $\mathbf{X} = \mathbf{P}^+ \mathbf{Q}^+$ and for any function $x \neq 0$ on the OP-axis that $|\mathbf{P}^+ \mathbf{Q}^+ x| < |\mathbf{I}x| = |x|$ since $\mathbf{P}^+ \mathbf{Q}^+ x$ is closer to the origin. That is always true as long as \mathbf{P}^+ and \mathbf{Q}^+ (as here) are some kind of projection operators. For the case of Fredholm integral equations, the rate of convergence can be improved by replacing Neumann style iterative solutions by various alternatives, such as the conjugate gradient method (*cf.* [68]). It would be expected that similar improvements can be achieved if the same methods apply in non-Fredholm non-commutative situation here.

When converting an implementation of the transmissive problem into an implementation of the reflective problem some care must be taken. Validity of the conversion relies on the resulting implementation meeting certain conditions required of the reflective solution, but not of the transmissive solution. In principle, basis functions which support singularities at the corners and edges are required. Use of bilinear functions as here cannot be expected to yield optimal results. With the new basis functions, methods of integration must be chosen accordingly; *i.e.*, to support (integrable) singularities at the limits of the integration. Doing so eliminates the need for the angular ratios in Table 4.1 at the corners and edges of the cube which, in the case of the reflective problems, are unknown.

6.2 Future Research

The scope of the work here has been limited to the most simple cases in three ways: theoretical, numerical and applied.

Theory Here the theory used applies only to the case of perfect transmissive and perfectly reflection objects. Although there are many real applications for which this theory is sufficient, there are also applications such as dielectrically loaded waveguides, where the theory of partially reflective and transmissive objects needs to be used instead. Further work is required at theoretical level to accommodate these applications. For example, it is not clear if the simple iterative solution described here is appropriate for partially reflective and transmissive objects. The reason for some doubt is that for these objects the geometrical constructions on which the solution here is based, are not longer simple and straightforward.

Numerical Methods The numerical techniques used here are limited by shape, integrations, basis functions, and speed.

1. Shape is limited to rectilinear objects. That is not useful for most engineering applications. Further work us required to extend the implementation so that it also applies to smoothly curving surfaces.
2. Integration are limited to cases where the normal is everywhere known, and the functions (fields) on the boundary are everywhere finite. In practice the (field density) functions should be free to approach infinity at sharp edges and corners, and the normals there are undefined. Further work is required to incorporate integration techniques which accommodate integrable singularities at the corners and edges, and are insensitive to the normal at those points.
3. The basis functions here are simpler than strictly necessary to properly represent all fields in the surfaces of all objects. Further work is required to incorporate basis functions which support integrable singularities at the corners and edges.
4. The iterative technique here has linear convergence, i.e. the number of decimal places of accuracy increases by the same amount every iteration (until close to convergence). Iterative techniques for the other problems have been developed which show convergence characteristics greater than linear, suggesting that it may be possible to improve the speed of convergence for the iteration used here. Further work is required to find out how to do that.

Applications The applications investigated here are useful for testing the technique but are too simple for real (engineering design) solutions. Further work is required to extend the technique (particularly in the numerical sense described above) and then apply it to problems of real engineering interest, such as the design of antennas and waveguides.

References

- [1] Balanis, C. A. Advanced Engineering Electromagnetics. New York : John Wiley & Sons, 1989.
- [2] Bluck, M. J., Hatzipetros, A., and Walker, S. Applications of differential forms to boundary integral equations. IEEE Trans. on Antennas and Propagation. 54 (June 2006): 1781–1796.
- [3] Garcia-Castillo, L., Salazar-Palma, M., Sarkar, T., and Adve, R. Efficient solution of differential form of Maxwell's equations in rectangular regions. IEEE Trans. on Microwave Theory and Techniques 43 (Mar. 1995): 647–654.
- [4] Miller, E. K. A selective survey of computational electromagnetics. IEEE Trans. on Antennas and Propagation 36 (Sept. 1988): 1281–1305.
- [5] Krishnan, A. Finite element analysis of lossless propagation in surface plasmon polariton waveguides with nanoscale spot-sizes. Journal of Lightwave Technology 27 (May 2009): 1114–1121.
- [6] Loveday, P. W. Simulation of piezoelectric excitation of guided waves using waveguide finite elements. IEEE Trans. on Ultrasonics, Ferroelectrics and Frequency Control 55 (Sept. 2008): 2038–2045.
- [7] Marais, N. and Davidson, D. B. Numerical evaluation of high-order finite element time domain formulations in electromagnetics. IEEE Trans. on Antennas and Propagation 56 (Dec. 2008): 3743–3751.
- [8] Balanis, C. A. Antenna Theory Analysis and Design. New York : John Wiley & Sons, 3rd ed., Apr. 2005.
- [9] Davidson, D. B. Computational Electromagnetics for RF and Microwave Engineering. Cambridge : Cambridge University Press, 2005.
- [10] Ishimaru, A. Electromagnetic Wave Propagation, Radiation, and Scattering. London : Prentice-Hall International, 1991.
- [11] Petre, P. and Sarkar, T. K. Planar near-field to far-field transformation using an equivalent magnetic current approach. IEEE Trans. on Antennas and Propagation 40 (Nov. 1992): 1348–1356.
- [12] Petre, P. and Sarkar, T. K. Planar near-field to far-field transformation using an array of dipole probes. IEEE Trans. on Antennas and Propagation 42 (Apr. 1994): 534–537.
- [13] Taaghjol, A. and Sarkar, T. K. Near-field to near/far-field transformation for arbitrary near-field geometry, utilizing an equivalent magnetic current. IEEE Trans. on Electromagnetic Compatibility 38 (Aug. 1996): 536–542.

- [14] Sarkar, T. K. and Taaghoul, A. Near-field to near/far-Field transformation for arbitrary near-Field geometry utilizing an equivalent electric current and MoM. IEEE Trans. on Antennas and Propagation 47 (Mar. 1999): 566–573.
- [15] Knepp, D. L. and Goldhirsh, J. Numerical analysis of electromagnetic radiation properties of smooth conducting bodies of arbitrary shape. IEEE Trans. on Antennas and Propagation 20 (May 1972): 383–388.
- [16] Richmond, J. A wire-grid model for scattering by conducting bodies. IEEE Trans. on Antennas and Propagation 14 (Nov. 1966): 782–786.
- [17] Mautz, J. R. and Harrington, R. F. H-field, E-field and combined-field solution for conducting bodies of revolution. Arch. Elektron. Übertragungstech. (AEU) 32 (Apr. 1978): 157–164.
- [18] Harrington, R. F. Field Computation by Moment Methods. Wiley-IEEE Press, May 1993.
- [19] Burke, G. J., Poggio, A. J., Logan, J. C., and Rockway, J. W., NEC-numerical electromagnetics code for antennas and scattering. Proceedings of the IEEE Antennas and Propagation Society International Symposium 17 (1979): 147–150.
- [20] Butler, C. M. and Wilton, D. R. Analysis of various numerical techniques applied to thin-wire scatterers. IEEE Trans. on Antennas and Propagation 23 (July 1975): 534–540.
- [21] Butler, C. M. Evaluation of potential integral at singularity of exact kernel in thin-wire calculations. IEEE Trans. on Antennas and Propagation 23 (Mar. 1975): 293–295.
- [22] Tijhuis, A., Zhongqiu, P., and Bretones, A. R. Transient excitation of a straight thin-wire segment: a new look at an old problem. IEEE Trans. on Antennas and Propagation 40 (Oct. 1992): 1132–1146.
- [23] Wang, W. X. The exact kernel for cylindrical antenna. IEEE Trans. on Antennas and Propagation 39 (Apr. 1991): 434–435.
- [24] Werner, D. H. An exact formulation for the vector potential of a cylindrical antenna with uniformly distributed current and arbitrary radius. IEEE Trans. on Antennas and Propagation 41 (Aug. 1993): 1009–1018.
- [25] Caorsi, S., Moreno, D., and Sidoti, F. Theoretical and numerical treatment of surface integrals involving the free-space green's function. IEEE Trans. on Antennas and Propagation 41 (Sept. 1993): 1296–1301.
- [26] Graglia, R. D. On the numerical integration of the linear shape functions times the 3-D Green's function or its gradient on a plane triangle. IEEE Trans. on Antennas and Propagation 41 (Oct. 1993): 1448–1455.
- [27] Werner, D. H., Huffman, J. A., and Werner, P. L. Techniques for evaluating the uniform current vector potential at isolated singularity of the cylindrical wire kernel. IEEE Trans. on Antennas and Propagation 42 (Nov. 1994): 1549–1553.

- [28] Champagne, N. J., Wilton, D. R., and Rockway, J. D. The analysis of thin wires using higher order elements and basis functions. IEEE Trans. on Antennas and Propagation 54 (Dec. 2006): 3815–3821.
- [29] Khayat, M. A. and Wilton, D. R. Numerical evaluation of singular and near-singular potential integrals. IEEE Trans. on Antennas and Propagation 53 (Oct. 2005): 3180–3190.
- [30] Wilton, D. R. and Champagne, N. J. Evaluation and integration of thin wire kernel. IEEE Trans. on Antennas and Propagation 54 (Apr. 2006): 1200–1206.
- [31] Rao, S. M., Wilton, D. R., and Gilsson, A. Electromagnetic scattering by surface of arbitrary shape. IEEE Trans. on Antennas and Propagation 30 (May 1982): 409–418.
- [32] Taylor, D. J. Accurate and efficient numerical integration of weakly singular integrals in Galerkin EFIE solutions. IEEE Trans. on Antennas and Propagation 51 (July 2003): 1630–1637.
- [33] Albersen, N. C., Hansen, J. E., and Jensen, N. E. Computation of radiation from wire antennas on conducting bodies. IEEE Trans. on Antennas and Propagation 22 (Mar. 1974): 200–206.
- [34] Ergül, Ö. and Gürel, L., Investigation of the inaccuracy of the MFIE discretized with RWG basis functions. Proceedings of the IEEE Antennas and Propagation Society International Symposium 3 (2004): 3393–3396.
- [35] Peterson, A. F. and Kempel, L. C., Solution of the MFIE using curl-conforming basis functions. Proceedings of the IEEE Antennas and Propagation Society International Symposium 1 (2002): 70–73.
- [36] Ergül, Ö. and Gürel, L. Improved testing of the magnetic-field integral equation. IEEE Microwave and Wireless Components Letters 15 (Oct. 2005): 615–617.
- [37] Ergül, Ö. and Gürel, L., Improving the accuracy of the MFIE with the choice of basis functions. Proceedings of the IEEE Antennas and Propagation Society International Symposium 3 (2004): 3389–3392.
- [38] Davis, C. P. and Warnick, K. F. High-order convergence with a low-order discretization of the 2-d MFIE. IEEE Antennas and Wireless Propagation Letters 3 (2004): 355–358.
- [39] Gürel, L. and Ergül, Ö. Singularity of the magnetic-field integral equation and its extraction. IEEE Antennas and Wireless Propagation Letters 4 (2005): 229–232.
- [40] Ergül, Ö. and Gürel, L. Improving the accuracy of the magnetic field integral equation with the linear-linear basis functions. Radio Science 41 (2005): 1–15.
- [41] Peterson, A. F. and Bibby, M. M., Error trends in higher-order discretizations of the EFIE and MFIE. Proceedings of the IEEE Antennas and Propagation Society International Symposium 3 (2005): 52–55.

- [42] Lu, C. C., Chew, W. C., and Song, J. M., A study of disparate grid sizes for an irregular-shape scatterer on EFIE, MFIE, and CFIE. Proceedings of the IEEE Antennas and Propagation Society International Symposium 3 (1996): 1746–1749.
- [43] Kang, G., Song, J., Chew, W. C., Donepudi, K. C., and Jin, J.-M. A novel grid-robust higher order vector basis function for the method of moments. IEEE Trans. on Antennas and Propagation 49 (June 2001): 908–915.
- [44] Yla-Oijala, P. and Taskinen, M. Calculation of CFIE impedance matrix elements with RWG and $n \times$ RWG functions. IEEE Trans. on Antennas and Propagation 51 (Aug. 2003): 1837–1846.
- [45] Rao, S. M. and Wilton, D. R. E-field, h-field, and combined-field solution for arbitrarily shaped three-dimensional dielectric bodies. Electromagn. 10 (1990): 407–421.
- [46] Volakis, J. L., Chatterjee, A., and Kempel, L. C. Review of the finite element method for three dimensional electromagnetic scattering. J. Opt. Soc. Amer. A 11 (Apr. 1994): 1422–1433.
- [47] Sheng, X.-Q., Jin, J.-M., Song, J., Lu, C.-C., and Chew, W. C., On the formulation of hybrid finite-element and boundary-integral methods for 3-D scattering using multi-level fast multipole algorithm. Proceedings of the IEEE Antennas and Propagation Society International Symposium 1 (1998): 236–239.
- [48] Warnick, K. F., Selfridge, R. H., and Arnold, D. V. Teaching electromagnetic field theory using differential forms. IEEE Trans. on Education 40 (Feb. 1997): 53–68.
- [49] Kurz, S., Rain, O., Rischmüller, V., and Rjasanow, S. Discretization of boundary integral equation by differential forms on dual grid. IEEE Trans. on Magnetics 40 (Mar. 2004): 826–829.
- [50] Deschamps, G. A., Electromagnetics and differential forms. Proceedings of the IEEE 69 , 6 (1981): 676–696.
- [51] McIntosh, A., Clifford algebras and the higher-dimensional Cauchy integral. in *Approximation Theory and Function Spaces* (Ciesielski, Z., ed.), no. 22 in BCP series, pp. 253–267, Warsaw, Poland : Banach Center Publications, 1989.
- [52] Axelsson, A., Grogard, R., Hogan, J., and McIntosh, A., Harmonic analysis of Dirac operators on Lipschitz domains. Clifford Analysis and its Applications (Brackx, F., ed.), no. 25 in NATO Science Series II, Mathematics Physics and Chemistry, Dordrecht, Kluwer, (2001): 231–246. (Prague, 2000).
- [53] Burton, A. J. and Miller, G. F. The application of integral equation methods to the numerical solution of some exterior boundary-value problems. Proceedings of the Royal Society of London 323 (1971): 201–210.
- [54] Moisil, G. C. and Théodorescu, N. Fonctions holomorphes dans l'espace. Mathematica Cluj 5 (1931): 142–159.
- [55] Clifford, W. K. Applications of Grassmann's extensive algebra. American Journal of Mathematics 1 , 4 (1878): 350–358.

- [56] Chisholm, M. Such Silver Currents: the Story of William and Lucy Clifford 1845-1929. Cambridge : Lutterworth Press, Mar. 2002.
- [57] Lasenby, A. C., Doran, C., and Arcaute, E., Applications of geometric algebra in electromagnetism, quantum theory and gravity. In R. Ablamowicz, editor, Proc, Sixth International Conference on Clifford Algebras and Their Application, (2003): 467.
- [58] Axelsson, A., Transmission Problems for Dirac's and Maxwell's Equations with Lipschitz Interfaces. Ph.D. dissertation Australian National University, 2002.
- [59] Dhia, A. S. B. B., Hazard, C., and Lohrengel, S. A singular field method for the solution of Maxwell's equations in polyhedral domains. SIAM J. Appl. Math. 59 (1999): 2028–2044.
- [60] Hazard, C. and Lohrengel, S. A singular field method for Maxwell's equations: Numerical aspects for 2D magnetostatics. SIAM J. Numer. Anal. 40, 3 (2002): 1021–1040.
- [61] Mitrea, D. and Mitrea, M. Finite energy solutions of Maxwell's equations and constructive hodge decompositions on nonsmooth Riemannian manifolds. Journal of Functional Analysis 190, 2 (2002): 339–417.
- [62] McIntosh, A. and Mitrea, M. Clifford algebras and Maxwell's equations in Lipschitz domains. Mathematical Methods in the Applied Sciences. 22 (1999): 1599–1620.
- [63] Duffy, D. G. Green's Functions with Applications. New York : Chapman & Hall/CRC, 2000.
- [64] Press, W. H., Teukolsky, S. A., Vetterling, W. T., and Flannery, B. P. Numerical Recipes – The Art of Scientific Computing. Cambridge : Cambridge University Press, 3rd ed., Sept. 2007.
- [65] Yaghjian, A. D. and McGhan, R. V. Broadside radar cross section of the perfectly conducting cube. IEEE Trans. on Antennas and Propagation 33, 3 (1985): 321–329.
- [66] Cote, M. G., Woodworth, M. B., and Yaghjian, A. D. Scattering from of the perfectly conducting cube. IEEE Trans. on Antennas and Propagation 36, 9 (1988): 1321–1329.
- [67] Yaghjian, A. D. Augmented electric- and magnetic-field integral equations. Radio Sci. 16, 6 (1981): 987–1001.
- [68] Yuan, M., Berg, P. M., and Sarkar, T. K. Direct extrapolation of a causal signal using low-frequency and early-time data. IEEE Antennas and Propagation Magazine 53 (July 2005): 2290–2298.



Appendices

ศูนย์วิทยทรัพยากร
จุฬาลงกรณ์มหาวิทยาลัย

Appendix A

Clifford Algebra

This section is to introduce Clifford number and Clifford arithmetic for supporting the proposed material in the research. There are two operations of Clifford algebra such as addition and multiplication. These operations can explain the three main products in vector form, such as inner product, outer product and cross product. Moreover, the differential operators such as the divergence and curl that are expressed in Maxwell's equations in the differential form, are described with Clifford algebra.

A.1 Clifford numbers

Numbers on Clifford algebra are called "Clifford number" which can represent electromagnetic fields in various dimensions. For problems in electromagnetics, 3-dimensional and 4-dimensional Clifford numbers are the most useful.

Dimensions: Dimensions of Clifford number depends on the kind of problem. Static field problems and time dependent field problems are embedded in three and four dimensions respectively. For example of Clifford number in three dimensions is shown as:

$$\mathbf{a} = a_0 + a_1\mathbf{e}_0 + a_2\mathbf{e}_1 + a_3\mathbf{e}_0\mathbf{e}_1 + a_4\mathbf{e}_2 + a_5\mathbf{e}_0\mathbf{e}_2 + a_6\mathbf{e}_1\mathbf{e}_2 + a_7\mathbf{e}_0\mathbf{e}_1\mathbf{e}_2$$

and four dimensions is shown as:

$$\begin{aligned} \mathbf{a} = & a_0 + a_1\mathbf{e}_0 + a_2\mathbf{e}_1 + a_3\mathbf{e}_2 + a_4\mathbf{e}_3 + a_5\mathbf{e}_0\mathbf{e}_1 + a_6\mathbf{e}_0\mathbf{e}_2 + a_7\mathbf{e}_1\mathbf{e}_2 + a_8\mathbf{e}_0\mathbf{e}_3 + a_9\mathbf{e}_1\mathbf{e}_3 \\ & + a_{10}\mathbf{e}_2\mathbf{e}_3 + a_{11}\mathbf{e}_0\mathbf{e}_1\mathbf{e}_2 + a_{12}\mathbf{e}_0\mathbf{e}_1\mathbf{e}_3 + a_{13}\mathbf{e}_0\mathbf{e}_2\mathbf{e}_3 + a_{14}\mathbf{e}_1\mathbf{e}_2\mathbf{e}_3 + a_{15}\mathbf{e}_0\mathbf{e}_1\mathbf{e}_2\mathbf{e}_3 \end{aligned}$$

Components: Number of components is all terms of a Clifford number which depends on the dimensions. This is similar to complex numbers, where there are two components: Real and Imaginary parts. For example of three dimensional Clifford number contains eight terms, so that the number of components is eight. Each component is made form two parts: numeric and symbolic parts. In the numeric part is a complex number and it is commonly called the 'coefficient'. The symbolic part is either invisible, or is a combination of the symbol 'e' and digits '0-9'. This part is commonly called the unit which is described latter. The eight components are enough to provide storage for two complex scalars and two complex 3-dimensional vectors. It is normal to use one of vectors for the electric field and one of vectors for magnetic field.

In general an n-dimensional Clifford number C_n has 2^n complex-valued components.

Grades: The internal structure of Clifford numbers places the different components into different groups. All components in each group have some common characteristics, which are different from the characteristics of the other groups. The characteristic of the groups are described by the term 'Grade'.

Grades are given numeric names so that each grade can be easily identified, e.g. grade 0, grade 1, etc. The symbol, which normally used to represent grades, is a capital lambda

Λ with a numeric superscript. For example, $\Lambda^0 = \text{grade } 0$ and $\Lambda^k = \text{grade } k$. The number of grades (groups of components) in a Clifford number is determined if the dimension of Clifford number is specified.

Units: In order to determine how each component in Clifford numbers should behave under arithmetic operation each component is given specific (individual) characteristics. This is similar to complex numbers where the real component is given the characteristic of 'multiplication by 1' and the imaginary component is given the characteristic of 'multiplication by $\sqrt{-1}$ '. For Clifford numbers the appropriate characteristics are first assigned to the components in grade 0 and grade 1, and then used along with some simple rules to construct the characteristics for the components in all other grades. The characteristics of the components are described by the term 'unit'.

Units are given symbolic names according to a particular convention, chosen so that the characteristics of each component are clearly defined by the name of its unit. The units can not be determined until the dimension of the Clifford number is specified. For example of units in the three dimensional Clifford number, the unit in Λ^0 is 1 which is an invisible unit. The units in Λ^1 , which is called the basis units, are e_0 , e_1 and e_2 . The units in Λ^2 are constructed by multiplying in pairs all of the basis units i.e. e_0e_1 , e_0e_2 and e_1e_2 . The units in Λ^3 are constructed by multiplying in triples all of the basis units i.e. $e_0e_1e_2$.

In general an n-dimensional Clifford number has an invisible unit in Λ^0 and the basis units e_0, e_1, \dots, e_n in Λ^1 . The units of in $\Lambda^k > \Lambda^1$ are constructed by multiplying in k-tuples all of the units in Λ^1 ; i.e.

$$\prod_{i=1}^k e_{u_i}$$

where $u_i < u_{i+1}$ and $u_i \in \{1, 2, \dots, k\}$. The order of multiplication is very important! In Clifford numbers the units $e_m e_n$ is not normally the same as the units $e_n e_m$. One is normally the negative of the order (unless $m = n$, in which case they are equal). It does not matter whether $e_n e_m$ or $e_m e_n$ is used as long as care is taken to get the \pm sign correct. However, it is normal to use units with the subscripts running smallest to largest in the direction from left to right, i.e. $e_m e_n$ if $m > n$, or $e_n e_m$ if $n > m$.

A.2 Addition of Clifford numbers

Addison of Clifford numbers is similar to addition vectors which is performed by adding all of the components that have the same units. However, the coefficients of the components need to use the addition of complex number, in vector case use the addition of real number. Adding two n-dimensional Clifford numbers requires 2^n complex addition operations. For examples of addition of two 3-dimensional Clifford numbers: $c_3 = a_3 + b_3$,

$$a_3 = a_0 + a_1e_0 + a_2e_1 + a_3e_0e_1 + a_4e_2 + a_5e_0e_2 + a_6e_1e_2 + a_7e_0e_1e_2$$

$$b_3 = b_0 + b_1e_0 + b_2e_1 + b_3e_0e_1 + b_4e_2 + b_5e_0e_2 + b_6e_1e_2 + b_7e_0e_1e_2$$

$$c_3 = a + b$$

$$= c_0 + c_1e_0 + c_2e_1 + c_3e_0e_1 + c_4e_2 + c_5e_0e_2 + c_6e_1e_2 + c_7e_0e_1e_2$$

where:

$$c_0 = a_0 + b_0 \quad c_2 = a_2 + b_2 \quad c_4 = a_4 + b_4 \quad c_6 = a_6 + b_6$$

$$c_1 = a_1 + b_1 \quad c_3 = a_3 + b_3 \quad c_5 = a_5 + b_5 \quad c_7 = a_7 + b_7$$

A.3 Multiplication of Clifford numbers

Multiplication of Clifford number is not really difficult, but there are an awful lot of operations involved. It necessary uses two important rules: the rules of multiplying complex number and the rules of combining units of Clifford number. Multiplying two n-dimensional Clifford numbers requires 2^{2n} complex multiplication operations, and after that the 2^{2n} intermediate results must be sorted into components, and all the immediate results for each 2^{2n} components must be added together.

The rule of multiplying complex number is the basic rule in complex algebra, but the rules of multiplying units of Clifford numbers are many alternatives. For example of the common choice is $e_n e_n = +1$ or $e_n e_n = 0$. Any of these choice can be adopted. Each gives a different formalism of the Clifford framework, and Maxwell's equations can be embedded in any of these. It seems that none of these formalisms has any overwhelming advantage. In this thesis, the rules of multiplying Clifford's units are following by (2.2) that is made to accord with history convention.

Multiplying two 2-dimensional Clifford numbers of A and B:

$$\begin{cases} \mathbf{A}_{(2)} = a_0 + a_1 \mathbf{e}_1 + a_2 \mathbf{e}_2 + a_3 \mathbf{e}_1 \mathbf{e}_2 \\ \mathbf{B}_{(2)} = b_0 + b_1 \mathbf{e}_1 + b_2 \mathbf{e}_2 + b_3 \mathbf{e}_1 \mathbf{e}_2 \end{cases}$$

gives the result:

$$\begin{cases} C_{(2)} = a_0 b_0 + a_0 b_1 \mathbf{e}_1 + a_0 b_2 \mathbf{e}_2 + a_0 b_3 \mathbf{e}_1 \mathbf{e}_2 \\ + a_1 b_0 \mathbf{e}_1 + a_1 b_1 \mathbf{e}_1 \mathbf{e}_1 + a_1 b_2 \mathbf{e}_1 \mathbf{e}_2 + a_1 b_3 \mathbf{e}_1 \mathbf{e}_1 \mathbf{e}_2 \\ + a_2 b_0 \mathbf{e}_2 + a_2 b_1 \mathbf{e}_2 \mathbf{e}_1 + a_2 b_2 \mathbf{e}_2 \mathbf{e}_2 + a_2 b_3 \mathbf{e}_2 \mathbf{e}_1 \mathbf{e}_2 \\ + a_3 b_0 \mathbf{e}_1 \mathbf{e}_2 + a_3 b_1 \mathbf{e}_1 \mathbf{e}_2 \mathbf{e}_1 + a_3 b_2 \mathbf{e}_1 \mathbf{e}_2 \mathbf{e}_2 + a_3 b_3 \mathbf{e}_1 \mathbf{e}_2 \mathbf{e}_1 \mathbf{e}_2 \end{cases}$$

Therefore;

$$\begin{cases} C_{(2)} = (a_0 b_0 - a_1 b_1 - a_2 b_2 - a_3 b_3) \\ + (a_0 b_1 + a_1 b_0 + a_2 b_3 - a_3 b_2) \mathbf{e}_1 \\ + (a_0 b_2 - a_1 b_3 + a_2 b_0 + a_3 b_1) \mathbf{e}_2 \\ + (a_0 b_3 + a_1 b_2 - a_2 b_1 + a_3 b_0) \mathbf{e}_1 \mathbf{e}_2 \end{cases}$$

Notice that the coefficients of the components involve sums and differences of pairs of complex numbers. This similar to complex arithmetic, where the coefficients of the components involve sums and differences of pairs of the real numbers.

A.4 Involution

Involution (or inversion) is an operation which changes the signs of some components of a Clifford number. The operation can be performed as three step:

1. breaking all Clifford units from grade Λ^k into a product of separate units from grade Λ^1 ,
2. multiplying all the Λ^1 units by -1, and
3. putting all the Λ^1 units back together into units from Λ^k

The effect is to introduce in every unit a factor of $(-1)^k$. This introduces a change of sign for all odd grades, and has no effect on even grades. For example: If $\mathbf{x} = a_0 + a_1\mathbf{e}_1 + a_2\mathbf{e}_2 + a_3\mathbf{e}_1\mathbf{e}_2$ is 2-dimensional Clifford number, then the involution of \mathbf{x} is:

$$\begin{cases} \bar{\mathbf{x}} = a_0 + a_1\mathbf{e}_1 + a_2\mathbf{e}_2 + a_3\mathbf{e}_1\mathbf{e}_2 \\ = a_0 + a_1(-\mathbf{e}_1) + a_2(-\mathbf{e}_2) + a_3(-\mathbf{e}_1)(-\mathbf{e}_2) \\ = a_0 - a_1\mathbf{e}_1 - a_2\mathbf{e}_2 + a_3(-\mathbf{e}_1)(-\mathbf{e}_2) \end{cases}$$

where the symbol $\bar{}$ is used to indicate the involution operation. Involution can be used to help write some algebraic results in a more concise form as with, for example, the recursive product in next section.

A.5 Recursive Product

The product of Clifford numbers of any dimension can be recursively defined in terms of Clifford numbers of lower dimension, in a form similar to the (more familiar) product of complex numbers. For complex numbers $u = v + iw$ and $z = x + iy$ the product is:

$$uz = (v + iw)(x + iy) = [vx - wy] + i[vy + wx] \quad (1)$$

For n-dimensional Clifford numbers $\mathbf{U}_{(n)} = \mathbf{V}_{(n-1)} + \mathbf{W}_{(n-1)}\mathbf{e}_n$ and $\mathbf{Z}_{(n)} = \mathbf{X}_{(n-1)} + \mathbf{Y}_{(n-1)}\mathbf{e}_n$ the product is:

$$\begin{aligned} \mathbf{U}_{(n)}\mathbf{Z}_{(n)} &= (\mathbf{V}_{(n-1)} + \mathbf{W}_{(n-1)}\mathbf{e}_n)(\mathbf{X}_{(n-1)} + \mathbf{Y}_{(n-1)}\mathbf{e}_n) \\ &= (\mathbf{V}_{(n-1)}\mathbf{X}_{(n-1)} + \mathbf{W}_{(n-1)}\mathbf{e}_n\mathbf{Y}_{(n-1)}\mathbf{e}_n) + (\mathbf{V}_{(n-1)}\mathbf{Y}_{(n-1)}\mathbf{e}_n + \mathbf{W}_{(n-1)}\mathbf{e}_n\mathbf{X}_{(n-1)}) \end{aligned}$$

Changing the order of $\mathbf{e}_n\mathbf{X}_{(n-1)}$ to $\mathbf{X}_{(n-1)}\mathbf{e}_n$ introduces minus signs in all odd grade of \mathbf{X} . The same effect can be achieved by applying the involution operator so that:

$$\mathbf{e}_n\bar{\mathbf{X}}_{(n-1)} = \mathbf{X}_{(n-1)}\mathbf{e}_n$$

Multiplying both sides from left and right by \mathbf{e}_n now gives:

$$\begin{aligned} \mathbf{e}_n\mathbf{e}_n\bar{\mathbf{X}}_{(n-1)}\mathbf{e}_n &= \mathbf{e}_n\mathbf{X}_{(n-1)}\mathbf{e}_n\mathbf{e}_n \\ \bar{\mathbf{X}}_{(n-1)}\mathbf{e}_n &= \mathbf{e}_n\mathbf{X}_{(n-1)} \end{aligned}$$

Using this result for both $\mathbf{e}_n\mathbf{X}_{(n-1)}$ and $\mathbf{e}_n\mathbf{Y}_{(n-1)}$ gives:

$$\begin{aligned} \mathbf{U}_{(n)}\mathbf{Z}_{(n)} &= (\mathbf{V}_{(n-1)}\mathbf{X}_{(n-1)} + \mathbf{W}_{(n-1)}\bar{\mathbf{Y}}_{(n-1)}\mathbf{e}_n\mathbf{e}_n) + (\mathbf{V}_{(n-1)}\mathbf{Y}_{(n-1)}\mathbf{e}_n + \mathbf{W}_{(n-1)}\bar{\mathbf{X}}_{(n-1)}\mathbf{e}_n) \\ &= (\mathbf{V}_{(n-1)}\mathbf{X}_{(n-1)} - \mathbf{W}_{(n-1)}\bar{\mathbf{Y}}_{(n-1)}) + (\mathbf{V}_{(n-1)}\mathbf{Y}_{(n-1)} + \mathbf{W}_{(n-1)}\bar{\mathbf{X}}_{(n-1)})\mathbf{e}_n \end{aligned}$$

Comparison of the case for the multiplication of Clifford numbers and the case for multiplication of complex numbers shows strong similarities. Structurally the equations are the same, with the only added complication in the case of Clifford multiplication being the need to apply the involution operation to some of the terms. The simple form of equation can be exploited to develop simple (although recursive) computer implementations of Clifford multiplication.

A.6 Geometric operation

The inner, cross and outer products are always described by vector form in engineering, the transformation of vectors and Clifford numbers are appeared in here for applying and understanding easier. Moreover, the construction about the differentiation of the fields based on Clifford algebra is presented. The representations of geometric object perform in three dimensions; therefore, the forms of fields that are presented in three dimensional vector forms are considered in three dimensional Clifford numbers.

Transformation between vectors and Clifford numbers: To describe in details of (2.4) the transformation of vectors and Clifford numbers for explaining the geometric operation and differentiation of Clifford algebra. Vectors are presented in the Cartesian system are constructed from basis vectors: \vec{a}_x , \vec{a}_y and \vec{a}_z that shown as:

$$\vec{v} = v_x \vec{a}_x + v_y \vec{a}_y + v_z \vec{a}_z$$

These vectors in three dimensions are a subset of Clifford numbers in three dimensions. The subset used consists of number whose components are zero in all grades except Λ^1 . It is possible to encode the coordinates of the vector \vec{v} into Λ^1 of the Clifford number: \mathbf{u} :

$$\mathbf{u} = v_x \mathbf{e}_1 + v_y \mathbf{e}_2 + v_z \mathbf{e}_3 = [\vec{v}]^1$$

The notation $[\vec{v}]^1$ indicates the vector \vec{v} encoded into a Clifford number by copying its coordinates into corresponding coefficients of Λ^1 . It is now possible to perform geometric operations on the vector \vec{v} by making algebraic operations on Clifford image \mathbf{u} of the vector \vec{v} .

Product operation: When working with vectors there are three products that are frequently used Inner product (or scalar product), Cross product (or vector product) and Outer product (or wedge product).

All three of these products are produced if two vectors \vec{p} and \vec{q} are encoded as Clifford numbers, and those numbers are then multiplied together. Vector \vec{p} has coordinates (p_x, p_y, p_z) and Vector \vec{q} has coordinates (q_x, q_y, q_z) . Then vector \vec{p} and \vec{q} are encoded into Clifford numbers \mathbf{p} and \mathbf{q} respectively.

$$\begin{aligned} \vec{p} &= p_x \vec{a}_x + p_y \vec{a}_y + p_z \vec{a}_z & \mathbf{p} &= [\vec{p}]^1 = p_x \mathbf{e}_1 + p_y \mathbf{e}_2 + p_z \mathbf{e}_3 \\ \vec{q} &= q_x \vec{a}_x + q_y \vec{a}_y + q_z \vec{a}_z & \mathbf{q} &= [\vec{q}]^1 = q_x \mathbf{e}_1 + q_y \mathbf{e}_2 + q_z \mathbf{e}_3 \end{aligned}$$

In Clifford algebra, *Scalar product* can be recovered after adding the two Clifford products $\mathbf{p}\mathbf{q}$ and $\mathbf{q}\mathbf{p}$. The result ends up in Λ^0 , which is a scalar.

$$\vec{p} \cdot \vec{q} = \left[-\frac{1}{2} (\mathbf{p}\mathbf{q} + \mathbf{q}\mathbf{p}) \right]_0$$

Cross product can be recovered after subtracting two Clifford products $\mathbf{p}\mathbf{q}$ and $\mathbf{q}\mathbf{p}$. The result ends up in Λ^2 , which does not decoded into a vector. So that we must post-multiply by (minus) the unit of Λ^3 to transfer the result into Λ^1 .

$$\vec{p} \times \vec{q} = \left[-\frac{1}{2} (\mathbf{p}\mathbf{q} - \mathbf{q}\mathbf{p}) \mathbf{e}_1 \mathbf{e}_2 \mathbf{e}_3 \right]_1$$

Outer product can be recovered directly after subtracting two Clifford products \mathbf{pq} and \mathbf{qp} . The results ends up in Λ^2 , which is bi-vector.

$$\vec{p} \wedge \vec{q} = \left[\frac{1}{2} (\mathbf{pq} - \mathbf{qp}) \right]_2$$

A.7 Differentiation of Clifford number

Three important operators of vectors in three dimensions are gradient, divergence and curl operations can be described on three dimensional Clifford number. These operators are used to present the relationship of the electromagnetic fields in Maxwell's equations. The gradient operator ∇ of vector form can encode into Clifford number in Λ^1 :

$$\begin{aligned} \nabla &= \frac{\partial}{\partial x} \vec{a}_x + \frac{\partial}{\partial y} \vec{a}_y + \frac{\partial}{\partial z} \vec{a}_z \\ \mathbf{D} &= \frac{\partial}{\partial x} \mathbf{e}_1 + \frac{\partial}{\partial y} \mathbf{e}_2 + \frac{\partial}{\partial z} \mathbf{e}_3 \end{aligned}$$

where the differential operator 'D' is called 'Dirac operator' or 'Clifford gradient'. The scalar ' ϕ ' and vector ' \vec{F} ', that are represented in vector form are encoded into three dimensional Clifford number \mathbf{u} in Λ^0 and Λ^1 , respectively.

$$\begin{aligned} \phi &= \phi(x, y, z) \\ \vec{F} &= F_x \vec{a}_x + F_y \vec{a}_y + F_z \vec{a}_z \\ \mathbf{u} &= [\phi]^0 + [\vec{F}]^1 = \phi + F_x \mathbf{e}_1 + F_y \mathbf{e}_2 + F_z \mathbf{e}_3 \end{aligned}$$

In Clifford algebra, three operators can be constructed by using the multiplication of the gradient operator \mathbf{D} and Clifford number \mathbf{u} :

$$\begin{aligned} \mathbf{D}\mathbf{u} &= \left(\frac{\partial}{\partial x} \mathbf{e}_1 + \frac{\partial}{\partial y} \mathbf{e}_2 + \frac{\partial}{\partial z} \mathbf{e}_3 \right) (\phi + F_x \mathbf{e}_1 + F_y \mathbf{e}_2 + F_z \mathbf{e}_3) \\ &= - \left(\frac{\partial F_x}{\partial x} + \frac{\partial F_y}{\partial y} + \frac{\partial F_z}{\partial z} \right) \in \Lambda^0 \\ &+ \left(\frac{\partial \phi}{\partial x} \mathbf{e}_1 + \frac{\partial \phi}{\partial y} \mathbf{e}_2 + \frac{\partial \phi}{\partial z} \mathbf{e}_3 \right) \in \Lambda^1 \\ &+ \left(\frac{\partial F_z}{\partial y} - \frac{\partial F_y}{\partial z} \right) \mathbf{e}_2 \mathbf{e}_3 - \left(\frac{\partial F_z}{\partial x} - \frac{\partial F_x}{\partial z} \right) \mathbf{e}_3 \mathbf{e}_1 + \left(\frac{\partial F_y}{\partial x} - \frac{\partial F_x}{\partial y} \right) \mathbf{e}_1 \mathbf{e}_2 \in \Lambda^2 \end{aligned}$$

Divergence of vector \vec{F} can be recovered from some components of $\mathbf{D}\mathbf{u}$ in Λ^0 is a scalar and define as:

$$\begin{aligned} \nabla \cdot \vec{F} &= -[\mathbf{D}\mathbf{u}]_0 \\ &= \left(\frac{\partial F_x}{\partial x} + \frac{\partial F_y}{\partial y} + \frac{\partial F_z}{\partial z} \right) \end{aligned}$$

Gradient of scalar function ϕ can be recovered from some components of $\mathbf{D}\mathbf{u}$ in Λ^1 is a vector and define as:

$$\begin{aligned} \nabla \phi &= [\mathbf{D}\mathbf{u}]_1 \\ &= \left(\frac{\partial \phi}{\partial x} \mathbf{e}_1 + \frac{\partial \phi}{\partial y} \mathbf{e}_2 + \frac{\partial \phi}{\partial z} \mathbf{e}_3 \right) \end{aligned}$$

Curl of vector \vec{F} can be recovered from some components of \mathbf{Du} in Λ^2 is a bi-vector which can be decoded the curl of vector \vec{F} into a vector by post-multiplying by (minus) the units of Λ^3 and then decoding into Λ^1 is a vector, that define as:

$$\begin{aligned}\nabla \times \vec{F} &= -[(\mathbf{Du}) \mathbf{e}_1 \mathbf{e}_2 \mathbf{e}_3]_1 \\ &= \left(\frac{\partial F_z}{\partial y} - \frac{\partial F_y}{\partial z} \right) \mathbf{e}_1 - \left(\frac{\partial F_z}{\partial x} - \frac{\partial F_x}{\partial z} \right) \mathbf{e}_2 + \left(\frac{\partial F_y}{\partial x} - \frac{\partial F_x}{\partial y} \right) \mathbf{e}_3\end{aligned}$$

Notice, if the scalar function is zero, $\phi = 0$, \mathbf{u} is encoded by vector field \vec{F} only, and the differential operation in Clifford number gives only Λ^0 and Λ^2 .

$$\begin{aligned}\mathbf{Du} &= \left(\frac{\partial}{\partial x} \mathbf{e}_1 + \frac{\partial}{\partial y} \mathbf{e}_2 + \frac{\partial}{\partial z} \mathbf{e}_3 \right) (\phi + F_x \mathbf{e}_1 + F_y \mathbf{e}_2 + F_z \mathbf{e}_3) \\ &= - \left(\frac{\partial F_x}{\partial x} + \frac{\partial F_y}{\partial y} + \frac{\partial F_z}{\partial z} \right) \in \Lambda^0 \\ &+ \left(\frac{\partial F_z}{\partial y} - \frac{\partial F_y}{\partial z} \right) \mathbf{e}_2 \mathbf{e}_3 - \left(\frac{\partial F_z}{\partial x} - \frac{\partial F_x}{\partial z} \right) \mathbf{e}_3 \mathbf{e}_1 + \left(\frac{\partial F_y}{\partial x} - \frac{\partial F_x}{\partial y} \right) \mathbf{e}_1 \mathbf{e}_2 \in \Lambda^2 \\ &= - [\nabla \cdot \vec{F}]^0 - [\nabla \times \vec{F}]^1 \mathbf{e}_1 \mathbf{e}_2 \mathbf{e}_3\end{aligned}$$

Therefore, two differential operations on vector calculus, such as divergence and curl products, can be produced with a single differential operation on Clifford algebra.

A.8 Hybrid Vector/Clifford Notation

The rules governing manipulations of Clifford numbers are very simple, but when there are many components it is easy to make a mistake and to lose a minus sign. Often we wish to perform geometric operation (primarily in 3 spatial dimensions or 3 spatial + 1 temporal or frequency dimension) rather than numeric operations. In this case it is often easier for manipulations performed by hand to adopt a hybrid notation and a set of rules which exploit both the Clifford structure and the engineer's familiarity with vector calculus. This approach also makes it easier to recognize important results which fall into the form of cross products and dot products (such as Maxwell's equations); something not always easily recognized if scattered around the page as isolated components.

The hybrid notation unites, where possible, groups of components in a Clifford number either in terms of a single vector, or a dot product or cross product of a pair of vectors, all suitably encoded and transferred into the required grades. For example of the product of two vectors \mathbf{p} , \mathbf{q} encoded into two Clifford number \mathbf{u} , \mathbf{v} can be written:

$$\mathbf{uv} = [\vec{p} \cdot \vec{q}]^0 - [\vec{p} \times \vec{q}]^1 \vec{e}_1 \vec{e}_2 \vec{e}_3$$

The unit $\mathbf{e}_1 \mathbf{e}_2 \mathbf{e}_3$ of Λ^3 appears so often (with a minus sign) that is accorded for convenience with a single symbol σ . This new unit has the following properties:

$$\begin{aligned}\sigma &= -\mathbf{e}_1 \mathbf{e}_2 \mathbf{e}_3 \\ \sigma^2 &= 1 \\ \sigma \mathbf{e}_1 &= \mathbf{e}_1 \sigma \\ \sigma \mathbf{e}_2 &= \mathbf{e}_2 \sigma \\ \sigma \mathbf{e}_3 &= \mathbf{e}_3 \sigma\end{aligned}$$

Note that the unit σ commutes with all of the other units. The product of \mathbf{u} and \mathbf{v} can now be written:

$$\mathbf{uv} = [\vec{p} \cdot \vec{q}]^0 - [\vec{p} \times \vec{q}]^1 \sigma$$

It is difficult to remember which particular vector \mathbf{p} or \mathbf{q} is coded into which particular Clifford number \mathbf{u} or \mathbf{v} , especially when there are a lot of vectors and Clifford numbers. It is therefore safer to write as:

$$\mathbf{uv} = -[[\mathbf{u}]_1 \cdot [\mathbf{v}]_1]^0 + [[\mathbf{u}]_1 \times [\mathbf{v}]_1]^1 \sigma$$

The equation reads from left to right:

“the product of the Clifford number \mathbf{u} with the Clifford number \mathbf{v} is equal to minus the dot product of the vector decoded from grade 1 of the Clifford number \mathbf{u} with the vector decoded from grade 1 of the Clifford number \mathbf{v} then recoded into grade of another Clifford number plus the cross product of the vector decoded from grade 1 of the Clifford number \mathbf{u} with the vector decoded from grade 1 of the Clifford number \mathbf{v} then recoded into grade 1 of yet another Clifford number and multiplied by the unit σ .”

It is important to note three things:

1. It is only true for Clifford numbers which have vectors encoded into Λ^1 and nothing in any other grade,
2. It is really clumsy when written in words, and
3. It is also really clumsy when written as an equation!

The first point is usually not a problem, because we are normally interested only in that situation (or very similar situation). The second point is not a problem because we never use a complete verbal description. The third point can be eliminated by throwing away the notation $[\dots]^0$ and $[\dots]^1$ for encoding scalars and vectors into Clifford numbers and $[\dots]_0$ and $[\dots]_1$ for decoding Clifford numbers into vectors or scalars. The multiplication of \mathbf{uv} can then be written:

$$\mathbf{uv} = -(\mathbf{u} \cdot \mathbf{v}) + (\mathbf{u} \times \mathbf{v})\sigma$$

Care must be taken when reading equations in this hybrid “Clifford plus vector” form. On the left the symbols \mathbf{u} and \mathbf{v} represent Clifford numbers. On the right the symbols \mathbf{u} and \mathbf{v} represent equivalent vectors, but the whole expression on the right denotes a Clifford numbers.

The reader must note for themselves that the dot product and the cross product only make sense with vectors, so the symbols \mathbf{u} and \mathbf{v} on the right hand side must be intended into vectors. There is explicit notation for recoding the results of the vector dot and cross products into Clifford numbers. The reader must also note that the dot product of two vectors is a scalar so must be recoded into Λ^0 , and that the cross product of two vectors is a vector so must be recoded into Λ^1 . In this example the recoded result of the cross product is then transferred into Λ^2 by multiplying by the (specially defined) Clifford unit σ .

If an outer product notation is preferred to the cross product notation, it can be written instead as:

$$\mathbf{uv} = -(\mathbf{u} \cdot \mathbf{v}) - (\mathbf{u} \wedge \mathbf{v})$$

The same approach can be used for rewriting the Clifford gradient of Clifford number \mathbf{u} with vector field. First gritting the full expression gives:

$$\mathbf{Du} = -[\nabla \cdot [\vec{u}]_1]^0 + [\nabla \times [\vec{u}]_1]^1 \sigma$$

Now, as before, leaving the notation for encoding and decoding unwritten gives:

$$\mathbf{D}\mathbf{u} = -(\nabla \cdot \mathbf{u}) + (\nabla \times \mathbf{u})\sigma$$



ศูนย์วิทยทรัพยากร
จุฬาลงกรณ์มหาวิทยาลัย

Appendix B

Static Electric and Magnetic Fields

B.1 Static Field on Maxwell's Equations

The time-harmonic Maxwell's equations in vector form are referred for describing the static electric and magnetic fields. They do not change in time; therefore, we can let $\omega \rightarrow 0$ in (2.9). The four basic equations of electromagnetism can be found immediately

$$\begin{cases} \nabla \cdot \vec{E} = 0 \\ \nabla \times \vec{H} = 0 \\ \nabla \times \vec{E} = 0 \\ \nabla \cdot \vec{H} = 0. \end{cases}$$

These four equations can describe into a single equation on Clifford framework.

B.2 Static Field on Maxwell-Dirac equations

Maxwell-Dirac equations in Clifford form as (2.16) that are used to model the general electromagnetic fields are referred in here. They are made by multiplying the k -Dirac operator and the Clifford field. For static field the k -Dirac operator as (2.15) is specified to:

$$\mathbf{D}_{k=0} = \mathbf{D}$$

where \mathbf{D} is Clifford gradient operator, and the Clifford field as (2.7) is same style as the electromagnetic field. Therefore the static domain version of homogenous form of Maxwell's equations is given by:

$$\mathbf{D}\mathbf{u} = \begin{cases} -j\sqrt{\epsilon} [\nabla \cdot \vec{E}]^0 \mathbf{e}_0 \in T\Lambda^1 \\ + \sqrt{\mu} [\nabla \times \vec{H}]^1 \in S\Lambda^1 \\ + j\sqrt{\epsilon} [\nabla \times \vec{E}]^1 \sigma \mathbf{e}_0 \in T\Lambda^3 \\ - \sqrt{\mu} [\nabla \cdot \vec{H}]^0 \sigma \in S\Lambda^3 \end{cases} = 0.$$

The resulting Clifford number occupies time-like components T (containing the time unit \mathbf{e}_0) and space-like components S (where the unit \mathbf{e}_0 is missing) of both Λ^1 and Λ^3 . These four components in the order listed represent respectively source free differential statements of Gauss's law, the Ampere-Maxwell law, Faraday's law, and a magnetic version of Gauss's law.

B.3 Fundamental Solutions of k -Dirac Operator for Static Fields

The fundamental solution of the static Maxwell-Dirac operator is given by:

$$\mathbf{F}_0(\mathbf{p}) = \frac{-1}{4\pi r^3}$$

where $r = |\mathbf{p}|$. The fundamental solution of k -Dirac operator for static field by three dimensional Clifford number. The part of temporal component does not appear (the wavenumber is zero).



ศูนย์วิทยทรัพยากร
จุฬาลงกรณ์มหาวิทยาลัย

Appendix C

Reflection and Projection Operators for Clifford Functions

C.1 General Reflection and Projection Operators

In general, from a mathematical viewpoint, any operator \mathcal{R} is a reflection operator if it acts as its own inverse, i.e. $\mathcal{R}^2 = I$, and any operator \mathcal{P} is a projection operator if it is idempotent. This means only the first of a sequence of n identical operators can produce any effect. In general for $n > 1$, $\mathcal{P}^n = \mathcal{P}$. In particular for $n = 2$, $\mathcal{P}^2 = \mathcal{P}$.

In addition, any pair of operators \mathcal{P}^+ , \mathcal{P}^- constructed from a reflection operator \mathcal{R} according to the relations

$$\begin{cases} \mathcal{P}^+ &= \frac{1}{2}(I + \mathcal{R}) \\ \mathcal{P}^- &= \frac{1}{2}(I - \mathcal{R}) \end{cases} \quad (2)$$

are encoded with the following properties:

$$\begin{cases} (\mathcal{P}^\pm)^2 &= \mathcal{P}^\pm \\ \mathcal{P}^+ \mathcal{P}^- &= 0 \\ \mathcal{P}^+ + \mathcal{P}^- &= I \end{cases} \quad (3)$$

The first property ensures that \mathcal{P}^+ and \mathcal{P}^- are projection operators. The second property is useful for splitting fields into two orthogonal components. The third property is useful for reconstructing a field from its orthogonal components.

C.2 Space and Time

Here, the operator \mathcal{T}

$$\mathcal{T}(\mathbf{w}) = \sigma \mathbf{w} \sigma \quad (4)$$

is chosen as the basis on which to construct projection operators which extract the 'space-like' and 'time-like' components of Clifford numbers. The operator \mathcal{T} acts as its own inverse:

$$\mathcal{T}^2(\mathbf{w}) = \sigma^2 \mathbf{w} \sigma^2 = I \mathbf{w} \quad (5)$$

so that it has the general behavior of a reflection operator, as is required. Its particular behavior is to reflect any Clifford number \mathbf{w} in the hyper plane (mirror) represented by the unit of Λ^3 , $\sigma = -\mathbf{e}_1 \mathbf{e}_2 \mathbf{e}_3$. Components containing only space-like units are invariant since (geometrically) they sit on the (hyper) surface of the mirror, and (mathematically) they commute with the unit σ . Components containing the time unit $\hat{\mathbf{e}}$ undergo a change of sign since (mathematically) they anti-commute with the unit σ :

$$\sigma \hat{\mathbf{e}} = -\hat{\mathbf{e}} \sigma \quad (6)$$

are (geometrically) they are transported from one side of the mirror to the other.

Subjecting a four dimensional Clifford space-time vector $\mathbf{u} \in \Lambda^1$ to the operator \mathcal{T} simply reverses the sign on the time dimension, $\hat{e} \rightarrow -\hat{e}$, leaving all of the spatial dimensions $\mathbf{e}_1, \mathbf{e}_2, \mathbf{e}_3$ unaltered:

$$\begin{aligned} \mathcal{T}(u_1\mathbf{e}_1 + u_2\mathbf{e}_2 + u_3\mathbf{e}_3 + \hat{u}\hat{e}) &= u_1\sigma\mathbf{e}_1\sigma + u_2\sigma\mathbf{e}_2\sigma + u_3\sigma\mathbf{e}_3\sigma + \hat{u}\sigma\hat{e}\sigma \\ &= u_1\mathbf{e}_1 + u_2\mathbf{e}_2 + u_3\mathbf{e}_3 - \hat{u}\hat{e} \end{aligned} \quad (7)$$

Projection operators that reject and select components containing the time unit are now constructed from the reflection operator \mathcal{T} :

$$\begin{cases} S &= \frac{1}{2}(I + \mathcal{T}) \\ T &= \frac{1}{2}(I - \mathcal{T}) \end{cases} \quad (8)$$

As in the general case, these operators are idempotent ($S^2 = S, T^2 = T$), mutually exclusive ($ST = TS = 0$) and complementary ($S + T = I$).

Subjecting a four dimensional Clifford space-time vector $\hat{\mathbf{u}} \in \Lambda^1$ to the S operator gives:

$$\begin{aligned} S(\hat{\mathbf{u}}) &= S(u_1\mathbf{e}_1 + u_2\mathbf{e}_2 + u_3\mathbf{e}_3 + \hat{u}\hat{e}) \\ &= \frac{1}{2}(u_1\mathbf{e}_1 + u_2\mathbf{e}_2 + u_3\mathbf{e}_3 + \hat{u}\hat{e}) + \frac{1}{2}(u_1\mathbf{e}_1 + u_2\mathbf{e}_2 + u_3\mathbf{e}_3 - \hat{u}\hat{e}) \\ &= (u_1\mathbf{e}_1 + u_2\mathbf{e}_2 + u_3\mathbf{e}_3) \end{aligned} \quad (9)$$

Subjecting a four dimensional Clifford time-time vector $\hat{\mathbf{u}} \in \Lambda^1$ to the T operator gives:

$$\begin{aligned} T(\hat{\mathbf{u}}) &= T(u_1\mathbf{e}_1 + u_2\mathbf{e}_2 + u_3\mathbf{e}_3 + \hat{u}\hat{e}) \\ &= \frac{1}{2}(u_1\mathbf{e}_1 + u_2\mathbf{e}_2 + u_3\mathbf{e}_3 + \hat{u}\hat{e}) - \frac{1}{2}(u_1\mathbf{e}_1 + u_2\mathbf{e}_2 + u_3\mathbf{e}_3 - \hat{u}\hat{e}) \\ &= \hat{u}\hat{e} \end{aligned} \quad (10)$$

The operator T selects components which contain the time unit, either alone or in the form of a product with space units. The operator S does exactly the opposite. It selects all other components. This includes all components which contain only space units, either alone or in the form of a product with one another. It also includes all components which contain only the invisible unit, i.e. scalars. In view of their behavior, the S and T operators are called the *space-like* and *time-like* projection operators respectively. However, don't forget that the S operator is really space+scalar.

C.3 Boundary Data and Boundary Field

Boundary conditions for problems in electromagnetics are usually described for the field \mathbf{u} on the boundary Σ , in terms of either the field's normal component or its tangential component.

In the Clifford framework vectors and fields can be split into a mixture of different normal or tangential components by employing two projection operators \mathbf{Q}^+ and \mathbf{Q}^- , which themselves are derived from a single reflection operator \mathbf{Q} .

For the purposes of numerical implementation it is usual to embed any given problem into whatever coordinate system seems most appropriate. In some case it is convenient to

decompose the boundary into a set of matching elements (pieces), and to perform some of the calculations using a coordinate system local to each element. The local results must subsequently be transformed into a common coordinate system before they can be used together to form a solution. This requires simple rigid body transformations, i.e. translation and rotation.

In the Clifford framework translation of vectors and fields can be effected by adding a constant vector to the independent variable, and rotation can be achieved by employing a rotation operator constructed specifically for that purpose.

- Boundary data Projection Operator

1. A Boundary Reflection Operator Firstly, a reflection operator \mathbf{Q} for any Clifford number \mathbf{u} is defined as

$$\mathbf{Q}\mathbf{u} = \mathbf{n}\mathbf{u}\mathbf{n} \quad (11)$$

where \mathbf{n} is a unit vector encoded as a Clifford number (i.e. $\mathbf{n} \in S\Lambda^1$ and $\mathbf{n}^2 = -1$). Note that $\mathbf{Q}^2\mathbf{u} = (\mathbf{n}\mathbf{u}\mathbf{n})^2 = \mathbf{u} = \mathbf{I}\mathbf{u}$. This shows \mathbf{Q} is its own inverse and therefore confirms that \mathbf{Q} is a reflection operator. The unit vector \mathbf{n} can be chosen arbitrarily, but it is often most useful to choose \mathbf{n} as the unit normal vector to the boundary Σ .

2. Two Boundary Projection Operators Two projection operators \mathbf{Q}^+ , \mathbf{Q}^- are now defined as:

$$\mathbf{Q}^+ = \frac{1}{2}(\mathbf{I} + \mathbf{Q})\mathbf{u} \quad (12)$$

$$\mathbf{Q}^- = \frac{1}{2}(\mathbf{I} - \mathbf{Q})\mathbf{u} \quad (13)$$

As in the general case, these operators are idempotent $(\mathbf{Q}^+)^2 = \mathbf{Q}^+$, $(\mathbf{Q}^-)^2 = \mathbf{Q}^-$, mutually exclusive $(\mathbf{Q}^+\mathbf{Q}^- = \mathbf{Q}^-\mathbf{Q}^+ = 0)$ and complementary $(\mathbf{Q}^+ + \mathbf{Q}^- = \mathbf{I})$.

3. Application to Vectors. The positions of points on the boundary can be encoded into $S\Lambda^1$ of a Clifford number \mathbf{u} . Applying the reflection operator \mathbf{Q} to any vector $\mathbf{u} \in S\Lambda^1$ gives:

$$\begin{aligned} \mathbf{Q}\mathbf{u} &= \mathbf{n}\mathbf{u}\mathbf{n} \\ &= [-(\mathbf{n} \cdot \mathbf{u}) + (\mathbf{n} \times \mathbf{u})\sigma]\mathbf{n} \\ &= -(\mathbf{n} \cdot \mathbf{u})\mathbf{n} + \{-(\mathbf{n} \times \mathbf{u})\sigma \cdot \mathbf{n} + [(\mathbf{n} \times \mathbf{u})\sigma \times \mathbf{n}]\sigma\} \end{aligned} \quad (14)$$

The first term of in braces is zero because $\mathbf{n} \times \mathbf{u}$ is perpendicular to \mathbf{n} , and the second term simplifies with $\mathbf{n}\sigma = \sigma\mathbf{n}$ and then $\sigma^2 = 1$. Therefore:

$$\begin{aligned} \mathbf{Q}\mathbf{u} &= -(\mathbf{n} \cdot \mathbf{u})\mathbf{n} + (\mathbf{n} \times \mathbf{u}) \times \mathbf{n} \\ &= -\mathbf{u}_n + \mathbf{u}_t \end{aligned} \quad (15)$$

where \mathbf{u}_n and \mathbf{u}_t are two orthogonal components of the vector \mathbf{u} . The component \mathbf{u}_n is parallel to the vector \vec{n} , and the component \mathbf{u}_t is perpendicular to it. The general behavior of the reflection operator is to reverse the component of any vector parallel to the unit (reference) vector \vec{n} . In the case where \vec{n} is the unit

normal to the boundary Σ then \mathbf{u}_n and \mathbf{u}_t are the normal and tangential components of the field respectively. In this case the behaviour of the operator \mathbf{Q} is to reflect the vector \mathbf{u} in the boundary.

Applying the projection operators \mathbf{Q}^+ and \mathbf{Q}^- now gives:

$$\begin{aligned}\mathbf{Q}^+\mathbf{u} &= \frac{1}{2}(\mathbf{I} + \mathbf{Q})\mathbf{u} = \frac{1}{2}(\mathbf{u}_n + \mathbf{u}_t - \mathbf{u}_n + \mathbf{u}_t) = \mathbf{u}_t \\ \mathbf{Q}^-\mathbf{u} &= \frac{1}{2}(\mathbf{I} - \mathbf{Q})\mathbf{u} = \frac{1}{2}(\mathbf{u}_n + \mathbf{u}_t + \mathbf{u}_n - \mathbf{u}_t) = \mathbf{u}_n\end{aligned}\quad (16)$$

The projection operator $\mathbf{Q}^+\mathbf{u}$ and $\mathbf{Q}^-\mathbf{u}$ therefore split any Clifford vector $\mathbf{u} \in S\Lambda^1$ into normal and tangential components with respect to the normal vector \mathbf{n} .

4. Application to Electromagnetic Field The Electromagnetic (bi-vector) field $\mathbf{u} \in \Lambda^2$ is encoded into a Clifford number as:

$$\mathbf{u} = ab\mathbf{H}\sigma + jb\mathbf{E}\hat{\mathbf{e}} \quad (17)$$

Applying the reflection operator \mathbf{Q} gives:

$$\begin{aligned}\mathbf{Q}\mathbf{u} &= \mathbf{n}\mathbf{u}\mathbf{n} \\ &= ab\mathbf{n}\mathbf{H}\sigma\mathbf{n} + jb\mathbf{n}\mathbf{E}\hat{\mathbf{e}}\mathbf{n} \\ &= ab(\mathbf{n}\mathbf{H}\mathbf{n})\sigma - jb(\mathbf{n}\mathbf{E}\mathbf{n})\hat{\mathbf{e}} \\ &= ab(\mathbf{Q}\mathbf{H})\sigma - jb(\mathbf{Q}\mathbf{E})\hat{\mathbf{e}}\end{aligned}\quad (18)$$

Both the magnetic and electric parts of the field are subject to the influence of the operator, with the electric part subject also to a change of sign.

Applying the projection operators \mathbf{Q}^+ and \mathbf{Q}^- gives:

$$\begin{aligned}\mathbf{Q}^+\mathbf{u} &= \frac{1}{2}[ab\mathbf{H}\sigma + jb\mathbf{E}\hat{\mathbf{e}} + ab(\mathbf{Q}\mathbf{H})\sigma - jb(\mathbf{Q}\mathbf{E})\hat{\mathbf{e}}] \\ &= ab\frac{1}{2}(\mathbf{I} + \mathbf{Q})\mathbf{H}\sigma + jb\frac{1}{2}(\mathbf{I} - \mathbf{Q})\mathbf{E}\hat{\mathbf{e}} \\ &= ab(\mathbf{Q}^+\mathbf{H})\sigma + jb(\mathbf{Q}^-\mathbf{E})\hat{\mathbf{e}} \\ &= ab\mathbf{H}_t\sigma + jb\mathbf{E}_n\hat{\mathbf{e}}\end{aligned}\quad (19)$$

and:

$$\begin{aligned}\mathbf{Q}^-\mathbf{u} &= \frac{1}{2}[ab\mathbf{H}\sigma + jb\mathbf{E}\hat{\mathbf{e}} - ab(\mathbf{Q}\mathbf{H})\sigma + jb(\mathbf{Q}\mathbf{E})\hat{\mathbf{e}}] \\ &= ab\frac{1}{2}(\mathbf{I} - \mathbf{Q})\mathbf{H}\sigma + jb\frac{1}{2}(\mathbf{I} + \mathbf{Q})\mathbf{E}\hat{\mathbf{e}} \\ &= ab(\mathbf{Q}^-\mathbf{H})\sigma + jb(\mathbf{Q}^+\mathbf{E})\hat{\mathbf{e}} \\ &= ab\mathbf{H}_n\sigma + jb\mathbf{E}_t\hat{\mathbf{e}}\end{aligned}\quad (20)$$

The projection operators \mathbf{Q}^+ and \mathbf{Q}^- therefore split the Clifford representation of the electromagnetic field into one part containing tangential magnetic field paired with normal electric field, and another part containing normal magnetic field paired with tangential electric field.

- A vector and Field Rotation Operator

A rotation operator Θ for any Clifford number \mathbf{u} is defined as:

$$\Theta \mathbf{u} = \mathbf{n}_2 \mathbf{n}_1 \mathbf{u} \mathbf{n}_1 \mathbf{n}_2 \quad (21)$$

where \mathbf{n}_1 and \mathbf{n}_2 are unit vectors encoded as Clifford numbers (i.e. $\mathbf{n} \in S\Lambda^1$ and $\mathbf{n}^2 = -1$). Note that $\Theta \mathbf{u} = \mathbf{Q}_2 \mathbf{Q}_1 \mathbf{u}$, where $\mathbf{Q}_1 = \mathbf{n}_1 \mathbf{u} \mathbf{n}_1$ and $\mathbf{Q}_2 = \mathbf{n}_2 \mathbf{u} \mathbf{n}_2$ are two different reflection operators.

1. Application to Scalar

For any scalar $\mathbf{u} \in \Lambda^0$:

$$\Theta \mathbf{u} = \mathbf{n}_2 \mathbf{n}_1 \mathbf{u} \mathbf{n}_1 \mathbf{n}_2 = \mathbf{n}_2 \mathbf{n}_1 \mathbf{n}_1 \mathbf{n}_2 \mathbf{u} = \mathbf{u} \quad (22)$$

The rotation operator has no effect on scalars.

2. Application to Vector

For any vector $\mathbf{u} \in \Lambda^1$:

$$\Theta \mathbf{u} = \mathbf{n}_2 \mathbf{n}_1 \mathbf{u} \mathbf{n}_1 \mathbf{n}_2 \quad (23)$$

3. Application to Bi-vector

For any electromagnetic field $\mathbf{u} = ab\mathbf{H}\sigma + ib\mathbf{E}\hat{\mathbf{e}} \in \Lambda^2$:

$$\Theta \mathbf{u} = ab(\Theta \mathbf{H})\sigma + ib(\Theta \mathbf{E})\hat{\mathbf{e}} \quad (24)$$

4. Application to Sum

For any Clifford numbers \mathbf{u} and \mathbf{v} :

$$\begin{aligned} \Theta(\mathbf{u} + \mathbf{v}) &= \mathbf{n}_2 \mathbf{n}_1 (\mathbf{u} + \mathbf{v}) \mathbf{n}_1 \mathbf{n}_2 \\ &= \mathbf{n}_2 \mathbf{n}_1 \mathbf{u} \mathbf{n}_1 \mathbf{n}_2 + \mathbf{n}_2 \mathbf{n}_1 \mathbf{v} \mathbf{n}_1 \mathbf{n}_2 \\ &= \Theta \mathbf{u} + \Theta \mathbf{v} \end{aligned}$$

The rotation operator has a distributive property over sums of Clifford numbers.

5. Application to Products

For any Clifford number \mathbf{u} and \mathbf{v} :

$$\begin{aligned} \Theta(\mathbf{u}\mathbf{v}) &= \mathbf{n}_2 \mathbf{n}_1 (\mathbf{u}\mathbf{v}) \mathbf{n}_1 \mathbf{n}_2 \\ &= (\mathbf{n}_2 \mathbf{n}_1 \mathbf{u})(\mathbf{v} \mathbf{n}_1 \mathbf{n}_2) \\ &= (\mathbf{n}_2 \mathbf{n}_1 \mathbf{u})(\mathbf{n}_1 \mathbf{n}_2 \mathbf{n}_2 \mathbf{n}_1)(\mathbf{v} \mathbf{n}_1 \mathbf{n}_2) \\ &= (\mathbf{n}_2 \mathbf{n}_1 \mathbf{u} \mathbf{n}_1 \mathbf{n}_2)(\mathbf{n}_2 \mathbf{n}_1 \mathbf{v} \mathbf{n}_1 \mathbf{n}_2) \\ &= \Theta \mathbf{u} \Theta \mathbf{v} \end{aligned} \quad (25)$$

The rotation operator has a distributive property over products of Clifford numbers.

6. Application to Reproducing Kernel

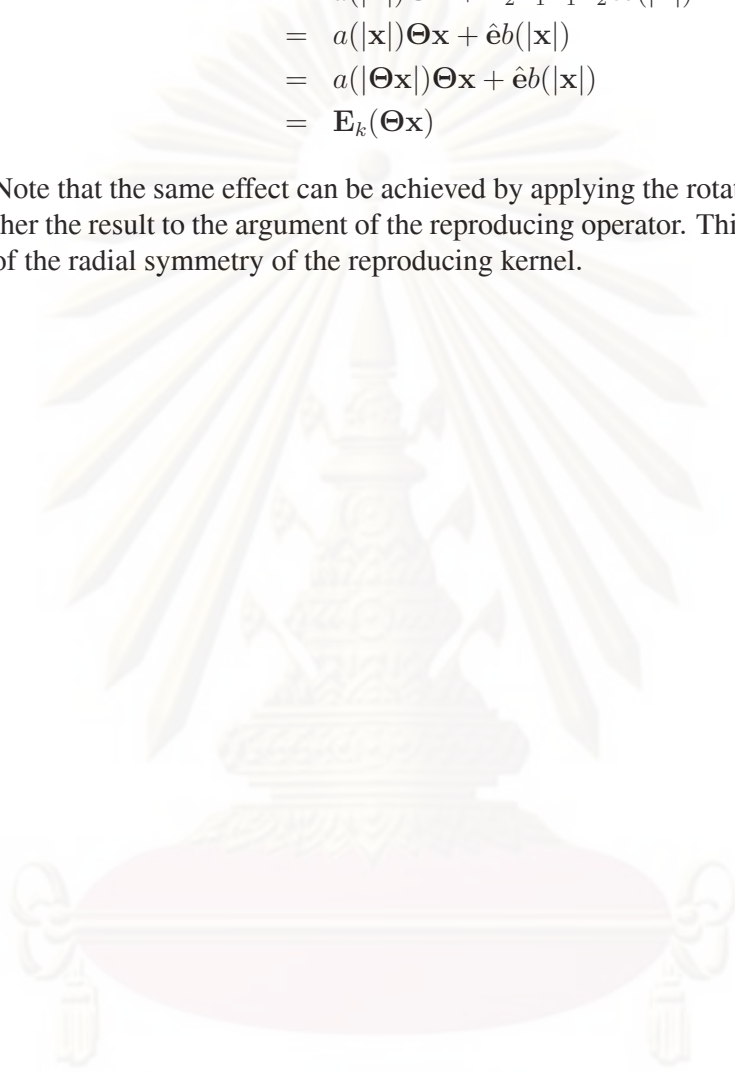
The reproducing kernel is of the form:

$$\mathbf{E}_k(\mathbf{x}) = a(|\mathbf{x}|)\mathbf{x} + \hat{\mathbf{e}}b(|\mathbf{x}|) \quad (26)$$

where a and b are scalar valued functions and $\mathbf{x} \in S\Lambda^1$. Applying the rotation operator gives:

$$\begin{aligned}
 \Theta \mathbf{E}_k(\mathbf{x}) &= \mathbf{n}_2 \mathbf{n}_1 \{a(|\mathbf{x}|)\mathbf{x} + \hat{e}b(|\mathbf{x}|)\} \mathbf{n}_1 \mathbf{n}_2 \\
 &= a(|\mathbf{x}|) \mathbf{n}_2 \mathbf{n}_1 \mathbf{x} \mathbf{n}_1 \mathbf{n}_2 + \mathbf{n}_2 \mathbf{n}_1 \hat{e}b(|\mathbf{x}|) \mathbf{n}_1 \mathbf{n}_2 \\
 &= a(|\mathbf{x}|) \Theta \mathbf{x} + \mathbf{n}_2 \mathbf{n}_1 \mathbf{n}_1 \mathbf{n}_2 \hat{e}b(|\mathbf{x}|) \\
 &= a(|\mathbf{x}|) \Theta \mathbf{x} + \hat{e}b(|\mathbf{x}|) \\
 &= a(|\Theta \mathbf{x}|) \Theta \mathbf{x} + \hat{e}b(|\mathbf{x}|) \\
 &= \mathbf{E}_k(\Theta \mathbf{x})
 \end{aligned} \tag{27}$$

Note that the same effect can be achieved by applying the rotation operator to either the result to the argument of the reproducing operator. This is a consequence of the radial symmetry of the reproducing kernel.



ศูนย์วิทยทรัพยากร
จุฬาลงกรณ์มหาวิทยาลัย

Appendix D

List of Abbreviations

PDE	Partial Differential Equation
FDM	Finite Difference Method
FEM	Finite Element Method
FDTD	Finite Difference Time Domain
FETD	Finite Element Time Domain
TLM	Transmission-Line Method
MoM	Method of Moment
BEM	Boundary Element Method
BIE	Boundary Integral Equation
EFIE	Electric Field Integral Equation
MFIE	Magnetic Field Integral Equation
CFIE	Combined Field Integral Equation
CSIE	Combined Source Integral Equation
NEC	Numerical Electromagnetics Code
MRW	Ma-Rohkin-Wandzura Quadrature Scheme
RWG	Rao-Wilton-Gilsson Basis Function
TL	Trintinalia-Ling Basis Function
PMCHW	Poggio-Miller-Chang-Harrington-Wu Formulation
DFs	Differential Forms
EMs	Electromagnetics
PEC	Perfect Electric Conductor
EHFD	Enhanced High Frequency Diffraction
P.V.	Principal Value

ศูนย์วิทยทรัพยากร
จุฬาลงกรณ์มหาวิทยาลัย

Appendix E

Publications and Presentations

Chantaveerod, A., Seagar, A. D. and Angkaew, T.

“Calculation of Electromagnetic Field with Integral Equation Based Clifford Algebra” is presented at Progress in Electromagnetics Research Symposium (PIERS 2007) on August 27-30, 2007, Prague, Czech Republic.

Chantaveerod, A. and Angkaew, T.

“Numerical Computation of Electromagnetic Far-Field from Near-Field using Integral Equation based on Clifford Algebra” is presented at Asia-Pacific Microwave Conference (APMC 2007) on December 11-14, 2007, Bangkok, Thailand.

Chantaveerod, A. and Seagar, A. D.

“Iterative Solutions of Electromagnetic Fields at Perfectly Reflective and Transmissive Interfaces using Clifford Algebra and the Multi-Dimensional Cauchy Integral” is published in the IEEE Transactions on Antennas and Propagations, on xxx, yyy, pages zzz-zzz.

Vitae

Ajalawit Chantaveerod was born in Hatyai, Songkhla, Thailand in 1979. He received the B.Eng. and M.Eng. degrees from the Department of Electrical Engineering at the Prince of Songkla University, Hatyai, Songkhla, Thailand, in 2001 and 2004 respectively. He has been pursuing the Doctoral degree in electrical engineering at Chulalongkorn University, Bangkok, Thailand, since 2004. His research areas are electromagnetic theory and computational electromagnetics.



ศูนย์วิทยทรัพยากร
จุฬาลงกรณ์มหาวิทยาลัย